

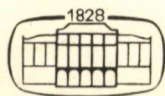
ACTA TECHNICA

ACADEMIAE SCIENTIARUM HUNGARICAE

EDITOR-IN-CHIEF: P. MICHELBERGER

VOLUME 102
NUMBERS 1—2

CIVIL ENGINEERING — C/2



AKADÉMIAI KIADÓ, BUDAPEST 1989

ACTA TECHN. HUNG.

ACTA TECHNICA

A JOURNAL OF THE HUNGARIAN ACADEMY OF SCIENCES

CENTRAL EDITORIAL BOARD

T. CZIBERE, K. GÉHER, L. KOLLÁR, P. MICHELBERGER (EDITOR-IN-CHIEF),
A. LÉVAI, J. PROHÁSZKA, K. REMÉNYI, J. SZABÓ,
GY. CZEGLÉDI (MANAGING EDITOR)

EDITORIAL COMMITTEE FOR CIVIL ENGINEERING (SERIES C.)

A. BÉNYEI, ZS. GÁSPÁR, L. KOLLÁR (CHAIRMAN), L. RÉTHÁTI,
L. SOMLYÓDY

Acta Technica publishes original papers, preliminary reports and reviews in English, which contribute to the advancement of engineering sciences.

Acta Technica is published by

AKADÉMIAI KIADÓ

Publishing House of the Hungarian Academy of Sciences
H-1117 Budapest, Prielle K. u. 19—35.

Subscription information

Orders should be addressed to

KULTURA Foreign Trading Company
H-1389 Budapest P.O. Box 149

or to its representatives abroad

Acta Technica is abstracted/indexed in Applied Mechanics Reviews, Current Contents-Engineering, Technology and Applied Sciences, GeoRef Information System, Science Abstracts.

CONTENTS

| | |
|--|-----|
| <u>Bognár, L.</u> : Stability of planar reinforced concrete column systems | 3 |
| <u>Bojtár, I. - Bagi, K.</u> : Micromechanical model for numerical analysis of granular materials. | 207 |
| <u>Gáspár, Zs. - Domokos, G.</u> : Global investigation of discrete models of the Euler buckling . | 227 |
| <u>Györgyi, J.</u> : Production of dynamic stiffness matrix in case of other than rigid joints and rigid elements | 239 |
| <u>Hegedűs, I. - Kollár, L.P.</u> : Wrinkling of faces of compressed and bent sandwich bars and its interaction with overall instability | 49 |
| <u>Imre, E.</u> : Some physical problems associated with the skin bearing capacity of axially loaded piles | 65 |
| <u>Iványi, M.</u> : Failure tests with steel frameworks | 247 |
| <u>Kaliszky, S. - Lógó, J.</u> : Optimal design of dynamically loaded reinforced concrete frames under single displacement constraint | 267 |
| <u>Kollár, L.</u> : Space structures: static relationships, structural forms | 281 |
| <u>Kurutz, M.</u> : Stability of structures of non-smooth energy functionals in one-dimensional case | 291 |
| <u>Páczelt, I. - Szabó, I.</u> : A bandwidth reduction process for substructural element method .. | 315 |
| <u>Popper, Gy.</u> : Identification of damping parameters in linear vibration systems | 327 |
| <u>Rédey, G. - Paál, I.</u> : Expert system for geotechnical testing of damaged buildings | 87 |
| <u>Roller, B.</u> : The general state change equation of bar structures | 339 |
| <u>Sajtos, I.</u> : Calculation of hyperbolic paraboloid segmental shell with protruding unsupported edge | 103 |
| <u>Scharle, P.</u> : Attractions and risks of the analogies | 355 |
| <u>Tarnai, I.</u> : Higher-order infinitesimal mechanisms | 363 |
| <u>Tarnai, I. - Makai, E.</u> : Kinematical indeterminacy of a pair of tetrahedral frames | 123 |
| <u>Türkóssy, A.</u> : Accuracy test of simplified continuum calculations of two-layer space grids | 147 |
| <u>Vásárhelyi, A. - Lógó, J.</u> : Analysis of the structures for dynamic effects with mathematical programming | 379 |
| <u>Vértes, Gy.</u> : Investigation of nonlinear behaviour of building structures under dynamic load | 391 |

BOOK REVIEWS

| | |
|--|-----|
| <u>Iványi, M.</u> (editor): Stability of steel structures (Gy. Czeglédi) | 199 |
| <u>Kaliszky, S.</u> : Plasticity (Mrs. P. Elter) | 405 |
| <u>Kézdi, Á. - Rétháti, L.</u> : Soil mechanics of earthworks, foundations and highway engineering (P. Scharle) | 201 |
| <u>Rétháti, L.</u> : Probabilistic solutions in geotechnics (P. Scharle) | 202 |

CONTENTS

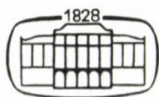
| | |
|--|-----|
| <u>Bognár, L.</u> : Stability of planar reinforced concrete column systems | 3 |
| <u>Hegedűs, I. - Kollár, L.P.</u> : Wrinkling of faces of compressed and bent sandwich bars and its interaction with overall instability | 49 |
| <u>Imre, E.</u> : Some physical problems associated with the skin bearing capacity of axially loaded piles | 65 |
| <u>Rédey, G. - Paál, T.</u> : Expert system for geotechnical testing of damaged buildings | 87 |
| <u>Sajtos, I.</u> : Calculation of hyperbolic paraboloid segmental shell with protruding unsupported edge | 103 |
| <u>Tarnai, T. - Makai, E.</u> : Kinematical indeterminacy of a pair of tetrahedral frames | 123 |
| <u>Türkössey, A.</u> : Accuracy test of simplified continuum calculations of two-layer space grids | 147 |
| BOOK REVIEWS | |
| <u>Iványi, M.</u> (editor): Stability of steel structures (Gy. Czeglédi) | 199 |
| <u>Kézdí, Á. - Rétháti, L.</u> : Soil mechanics of earthworks, foundations and highway engineering (P. Scharle) | 201 |
| <u>Rétháti, L.</u> : Probabilistic solutions in geotechnics (P. Scharle) | 202 |

ACTA TECHNICA

ACADEMIAE SCIENTIARUM HUNGARICAE

EDITOR-IN-CHIEF: P. MICHELBERGER

VOLUME 102
NUMBERS 1—4



AKADÉMIAI KIADÓ, BUDAPEST 1989

ACTA TECHN. HUNG.

STABILITY OF PLANAR REINFORCED CONCRETE COLUMN SYSTEMS

BOGNÁR, L.*

(Received: 30 September 1986)

A process is presented in this work, permitting the stability of a system of planar reinforced concrete columns to be investigated simply and accurately without the use of a computer. Instead of assuming a single-parameter load usually used in stability studies, the process considers the magnitude of vertical loads to be constant and determines the value of horizontal deflecting force, taking into consideration the effect of displacement on internal forces of the indeterminate beam, restraint due to ultimate cross sectional curvature as well as the creep of concrete.

1. Introduction

A supporting structure consisting of restrained columns and two-support beams interconnecting them (Fig. 1), essentially a special framework, is often used in the construction of industrial buildings. Different methods are known to calculate for supporting structure of this type /4/, /5/, /6/, /7/, /8/, /9/, /10/, having, however, a common feature in that they use neglects which make impossible to determine the behaviour of the structure accurately or they are rather sophisticated methods requiring the use of a high-capacity computer. Even accurate methods are applicable to structures of elastic-plastic material only /2/, /5/, /8/, /9/, the investigation of reinforced concrete systems being a field still unexplored.

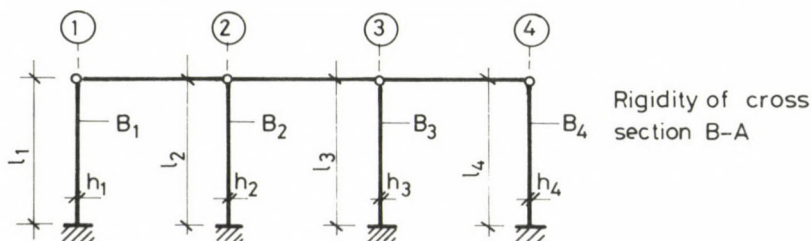


Fig. 1. Frame network

*Bognár, László, H-2400 Dunaújváros, Zalka M. u. 1, Hungary

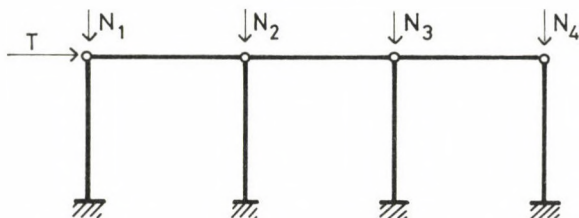


Fig. 2. Frame under compression and bending

A method has been presented in /19/ to investigate planar column systems under pressure and bending, made of elastic-plastic material (Fig. 2). Based on this method, a process applicable to reinforced concrete columns has been developed. The process is capable of describing the actual behaviour of the structure and it can be directly used by design engineers. The process is described below.

2. The problem posed

Methods suited for calculation of column systems are briefly summed up in /19/. Outlined in the present work are the most significant deficiencies of these methods, elimination of these deficiencies being the most important objective of this study.

In the methods used so far,

- a) the forces acting upon indeterminate supporting structures have been determined on the basis of the theory of elasticity of the first order and in stability studies, the internal forces have been assumed to increase proportionately with an increasing load intensity,
- b) a gradual reduction in rigidity of the support is usually left out of consideration,
- c) the effect of normal forces on the moment load capacity of the cross sections can not be taken into consideration or if indeed at all, only by means of some iteration process /2/,
- d) no limits are set to angular displacement of the different cross sections of the supporting structure, the angular displacement being assumed to be infinite in general,
- e) the effect of slow deformation is not taken into consideration.

This work deals with column systems where the load and/or rigidity conditions are such as to exclude three-dimensional twist buckling so that the columns will act as a planar supporting structure.

A theory of the second order has been taken as a basis for investigation. An elastic-plastic material model is used to describe the stress-strain ($\sigma - \epsilon$) diagram of concrete and reinforcement. The supporting structure includes columns of rectangular cross section with a symmetric reinforcement.

3. Description of the principle of the calculation method

The first step is to produce the moment-curvature ($M - \frac{1}{\rho}$) function of the reinforced concrete cross section (see later in Chapter 4), a rather complicated job requiring usually the use of a computer but for a symmetrically reinforced rectangular cross section, it can be found in the literature. To simplify the job, analytical functions are used to approximate numerical functions. The rigidity of the cross section is determined on the basis of this analytical relationship, the value of rigidity depending on the cross sectional and material characteristics as well as on the value of instantaneous load acting upon the cross section.

This rigidity function is used then to write the compatibility and equilibrium equations of the structure.

As has been outlined in detail in /19/, significant difficulties are encountered in assumption of a single-parameter load in stability calculations. Therefore, the vertical loads are assumed to be constant in this method and what we determine is the critical horizontal load associated with the vertical load of given magnitude.

To be on the safe side, the rigidity of the columns has been assumed to be the same as the rigidity of the restraint cross section along full length of the column. As a final result of the investigation, the function between displacement ω of the top point of given column system and horizontal force T is obtained (Fig. 3), the maximum value of this function, T_{\max} , being the critical horizontal load of the column system. It is checked whether T_{\max} and displacement ω associated with it can actually take place in case of a structure including reinforced concrete columns. Namely, the curvature of any column cross section may reach the value of ultimate curvature before T_{\max} takes place loses its load bearing capacity because of lost strength of a cross section. Without a curtailment of generality, the procedure of plotting of curve $T - \omega$ is illustrated for the case of a two-column system, the results obtained being applicable to multicolumn systems accordingly.

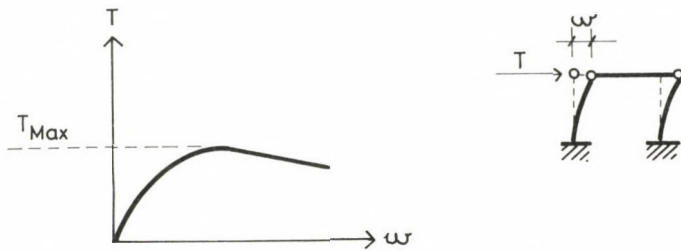


Fig. 3. Determination of critical horizontal load (T_{\max}) on the basis of $T - \omega$ function

4. Moment-curvature function of a symmetrically reinforced rectangular cross section

The procedure of calculation of the moment-curvature function for elastic-plastic cross sections has been described in detail in [19]. In case of a reinforced concrete cross section, a difference lies only in the internal forces of the reinforced concrete cross section when identifying the equilibrium state associated with the different extreme fibre compressions.

The shape of the function depends on the stress-strain diagram of concrete or reinforcement. There is a difference between functions given as a $\sigma - \epsilon$ diagram for concrete and steel by the different authors or standards of the different countries.

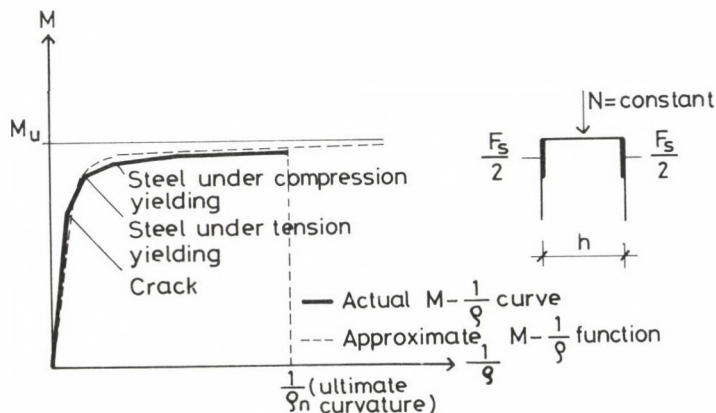


Fig. 4. Moment (M) - curvature ($\frac{1}{\rho}$) function of a symmetrically reinforced rectangular cross section with constant normal force acting upon it

For low values of curvature where the stress-strain relations are usually described on the basis of a linearly elastic relationship for both concrete and steel, the moment-curvature function of a symmetrically reinforced rectangular cross section under constant normal load increases relatively steeply (Fig. 4). Cracks take place in the cross section as the value of curvature increases and the neutral axis gets inside the cross section with the rigidity of the cross section reducing as a result. The moment-curvature function keeps flattening as the rigidity reduces. Depending on the magnitude of normal force as well as on the conditions of concrete and/or steel, this process will either discontinue due to destruction of the cross section resulting from breaking compression in the extreme fibre of the concrete or the reinforcement will yield before destruction with the curve, still more flattened, continuing until breaking compression takes place.

The flatness of function $M - \frac{1}{\phi}$ depends first of all on the concrete curve and within this, on the ratio of elastic and plastic sections. Authors of the international literature assume a relatively high value, usually $\epsilon_{c,u} = 3.5\%$, for ultimate compression of concrete and thus the moment-curvature function runs nearly horizontally over a relatively wide range of curvature after the first steep section until the value of ultimate curvature depending on ultimate compression of the concrete ($\frac{1}{\phi_u}$) is reached.

Examples of analysis of moment-curvature relations of reinforced concrete cross sections under constant normal load are given by authors of the international literature /20/, /21/, /22/. They use an elastic-plastic material model to describe the stress-strains relations for concrete. Some authors replace the elastic section with a linear curve or curve of the second order (Fig. 5). The $\sigma - \epsilon$ diagram of steel is a linearly elastic-plastic model (Fig. 6).

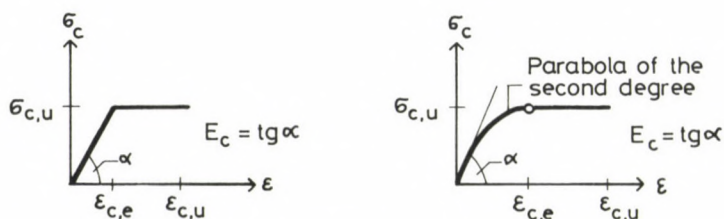


Fig. 5. Stress (σ) - strain (ϵ) diagrams of concrete according to different authors

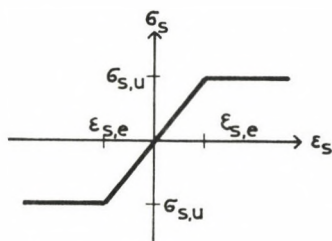


Fig. 6. Stress (σ) - strain (ϵ) diagram of reinforcement

From among Hungarian authors, Szalai /23/ investigated the moment-curvature relations for reinforced concrete cross sections. However, the results of these investigations can not be used in the present case directly because here the investigation is based rather on constancy of the initial eccentricity of forces acting upon the different reinforced concrete bars investigated than on constancy of normal force, acting upon the cross section, during increase of the curvature. In investigation of column systems, the eccentricity of forces acting upon the different columns (as an initial eccentricity) changes in the course of the loading process independently of whether single-parameter load or multiparameter load is assumed (depending on the rigidity or load conditions of the different columns). Moreover, as has been pointed out in /19/, different moment-curvature functions should be used as the intensity of load is increased unless vertical compressive forces for other than constant values were assumed. Szalai's investigations apply to a reinforced concrete cross section reinforced on one side and to linearly elastic-plastic concrete material model. For ultimate compression of concrete, a relatively low value, only $\epsilon_{c,u} = 2.5\%$ has been assumed by the author in agreement with the Hungarian standard for reinforced concrete.

Almási /24/ investigated the stability of prestressed concrete columns. The equilibrium equations of internal cross sectional forces in the moment-curvature relationship include also the effect of the prestressing wire, which is estimated to be insignificant but a more accurate investigation would be required to verify this insignificance. The moment-curvature functions have been written for constant normal force as a tensile force. A value of $\epsilon_{c,u} = 2\%$ has been assumed by the author for ultimate compression of the concrete based on earlier experiments and thus the moment-curvature function is restricted to a narrow range of curvature. Otherwise what has been said earlier applies to the shape of the function.

According to problem posed, the numerically determined function of moment-curvature described above is approximated analytically to facilitate computation. The following functions result in a relatively good approximation (see dash-line in Fig. 4):

$$\frac{1}{\xi} = \frac{M}{E_C I_0} \left[\frac{1}{1 - \left(\frac{M}{M_U} \right)^6} \right] \quad (1)$$

for a cross section under pure bending,

$$\frac{1}{\xi} = \frac{M}{E_C I_0} \left[\frac{1}{1 - \left(\frac{N}{N_{U,e}} \right)^6} \right] \quad (2)$$

in case of eccentric pressure,

where E_C initial modulus of elasticity of concrete

I_0 inertial moment of uncracked concrete cross section

N, M normal force and/or bending moment acting upon the cross section

M_U ultimate moment of cross section under pure bending

$N_{U,e}$ magnitude of ultimate force associated with eccentricity e (by ultimate force or ultimate moment we understand the force or moment resulting in destruction).

The accuracy of approximation depends on the geometry and load. The accuracy will be tested later in another work.

Ultimate moment in case of a rectangular cross section with symmetric reinforcement under pure bending (Fig. 7).

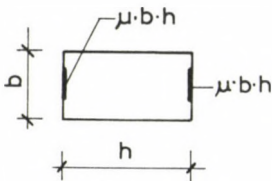


Fig. 7. Symmetrically reinforced rectangular concrete cross section

$$M_U = \frac{1}{2} N_S h \quad (3)$$

where

$$N_S = 2 \mu \cdot b \cdot h \cdot \sigma_{S,u} \quad (4)$$

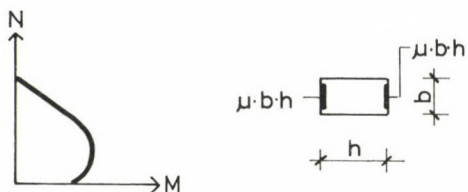


Fig. 8. Load capacity line of a reinforced concrete cross section

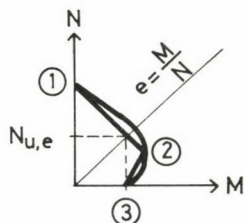


Fig. 9. Determination of ultimate force $N_{u,e}$ associated with eccentricity $e = \frac{M}{N}$ on the basis of the simplified load capacity line

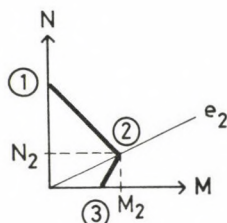


Fig. 10. Low-high eccentricity pressure transition

μ being the extent of reinforcement ($\mu = \frac{F_s}{2 \cdot F_c}$, where F_s is the area of reinforcement while F_c the area of the concrete cross section),
 b width of cross section,
 h height of cross section, and
 $\sigma_{s,u}$ is the ultimate stress of steel.

For a reinforced concrete cross section, $N_{u,e}$ in equation (2) that is the ultimate force associated with given eccentricity can be determined on the basis of the load bearing capacity line as in case of a reinforced concrete cross section, the boundary condition of the load bearing capacity for the cross section is determined by the load bearing capacity line (Fig. 8).

The value of $N_{u,e}$ is calculated as a co-ordinate of intersection of straight $e = \frac{M}{N}$ and the load bearing capacity line. The usual simplification is used here according to which a function set up of two straights is used to approximate the load bearing capacity line (Fig. 9). Determination of the ultimate force associated with given eccentricity is a still more difficult job than in case of a homogeneous cross section in spite of this approximation because in this case the investigation shall be divided in two as a function of the values of eccentricity. A different relationship is obtained for determination of $N_{u,e}$ in either case depending on whether straight $e = \frac{M}{N}$ intersects straight 1-2 or straight 2-3 (Fig. 9). In other

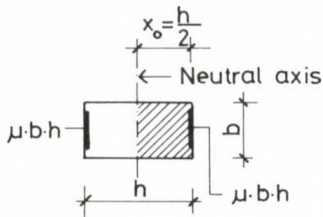


Fig. 11. Position of neutral axis at low-high eccentricity transition

words, a different relationship serves to calculate $N_{u,e}$ in the range of pressure of minor eccentricity and again a different relationship in the range of pressure of major eccentricity as two functions have been used instead of one function (like e.g. in case of steel cross sections) to obtain the load bearing capacity line expressing the boundary condition of load bearing capacity of the cross section. First thing to do is to determine eccentricity (straight e_2 in Fig. 10) associated with the state indicating the transition between minor and major eccentricity (2 in Fig. 10). This is necessary because for finding the value of $N_{u,e}$ of the ultimate force for given eccentricity e , one has to know if eccentricity e lies below or above eccentricity e as the relationship to be used to determine the ultimate force depends on this relation.

For a rectangular cross section with symmetric reinforcement, values M_2 and N_2 associated with eccentricity e_2 (Fig. 10) can be written, as follows (Fig. 11):

$$N_2 = \frac{N_c}{2}, \quad (5)$$

where $-N_c = b \cdot h \cdot \sigma_{c,u}$ ($\sigma_{c,u}$ being the ultimate stress of concrete),

$$M_2 = \frac{N_s \cdot h}{2} + \frac{N_c}{2} \cdot \frac{h}{4} \quad (6)$$

Now the value of e_2 :

$$e_2 = \frac{M_2}{N_2} = \frac{N_s \cdot h}{2 \cdot N_2} + \frac{N_c \cdot h}{8 \cdot N_2} \quad (7)$$

With the relationship of N_2 according to (5) as well as the values of N_s and N_c substituted into equation (6) and with the equation reduced, the following relationship is obtained:

$$e_2 = \frac{N_s \cdot h}{N_c} + \frac{h}{4} = \left(\frac{2 \mu \cdot \sigma_{s,u}}{\sigma_{c,u}} + \frac{1}{4} \right) \cdot h \quad (8)$$

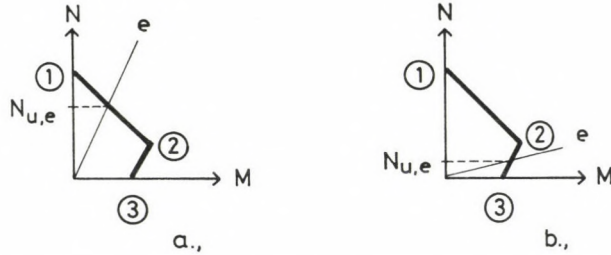


Fig. 12. Determination of ultimate force $N_{u,e}$ associated with eccentricity $e = \frac{M}{N}$ in the range of pressure of minor and major eccentricity

Having the value of e_2 , now we can return to the original problem that is to calculation of ultimate force $N_{u,e}$ associated with given eccentricity e .

If $e < e_2$, then co-ordinate $N_{u,e}$ of the intersection of straight e and straight 1-2 shall be found according to Fig. 12/a. If $e > e_2$, then the co-ordinate of the intersection of straight e and straight 2-3 will be required according to Fig. 12/b. These intersections can be simply determined by means of analytical geometry. Therefore, only the results are presented here with the derivations neglected.

Value $N_{u,e}$ of ultimate force associated with eccentricity e :
 — for $e < e_2$

$$N_{u,e} = \frac{N_s + N_c}{1 + A \frac{e}{h}} \quad (9)$$

where A is a factor depending on strength of reinforcement $\mu \cdot \frac{\sigma_{s,u}}{\sigma_{c,u}} / 12$, its value described by expression

$$A = \frac{1 + 4 \mu \frac{\sigma_{s,u}}{\sigma_{c,u}}}{0.25 + 2 \mu \frac{\sigma_{s,u}}{\sigma_{c,u}}} \quad (10)$$

— for $e > e_2$

$$N_{u,e} = \frac{2 N_s}{4 \cdot \frac{e}{h} - 1} \quad (11)$$

Summing up: The moment-curvature curve of a symmetrically reinforced rectangular reinforced concrete cross section has been approximated by means of analytical function (1) or (2).

The value of ultimate force $N_{u,e}$ associated with eccentricity e can be calculated on the basis of the load bearing capacity line of the cross section, the way of calculation being given by relationship (9) or (11) depending on whether the pressure is of minor or major eccentricity. To decide this, the transition between minor and major eccentricity has been determined (7).

On the basis of equation (1) or (2), the moment-curvature ratio of a reinforced concrete cross section can be written by means of a substitution rigidity, a quantity given in the form of a function comprising the effect of changes during load on rigidity.

Value of substitution rigidity in the course of load:

— For a cross section under bending only:

$$B = E_c \bar{I} = E_c \cdot I_0 \left[1 - \left(\frac{2 M}{N_s \cdot h} \right)^6 \right]; \quad (12)$$

— For a cross section under eccentric compression:

$$B = E_c \bar{I} = E_c I_0 \left\{ 1 - \left[\frac{N(1 + A \frac{e}{h})}{N_s + N_c} \right]^6 \right\}; \quad (13)$$

in case of an eccentricity within the range of minor eccentricity while

$$B = E_c \bar{I} = E_c I_0 \left\{ 1 - \left[\frac{N(4 \frac{e}{h} - 1)}{2 N_s} \right]^6 \right\} \quad (14)$$

in case of an eccentricity within the range of major eccentricity.

Explanation for the symbols used in the expressions has been given earlier.

5. Principle of determination of the critical load of a column system

As has been outlined above, what we shall do is essentially to plot the function between displacement of the top point of the column system and the horizontal load (Fig. 3), the critical horizontal load of the column system being given by value T_{\max} of this function. The method used to determine the critical load has been described in detail in /19/. According to this method, equations are written for the displacement of the top point of the different columns. In these equations, the internal contact forces and/or the rigidity of the different columns are given in the form of functions. Assuming that the different columns are equally displaced, the internal contact forces and/or the horizontal displacement force can be calculated for given displacement. Assuming a different displacement for each column and with force T determined for each displacement, function $T - \omega$ can be plotted.

To facilitate computation, a displacement-horizontal displacement force function has been plotted for each column and these functional values have been summed up to plot function $T - \omega$. This method has been preferred to direct solution of the equations.

Columns directly affected by normal force and unloaded columns have been dealt with in isolation. For unloaded columns, the displacement force relation can be written directly while for columns effected by normal force, the function between eccentricity e of forces acting upon the column and displacement ω has been determined first to write then the displacement-displacement force function on the basis of eccentricities associated with the different values of displacement.

The equations and function have been written usually in a dimensionless form. For this purpose, the following dimensionless quantities have been introduced, using the symbols of Figs 12 and 14:

$$\begin{aligned}
 \frac{H}{N_2} &= \tilde{\epsilon}_2 & \frac{T}{N_2} &= \alpha \\
 \frac{w_i}{h_i} &= \xi_i & \frac{N_1}{N_2} &= \mu \\
 \frac{N_i}{N_{u,i}} &= \tilde{\epsilon}_i & \frac{h_1}{h_2} &= \nu_1
 \end{aligned} \tag{15}$$

$$\frac{e_i}{h_i} = \Delta_i$$

$$\frac{\bar{H}_1}{N_{u,1}} = \epsilon_1^*$$

$$\frac{l_i}{h_i} = \gamma_i$$

$$\frac{N_{u,1}}{N_2} = \epsilon_1^*$$

$$\frac{E I_{0,i}}{N_i \cdot l_i^2} = q_i$$

$$\frac{E I_{0,1}}{N_{u,1} \cdot l_i^2} = q_1^*$$

From among symbols not defined earlier,

- H — internal contact force
- $N_{u,i}$ — ultimate force of i-th column for concentric pressure (in the present case, ultimate force of concrete cross section without reinforcement)
- H_1 — resultant of horizontal forces acting upon column 1 (or, depending on the static framework, $H_1 = H$ or $H_1 = T-H$)
- E — E_c in the present case.

Numbering of the columns in the static framework (Fig. 13) is not arbitrary. A column upon which normal forces are not directly acting is denoted by 1. Should normal forces act upon both columns, then the numbering is arbitrary. This stipulation has been necessary to write the equations.

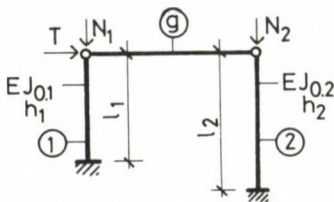


Fig. 13. Static framework of the column system

After introduction of the dimensionless quantities, the critical horizontal load of the column system is supplied by the extreme value of function $\alpha - \tilde{\xi}$.

Function $\alpha - \tilde{\xi}$ takes the following shape:

$$\alpha = -\frac{\tilde{\mu}}{\gamma_1} (\Delta_1 - \tilde{\xi}_1) + \tilde{\xi}_2, \quad (16)$$

where

$$\tilde{\xi}_2 = \frac{\Delta_2 - \tilde{\xi}_2}{\gamma_2}, \quad (17)$$

and

$$\tilde{\xi}_1 = \frac{\tilde{\xi}_2}{\nu_1} \quad (18)$$

For an unloaded column 1,

$$\alpha = \tilde{\xi}_2 + \xi_1^* \cdot \epsilon_1^* \quad (19)$$

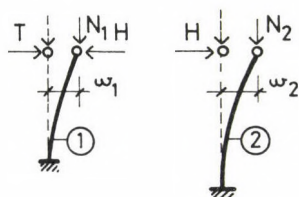


Fig. 14. Main girder of column system

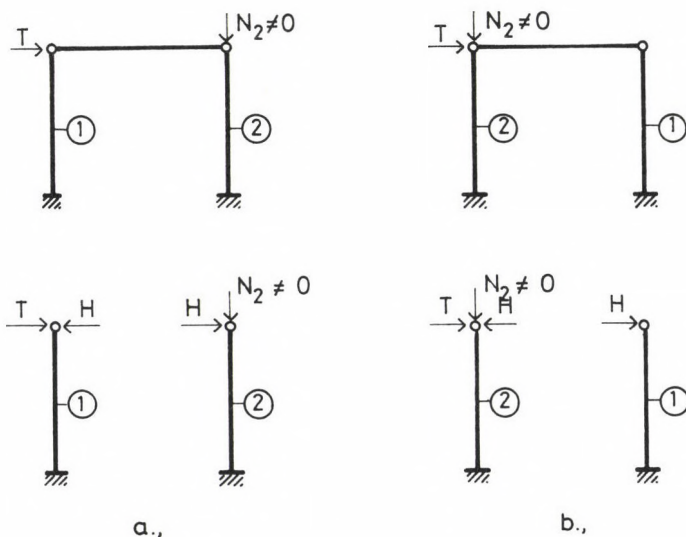


Fig. 15. Column system under different loads

where the value of $\tilde{\xi}_2$ is determined by means of equation (17) but it means dimensionless quantities $\frac{H}{N_2}$ (see Fig. 15/a) or $\frac{T-H}{N_2}$ (see Fig. 15/b), depending on the load.

The value of ξ_1^* can be determined by means of equation

$$\varrho_1^* = \frac{\bar{H}_1}{N_{U,1}} = \frac{3 \cdot B \cdot w_1}{l_1^3 \cdot N_{U,1}} \quad (20)$$

where the value of B is supplied by relationship (12).

After these equations have been written, the job can be essentially formulated, as follows:

In case of columns upon which normal forces are directly acting, it is the displacement (ω) — eccentricity (e) function or, in a dimensionless form, function $\xi_i - \Delta_i$ while in case of unloaded columns, the displacement (ω) — displacement force (\bar{H}_1) function or, in a dimensionless form, function $\varrho_1^* - \tilde{\xi}_1$ that shall be produced. This is described in Chapter 6. After these functions have been produced, the critical load of the column system is supplied in general by the extreme value of functions $\alpha - \tilde{\xi}$ that can be plotted on the basis of equation (16) or (19). An additional test is required after function $\alpha - \tilde{\xi}$ has been plotted in case of a system of reinforced concrete columns. Namely, in case of reinforced concrete cross section, the curvature of some restraining cross section may reach the value of ultimate curvature before function $\alpha - \tilde{\xi}$ reaches a maximum and the load capacity of the column system is fully exhausted as a result of destruction of this cross section (Fig. 16). Thus, in investigation of reinforced concrete columns, it is not enough to plot merely function $\Gamma - \omega$ or $\alpha - \tilde{\xi}$ but it shall also be tested whether the obtained value of Γ_{\max} can actually take place under given conditions without destruction of the cross sections due to lost strength. Practicably, this is made by determining first the value of displacement $\omega(\tilde{\xi})$ where the curvature of the cross section reaches the value of ultimate curvature (see value $\tilde{\xi}_{cr}$ in Fig. 16). It is then enough to test function $\alpha - \tilde{\xi}$ below this value of $\tilde{\xi}_{cr}$. Should function $\alpha - \tilde{\xi}$ have no extreme value in range $(0; \tilde{\xi}_{cr})$, then the critical horizontal load of the column system will be supplied by α_{cr} associated with the displacement as compared with $\tilde{\xi}_{cr}$.

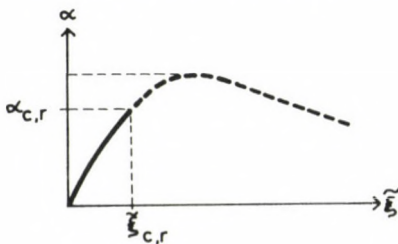


Fig. 16. Destruction of column system due to destruction of the restrained cross section

The necessity of this additional test comes from the fact that while the domain of definition of the analytical function used to approximate the moment-curvature relation lies between zero and infinite, actually the domain of definition can be imagined as lying between zero and $\frac{1}{\xi_u}$ (where $\frac{1}{\xi_u}$ means ultimate curvature, Fig. 4). Of course, the value of ultimate curvature depends also on the magnitude of normal force acting upon the cross section. Theoretically, breaking compression taking place in the extreme fibre of the reinforced concrete cross section should not necessarily be considered to be at the same time a limit of the load capacity of the entire structure. A local maximum of function $\Gamma - \omega$ will not necessarily take place as a result of breaking compression in some parts of the cross section of one of the columns with these parts contributing no longer to the force system. Assume that the moment-curvature line of a symmetrically reinforced rectangular cross section is continued after ultimate compression has taken place in the extreme fibres, using a descending function. In compliance with the specifications of the standard, breaking compression is considered to be the limit of destruction due to lost strength because, were a destruction of the different extreme fibres due to lost strength permissible, also a new definition of safety specified in the standard would be necessary. Namely, a case where some of the extreme fibres are destroyed while the structure as a whole is still stable might also occur.

6. Determination of the critical load of reinforced concrete column systems

As has been outlined above, essentially two cases are considered in the problem that is the case of columns upon which normal forces are directly acting and the case of unloaded columns for which a displacement-eccentricity function and a displacement-displacement force function shall be written, respectively.

6.1 Reinforced concrete columns under normal force

Assuming a deflection that can be described by a sine-wave function, the displacement (ω) — eccentricity (e) function for columns under normal force is described by equation

$$w_i = \frac{N_i \cdot e_i}{\frac{3EI_i}{l_i^2} \left(1 - \frac{4 \cdot N_i \cdot l_i^2}{\pi^2 \cdot EI_i} \right) + N_i} \quad (21)$$

/19/. Rigidities written in the form of functions for reinforced concrete cross sections in Chapter 4 shall be written in place of rigidities EI_i in the equation, the value of rigidity being described by a different equation in the range of pressures of minor eccentricity and by again a different equation in the range of pressures of major eccentricity (see Chapter 4):

a) Value of rigidity EI_i in the range of pressure of minor eccentricity ($e < e_2$):

$$EI_i = E_C \cdot I_{O,i} \left\{ 1 - \left[\frac{N_i \left(1 + A_i \frac{e_i}{h_i} \right)}{N_{S,i} + N_{C,i}} \right]^6 \right\} \quad (13)$$

With the value of A_i , $N_{S,i}$ and $N_{C,i}$ substituted into equation (13) and with a quantity $\theta_i = \frac{\mu_i \sigma_{S,u}}{\sigma_{C,u}}$ for reinforcement strength introduced, equation (13) takes the following shape:

$$EI_i = E_C \cdot I_{O,i} \left\{ 1 - \left[\frac{N_i \left(1 + \frac{1 + 4\theta_i}{0.25 + 2\theta_i} \cdot \frac{e_i}{h_i} \right)}{N_{U,i} (1 + 2\theta_i)} \right]^6 \right\} \quad (22)$$

With rigidity reducing factor

$$Z_i = 1 - \left[\frac{N_i \left(1 + \frac{1 + 4\theta_i}{0.25 + 2\theta_i} \cdot \frac{e_i}{h_i} \right)}{N_{U,i} (1 + 2\theta_i)} \right]^6 \quad (23)$$

introduced rigidity EI_i is described by simplified relationship

$$EI_i = E_C I_{O,i} \cdot Z_i \quad (24)$$

Now, with the functions obtained written in a dimensionless form, function $\tilde{\xi}_i - \Delta_i$ will be on the basis of equation (21)

$$\tilde{\xi}_i = \frac{\tilde{\epsilon}_i \cdot \Delta_i}{3 \cdot q_i \cdot \tilde{\epsilon}_i \cdot Z_i \left(1 - \frac{4}{\pi^2 \cdot q_i \cdot Z_i} \right) + \tilde{\epsilon}_i} \quad (25)$$

where, in a dimensionless form,

$$Z_i = 1 - \left[\frac{\tilde{\epsilon}_i \left(1 + \frac{1 + 4 \Theta_i}{0.25 + 2 \Theta_i} \cdot \Delta_i \right)}{1 + 2 \Theta_i} \right]^6 \quad (26)$$

b) Value of rigidity E_i in the range of pressure of major eccentricity ($e > e_2$):

$$EI_i = E_c I_{0,i} \left\{ 1 - \left[\frac{N_i \left(4 \frac{e_i}{h_i} - 1 \right)}{2 N_{s,i}} \right]^6 \right\} \quad (14)$$

In a dimensionless form, the value of rigidity reducing factor within the highly eccentric pressure range can be described by means of function

$$Z_i = 1 - \left[\frac{\tilde{\epsilon}_i (4 \Delta_i - 1)}{4 \Theta_i} \right]^6 \quad (27)$$

Value of eccentricity e_2 expressing the transition between minor and major eccentricity:

$$e_{2,i} = \left(\frac{2 \mu_i \sigma_{s,u}}{\sigma_{c,u}} + \frac{1}{4} \right) \cdot h_i \quad (8)$$

or, in a dimensionless form,

$$\Delta_{u,i} = \frac{e_{2,i}}{h_i} = 2 \Theta_i + \frac{1}{4} \quad (28)$$

Thus, relation $\tilde{\xi}_i - \Delta_i$ for reinforced concrete columns under normal force has been determined. As seen, the shape of the function varies depending on parameters ϵ_i , q_i and Θ_i .

6.2 Reinforced concrete columns with no normal force acting upon them

Displacement-displacement force function for columns upon which normal forces are not directly acting:

$$\bar{H}_1 = \frac{3 E I_1}{l_1^3} \cdot w_1, \quad (29)$$

Here rigidity $E I_1$ is determined by expression

$$E I_1 = E_c I_{o,1} \left[1 - \left(\frac{2 \cdot M_1}{N_{s,1} \cdot h_1} \right)^6 \right] \quad (12)$$

according to Chapter 4. Bending moment to be taken into consideration (M_1)

$$M_1 = \bar{H}_1 l_1 \quad (29)$$

Thus expression (20) takes the following shape:

$$\bar{H}_1 = \frac{3 E_c I_{o,1}}{l_1^3} \left[1 - \left(\frac{2 \cdot \bar{H}_1 \cdot l_1}{N_{s,1} \cdot h_1} \right)^6 \right] \cdot w_1 \quad (30)$$

Since the value of \bar{H}_1 is implicitly given in equation (30), displacement w shall reasonably be expressed from the equation. With the equation reduced, the following equation is obtained for a dimensionless $\tilde{\xi}_1 - \varrho_1^*$:

$$\tilde{\xi}_1 = \frac{\varrho_1^*}{\frac{3\varrho_1^*}{\gamma_1} \left[1 - \left(\frac{\varrho_1^*}{\theta_1} \cdot \gamma_1 \right)^6 \right]} \quad (31)$$

Relation $\tilde{\xi}_1 - \Delta_1$ has been determined for columns under normal force in par 6.2. Then, for unloaded columns, relation $\tilde{\xi}_1 - \varrho_1^*$ has been determined in par 6.2. In the knowledge of these relationships, function $\alpha - \tilde{\xi}$ can be plotted by means of equations written in Chapter 5.

7. Ultimate strain of symmetrically reinforced concrete columns of rectangular cross section

Next thing to do is to write for a reinforced concrete cross section under normal force of given magnitude ultimate curvature $\frac{1}{\xi_u}$ —resulting in ultimate compression $\epsilon_{c,u}$ in the concrete. Should the curvature reach this value in the restrained cross section of one of the columns during loading of a column system, this will mean at the same time that the load capacity of the entire column system is exhausted. Under given geometrical, strength and load conditions, a definite value of displacement of the column system is associated with this ultimate value. Since the stability of the column system is investigated on the basis of the displacement-force function, it is reasonable to reduce also the stipulation concerning ultimate angular displacement of the cross section to limits set to strain. In doing so, first the value of ultimate curvature shall be determined for a reinforced concrete cross section under normal force. In the knowledge of ultimate curvature and with the strain line of the column assumed to be sinusoid, displacement w_{cr} shall be determined for the upper end point of the column where ultimate curvature is just taking place in the restrained cross section.

In investigation of the column system as a whole, value w_{cr} or $\tilde{\xi}_{cr}$ is one of the possible limits set to the maximum horizontal load when function $T - w$ or $\alpha - \tilde{\xi}$ is plotted, respectively (see Chapter 5).

The internal force system of the reinforced concrete cross section and the strains have been plotted in Fig. 17 for writing of the ultimate curvature. The $\sigma - \epsilon$ diagrams for steel and for concrete are given in Fig. 18. According to the notation used in Fig. 17,

$$\beta = \frac{\epsilon_{c,e}}{\epsilon_c}$$

denotes utilization of the angular displacement of the cross section, where $\epsilon_{c,e}$ maximum elastic compression of the concrete (Fig. 18) and ϵ_c instantaneous compression of concrete in the extreme fibre of the cross section.

Distinctions can be made between two basic cases in respect of stress and strain state, such as

a) when the neutral axis lies outside the cross section (Fig. 17/a) that is

$$x = \xi \cdot h > h \quad \text{and}$$

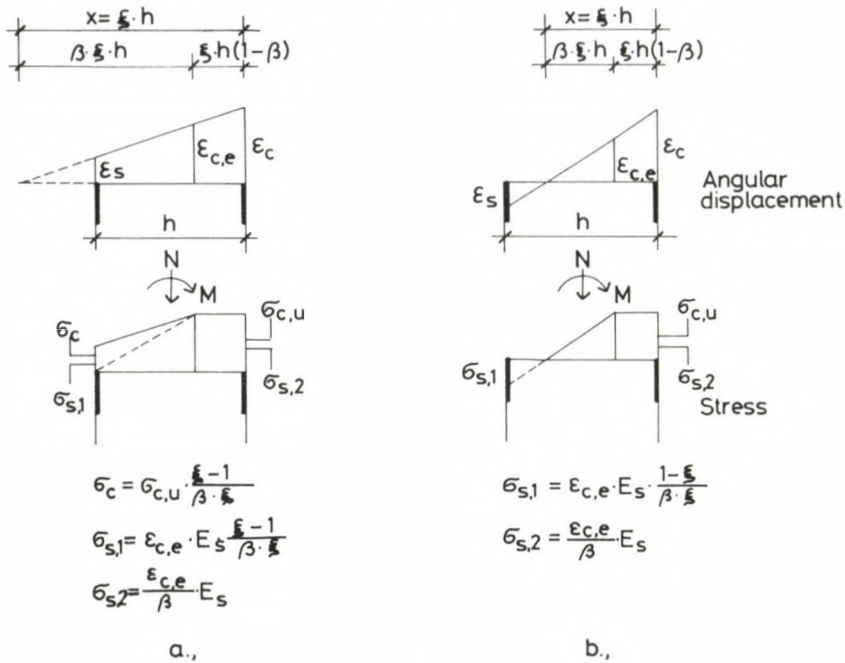
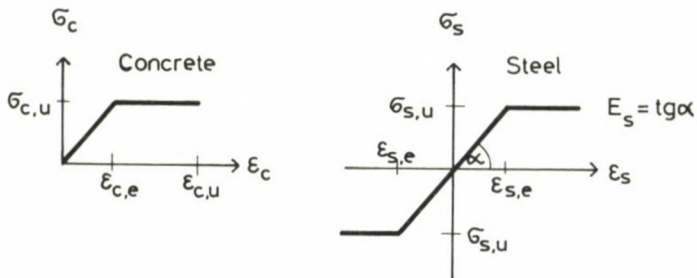


Fig. 17. Internal force system of reinforced concrete cross section


 Fig. 18. Stress (σ) - strain (ϵ) diagram for concrete and steel

b) when the neutral axis lies inside the cross section (Fig. 17/b) that is

$$x = \tilde{\xi} \cdot h < h$$

In both basic cases, what we need from among the equations expressing the equilibrium of external-internal forces are projective equations. (The magnitude of bending moment acting upon the cross section when the ultimate curvature occurs in case of given normal force is indifferent in respect of the investigation.)

In case a), the projective equation

$$N = N_C + N_S + H_S, \quad (32)$$

where N - external force acting upon the column as a compressive force acting upon the cross section

N_C - resultant of compressive forces arising in the concrete

N_S - force arising in the reinforcement on that side of the cross section where compression is higher

H_S - force arising in the reinforcement on that side of the cross section where compression is lower.

In case b), the projective equation

$$N = N_C + N_S - H_S, \quad (33)$$

where the notation complies with that used in equation (32).

With the projective equations written in detail using the notation of Fig. 17, the following relationships are obtained:

For case a):

$$N = b \cdot h \cdot \sigma_{C,u} \left[\xi - \beta \cdot \xi + 0.5 (1 - \xi + \beta \cdot \xi) \left(1 + \frac{\xi - 1}{\beta \cdot \xi} + \mu \cdot \frac{\epsilon_{C,e}}{\sigma_{C,u}} \cdot E_s \cdot \frac{\xi - 1}{\beta \cdot \xi} + \mu \frac{\epsilon_{C,e}}{\beta \cdot \sigma_{C,u}} \cdot E_s \right) \right], \quad (34)$$

for case b):

$$N = b \cdot h \cdot \sigma_{C,u} \left[\xi - 0.5 \cdot \beta \cdot \xi - \mu \frac{\epsilon_{C,e}}{\sigma_{C,u}} E_s \frac{1 - \xi}{\beta \cdot \xi} + \mu \frac{\epsilon_{C,e}}{\beta \cdot \sigma_{C,u}} \cdot E_s \right]. \quad (35)$$

With the equations written in a general form, the following relationship is obtained:

$$\frac{N}{b \cdot h \cdot \sigma_{c,u}} = \frac{1}{6\beta \cdot \xi} (a \cdot \xi^2 + b \cdot \xi + c), \quad (36)$$

where,

$$\begin{aligned} & \text{for } \xi > 1 & \text{for } \xi < 1 \\ a &= 6\beta - 3 \cdot \beta^2 - 3 & a &= 6\beta - 3\beta^2 \\ b &= 6 + 12\mu \frac{\epsilon_{c,e}}{\sigma_{c,u}} E_s & b &= 12\mu \frac{\epsilon_{c,e}}{\sigma_{c,u}} E_s \\ c &= - (3 + 6\mu \frac{\epsilon_{c,e}}{\sigma_{c,u}} E_s) & c &= - 6\mu \frac{\epsilon_{c,e}}{\sigma_{c,u}} E_s \end{aligned} \quad (37a)$$

After arrangement of equation (36), the following bigrade equation is obtained for ξ :

$$\frac{a}{6\beta} \cdot \xi^2 + \left(\frac{b}{6\beta} - \frac{N}{b \cdot h \cdot \sigma_{c,u}} \right) \cdot \xi + \frac{c}{6\beta} = 0 \quad (38)$$

When this bigrade equation is solved, the stipulation that no higher stresses than ultimate stress $\sigma_{s,u}$ can arise in the reinforcement shall, of course, be taken into consideration.

Hence:

$$\sigma_{s,1} = \left| \epsilon_{c,e} \cdot E_s \frac{\xi - 1}{\beta \cdot \xi} \right| \leq \sigma_{s,u} \quad (39)$$

and

$$\sigma_{s,2} = \frac{\epsilon_{c,e}}{\beta} E_s \leq \sigma_{s,u} \quad (40)$$

Should condition $\sigma_{s,1} < \sigma_{s,u}$; $\sigma_{s,2} = \sigma_{s,u}$ exist, equations (37/a) will change, as follows:

$$\begin{aligned} & \text{for } \xi > 1 & \text{for } \xi < 1 \\ a &= 6\beta - 3\beta^2 - 3 & a &= 6\beta - 3\beta^2 \\ b &= 6 + 12\mu \beta \frac{\sigma_{s,u}}{\sigma_{c,u}} & b &= 12\mu \beta \frac{\sigma_{s,u}}{\sigma_{c,u}} \\ c &= - \left(3 + 6\mu \beta \frac{\sigma_{s,u}}{\sigma_{c,u}} \right) & c &= - 6\mu \beta \frac{\sigma_{s,u}}{\sigma_{c,u}} \end{aligned} \quad (37/b)$$

If $\sigma_{s,1} = \sigma_{s,2} = \sigma_{s,u}$, then equation (37/a) will change, as follows:

$$\begin{array}{ll}
 \text{for } \xi > 1 & \text{for } \xi < 1 \\
 a = 6\beta - 3\beta^2 - 3 & a = 6\beta - 3\beta^2 \\
 b = 3 + 12\mu\beta \frac{\sigma_{s,u}}{\sigma_{c,u}} & b = 0 \\
 c = 0 & c = 0
 \end{array} \quad (37/c)$$

Using equation (38), the ultimate curvature of a reinforced concrete cross section under normal force of given magnitude can be determined by writing in place of β , utilization of angular displacement, a value $\beta_u = \frac{\epsilon_{c,e}}{\epsilon_{c,u}}$ that is the extreme value of β . The value of β can then be determined from equation (38).

Having the value of ξ , the value of ultimate curvature can be calculated on the basis of equation

$$\frac{1}{\xi_u} = \frac{\epsilon_{c,e}}{\beta_u \cdot \xi \cdot h} \quad (41)$$

In the knowledge of the value of ultimate curvature, it is possible to determine displacement w_{cr} of the top point of the restrained column where ultimate curvature $\frac{1}{\xi_u}$ takes place in the restrained cross section. Using the notation of Fig. 19 and assuming function

$$y = w \cdot \sin \frac{\pi}{2 \cdot l} \cdot x \quad (42)$$

for the strain line of the column, the usual approximation, $\sqrt{y'^2 + 1} \approx 1$, results in a function

$$\frac{1}{\xi} = y'' = w \frac{\pi^2}{(2l)^2} \cdot \sin \frac{\pi}{2 \cdot l} x \quad (43)$$

for the curvature.

Value of curvature at $x = l$:

$$\frac{1}{\xi} = w \cdot \frac{\pi^2}{4 \cdot l^2} \quad (44)$$

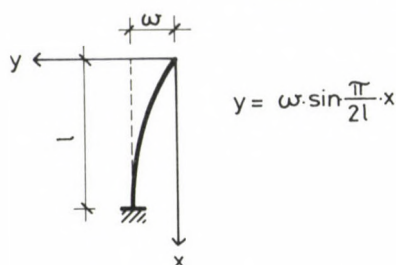


Fig. 19. Line of deformation of restrained column

With the value of ultimate curvature according to (41) substituted into (44), the critical displacement is given by the following equation:

$$w_{cr} = \frac{1}{\rho_u} \cdot \frac{4 \cdot l^2}{\pi^2} = \frac{\varepsilon_{c,e}}{\beta_u \cdot \xi \cdot h} \cdot \frac{4 \cdot l^2}{\pi^2} \quad (45)$$

In a dimensionless form:

$$\tilde{\xi}_{cr} = \frac{0.405 \cdot \gamma^2 \cdot \varepsilon_{c,e}}{\beta_u \cdot \xi} \quad (46)$$

8. Effect of creep of concrete on the critical load of a reinforced concrete column system

In investigation of the effect of creep of concrete, vertical loads and horizontal loads are assumed to be applied to the column system at times independent of each other in compliance with earlier calculation. The system experiences first vertical loads (dead load, useful load etc.) acting as a permanent load. Horizontal loads are considered to be an instantaneous load (wind load) and accordingly, the effect of creep on horizontal loads is neglected.

As a result of vertical loads, the concrete in the reinforced concrete columns experiences creep. This creep can be attributed to the viscoelastic behaviour of the concrete. The stability of the column system is affected in two ways by creep of the concrete.

— The internal forces are rearranged in the reinforced concrete cross section because the concrete evades the load. The stress reduces in the concrete while it increases in the reinforcement. The rearrangement of stresses affects also the strain of the concrete as stresses arising in the concrete, affecting the extent of creep, reduce gradually in the course of creep.

— The range of curvature where no breaking compression is taking place in the concrete reduces because, as compared with the instant at which vertical loads are applied to the column, the original compression of the extreme fibre in the concrete increases because of creep (Fig. 20).

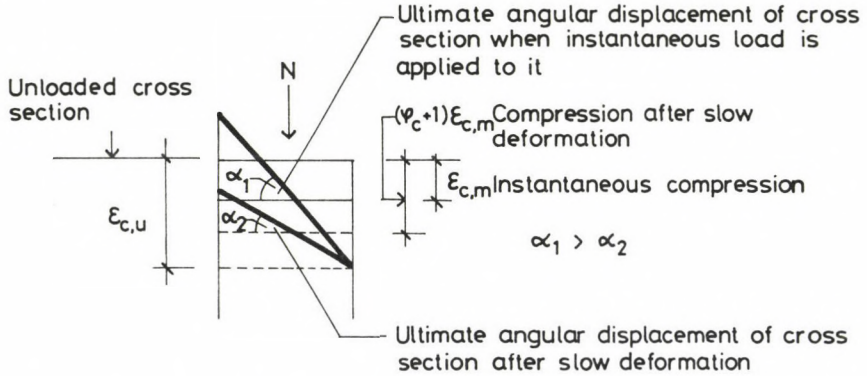


Fig. 20. Reduction of the value of ultimate curvature due to slow deformation

The first effect is not dealt with in this work. At a later date, it will be investigated in detail. The effect of reduction of the range of curvature can be taken into consideration by reducing the value of ultimate compression of the concrete, $\epsilon_{c,u}$ by the extent of creep when the value of ultimate curvature derived in Chapter 7 is determined. This is possible on consideration that the compression of the extreme fibre due to load must be less than (or equal to) ultimate compression. Compression is set up of two components that is compression due to instantaneous load on the one hand while additional compression as a result of creep on the other hand. Hence, failure condition for the extreme fibre of the cross section:

$$\epsilon_{c,m} + \epsilon_{c,c} = \epsilon_{c,u}$$

It follows that, at the instant the load is applied, permissible compression $\epsilon_{c,m}$ must be less than the ultimate strain minus creep strain:

$$\epsilon_{c,m} \leq \epsilon_{c,u} - \epsilon_{c,c}$$

Value of instantaneous strain $\epsilon_{c,m}$ resulting from normal force N which acts upon the cross section (with the effect of reinforcement neglected:

$$\epsilon_{c,m} = \frac{N}{b \cdot h \cdot E_c} \quad (47)$$

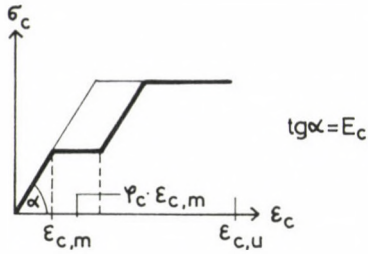


Fig. 21. Slow deformation of concrete due to sustained load

Creep (Fig. 21):

$$\varepsilon_{c,c} = \varphi_c \cdot \varepsilon_{c,m} = \varphi_c \frac{N}{b \cdot h \cdot E_c}, \quad (48)$$

where φ_c is the creep factor.

To determine ultimate curvature, ultimate compression $\varepsilon_{c,u}$ of the concrete shall be reduced by $\varepsilon_{c,c}$. Hence, on the basis of (41),

$$\frac{1}{\varrho_{u,c}} = \frac{\varepsilon_{c,e}}{\beta_{u,c} \cdot \xi_c \cdot h} \quad (49)$$

where $\varrho_{u,c}$ — ultimate curvature comprising also the effect of creep
 $\beta_{u,c}$ — utilization of angular displacement of the cross section, taking into consideration also the effect of creep
 ξ_c — value obtained by substitution for $\beta = \beta_{u,c}$ on the basis of (38).

Hence, the value of $\beta_{u,c}$ can be determined on the basis of relationship

$$\beta_{u,c} = \frac{\varepsilon_{c,e}}{\varepsilon_{c,u} - \varepsilon_{c,c}} \quad (50)$$

In investigation of the stability of a column system, the effect of creep can be taken into consideration by including the value of $\beta_{u,c}$ in the relationship for calculation of ultimate strain of the column system. Hence, on the basis of (45), ultimate strain $w_{cr,c}$ comprising also the effect of creep is

$$w_{cr,c} = \frac{1}{\varrho_{u,c}} \cdot \frac{4 l^2}{\pi^2} = \frac{\varepsilon_{c,e}}{\beta_{u,c} \xi_c \cdot h} \cdot \frac{4 l^2}{\pi^2} \quad (51)$$

or in a dimensionless form

$$\tilde{\xi}_{cr,c} = \frac{0.405 \cdot \gamma^2 \cdot \varepsilon_{c,e}}{\beta_{u,c} \cdot \xi_c} \quad (52)$$

9. Numerical examples

9.1 Example

Consider the reinforced concrete frame consisting of two columns illustrated schematically in Fig. 22. The columns are symmetrically reinforced and normal force is acting only upon column 2 from among both. Calculate critical horizontal load (T_{cr}) for the column system, taking into consideration the effect of creep.

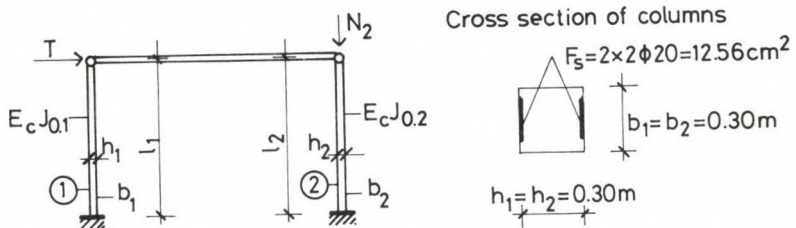


Fig. 22. Column system consisting of reinforced concrete columns with normal force acting upon column 2

Data:

a) geometrical and cross sectional characteristics:

$$\begin{aligned} l_1 &= l_2 = 6.00 \text{ m} \\ h_1 &= h_2 = 0.30 \text{ m} \\ b_1 &= b_2 = 0.30 \text{ m} \\ F_c &= 12.56 \text{ cm}^2 \\ \mu_1 &= \mu_2 = \frac{6.28}{30 \cdot 30} = 0.00697 \\ I_{o,1} &= I_{o,2} = \frac{30 \cdot 30^3}{12} = 67500 \text{ cm}^4 \end{aligned}$$

b) strength characteristics:

Grade C25 concrete

$$\begin{aligned} \sigma_{c,u} &= 1.9 \text{ kN/cm}^2 \\ E_c &= 2050 \text{ kN/cm}^2 \\ \epsilon_{c,u} &= 2.5 \% \\ \epsilon_{c,e} &= \frac{\sigma_{c,u}}{E_c} = 0.623 \% \\ \beta_u &= \frac{\epsilon_{c,e}}{\epsilon_{c,u}} = 0.249 \end{aligned}$$

Grade B 60.40 steel

$$\begin{aligned}\sigma_{s,u} &= 35 \text{ kN/cm}^2 \\ E_s &= 2100 \text{ kN/cm}^2 \\ \epsilon_{s,e} &= \frac{\sigma_{s,u}}{E_s} = 1.66 \%\end{aligned}$$

c) creep factor of concrete: $\varphi_c = 2$

d) load: $N_2 = 500 \text{ kN}$

9.1.1 Calculation of auxiliary quantities

$$\begin{aligned}N_{u,1} &= N_{u,2} = b_1 \cdot h_1 \cdot \sigma_{c,u} = b_2 \cdot h_2 \cdot \sigma_{c,u} = 30 \cdot 30 \cdot (1.9) = \\ &= 1710 \text{ kN}\end{aligned}$$

On the basis of relationships (13):

$$\begin{aligned}\tilde{\epsilon}_1 &= 0 \\ \tilde{\epsilon}_2 &= \frac{500}{1710} = 0.292 \\ \gamma_1 = \gamma_2 &= \frac{6.00}{0.3} = 20 \\ q_2 &= \frac{3050 \cdot 67500}{500 \cdot 600^2} = 1.143 \\ \gamma_1 &= \frac{0.30}{0.30} = 1 \\ \epsilon_1^* &= \frac{1710}{500} = 3.42 \\ q_1^* &= \frac{3050 \cdot 67500}{1710 \cdot 600^2} = 0.334 \\ \theta_1 = \theta_2 &= \frac{\mu_1 \cdot \sigma_{s,u}}{\sigma_{c,u}} = \frac{\mu_2 \cdot \sigma_{s,u}}{\sigma_{c,u}} = \\ &= \frac{0.00697 \cdot 35}{1.9} = 0.128\end{aligned}$$

9.1.2 Production of function $\tilde{\xi}_2 - \Delta_2$ of column 2 (as a column upon which normal forces are directly acting)

In the range of pressure of minor eccentricity, function $\tilde{\xi}_2 - \Delta_2$ can be determined on the basis of equation (25):

$$\tilde{\xi}_2 = \frac{0.292}{3.1 \cdot 1.143 \cdot 0.292 \cdot z_2 \left(1 - \frac{4}{\pi^2 \cdot 1.143 \cdot z_2}\right) + 0.292} \cdot \Delta_2,$$

where

$$z_2 = 1 - \left[\frac{0.292 \left(1 + \frac{1 + 4 \cdot 0.128}{0.25 + 2 \cdot 0.128} \cdot \Delta_2 \right)}{1 + 2 \cdot 0.128} \right]^6 .$$

Function

$$\tilde{\xi}_2 = \frac{0.292}{z_2 \left(1 - \frac{0.3546}{z_2} \right) + 0.292} \cdot \Delta_2$$

is then obtained after operations where

$$z_2 = 1 - \left(\frac{0.292 + 0.872 \cdot \Delta_2}{1.256} \right)^6 .$$

Function $\tilde{\xi}_2 - \Delta_2$ can be determined on the basis of equation (25) also within the pressure range of major eccentricity but here the value of rigidity reducing factor will be

$$z_2 = 1 - \left[\frac{0.292(4 \cdot \Delta_2 - 1)}{4 \cdot 0.128} \right]^6$$

After operations:

$$z_2 = 1 - \left(\frac{1.168 \cdot \Delta_2 - 0.292}{0.512} \right)^6$$

Transition between low and high eccentricity pressures is given by equation (28):

$$\Delta_{u,2} = 2 \cdot 0.128 + 0.25 = 0.506$$

Function $\tilde{\xi}_2 - \Delta_2$ has been plotted in Fig. 23, the value of ultimate strain $\tilde{\xi}_{2,cr}$ being calculated on the basis of equation (46),

$$\tilde{\xi}_{2,cr} = \frac{0.405 \cdot 20^2 \cdot 0.000623}{0.249 \cdot \xi} = \frac{0.405}{\xi} ,$$

and the value of ξ on the basis of equation (36).

Since $\epsilon_{s,e} = 1.66\% < \epsilon_{c,u} = 2.5\%$, ultimate stress $\sigma_{s,2} = \sigma_{s,u}$ arises in the reinforcement on that side of the cross section where the compression is higher. Accordingly, coefficients a, b, c in equation (38) shall be calculated according to equations (37/b) or (37/c). Determination of the applicable coefficient is a matter of trial and error. Let first

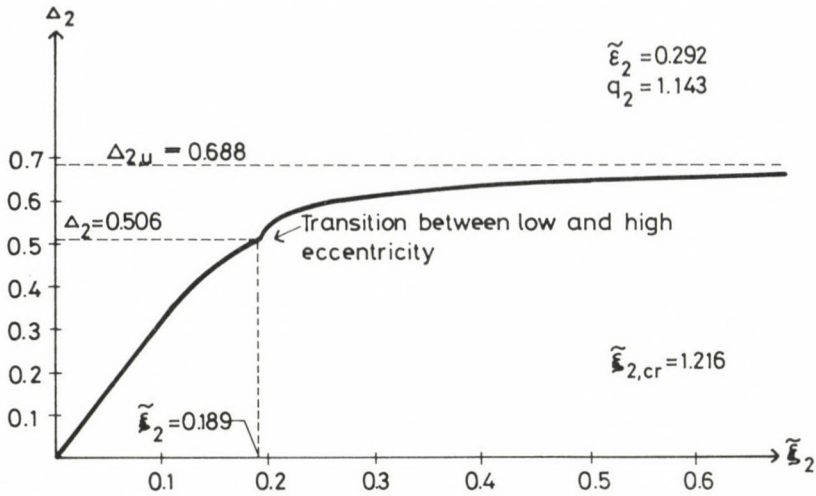


Fig. 23. $\xi_2 - \Delta_2$ function of column 2

case $\xi < 1$ from equations (37/c) be tested. Now equation (38) will take the following shape:

$$a = 6 \cdot 0.0249 - 3 \cdot 0.249^2 = 1.307$$

$$b = 0$$

$$c = 0$$

$$\frac{1.307}{6 \cdot 0.249} \cdot \xi^2 - 0.292 \xi = 0$$

From here, $\xi = 0.333$ is obtained. Check on the basis of equation (40) if the value of $\alpha_{s,1}$ actually reaches $\sigma_{s,u}$ for this ξ .

$$\sigma_{s,1} = 0.000623 \cdot 21000 \cdot \frac{1 - 0.333}{0.249 \cdot 0.333} = 105.2 \text{ kN/cm}^2$$

$\sigma_{s,1} > \sigma_{s,u}$ suggests that ultimate stress $\sigma_{s,1} = \sigma_{s,u}$ arises in the reinforcement also on the side where the compression (tension in this example) is lower. This is in agreement with equations (37/c) and accordingly, $\xi = 0.333$ complies with the actual value of ξ .

Now return to determination of $\xi_{2,cr}$. It has been written earlier on the basis of (46) that

$$\xi_{2,cr} = \frac{0.405}{\xi} = \frac{0.405}{0.333} = 1.216$$

This means that the function plotted in Fig. 23 comes to an end at value $\xi_{2,cr} = 1.216$.

If also creep of the concrete has to be taken into consideration, the ultimate strain shall be determined according to equation (52). The value of $\beta_{u,c}$, ξ_c in the equation shall be determined, as follows:

— On the basis of (47):

$$\varepsilon_{c,m} = \frac{500}{30 \cdot 30 \cdot 3050} = 0.000182 \quad .$$

— On the basis of (48):

$$\varepsilon_{c,c} = 2 \cdot 0.000182 = 0.000364 \quad .$$

— On the basis of (50):

$$\beta_{u,c} = \frac{0.000623}{0.0025 - 0.000364} = 0.291$$

— On the basis of 37/c):

$$\begin{aligned} a &= 6 \cdot 0.291 - 3 \cdot 0.291^2 = 1.491 \\ b &= 0 \\ c &= 0 \quad . \end{aligned}$$

— On the basis of (38):

$$\frac{1.491}{6 \cdot 0.291} \xi_c^2 - 0.292 \cdot \xi_c = 0$$

— On the basis of (39):

$$\xi_c = 0.34 \quad .$$

$$\sigma_{s,1} = \left| 0.000623 \cdot 21000 \frac{1 - 0.341}{0.291 - 0.341} \right| = 86.88 \text{ kN/cm}^2$$

Since $\sigma_{s,1} > \sigma_{s,u}$, the value of ξ_c shall be determined actually on the basis of (37/c).

— On the basis of (52):

$$\xi_{2,cr,c} = \frac{0.405 \cdot 20^2 \cdot 0.000623}{0.291 \cdot 0.341} = 1.01$$

9.1.3 Production of function $\tilde{\xi}_1 - e_1^*$ of column 1 (as a column upon which no normal force is directly acting)

According to relationship (31):

$$\tilde{\xi}_1 = \frac{e_1^*}{\frac{3 \cdot 0.334}{20} \left[1 - \left(\frac{e_1^*}{0.128} \cdot 20 \right)^6 \right]}$$

After operations we obtain a function

$$\tilde{\xi}_1 = \frac{e_1^*}{0.05 \left[1 - (156.25 \cdot e_1^*)^6 \right]}$$

The function has been plotted in Fig. 24.

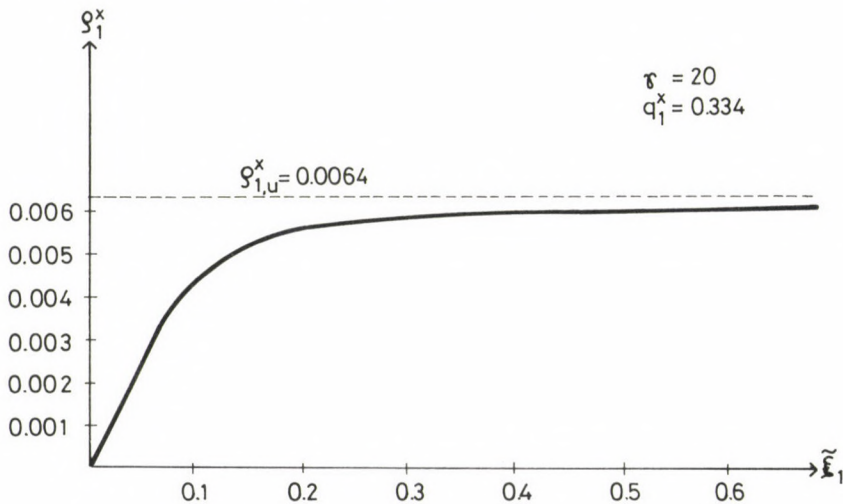


Fig. 24. $\tilde{\xi}_1 - e_1^*$ function of column 1

9.1.4 Determination of critical horizontal load for the column system

The functional values for plotting function $\alpha - \tilde{\xi}_1$ have been determined in Table 1 while the tabulated values are plotted in Fig. 25. $\alpha_{cr} = 0.0373$ has been obtained as an extreme value of function $\alpha - \tilde{\xi}_1$. Thus, the magnitude of critical horizontal load:

$$T_{cr} = \alpha_{cr} \cdot N_2 = 0.0373 \cdot 500 = 18.65 \text{ kN}.$$

Table 1 Determination of critical horizontal load (α_{cr}) of the column system according to example 9.1

| Serial No. | Column 1 | | Column 2 | | Frame | |
|------------|-----------------|----------------------------------|---|-----------------------------|---|--|
| | $\tilde{\xi}_1$ | ϑ_1^* (see Fig. 24) | $\tilde{\xi}_2 = \nu_1 \cdot \tilde{\xi}_1$ | Δ_2 (see Fig. 23) | $\tilde{\xi}_2 = \frac{\Delta_2 - \tilde{\xi}_2}{\gamma_2}$ | $\alpha = \tilde{\xi}_2^* + \vartheta_1^* \cdot \varepsilon_1^*$ |
| 1 | 0.1 | 0.0043 | 0.1 | 0.32 | 0.011 | 0.0257 |
| 2 | 0.189 | 0.0056 | 0.189 | 0.506 | 0.0158 | 0.0346 |
| 3 | 0.25 | 0.0058 | 0.25 | 0.6 | 0.175 | 0.0373 |
| 4 | 0.3 | 0.006 | 0.3 | 0.61 | 0.0155 | 0.0360 |
| 5 | 0.5 | 0.006 | 0.5 | 0.62 | 0.006 | 0.0265 |
| 6 | 0.6 | 0.006 | 0.6 | 0.62 | 0.001 | 0.0215 |

Displacement of the column system as a result of force T_{cr} :

$$w_{cr} = \tilde{\xi}_{1,cr} \cdot h = 0.25 \cdot 30 = 7.5 \text{ cm}.$$

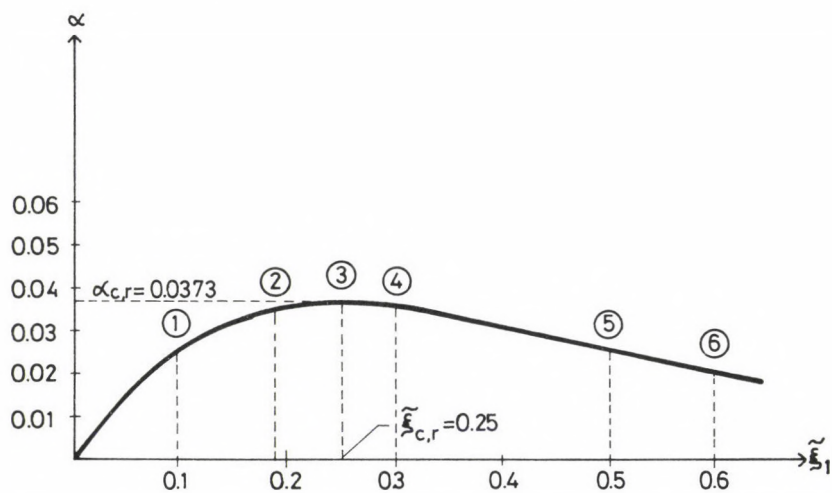


Fig. 25. Determination of critical horizontal load of the column system on the basis of function $\alpha - \tilde{\xi}_1$

Comments:

As seen from the result, the column system has lost its stability to arrive at ultimate load capacity. At a value of $\tilde{\xi}_{1,cr} = 0.25$ indicating the

limit of lost stability resulting in destruction, the lost strength of the different columns has not contributed yet as this would take place only at much greater displacements that is at $\tilde{\xi}_1 > 1$. The situation will not change even if creep is taken into consideration. This can be attributed to the fact that a structure of relatively high slenderness has been selected as an example. Should only the behaviour of column 2 be investigated (values $\tilde{\xi}_2$ in Table 1), it will be seen also column 2 will lose its stability only at $\tilde{\xi}_2 = 0.25$. An additional load bearing capacity of the column system would require more contribution to the overall supporting effort by column 1.

Let the results obtained be compared with the results obtainable by means of Hungarian Standard MSZ 15022. Consider first column 2 alone. A value of $\Delta e_t = 0.04 \left(\frac{l_0}{10 \cdot h} \right)^2 \cdot h$ is specified for increase in eccentricity of reinforced concrete columns under eccentric compression due to secondary effect ($l_0 = 2 \cdot l$) which amounts to $\Delta e_t = 0.64 \cdot 30 = 19.2$ cm in our case. For given loads of $N_2 = 500$ kN and $T_{cr,2} = \tilde{\xi}_2 \cdot N_2 = 0.0175 \cdot 500 = 8.75$ kN, the calculated initial eccentricity of $\Delta e_o = \frac{T_{cr,2} \cdot l}{N_2} = \frac{8.75 \cdot 6}{500} = 0.105$ m = 10.5 cm increases to an effective eccentricity of $\Delta e_M = \Delta e_o + \Delta e_t = 10.5 + 19.2 = 29.7$ cm. For a vertical load of $N_2 = 500$ kN, a restraint moment of $M_2 = N_2 \cdot \Delta e_M = 500 \cdot 0.297 = 148.5$ kNm is associated with this eccentricity. At the same time, the numerical example presented here resulted in a restraint moment of $M_2 = N_2 \cdot w_{cr,2} + T_{cr,2} \cdot l_2 = 500 \cdot 0.075 + 8.75 \cdot 6 = 90$ kNm. (Displacement $w_{cr,2} = 7.5$ cm can be calculated on the basis of $\tilde{\xi}_2 = 0.25$.) The difference between the value of restraint moment calculated on the basis of the standard and the value of actual restraint moment is more than 65% in favour of safety.

In investigation of the column system as a whole, the ratio of horizontal load per column is determined by the standard on the basis of the theory of elasticity of the first order, assuming an average value for increase in eccentricity due to the secondary effect. However, this average value depends only on the geometry of the different columns while it is independent of load.

In the present case, the geometry and initial rigidity of the two columns are identical and thus half of the horizontal displacement force is acting upon each column, the value of increase in secondary eccentricity being $\Delta e_t = 19.2$ cm also in this case. According to the standard, the value of restraint moment acting upon the different columns can be calcu-

lated as earlier in investigation of column 2. As a result of $T_{cr} = 18.65 \text{ kN}$ (that is horizontal load acting upon the column system) and vertical load $N_2 = 500 \text{ kN}$, restraint moment $M_1 = 55.95 \text{ kNm}$ arises in column 1 while $M_2 = 151.96 \text{ kNm}$ in column 2. Using the results of the numerical example, $M_1 = 59.50 \text{ kNm}$ and $M_2 = 90.0 \text{ kNm}$ are obtained for the restrained cross section of column 1 and column 2, respectively. It can be seen that a lower value is obtained for the restraint moment of the unloaded column by the standard because the mutual supporting effort of the columns is not taken into consideration while at the same time there is a difference of 70% in moment in the restrained cross section because of the exaggerated value of increase in eccentricity for the loaded column. Should the rigidity of column 1 be further increased, the supporting effect of this column upon column 2 will be increasingly appreciable with the results increasingly differing from the values according

9.2 Example

Consider the two-column frame illustrated in Fig. 26. The columns are symmetrically reinforced and normal force is acting upon column 2. Let the critical horizontal load of the column system be calculated, taking into consideration also the effect of creep of the concrete.

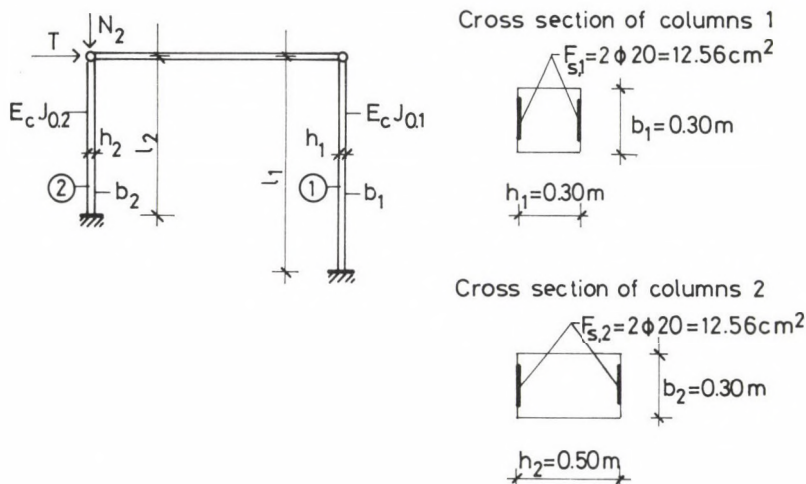


Fig. 26. Two-column frame with normal force acting upon column 2

Specifications:

(a) geometrical and cross sectional characteristics:

$$\begin{aligned}
 \ell_1 &= 6 \text{ m} \\
 \ell_2 &= 3 \text{ m} \\
 h_1 &= 0.30 \text{ m} \\
 h_2 &= 0.50 \text{ m} \\
 F_{s,1} &= F_{s,2} = 12.56 \text{ cm}^2 \\
 \mu_1 &= \frac{6.28}{30.30} = 0.00697 \\
 \mu_2 &= \frac{6.28}{30.50} = 0.00411 \\
 I_{o,1} &= \frac{30.30^3}{12} = 67.500 \text{ cm}^4 \\
 I_{o,2} &= \frac{30.50^3}{12} = 312.500 \text{ cm}^4
 \end{aligned}$$

(b) strength characteristics:

same as in example 9.1.

(c) creep factor of concrete: $\varphi_c = 2$

(d) loads: $N_2 = 2000 \text{ kN}$

9.2.1 Calculation of auxiliary quantities

$$N_{u,1} = b_1 \cdot h_1 \cdot \sigma_{c,u} = 30.30 \cdot 1.9 = 1710 \text{ kN}$$

$$N_{u,2} = b_2 \cdot h_2 \cdot \sigma_{c,u} = 30.50 \cdot 1.9 = 2850 \text{ kN}$$

On the basis of equations (13):

$$\tilde{\epsilon}_1 = 0$$

$$\tilde{\epsilon}_2 = \frac{2000}{2850} = 0.701$$

$$\gamma_1 = \frac{6.00}{0.30} = 20$$

$$\gamma_2 = \frac{3.00}{0.50} = 6$$

$$q_2 = \frac{3050 \cdot 312 \cdot 500}{2000 \cdot 300^2} = 5.295$$

$$\nu_1 = \frac{0.30}{0.50} = 0.6$$

$$\epsilon_1^* = \frac{1710}{2000} = 0.855$$

$$q_1^* = \frac{3050 - 67 \cdot 500}{1710 \cdot 600^2} = 0.334$$

$$\theta_1 = \frac{\mu_1 \cdot \sigma_{s,u}}{\sigma_{c,u}} = \frac{0.00697 \cdot 35}{1.9} = 0.128$$

$$\theta_2 = \frac{\mu_2 \cdot \sigma_{s,u}}{\sigma_{c,u}} = \frac{0.00411 \cdot 35}{1.9} = 0.0757$$

9.2.2 Production of function $\tilde{\xi}_2 - \Delta_2$ of column 2 (as a column upon which normal forces are directly acting)

In the range of eccentric pressure, function $\tilde{\xi}_2 - \Delta_2$ is described by equation (25):

$$\tilde{\xi}_2 = \frac{0.701}{3.5.295 \cdot 0.701 \cdot z_2 \left(1 - \frac{4}{\pi^2 \cdot 5.295 \cdot z_2}\right) + 0.701} \cdot \Delta_2$$

where

$$z_2 = 1 - \left[\frac{0.701 \left(1 + \frac{1 + 4 \cdot 0.0757}{0.25 + 2 \cdot 0.0757} \cdot \Delta_2\right)}{1 + 2 \cdot 0.0757} \right]^6$$

After operations, function

$$\tilde{\xi}_2 = \frac{0.701}{11.13 - z_2 \left(1 - \frac{0.0765}{z_2}\right) + 0.701} \cdot \Delta_2$$

is obtained where

$$z_2 = 1 - \left[\frac{0.701 + 2.275 \Delta_2}{1.151} \right]^6$$

Value of z_2 within the range of highly eccentric pressure:

$$z_2 = 1 - \left[\frac{0.701(4 \cdot \Delta_2 - 1)}{4 \cdot 0.0757} \right]^6$$

After operations:

$$z_2 = 1 - \left(\frac{2.804 \cdot \Delta_2 - 0.701}{0.3028} \right)^6$$

Minor and major eccentricity pressure transition according to (28):

$$\Delta_{u,2} = 2 \cdot 0.0757 + 0.25 = 0.41$$

As seen, the value of rigidity reducing factor z_2 is zero for $0.1978 = \Delta_2$ in the range of minor eccentricity. Since this $\Delta_2 < \Delta_{u,2}$, this means that the entire stability test takes place in the range of pressure of low eccentricity.

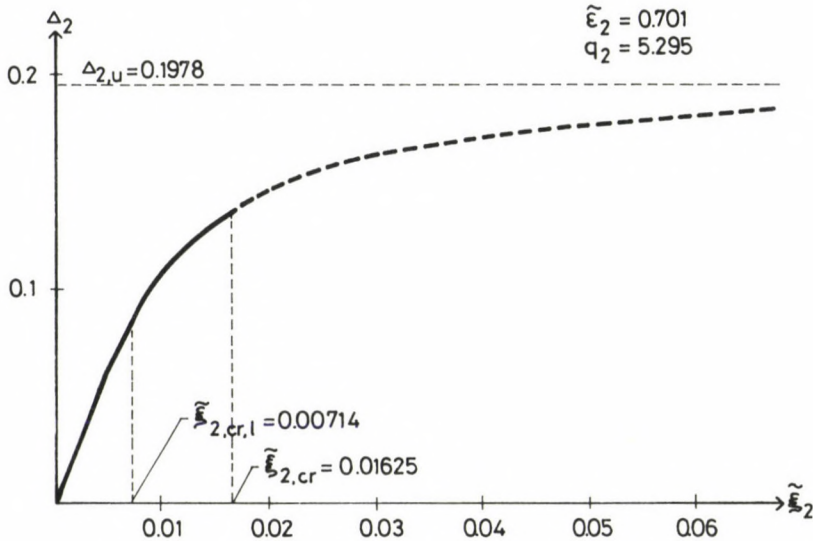


Fig. 27. $\tilde{\xi}_2 - \Delta_2$ function of column 2

Function $\tilde{\xi}_2 - \Delta_2$ has been plotted in Fig. 27. The value of $\tilde{\xi}_{2,cr}$ can be calculated on the basis of equation (46):

$$\tilde{\xi}_{2,cr} = \frac{0.405 \cdot 6^2 \cdot 0.000523}{0.249 \cdot \xi} = \frac{0.0354}{\xi}.$$

The value of ξ is supplied by equation (38) where the coefficients can be calculated on the basis of equation (37/b). Since we face the case of low-eccentricity pressure, equations associated with $\xi > 1$ apply:

$$\begin{aligned} a &= 6 \cdot 0.249 - 3 \cdot 0.249^2 - 3 = -1.592 \\ b &= 6 + 12 \cdot 0.00411 \cdot 0.249 \cdot \frac{35}{1.9} = 6.226 \end{aligned}$$

$$\begin{aligned}
 c &= -(3 + 6 \cdot 0.00411 \cdot 0.249 \cdot \frac{35}{1.9}) = -3.113 \\
 -\frac{1.692}{6 \cdot 0.249} \cdot \xi^2 + \left(\frac{6.226}{6 \cdot 0.249} - 0.701 \right) \cdot \xi - \frac{3.113}{6 \cdot 0.249} &= 0 \\
 -1.132 \xi^2 + 3.466 \xi - 2.083 &= 0 \\
 \xi &= 2.24
 \end{aligned}$$

Value of stress in reinforcement on the side under minor compression:

$$\sigma_{s,l} = 0.000623 \cdot 21000 \cdot \frac{2.24 - 1}{0.249 \cdot 2.24} = 29.08 \text{ kN/cm}^2$$

Hence, equations $\sigma_{s,l} < \sigma_{s,u}$ and thus equations (37/b) have been rightly used.

Accordingly, the value of critical strain:

$$\tilde{\xi}_{2,cr} = \frac{0.0364}{2.24} = 0.01625$$

That means that function $\tilde{\xi}_2 - \Delta_2$ plotted in Fig. 27 discontinues at $\tilde{\xi}_2 = \tilde{\xi}_{2,cr}$.

Taking into consideration the creep of concrete, the ultimate strain can be calculated, as follows:

— On the basis of (47):

$$\varepsilon_{c,m} = \frac{2000}{30 \cdot 50 \cdot 3050} = 0.000437$$

— On the basis of (48):

$$\varepsilon_{c,c} = 2 \cdot 0.000437 = 0.000874$$

— On the basis of (50):

$$\beta_{u,c} = \frac{0.00623}{0.0025 - 0.000874} = 0.383$$

— On the basis of (37/b):

$$a = 6 \cdot 0.383 - 3 \cdot 0.383^2 - 3 = -1.142$$

$$b = 6 + 12 \cdot 0.00411 \cdot 0.383 \cdot \frac{35}{1.9} = 6.347$$

$$c = -\left(3 + 6 \cdot 0.00411 \cdot 0.383 \cdot \frac{35}{1.9}\right) = -3.173$$

— On the basis of (38):

$$-\frac{1.142}{6 \cdot 0.383} \cdot \xi_c^2 + \left(\frac{6.347}{6 \cdot 0.383} - 0.701\right) \cdot \xi_c - \frac{3.173}{6 \cdot 0.383} = 0$$

$$-0.496 \cdot \xi_c^2 + 2.06 \cdot \xi_c - 1.380 = 0$$

$$\xi_c = 3.32$$

Stress arising in reinforcement on the side under minor compression:

$$\sigma_{s,1} = 0.00063 \cdot 21000 \frac{3.32 - 1}{0.383 \cdot 3.32} = 24.13 \text{ kN/cm}^2$$

Since $\sigma_{s,1} < \sigma_{s,u}$, equations (37/b) have been rightly used.

Value of ultimate strain with creep of the concrete taken into consideration:

$$\tilde{\xi}_{2,cr,c} = \frac{0.405 \cdot 6^2 \cdot 0.000623}{0.383 \cdot 3.32} = 0.00714$$

on the basis of (52).

9.2.3 Production of function $\tilde{\xi}_1 - e_1^*$ of column 1 (as a column upon which normal forces are not directly acting)

The function is identical with that determined in example 9.1 (Fig. 24).

9.2.4 Determination of critical horizontal load of the column system

The functional values for plotting of function $\alpha - \tilde{\xi}_1$ have been tabulated in Table 2 while plotted in Fig. 28. $\alpha_{cr} = 0.0209$ has been obtained as a value determining the magnitude of critical horizontal load an

thus

$$T_{cr} = \alpha_{cr} \cdot N_2 = 0.0209 \cdot 2000 = 41.8 \text{ kN.}$$

Displacement of the column system as a result of critical load:

$$w_{cr} = \tilde{\xi}_{1,cr} \cdot h_1 = 0.027 \cdot 30 = 0.81 \text{ cm.}$$

With the effect of creep taken into consideration:

$$T_{cr,c} = \alpha_{cr,c} \cdot N_2 = 0.0133 \cdot 2000 = 25.5 \text{ kN}$$

$$w_{cr,c} = \tilde{\xi}_{1,cr,c} \cdot h_1 = 0.0119 \cdot 30 = 0.357 \text{ cm.}$$

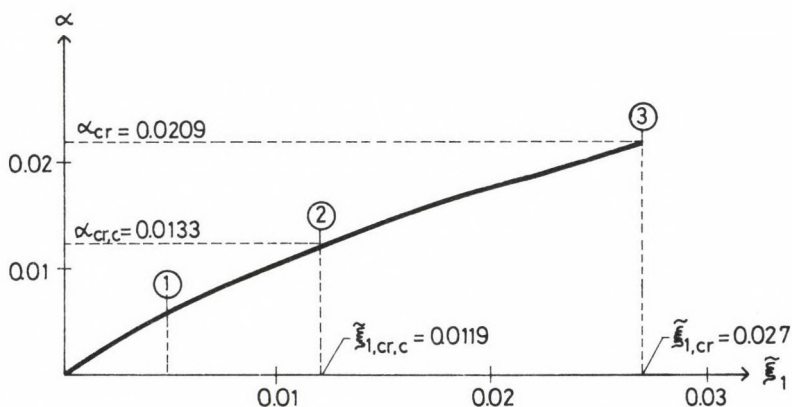


Fig. 28. Determination of critical horizontal load of the column system on the basis of function $\alpha - \tilde{\xi}_1$

Table 2 Determination of critical horizontal load (α_{cr}) of the column system according to example 9.2

| Serial No. | Column 1 | | Column 2 | | Frame | |
|---------------|-----------------|--------------------------------|---|-----------------------------|---|--|
| | $\tilde{\xi}_1$ | ϱ_1^* (see Fig. 24) | $\tilde{\xi}_2 = \nu_1 \cdot \tilde{\xi}_1$ | Δ_2 (see Fig. 27) | $\tilde{\varrho}_2 = \frac{\Delta_2 - \tilde{\xi}_2}{\gamma_2}$ | $\alpha = \tilde{\varrho}_2^* + \varrho_1^* \tilde{\xi}_1$ |
| 1 | 0.005 | 0 | 0.003 | 0.036 | 0.0055 | 0.0055 |
| 2 | 0.0119 | 0.0005 | 0.00714 | 0.084 | 0.0128 | 0.0133 |
| 3 | 0.0270 | 0.0012 | 0.01625 | 0.136 | 0.0199 | 0.0209 |

Comments:

The column system has arrived at ultimate load capacity when column 2 has been destroyed due to lost strength. Breaking compression takes place at a low value of displacement in the extreme fibre of the cross section of the relatively stubby column under significant load. The effect of column 1 upon the force system is minimal. Creep results in a significant reduction in load capacity when taken into consideration.

In comparison of the results obtained with the values that can be calculated for the reinforced concrete structure according to the standard, let first only column 2 be investigated as if it were an independent column. Should a vertical load of $N_2 = 2000$ kN and a horizontal load of $T_{2,cr,c} = \tilde{\xi}_{2,c} \cdot N_2 = 0.0128 \cdot 2000 = 25.6$ kN act upon the column, a value of $e_M = 6.72$ cm will be obtained for effective eccentricity in the restrained cross section according to the standard. (Values of $T_{cr,c}$ and $\tilde{\xi}_{2,c}$ taking into consideration also the effect of creep are used because creep of the concrete is taken into consideration also by the values according to the standard.) This results in a restraint moment of $M_2 = N_2 \Delta e_M = 2000 \cdot 0.0672 = 134.4$ kNm while in the numerical example, a restraint moment of $M_2 = T_{2,cr,c} \cdot \ell_2 + N_2 \cdot w_{2,cr,c} = 25.6 \cdot 3 + 2000 \cdot 0.00357 = 83.94$ kNm has been obtained, the difference being about 60%.

According to the standard, the ratio of horizontal load per column can be determined on the basis of the theory of elasticity of the first order in investigating the column system as a whole. Thus a load of $T_{2,cr,c} = 25.8$ kN that is 97% of the overall load of $T_{cr,c} = 26.6$ kN is applied to column 2 while $T_{1,cr,c} = 0.8$ kN that is only 3% of the overall load to column 1. Increase in eccentricity is determined by the standard on the basis of average length of deflection of both columns. For column 2, an increase in eccentricity of $\Delta e_{t,2} = 13.52$ cm is obtained in this way, the effective eccentricity being $\Delta e_{M,2} = 17.22$ cm for which a restraint moment of $M_2 = N_2 \cdot \Delta e_{M,2} = 2000 \cdot 0.1722 = 344.4$ kNm arises as a result of compressive force $N_2 = 2000$ kN. The difference between this value and the value determined in the numerical example, $M_2 = 83.94$ kNm, amounts to more than 300% due to the fact that, although the effect of column 1 upon the force system is minimum, the average slenderness of the columns is taken as a basis for determining the increase in eccentricity by the standard.

REFERENCES

1. Kaliszky, S.: Plasticity: Theory and Engineering (in Hungarian). Akadémiai Kiadó, Budapest, 1975
2. Halász, O.: Stability calculation of steel structures (in Hungarian). DSc. thesis. Budapest, 1976
3. Halász, O.: Materials and Mechanics of Lightweight Structures (in Hungarian). Műszaki Tudomány, Vol. 44, 1971
4. Korányi, I.: Elastic Buckling (Stability Problems in Engineering I). (In Hungarian.) FJV, Budapest, 1957
5. Korányi, I.: Plastic Buckling (Stability Problems in Engineering II). (In Hungarian.) FJV, Budapest, 1957
6. Korányi, I.: Stability Problems in Engineering (in Hungarian). Akadémiai Kiadó, Budapest, 1965
7. Horne, M.R. - Merchant, W.: The Stability of Frames. Pergamon Press, Oxford, 1965
8. Csonka, P.: Contribution to the Theory of Buckling (in Hungarian). Publications of the Section of Technical Sciences of the Hungarian Academy of Sciences, Vol. VI, (1951), p. 281.
9. Ježek, K.: Die Festigkeit von Druckstäben aus Stahl. Verlag Julius Springer, Wien, 1937
10. Timoshenko, S.P. - Gere, J.M.: Theory of Elastic Stability. McGraw-Hill, New York, 196.
11. Dulácska, E.: Elastic buckling of slender reinforced concrete supports. Architectural Research and Development, 1985
12. Bölcskei, E. - Dulácska, E.: Handbook of Static Engineers. Műszaki Könyvkiadó, Budapest, 1974
13. Hungarian Standard MSZ 15024/1-75; Mechanical design of the supporting structure of buildings. Steel structures. 1975
14. Korondi, D.: Approximate Stability Test of Multilevel Single-level Planar Frames. (Post-graduate Diploma Work) 1972
15. Stability of Frames and Column Systems. BVTV-Aid. 1972.
16. Raboldt, K. - Warnstedt, G. - Werner, F.: Verfahren der elastisch-plastischen Berechnung von Stabtragwerken des Stahlhochbaus. Bauplanung-Bautechnik 1986/6.
17. Palotás, L.: Handbook of Engineering. Műszaki Könyvkiadó, Budapest, 1984
18. Plastic Strength Calculation of Steel Structures. Sectoral Directives of Architectural Engineering MI-04.188-80. Architectural Information Center, Budapest, 1980
19. Bognár, L.: Stability of Elastic-Plastic Planar Column Systems. Acta Technica. Vol. 101. (1988), 5-47.
20. Betonkalender 1983. Tragsicherheitsnachweis mit vereinfachten Rechengrundlagen. Verlag von Wilhelm Ernst & Sohn, Berlin - München 1983
21. Sparowitz, L.: Ein halbgrafisches Verfahren zur Bemessung von beliebig belasteten Stahlbetondruckstäben. Bemessung und Sicherheit von Stahlbeton - Druckgliedern. Symposium. Québec 1974
22. F. Chen, W. - Chen, C.T.: Strength of Laterally Loaded Reinforced Concrete Columns. Design and Safety of Reinforced Concrete Compression Members. Symposium. Quebec 1974

23. Szalai, K.: Load capacity of Reinforced Concrete Bar under Compression. Mélyépítéstudományi Szemle, 1967/6
24. Almási, J.: Some Problems of Load Capacity and Deformation of Pre-stressed Concrete Columns. (MSc Diploma Work) 1971
25. Hungarian Standard MSZ 15022/1-71: Mechanical design of the supporting structure of buildings. Reinforced concrete structures. 1981.
26. Dulácska, E.: Buckling of Elastic Reinforced Concrete bar. Építés- és Építészettudomány, 1978. Vol. X, 1-2.

WRINKLING OF FACES OF COMPRESSED AND BENT SANDWICH BARS AND ITS INTERACTION WITH OVERALL INSTABILITY

HEGEDŰS, I.* - KOLLÁR, L.P.**

(Received: 15 June 1988)

The paper deals with the stability analysis of triple-layer sandwich bars (or cylindrical buckling of sandwich plates) taking the compression of the core also into account. It shows that in the case of an antiplane core the effect of wrinkling on the overall buckling load can be taken into consideration analogously to the Föppl-Papkovich formula.

The case of not equally loaded faces (e.g. flexural wrinkling) is also treated.

1. Introduction

In Allen's book /1/ the problem of wrinkling of faces of triple-layer sandwiches is presented on the basis of the studies of Gough, Elam and Bruyne /3/, Hoff and Mautner /5/, Williams, Leggett and Hopkins /8/, Goodier and Neou /2/. Chapter 8 deals in detail with three principal types of wrinkling instability as shown in Fig. 1.

Case I represents a sandwich beam in which wrinkling is likely to occur only in the compression face, while the tensile face, is assumed to remain perfectly flat.

Cases II and III represent antisymmetrical and symmetrical wrinkling respectively in a sandwich strut in which the two faces carry equal axial thrusts. It also deals with the interaction of wrinkling (Case II) and overall instability. The results presented in the book are valid for sandwiches with isotropic core, their use may cause significant errors in the



Fig. 1.

*Hegedűs, István H-2083 Solymár, Váci M. u. 10, Hungary

**Kollár, László P., H-1122 Budapest, Karap u. 9, Hungary

analysis of sandwiches with anisotropic core. The excellent work of Benson and Mayers /9/ deals with the buckling of compressed sandwich plates and bars with ideally orthotropic (honeycomb) cores.

Pomázi presents in /11, 12/ a detailed stability analysis of non-symmetrically loaded orthotropic sandwich panels. Among the basic assumptions he postulates that the transverse stresses and deformations are constant along the thickness of the core. This common assumption is widely used in the technical sandwich theory, however, the comparison of the results of /9/ with those of /11, 12/ shows that this assumption may a priori exclude any interaction between wrinkling and "global" buckling modes.

The aim of our paper is to extend the previous results /9/ for not equally loaded faces. We also show, that in the case of sinusoidal buckling shape the effect of the compressibility of the core can be taken into account in a very simple way analogously to the Föppl-Papkovich formula /6, 7/.

We generalized our results for sandwich plates in /13/.

Let us consider a sandwich bar with ideally orthotropic /9/ or — with another word — "antiplane" core /1/. The relationships between the stresses and strains are as follows:

$$\begin{bmatrix} \sigma_x \\ \sigma_z \\ \tau \end{bmatrix} = \begin{bmatrix} 0 & 0 & 0 \\ 0 & E_c & 0 \\ 0 & 0 & G \end{bmatrix} \begin{bmatrix} \epsilon_x \\ \epsilon_z \\ \gamma \end{bmatrix}, \quad (1.1)$$

i.e. the core is perfectly soft in the x direction. Between the strains and the displacements the well-known relations

$$\begin{aligned} \epsilon_x &= \frac{\partial u}{\partial x} = u', \\ \epsilon_z &= \frac{\partial w}{\partial z} = \dot{w}, \\ \gamma &= \frac{\partial u}{\partial z} + \frac{\partial w}{\partial x} = \dot{u} + w' \end{aligned} \quad (1.2 \text{ a-c})$$

hold.

As usual in the technical theory of sandwiches, we shall suppose (Fig. 2) that $c \gg t$ and, consequently, the displacements of the surfaces of the core are equal to those of the middle planes of the faces.

Let us introduce the notations of Fig. 2. Furthermore, let the "local" and "global" bending rigidities be denoted by B_l and B_0 , resp.:

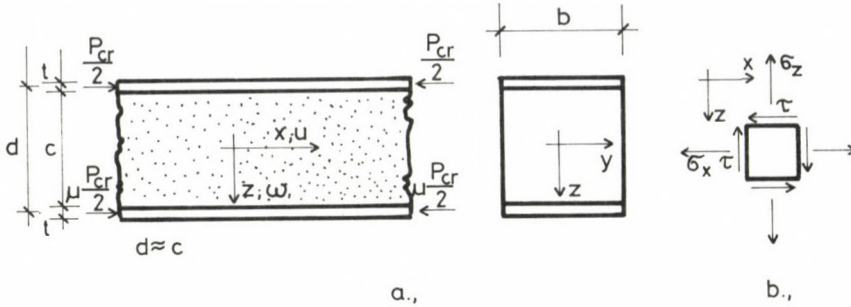


Fig. 2.

$$B_l = 2 \frac{E_f b t^3}{12}, \quad B_0 = \frac{E_f b t d^2}{2}. \quad (1.3)$$

(E_f is the modulus of elasticity of the faces.) The shearing rigidity is

$$S = G b c \quad (1.4)$$

(G is the shear modulus). We also introduce the critical loads belonging to the local and global bending rigidities

$$P_l = \frac{B_l \pi^2}{l^2}, \quad P_0 = \frac{B_0 \pi^2}{l^2}, \quad (1.5)$$

respectively (l is the half wavelength of a sinusoidal buckling shape); and another critical load

$$R = \frac{E_c b}{c} \cdot \frac{l^2}{\pi^2} \quad (1.6)$$

which characterizes the transversal compressibility of the core. The fictitious critical loads P_l , P_0 and R will be used in the formulas for the actual critical forces analyzed in the next section.

2. Governing equations

Let us write the equilibrium equations of the buckled sandwich bar shown in Fig. 2 on the basis of the stationarity condition for the total potential energy. We neglect the pre-buckling deformations, that is, the

axis of the bar is considered to be a straight line also in the case of bent bars before buckling. Furthermore, we assume negligible the effect of stresses which arise in the core before buckling.

The total potential energy π consists of three parts:

$$\pi = \pi_c + \pi_f - \pi_e \quad (2.1)$$

where

$$\pi_c = \frac{1}{2} b \int_{(x)} \int_{(z)} [G(\dot{u} + w')^2 + E_c (\dot{w})^2] dz dx \quad (2.2)$$

is the strain energy of the core,

$$\pi_f = \frac{1}{2} \frac{B_f}{2} \int_{(x)} [(w_1'')^2 + (w_2'')^2] dx + \frac{1}{2} E_f b t \int_{(x)} [(u_1')^2 + (u_2')^2] dx \quad (2.3)$$

is the strain energy of the faces, and

$$\pi_e = \frac{P_{cr}}{2} \frac{1}{2} \int_{(x)} [(w_1')^2 + \mu(w_2')^2] dx \quad (2.4)$$

is the work done by the external load. The integrals are extended to the total length of the beam in the x direction and from -c/2 to c/2 in the z direction.

In Eqs (2.3) and (2.4) 1 and 2 refer to the upper and lower faces, for example u_1, u_1', \dot{u}_1 , and w_1 are equal to u, u', \dot{u} and w , respectively, substituting $-\frac{c}{2}$ into the latter ones.

We have to find the displacement functions u , and w which meet the boundary conditions at the ends of the bar, and the condition

$$\pi = \text{stationary} !$$

For that purpose, let us replace u , and w by functions

$$\begin{aligned} u(x, z) &+ \varepsilon_u \eta_u(x, z) , \\ w(x, z) &+ \varepsilon_w \eta_w(x, z) , \end{aligned} \quad (2.5)$$

respectively, in the expression (2.1). Variations $\delta u = \varepsilon_u \eta_u$, and $\delta w = \varepsilon_w \eta_w$ are arbitrary smooth functions, ε_u and ε_w are multipliers of small absolute value.

If functions u , and w meet the stationarity condition for π (i.e. they are extremal functions of the variational problem) then the partial derivatives $\partial\pi/\partial\varepsilon_u$, and $\partial\pi/\partial\varepsilon_w$ must vanish at $\varepsilon_u = \varepsilon_w = 0$:

$$\left[\frac{\partial\pi}{\partial\varepsilon_u} \right]_{\varepsilon_u = \varepsilon_w = 0} = b \int \int_{(x)(z)} G(\dot{u}+w') \dot{\eta}_u \, dzdx + E_f b t \int_{(x)} [u'_1 \eta'_{u1} + u'_2 \eta'_{u2}] dx = 0, \quad (2.6a)$$

$$\begin{aligned} \left[\frac{\partial\pi}{\partial\varepsilon_w} \right]_{\varepsilon_u = \varepsilon_w = 0} &= b \int \int_{(x)(z)} [G(\dot{u}+w') \eta'_w + E_c \dot{w} \eta_w] \, dzdx + \\ &+ \int_{(x)} \left\{ \frac{B\ell}{2} [w''_1 \eta''_{w1} + w''_2 \eta''_{w2}] - \frac{P_{cr}}{2} [w'_1 \eta'_{w1} + \mu w'_2 \eta'_{w2}] \right\} dx = 0. \end{aligned} \quad (2.6b)$$

After integrating (2.6a,b) by parts, we obtain

$$\begin{aligned} &-b \int \int_{(x)(z)} G(\dot{u}+w') \dot{\eta}_u \, dzdx + \\ &+ \int_{(x)} [b G(\dot{u}_2 + w'_2) - E_f b t u''_2] \eta_{u2} \, dx + \\ &+ \int_{(x)} [-b G(\dot{u}_1 + w'_1) - E_f b t u''_1] \eta_{u1} \, dx + \\ &+ E_f b t \left\{ [u'_2 \eta_{u2} + u'_1 \eta_{u1}] \right\}_{(x)} = 0, \end{aligned} \quad (2.6c)$$

$$\begin{aligned} &-b \int \int_{(x)(z)} [G(\dot{u}+w')' + E_c \dot{w}] \eta_w \, dzdx + \\ &+ \int_{(x)} \left[E_c b \dot{w}_2 + \frac{B\ell}{1} w''''_2 + \mu \frac{P_{cr}}{2} w''_2 \right] \eta_{w2} \, dx + \\ &+ \int_{(x)} \left[-E_c b \dot{w}_1 + \frac{B\ell}{2} w''''_1 + \frac{P_{cr}}{2} w''_1 \right] \eta_{w1} \, dx + \\ &+ \left\{ b \int_{(z)} [G(\dot{u}+w') \eta_w] \, dz + \frac{B\ell}{2} w''_1 \eta'_{w1} + w''_2 \eta'_{w2} - \right. \end{aligned} \quad (2.6d)$$

$$-\frac{B\ell}{2} \left[w_1'''' \eta_{w1} + w_2'' \eta_{w2} \right] - \frac{P_{cr}}{2} \left[w_1' \eta_{w1} + \mu w_2' \eta_{w2} \right]_{(x)} = 0,$$

where the lower (x) refer to the boundaries in the x direction.

Since η_u , and η_w are supposed to be arbitrary smooth functions, these equations hold only if their terms separately vanish, that is, the respective multipliers of η_u , and η_w vanish in the integrals of (2.6c) and (2.6d). Hence, the following differential equations must hold:

$$bG (\dot{u}+w')' = 0 \quad , \quad (2.7)$$

$$- bG (\dot{u}_1+w_1') - E_f b t u_1'' = 0 \quad , \quad (2.8a)$$

$$bG (\dot{u}_2+w_2') - E_f b t u_2'' = 0 \quad , \quad (2.8b)$$

$$bG (\dot{u}+w')' + bE_c w'' = 0 \quad , \quad (2.9)$$

$$- bE_c w_1' + \frac{B\ell}{2} w_1'''' + \frac{P_{cr}}{2} w_1'' = 0 \quad , \quad (2.10a)$$

$$bE_c w_2' + \frac{B\ell}{2} w_2'''' + \mu \frac{P_{cr}}{2} w_2'' = 0 \quad . \quad (2.10b)$$

In the case of $\mu = 1$ eqs (2.7) to (2.10) are in agreement with (8), and (9) of /9/ if there the difference between c, and d is neglected.

3. Buckling of symmetrically loaded sandwich bars

Let $\mu = 1$, i.e. the bar is subjected to a symmetrical load. We assume the functions which satisfy the equations (2.7) to (2.10) in the form

$$u(x, z) = u(x) u(z) \quad , \quad (3.1)$$

$$w(x, z) = w(x) w(z) \quad , \quad (3.2)$$

where

$$u(x) = \cos \frac{\pi x}{\ell} \quad ,$$

$$w(x) = \sin \frac{\pi x}{\ell} \quad ,$$

and ℓ is the half wavelength of the buckling shape not known yet.

These functions meet equations (2.7), and (2.9) only if

$$u(z) = -\frac{\pi}{l} f(z) + 6f_3 \frac{E_c}{G} \frac{l}{\pi} z, \quad (3.3)$$

$$w(z) = f(z), \quad (3.4)$$

where $f(z)$ is a polynomial of the third order:

$$f(z) = f_3 z^3 + f_2 z^2 + f_1 z + f_0. \quad (3.5)$$

Displacement functions (3.3), and (3.4) contain four unknown coefficients, which can be determined using (2.8a,b), and (2.10a,b). From (2.8a,b) we obtain:

$$f_2 \frac{c^2}{4} + f_0 = 0, \quad (3.6)$$

$$6 E_c f_3 \frac{l}{\pi} = E_f t \frac{\pi^2}{l^2} \left[\frac{\pi}{l} \left(f_3 \frac{c^3}{8} + f_1 \frac{c}{2} \right) - f_3 \frac{E_c}{G} \frac{l}{\pi} c \right], \quad (3.7)$$

and from (2.10a,b)

$$\frac{1}{2} (P_{cr} - P_\ell) \left(\frac{3}{2} f_3 c^2 + 2 f_1 \right) = 6 R c^2 f_3, \quad (3.8)$$

$$\frac{1}{2} (P_{cr} - P_\ell) 2 f_2 c = 4 R c f_2. \quad (3.9)$$

(3.6) to (3.9) constitute a system of homogeneous linear algebraic equations in the unknown constants f_0 , f_1 , f_2 , and f_3 . A nontrivial solution is possible only if the determinant of the equation system vanishes.

Using this condition we obtain two different values for the critical load; the first value belongs to a symmetrical buckling shape:

$$\frac{1}{2} P_{cr}^s = \frac{1}{2} P_\ell + 2 R = \frac{\pi^2 B l}{l^2 2} + \frac{2 E_c b}{c} \frac{l^2}{\pi^2} \quad (3.10)$$

and the second value belongs to an antisymmetrical one:

$$P_{cr}^a = \left(\frac{1}{P_c} + \frac{1}{S} + \frac{1}{12R} \right)^{-1} + P_\ell. \quad (3.11)$$

Eq. (3.10) is formally identical with the formula of the critical load of a bar on elastic (Winkler type) foundation, where the bending rigidity of the bar is $\frac{B l}{2}$ and the stiffness of the foundation is

$$\frac{2 E_c b}{c}.$$

In the case of an incompressible core $E_c \longrightarrow \infty$ and, therefore, $R \longrightarrow \infty$, consequently, (3.10) becomes infinite, which means, that symmetrical buckling cannot develop. Under the same conditions (3.11) turns into

$$P_{cr} = \left(\frac{1}{P_0} + \frac{1}{S} \right)^{-1} + P_\ell, \quad (3.12)$$

which is the formula known as that for the critical load of a sandwich bar with thick faces /1, (3.13); 4, (9)/. Equation (3.11) can be considered a refinement of (3.12) because it takes into account the interaction of the wrinkling and the overall behaviour.

The structure of (3.11) is surprisingly simple. It takes into account the transverse compressibility of the core in the same way as if we used the Föppl-Papkovich theorem for calculating an approximate critical load of the sandwich bar /6, 7/.

Our results can be used not only in the case of an antiplane core but, as a good approximation, in the case of isotropic cores as well. The antiplane core (see (1.1)) is "softer" than the isotropic one, hence — according to the Föppl-Papkovich theorem — the approximate critical load is not greater than the exact one. (See also the numerical example.)

3.1 Wrinkling of faces without interaction of overall instability

In the case of "pure wrinkling" we have to take into consideration the conditions

$$u_1 = u_2 = 0 \quad (3.13a,b)$$

instead of (2.8a,b). Hence, we obtain the equations

$$f_0 = -f_2 \frac{c^2}{4}, \quad (3.14)$$

$$f_1 = f_3 c^2 \left(6 \frac{R}{S} - \frac{1}{4} \right), \quad (3.15)$$

where (3.14) is identical with (3.6) but (3.15) differs from (3.7).

From the homogeneous linear equation system consists of equations (3.14), (3.15), (3.8) and (3.9) we can determine two different critical loads:

Case III. (Fig. 1): In the case of a symmetrical buckling shape:

$$u = -f_2 \left(z^2 - \frac{c^2}{4} \right) \frac{\pi}{\ell} \cos \frac{\pi x}{\ell},$$

$$w = 2 f_2 z \sin \frac{\pi x}{l},$$

we obtain the critical load

$$\frac{1}{2} P_{\text{CR}}^{\text{III}} = \frac{1}{2} P_{\ell} + 2R \quad (3.16)$$

which is identical with (3.10). The stresses in the core are:

$$\tau = 0, \quad \sigma_z = 2 f_2 E_c \sin \frac{\pi x}{l}.$$

Case II. In the case of an antisymmetrical buckling shape:

$$u = \frac{\pi}{l} f_3 \left[-z^3 + \left(\frac{c^2}{4} - 6 c^2 \frac{R}{S} + 6 \frac{E_c}{G} \frac{l^2}{\pi^2} \right) z \right] \cos \frac{\pi x}{l},$$

$$w = f_3 \left[3 z^2 - \frac{c^2}{4} + 6 c^2 \frac{R}{S} \right] \sin \frac{\pi x}{l},$$

we obtain

$$\frac{1}{2} P_{\text{CR}}^{\text{II}} = \frac{1}{2} P_{\ell} + \left(\frac{2}{S} + \frac{2}{12 R} \right)^{-1}. \quad (3.17)$$

The stresses in the core are

$$\tau = 6 f_3 E_c \frac{l}{\pi} \cos \frac{\pi x}{l},$$

$$\sigma_z = -6 E_c f_3 z \sin \frac{\pi x}{l}.$$

If $P_0 \longrightarrow \infty$, then (3.17) is identical with (3.11).

Case I. This is — in the case of an antiplane core — physically not possible.

As we have shown, the overall instability combines only with the antisymmetrical wrinkling.

3.2 Numerical example

Let us consider the example of Goodier and Neou /2/, presented also in /1, Fig. 8, 14/.

The data of the analysed sandwich plate are:

$$\frac{t}{c} = 0.02 ;$$

Poisson's ratios of the core and of the faces are

$$\nu_c = 0 \quad , \quad \nu_f = \frac{1}{3}$$

respectively, and there are three different investigated ratios of the moduli of elasticity of the faces and of the core:

$$\frac{E_f^P}{E_c} = 500 \quad , \quad \frac{E_f^P}{E_c} = 1000 \quad \text{and} \quad \frac{E_f^P}{E_c} = 10\,000 \quad .$$

The full lines in Fig. 3 show the results of Goodier and Neou in the case of an isotropic core.

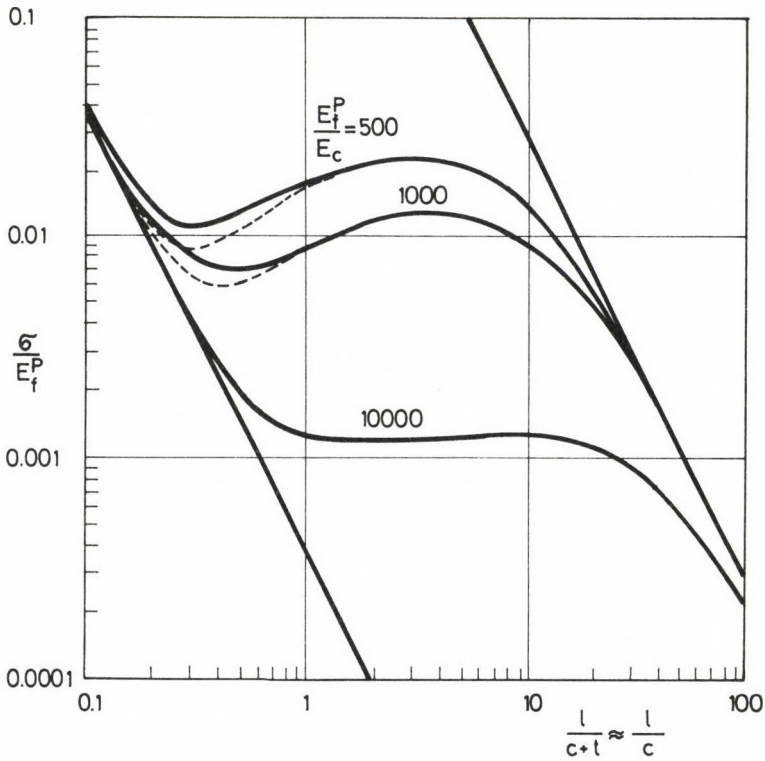


Fig. 3.

Let us consider a sandwich bar with an antiplane core. The data agree with those of the previously treated sandwich plate with an isotropic core, provided the modulus of elasticity of the faces is divided by $(1 - \nu_f^2)$:

$$\frac{E_f}{E_c} = \frac{500}{1 - \frac{1}{9}}, \quad \frac{E_f}{E_c} = \frac{1000}{1 - \frac{1}{9}} \quad \text{or} \quad \frac{E_f}{E_c} = \frac{10\,000}{1 - \frac{1}{9}}.$$

The shear modulus is $G = \frac{E_c}{2}$,
and $\frac{t}{c} = 0.02$.

Using the expressions (1.3) to (1.6) and (2.23) we obtain the results very easily:

$$\frac{\sigma}{E_f} = \frac{P_{cr}}{b t E_f} = \left\{ \frac{2 (1 - \nu_f^2) \ell^2}{\pi^2 c^2} + \frac{4 E_f t}{E_c c} + \frac{E_f t c^2}{b E_c c} \frac{\pi^2}{\ell^2} \right\}^{-1} + \frac{\pi^2 t^2}{12 (1 - \nu_f^2) \ell^2}.$$

The chain lines in Fig. 3 show that these approximate results give a very good upper limit for the critical force. In the case of

$\frac{E_f^P}{E_c} = 10\,000$ the chain and full lines practically coincide.

4. Buckling of not symmetrically loaded sandwich bars

Let us consider a sandwich bar with an antiplane core presented in Chapter 2, and let the forces acting in the faces be different (Fig. 2a).

In determining the critical load we can use the same method as in Chapter 3.

After a lengthy but straightforward procedure we obtain the following simple quadratic equation for the critical load:

$$\left(\frac{P_{cr}}{2} \right)^2 \mu - \frac{P_{cr}}{2} \frac{1 + \mu}{2} \left(\frac{P_{cr}^S}{2} + \frac{P_{cr}^a}{2} \right) + \frac{P_{cr}^S}{2} \frac{P_{cr}^a}{2} = 0, \quad (4.1)$$

where P_{cr}^S and P_{cr}^a are defined by formulas (3.10) and (3.11) respectively.

a) In the case of $\mu = 1$ (i.e. pure compression) Equation (4.1) yields the same results as we have obtained in, Chapter 3:

$$\left(\frac{P_{cr}}{2} \right)_{1,2} = \begin{cases} \frac{P_{cr}^S}{2} \\ \frac{P_{cr}^a}{2} \end{cases}. \quad (4.2)$$

In the case of $\mu = 0$ we obtain from (4.1)

$$\frac{P_{cr}}{2} = 2 \left[\left(\frac{P_{cr}^s}{2} \right)^{-1} + \left(\frac{P_{cr}^a}{2} \right)^{-1} \right]^{-1} \quad (4.3)$$

In the case of $\mu = -1$ (pure "global" bending) Eq. (4.1) yields

$$\frac{P_{cr}}{2} = \pm \sqrt{\frac{P_{cr}^s}{2} \frac{P_{cr}^a}{2}}, \quad (4.4)$$

and in the case of $\mu = -\infty$ (so that the tensile face remains perfectly flat; see Fig. 1, Case I.), we obtain from (4.1):

$$\frac{P_{cr}}{2} = \frac{1}{2} \left(\frac{P_{cr}^s}{2} + \frac{P_{cr}^a}{2} \right). \quad (4.5)$$

The results are presented in Fig. 4.

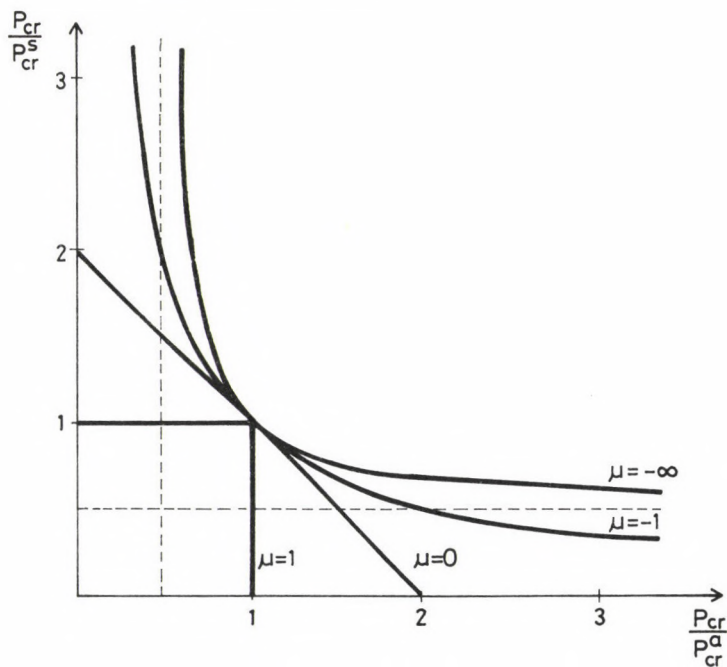


Fig. 4.

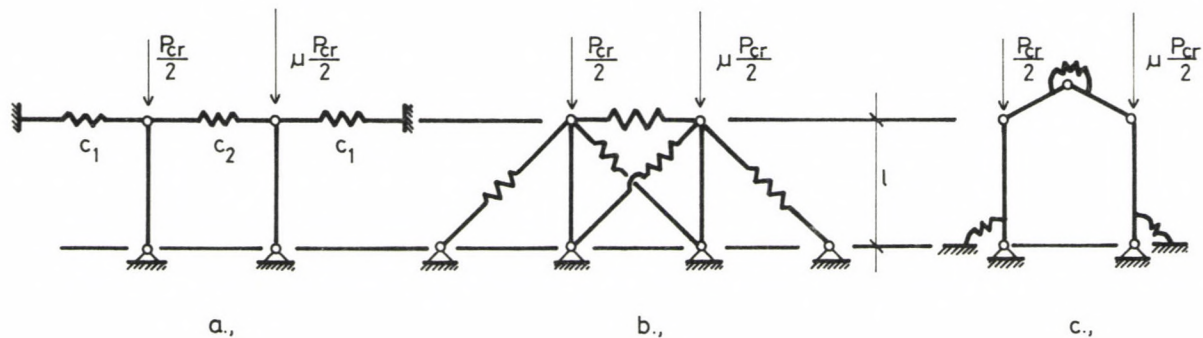


Fig. 5.

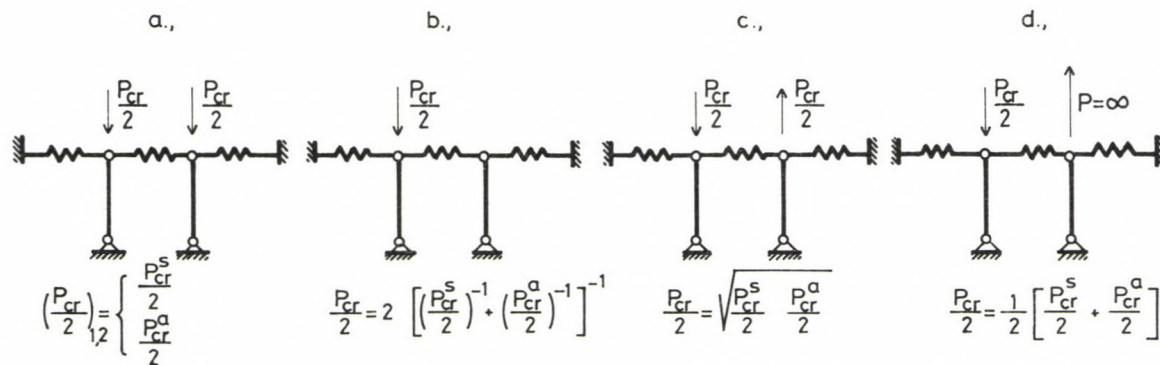


Fig. 6.

As can be seen, we obtained for the different cases the harmonic (4.3), the geometric (4.4) and the arithmetic (4.5) mean values of

$$\frac{p_{cr}^s}{2} \text{ and } \frac{p_{cr}^a}{2} .$$

In the analysis of flexural wrinkling of sandwich panels /10/ assumes that the tensile face is perfectly flat. This assumption can be used only if the wrinkling of the faces can be considered independent, but in the case of "antiplane" core the validity of this assumption requires an infinite large tensile stress in the tensile face.

4.1 Analogy with other symmetric quadratic eigenvalue problems

We have obtained analogous results investigating some symmetrical structures which have two independent displacements (e.g. that in Fig. 5). As an example, let us consider the structure shown in Fig. 5a. The coefficients of the springs are C_1 and C_2 .

The analysis for the stability of this structure yields the buckling condition in the form of Eq. (4.1) where

$$\frac{p_{cr}^s}{2} = l(C_1 + C_2) , \quad \frac{p_{cr}^a}{2} = l C_1 .$$

The results are presented in Fig. 6.

The mathematical analysis of this peculiar behaviour of symmetrical structures is the subject of /14/, which will be published in the near future.

REFERENCES

1. Allen, H.G.: Analysis and Design of Structural Sandwich Panels. Oxford etc.: Pergamon Press, 1969.
2. Goodier, J.N. - Neou, I.M.: The evaluation of theoretical critical compression in sandwich plates. J. Aero. Sci. 18, 10, Oct. (1951), 649-57.
3. Gough, C.S. - Elam, C.F. - DeBruyne, N.A.: The stabilization of a thin sheet by a continuous supporting medium. J. Roy. Aero. Soc. 44, 349, Jan., 1940, 12-43.
4. Hegedűs, I. - Kollár, L.P.: Buckling of Sandwich Columns with Thick Faces Subjected to Axial Loads of Arbitrary Distribution. Acta Techn. Hung., 97 (1-4), (1984), 123-131.
5. Hoff, N.J. - Mautner, S.E.: Buckling of sandwich-type panels. J. Aero. Sci., 12, 3, July 1945. 285-297.

6. Pflüger, A.: Stabilitätsprobleme der Elastostatik. Berlin: Springer 1964.
7. Tarnai, T.: Generalization of Southwell's and Dunkerley's theorems for quadratic eigenvalue problems. Acta Techn. Hung., 91 (3-4), (1980) 203-223.
8. Williams, D. - Leggett, D.M.A. - Hopkins, H.G.: Flat Sandwich Panels under compressive End Loads, A.R.C., R&M 1987. 1941.
9. Benson, A. - Mayers, I.: General Instability and Face Wrinkling of Sandwich Plates- Unified Theory and Applications. AIAA Journal, 5 (4) (1967), 729-739.
10. Chong, K.P. - Hartsock, J.A.: Flexural Wrinkling in Foam - Filled Sandwich Panels. J. Eng. Mech. Div., ASCE, 95 (1969), 585-610.
11. Pomázi, L.: Stability of Rectangular Sandwich Plates with Constructionally Orthotropic Hard Layers. Periodica Polytechnica, Mech. Eng. Part I., 24 (1980), 203-221.; Part II., (1989) (in press).
12. Pomázi, L.: Remarks to the stability of asymmetrically built and loaded sandwich plates. Proceedings of the Euromech Colloquium No 200, Mátrafüred, Hungary, 5-7 October 1985. Post-buckling of elastic structures, Edited by J. Szabó, assistant editors: Zs. Gáspár and T. Tarnai. Akadémiai Kiadó, Budapest, 1986, 253-275.
13. Hegedűs, I. - Kollár, L.P.: Vastag héjalású szendvics lemez horpadása. (Buckling of sandwich plates with thick faces.) (In Hungarian.) Mélyépítéstudományi Szemle, 38, (1988), 173-176.
14. Hegedűs, I. - Kollár, L.P.: Buckling of symmetrical structures under non-symmetrical loads. (It is submitted and accepted for publication to the journal: Mechanics of Structures and Machines.)

SOME PHYSICAL PROBLEMS ASSOCIATED WITH THE SKIN BEARING CAPACITY OF AXIALLY LOADED PILES^{**}

IMRE, E.^{*}

(Received: 18 August 1988)

Reasons for the failure of the plastic limit equilibrium method to predict the ultimate side resistance of axially loaded piles has been discussed. The following two comments have been made on the basis of some theoretical considerations.

1) Soil does not behave as a rigid body in the vicinity of the slip surface around the shaft because time dependent vertical consolidation settlements take place under newly applied load. It has been shown that a time dependent pile-soil interaction process is triggered and controlled by these settlements resulting in a relaxation type stress change and plane strain condition in vertical direction.

2) Well-known pile-soil interaction models generally do not deal with arching which takes place at the beginning of the point load transfer. The hypothesis has been investigated that this kind of arching influences the shaft load transfer in such a way that side resistance mobilized before the beginning of the point load transfer cannot be further increased.

Introduction

The ultimate load capacity of a single pile is generally accepted to be equal to the sum of the ultimate shaft and base resistance. It is an implicit assumption that shaft and base resistance are not interdependent.

According to the generally accepted plasticity approach the ultimate shaft resistance equals the integral of the unit skin resistance along a surface being parallel or coinciding with the pile surface, where the above mentioned integral is minimum.

The unit skin resistance $\tau_u(z)$:

$$\tau_u(z) = c'_a(z) + \sigma'(z) \operatorname{tg} \varphi'(z) \quad (1)$$

^{*}Miss Imre, Emőke, H-1024 Budapest, Káplár u. 4, Hungary

^{**}Section 1 of this paper was presented on the 1st Geotechnical Seminar of Deep Foundations on Bored and Auger Piles, June 10, 1988, Ghent Belgium, as an oral contribution

where c'_a = adhesion or cohesion in terms of the effective stress, σ' = effective normal stress acting on the slip surface, ϕ' = maximum angle of friction along the slip surface in terms of the effective stress.

On the other hand, several evidences indicate that the unit skin resistance depends on the pile geometry and, weak layers or local decompaction of soil around piles may have detrimental effect on it /2/, /3/, /10/, /12/, /21/.

These experiences show that Eq. (1) does not give a realistic estimate for the unit skin resistance of piles. "The design of limiting skin friction is based on empirical methods (e.g. the α , β and γ methods), which can easily differ by a factor of two in estimating the unit skin resistance" /1/.

In the following discussion, an attempt is made to reveal some physical reasons for the failure of the theoretical approach.

1. The load redistribution process of piles

It is well known that as the soil around the pile shaft compresses and creeps under newly applied stresses, downward movement of the soil with respect to pile causes load redistribution.

The load redistribution process of semi-rigid or intermediate piles is presented through the results of the step by step loading test of a diaphragm wall (0.5 x 1.5 x 24.4 m, soil: overconsolidated clay). The following characteristics were observed /14/. During the load redistribution process side load decrement and point load increment occurred, and the process was complete after 60 min (Fig. 1).

In the case of long compressible piles the load redistribution takes place similarly. The only difference that some load initially taken by the upper part of the pile is transferred not only to the point but also to the lower part of the shaft (Fig. 2).

Despite of the fact that the soil settlements may essentially change the load distribution of piles, this process has not been analysed in the literature.

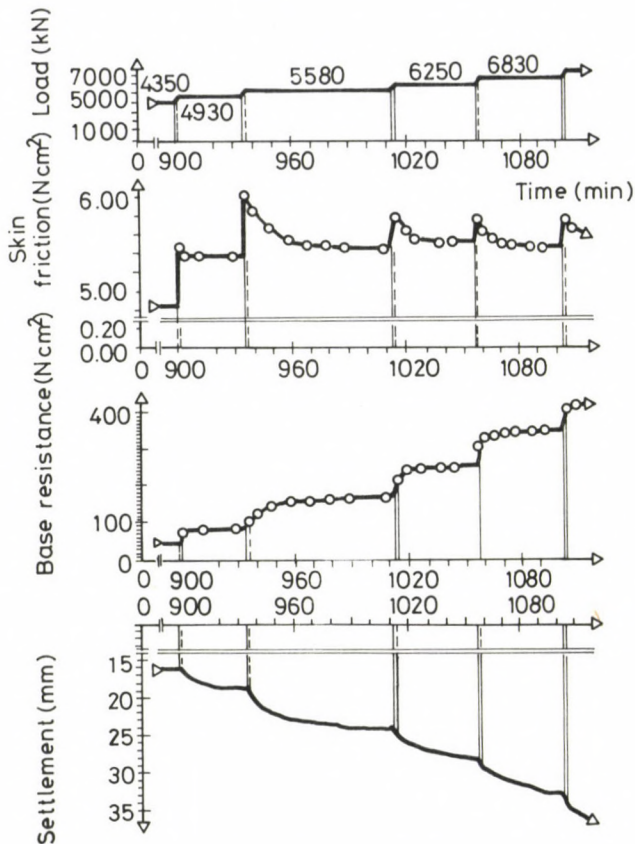


Fig. 1. Stress redistribution of characteristic load steps /14/

1.1 The physical equation of the side load transfer

In this paper it is viewed, that the physical equation of the side load transfer can be expressed in the function of the relative displacement between the shaft and the adjacent soil.*

*There have been two fundamental approaches to predict the shaft load transfer. The first considers the distortion of the whole soil body around the pile with zero relative displacement at the pile-soil interface and the second considers the relative displacement at the pile-soil interface generally assuming that soil behaves as a rigid body. Typical first approaches: the integration of the Mindlin's equation /13/, the method of Randolph and Wroth /15/; typical second approach are the transfer function methods of Seed and Reese /17/ or Kézdi /8/, and models of Scott /18/ and Trochanis /19/. An attempt is known to compile these two approaches /9/.

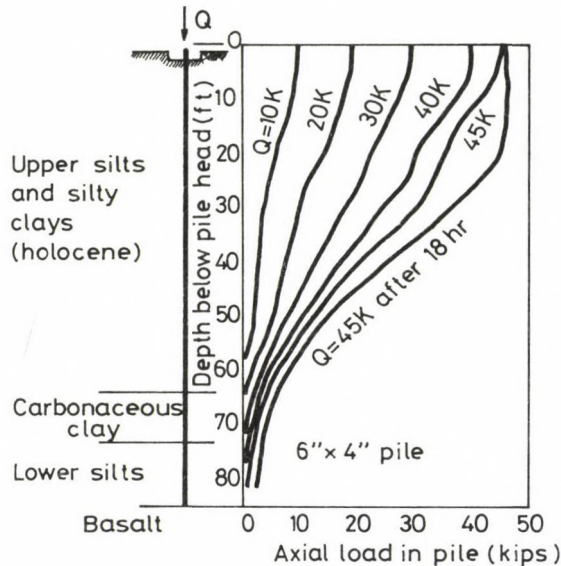


Fig. 2. Load transfer from a steel pile driven through compressible silt to rock /5/

The following model is suggested for the description of the side load transfer:

$$\tau(z) = \sigma(z) \operatorname{tg} \varphi(z) \quad (2)$$

$$\operatorname{tg} \varphi(z) = F(s(z)) \quad (3)$$

$$s(z) = w_p(z) - w_s(z) \quad (3a)$$

where σ = effective normal stress acting on the pile surface, φ = the friction angle at the pile soil interface which is dependent on the relative displacement (s) between pile and soil as can be seen on Fig. 3, w_p, w_s : vertical pile and soil displacement at the pile-soil interface.

1.2 Some consequences of the vertical force equilibrium condition

The equilibrium condition of the pile-soil system is considered. The horizontal force and the moment equilibrium conditions are satisfied because of the axial symmetry. The vertical equilibrium condition of the pile-soil system is analysed in the following.

It is assumed, that a finite radius does exist around the deep foundation at which the stresses originated from shaft load transfer become negligible. This assumption is widely accepted and used in load transfer

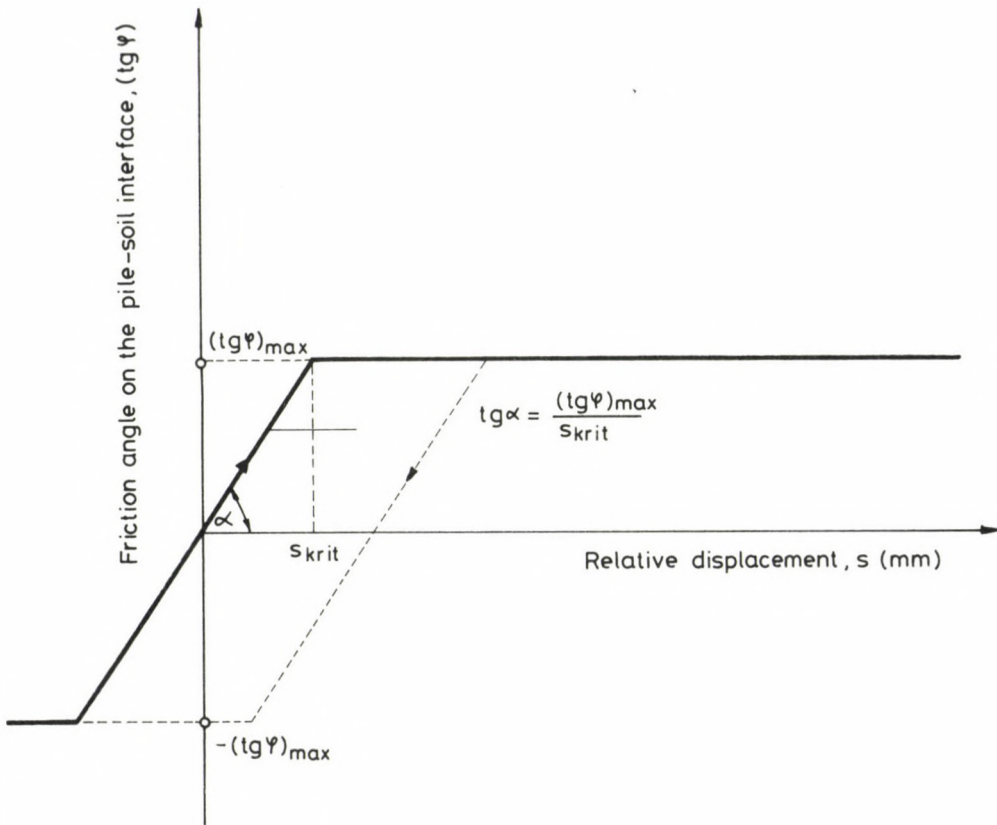


Fig. 3. The friction on the pile-soil interface versus the relative displacement

theories (i.e. /15/. This assumption is considered to be valid until the depth of $z = \ell$, where ℓ = the length of the deep foundation.

A pile-soil body is separated from the infinite half space along this zero stress cylinder boundary, and bounded by a horizontal plane at an arbitrary depth of z (Fig. 4). This pile-soil body can be further separated into a hollow soil cylinder and into a piece of pile (Fig. 5). The vertical forces acting upon these elements (neglecting the self-weight forces) are as follows: P_{p0} = pile load, $P_p(z)$ = normal force in pile at depth of z , $T(z)$ = total skin friction force at depth of z , $P_s(z)$ = vertical normal soil force at depth of z .

The skin friction force (T') transferred between depths of z_1 and z_2 can be computed as follows:

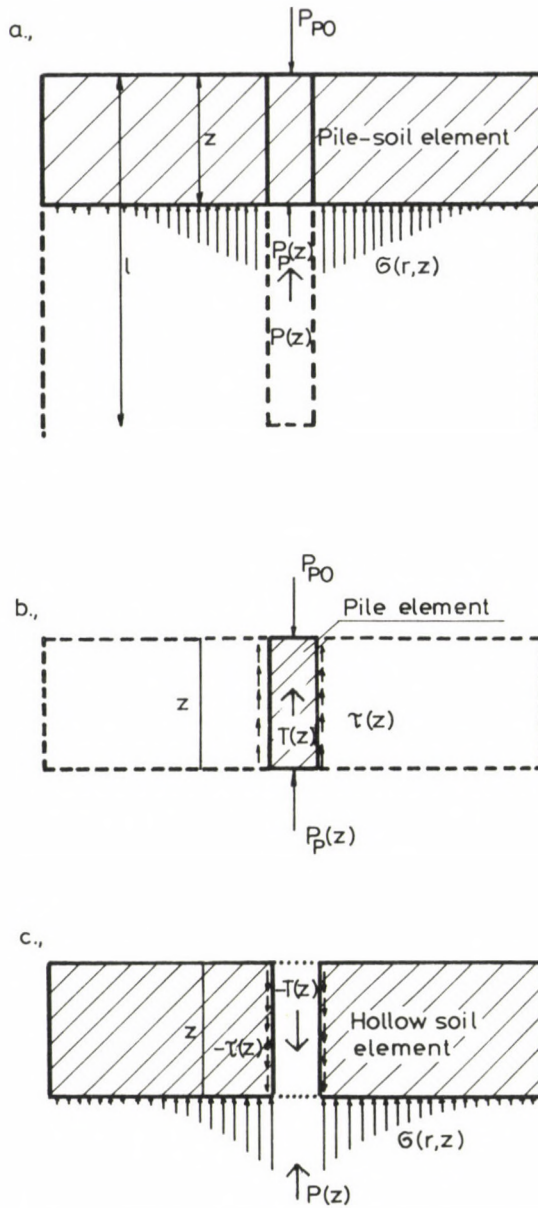


Fig. 5. Vertical forces on the a) zero pressure cylinder with depth of z ; b) pile element with depth of z ; c) hollow soil cylinder with depth of z

Three vertical equilibrium equations can be written for the three bodies and three unknown forces, only two of them are independent. For the soil-pile system:

$$P_p(z) + P_s(z) = -P_{P_0} = \text{const.} \quad (6)$$

For the pile element:

$$P_p(z) + T(z) = -P_{P_0} = \text{const.} \quad (7)$$

For the hollow soil cylinder:

$$P_s(z) - T(z) = 0 \quad (8)$$

It can be mentioned that Eqs (6) – (8) are still valid, if the radius of the zero stress boundary is increased to the infinity.

The corollaries of Eqs (6) – (8) – are as follows. (1) The total skin friction force and the vertical normal soil force equal. If one of them has a physical limiting value, so does the other. (2) The vertical normal soil force is steadily increasing with depth if the unit skin friction is positive. (3) All the vertical forces can be visualized on a simple diagram with constant abscissa of P_{P_0} , as it can be schematically seen on

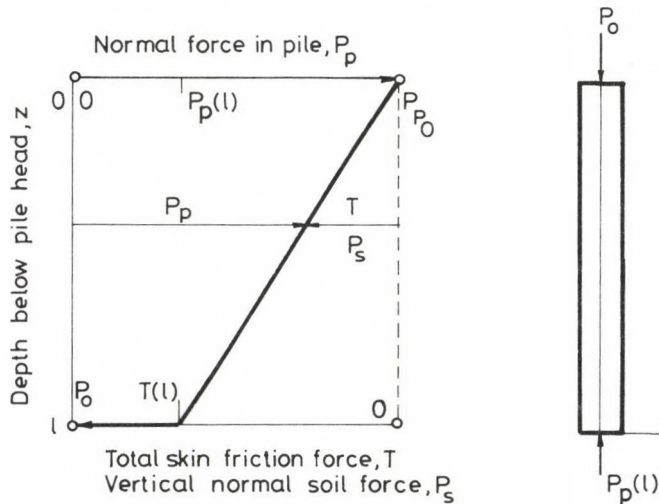


Fig. 6. Schematical representation of the vertical force diagram

Fig. 6. Note the discontinuity of the vertical normal soil force diagram at the pile tip.

1.3 The limiting nature of the long term vertical normal soil force

The load distribution process is analysed by means of an experiment of thought. The object of this analysis is to prove that the long term vertical normal soil force may have a limiting value and in this case the total skin friction force is also limited.

The following model is established (Fig. 7). The stratification around the pile can be characterized by three layers, between two stiff layers a weak, thin layer is found. It is assumed, the soil is with low permeability and the load application entails undrained condition. Due to load application the total vertical stress in the weak layer exceeds the yield stress of the soil adjacent to the pile, within a radius or r_1 . The immediate force distribution is schematically shown on Fig. 7. It is assumed, that the side load transfer can be described by Eqs (2) and (3); the pile can be considered as motionless; there is a direct relationship between the total vertical normal soil stress and the total vertical normal soil force at a given depth, only the primary consolidation deformation is time dependent; the yield limit of soil does not vary during the process.

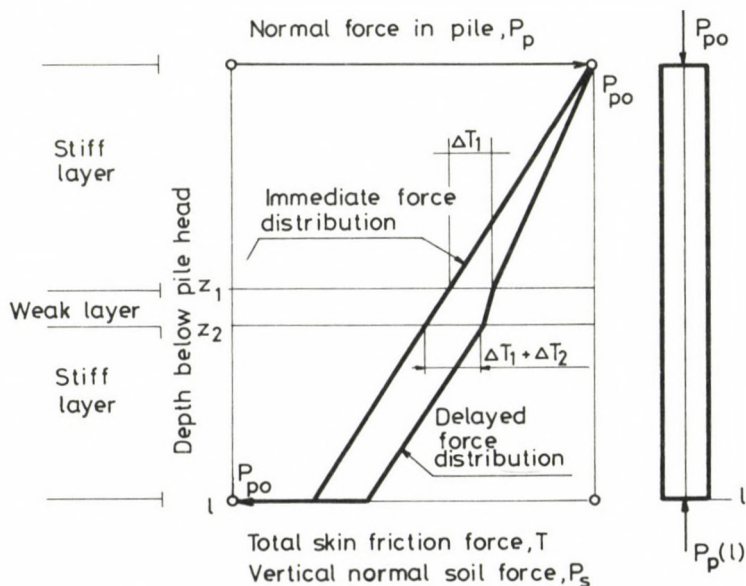


Fig. 7. Schematical representation of the load redistribution process

The load redistribution process of the above defined model is described by the following statements.

a) It can be stated that primary consolidation settlement in the intermediate layer is steadily increasing if the total vertical normal soil stress is greater than the yield stress of the soil.

b) Total skin friction force decrement is caused by the downward consolidation settlement in the intermediate layer.

c) The continuity of the soil mass results in a downward movement and in a total skin friction force decrement in the upper layer.

d) The negative skin friction force increment changes the immediate force distribution as it is schematically shown on Fig. 7. The total skin friction force decreases in depths z_1 , z_2 . According to Eqs (5), (6); the vertical normal soil force decreases and the normal force in pile increases by the same amount. This amount of load will be transferred to the soil in a greater depth.

e) The decrement of the vertical normal soil force in the soft layer results in the reduction of the total normal stress. The rate of the primary consolidation settlement decreases not only because of the very nature of the consolidation, but also because of the decreasing value of the vertical normal total soil stress.

f) Once the decreasing vertical total soil stress becomes less than the yield stress at the depth of the weak layer, the process ceases.

One can conclude that the long term vertical soil stress has a limiting value in the weak layer. Consequently the long term vertical normal soil and skin friction forces have a common limiting value in the weak layer. If the unit skin friction is positive (and the vertical normal soil force is steadily increasing with depth), this statement is valid for every depth of z above the weak layer.

1.4 Design of shaft capacity above weak layers

The long term shaft resistance can be defined as a limit value as follows (1) shaft resistance if the loading is with infinitely low rate (2) shaft resistance at infinite elapsed time after a loading with finite rate.

The yield point of the shaft load-settlement curve can be characterized by a marked decrease in stiffness as it is visualized on Fig. 8.

If the loading rate is finite, the shaft yield load is less than the maximum shaft load capacity. It is a well-known assumption that the

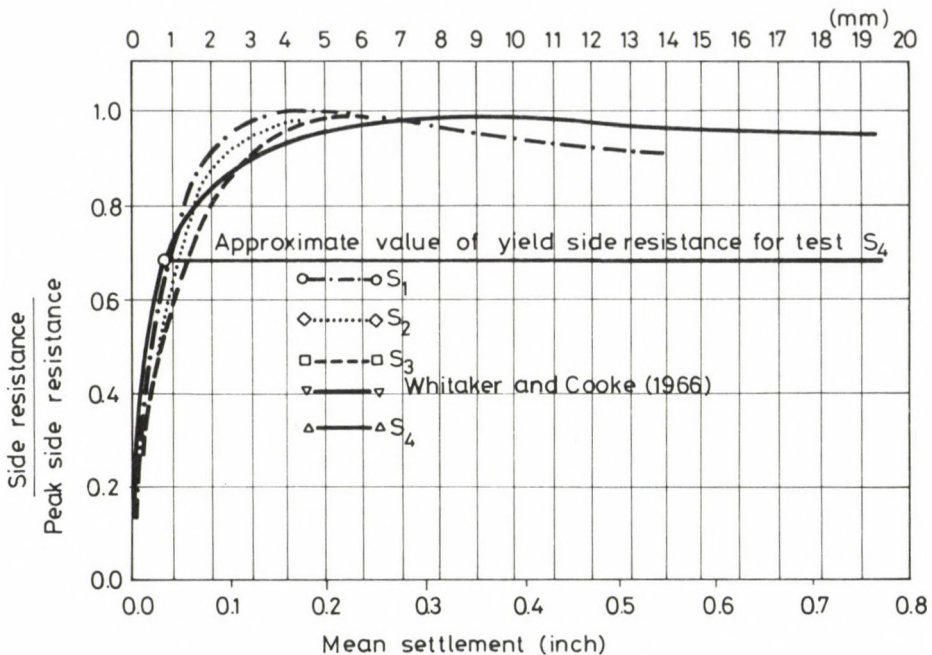


Fig. 8. Dimensionless side load - settlement relationship /11/ with the indication of the yield limit

yield load of the load-settlement curve does not depend on the rate of loading, and its value equals the ultimate long term shaft resistance (see for example the design of "creep piles"). This assumption is used hereafter in this paper.

In earlier papers /6, 7/ a heuristic method was suggested to compute the ultimate long term skin resistance of axially loaded piles for layered soil condition. Its basic idea is that the unit skin resistance of the upper stiff layer is reduced to the value of the lower weak layer.

Earlier results supporting the reliability of this approximate method are recapitulated as follows. The long term shaft resistance of five deep foundations (listed in Table 1) was estimated on the basis of cone penetrometer test local side friction data. Both "continuous" and "relaxation" type cone penetrometer data were taken into consideration.

The long term shaft resistance was approximately determined from pile load tests, the pile load at shaft yield condition by a new method /7/.

The ultimate shaft resistance was calculated in two different ways.

Table 1

| No. | Type of foundation | Cross section (m.m) | Peri-phery (m) | Cross section area (m^2) | Equivalent radius (m) | Length (m) | Soil type |
|-----|--------------------|---------------------|----------------|------------------------------|-----------------------|------------|------------------------|
| 1 | diaphragm | 0.6.2.6 | 6.40 | 1.56 | 0.70 | 15.0 | soft clay |
| 2 | diaphragm | 0.6.1.7 | 4.60 | 1.02 | 0.57 | 14.0 | soft clay |
| 3 | diaphragm | 0.7.1.6 | 4.60 | 1.13 | 0.60 | 10.0 | soft silt soft clay |
| 4 | Franki | Ø 0.6 | 1.88 | 0.28 | 0.30 | 10.5 | soft silt soft clay |
| 5 | diaphragm | 0.5.1.4 | 3.80 | 0.7 | 0.47 | 8.0 | silty sand |

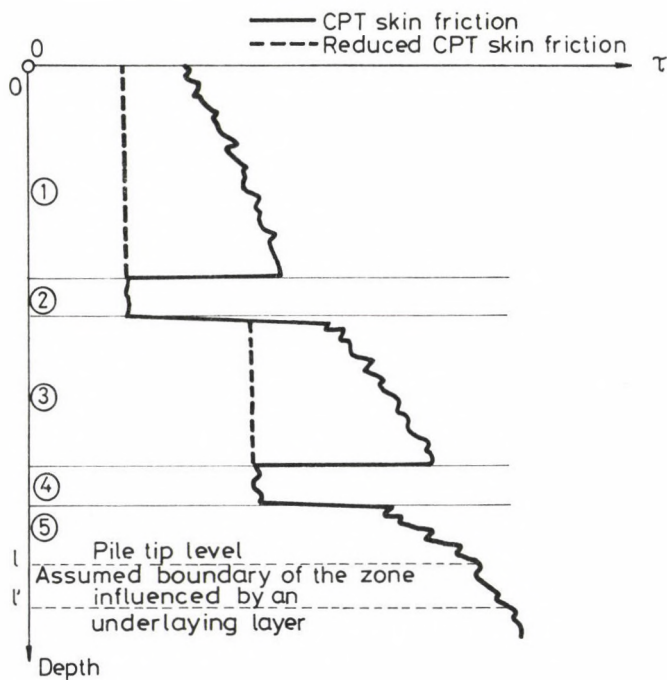


Fig. 9. Reduction in CPT data

Firstly slip surface was assumed on the pile surface and — according to the plasticity approach — the ultimate shaft resistance was considered as the integral of the measured CPT local side friction data on the pile surface. Secondly the ultimate shaft resistance was calculated as the integral of the reduced CPT local side friction data on the pile surface. Reduction was made if the local side friction measured at depth of z was greater than the minimum value measured below the depth of z and above the depth of $l + 1.0$ m (depth one meter below the pile tip) in such a way that the local side friction at depth of z was set to be equal to the above mentioned minimum value (Fig. 9). Data and results are shown in Tables 2, 3 where the computed ultimate shaft resistance values are expressed in the percentage of the measured pile load associated with the shaft yield condition /6/. As it can be seen, the conventional method gave highly overestimated results. The suggested method resulted in more realistic estimations.

Table 2

| No. | Conventional method using | | Suggested method using | |
|-----|-----------------------------------|----------|-----------------------------------|----------|
| | Continuous Relaxation CPT data | CPT data | Continuous Relaxation CPT data | CPT data |
| | (%) | (%) | (%) | (%) |
| 1 | 234 | 139 | 110 | 93 |
| 2 | 193 | 120 | 105 | 96 |
| 3 | 244 | 148 | 152 | 104 |
| 4 | 233 | 220 | 167 | 120 |
| 5 | 268 | 220 | 92 | 116 |

Table 3

| No. | $\frac{1}{\frac{w_{Es}}{w_{Ts}}} \cdot 100(\%)$ | $\frac{2}{\frac{w_{Es}}{w_{Ts}}} \cdot 100(\%)$ | $\frac{3}{\frac{w_{Es}}{w_{Ts}}} \cdot 100(\%)$ | Sign |
|-----|---|---|---|---------|
| | | | | |
| 1 | 51 | 59 | 43 | 131 |
| 2 | 86 | 110 | 66 | 130 |
| 3 | 41 | 46 | 38 | 75/1406 |
| 4 | 80 | 114 | 72 | 79/664 |
| 5 | 55 | 72 | 53 | 75/870 |

2. A hypothesis with regard to the effect of the starting of the point load transfer on the shaft load transfer

It is known that the settlement of piles can be split up into an elastic compression and a base component as follows

$$w_T = w_B + w_E \quad (9)$$

where w_T = top settlement, w_B = base settlement, w_E = elastic compression settlement arising from the elastic compression of the pile material.

2.1 Critical base settlement for deep foundations

It is well known that the ultimate skin resistance of piles is mobilized much sooner than the point resistance /23/. According to the Mindlin's solution, the point load transfer induces significant tensile stresses beyond the point. Most soils can take little stress if any, in tension. It is a general opinion that unless these tensile stresses are compensated by compressive stresses coming from loads applied above the pile point, they are not transmitted by the soil /23/. However the application of the principle of superposition is legitimate only in the case of linearly elastic soil. It is viewed that once point load transfer begins, arching (discontinuity in the stress and strain field) will be caused around the shaft, if soil takes no stress in tension.

It is hypothesized, that the long term shaft load transfer terminates at the beginning of the point load transfer. It is assumed that the base settlement needed for the starting of the point load transfer is small and independent of the geometry of the pile. This base settlement will be called as critical base settlement.

These hypothesis and assumption are attempted to be verified as follows.

2.2 Evaluation of the critical base settlement for five deep foundations

Shaft yield load and long term shaft resistance equal, therefore the above mentioned hypothesis has the following corollary: yielding appears in shaft load transfer at the critical base settlement.

The assumption that the critical base settlement is small and independent of pile geometry was investigated in such a way that settlement at shaft yield load for the aforementioned five foundations was determined.

Table 4

| No. | Back calculated transfer function constant | Transfer function constant (Randolph, Wroth,1979) | Measured total settlement at skin yield | Calculated elastic settlement at skin yield | Calculated base settlement at skin yield | Calculated point load at skin yield / Measured total load at skin yield ratio |
|-----|--|---|---|---|--|---|
| | ξ^{bc} | ξ | $\frac{M}{w_{Ts}}$ (mm) | $\frac{3}{w_{Es}}$ (mm) | w_{Bs} (mm) | (%) |
| 1 | 0.0618 | 3.62 | 0.83 | 0.36 | 0.47 | 2.12 |
| 2 | 0.0367 | 3.76 | 0.65 | 0.43 | 0.22 | 0.61 |
| 3 | 0.0498 | 3.37 | 0.49 | 0.19 | 0.29 | 2.21 |
| 4 | 0.0837 | 4.11 | 0.70 | 0.51 | 0.18 | 1.03 |
| 5 | 0.0334 | 3.39 | 0.47 | 0.25 | 0.22 | 1.30 |

Total settlement at shaft yield load was determined by a new method /6/. The measured total settlement at shaft yield load was as little as 0.47-0.83 mm (Table 4) which is in accordance with the result of O'Neill and Reese (Fig. 8). The total settlement was split up into elastic and base settlement components in such a way, that the elastic compression settlement was evaluated at first, then the calculated elastic component was subtracted from the measured total settlement according to Eq. /9/. Three methods were used for the calculation of the elastic settlement component. Methods 1 and 2 were used to check the result of Method 3.

Method 1: It was assumed, that the total load associated with the shaft yield condition is equally distributed along the shaft, and the point load is equal to zero.

$$w_{Es}^1 = \frac{1}{2} \frac{P}{E_p \cdot F} \cdot l \quad (10)$$

where P = total load associated with the skin yield condition, $E_p = 20\,000$ MN/m², F = cross section area, l = length of deep foundation.

Method 2: It was assumed that the side friction distribution is identical to the modified skin friction diagram determined from relaxation CPT data, and the point load is equal to zero.

$$w_{Es}^2 = \frac{1}{E_p \cdot F} \int_l^0 P_p(z) dz \quad (11)$$

$$P_p(z) = T'(z, l) = \int_z^l U \tau_T(z) dz \quad (12)$$

where $P_p(z)$ = vertical force of deep foundation, U = periphery, $\tau_T(z)$ reduced skin friction determined on the basis of relaxation type CPT test.

Method 3: The Randolph and Wroth (1978) method^{*} was used as follows. The shear modulus of the soil (G_s) and the Young's modulus of the pile (E_p) were estimated beforehand, and transfer function constant was back calculated on the basis of the measured load-settlement data at the skin yield point using Eq. (30) in the paper of Randolph and Wroth /15/. Then the compression settlement was calculated as follows:

$$w_{Es}^3 = w_{Ts} \left[1 - \frac{1}{\cosh \sqrt{\frac{2 G_s}{\xi^{bc} E_p} \frac{l}{r_o}}} \right] \quad (13)$$

where ξ^{bc} = back calculated transfer function constant, $G_s = 2 \text{ MN/m}^2$, r_o = equivalent radius, w_{Ts} = measured total settlement at skin yield load. (The ξ load transfer constant was also calculated by using the pile load-transfer model, suggested by Randolph and Wroth /15/. The back calculated and the estimated values differ by two orders from each other, as can be seen on Table 4.)

As can be seen in Table 4, the elastic compression component was greater than the base settlement component in the case of three foundations.

The calculated base settlement was as little as 0.18–0.47 mm, the calculated point load was less than 3% of total load at shaft yield condition indicating that shaft yield load was reached at an early stage of the point load transfer.

2.3 Dimension dependence of shaft capacity

It is well known that the ultimate unit skin resistance of piles depends on the pile geometry and the pile-soil stiffness ratio /2/. This

^{*}This method applies the following side load transfer model. The settlement of the pile shaft equals the settlement of the soil adjacent to the pile. The settlement of the pile shaft can be written: $w(z) = \tau(z)/\alpha$ where $\alpha = G/(\xi r_o)$; $\xi = \ln(r_o/r_m)$; $r_m = 2.5 l(1-\nu)$; l = length; r_o = radius of pile. This model can be substituted by the following - mathematically equivalent^o - relative displacement type side load transfer equation. It is assumed that relative displacement between soil and pile is arising only from pile settlement. The α term: $\alpha = \tau_{\max}/s_{\text{krit}}$ if $w(z) \geq s_{\text{krit}}$ and $\alpha = \tau_{\max}/w(z)$ if $w(z) < s_{\text{krit}}$; where notations are in accordance with the model presented in Part 1.1.

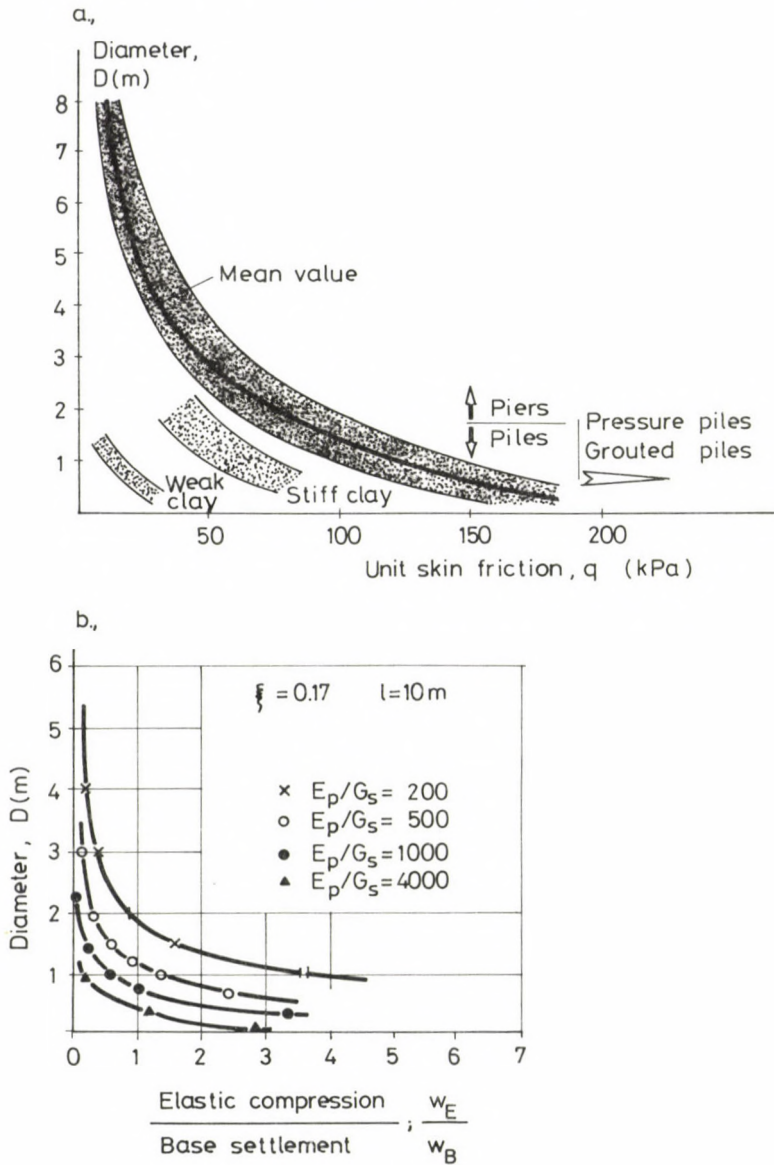


Fig. 10. a) Diameter and soil dependence of unit skin resistance (result from field tests, /2/); b) Diameter and stiffness ratio dependence of elastic/base settlement ratio (result of the parametric study)

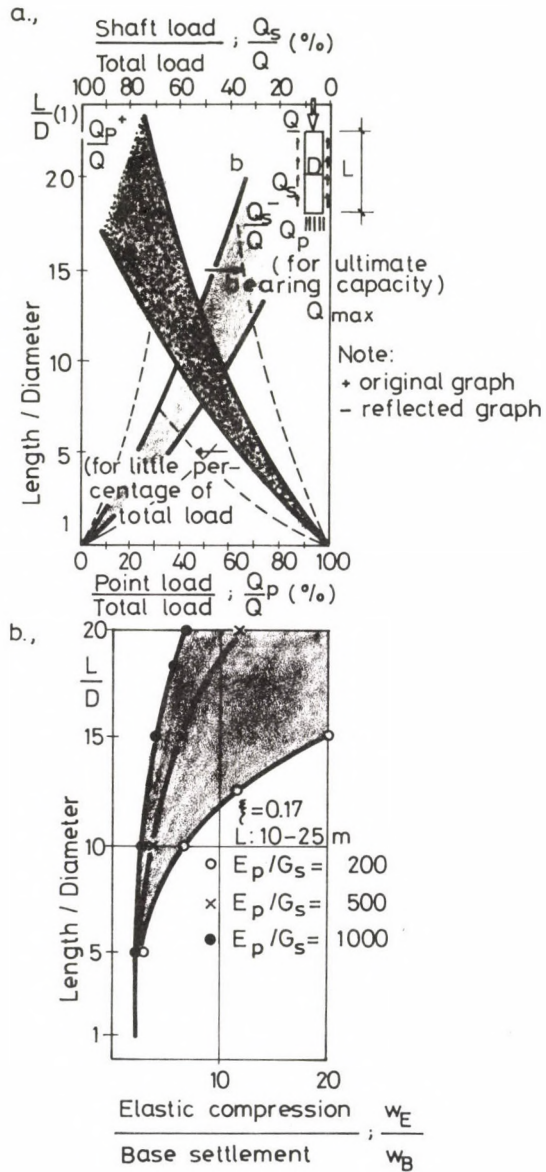


Fig. 11. a) Relationship between skin/total load ratio (Q_s/Q) and L/D ratio (after /2/);
b) Relationship among Q_s/Q ratio, stiffness ratio and L/D ratio (result of the parametric study)

fact can be explained as a corollary of the model, the hypothesis and assumption described in Sections 1.1, 2.1 as follows.

The relative displacement between soil and pile can be increased only by pile settlement (soil does not move upwards). If the critical base settlement is constant and independent of the pile geometry, dimension and stiffness ratio dependence of the unit skin resistance can be attributed exclusively to the dimension and stiffness ratio dependence of the elastic compression settlement incident to the critical base settlement.

The load transfer theory of Randolph and Wroth /15/ makes it possible to compute the elastic compression settlement for a given value of base settlement, in the function of the dimension of the pile and the stiffness ratio. The settlement of the pile top may be expressed in terms of the settlement of the pile base by /15/.

$$w_T = w_B \cdot \cosh \left(\sqrt{\frac{2 G_s}{\xi^{bc} E_p}} \cdot \frac{l}{r_o} \right) \quad (14)$$

Equations (13) and (14) can be compiled:

$$\frac{w_{Es}}{w_{Bs}} = \cosh \left(\sqrt{\frac{2 G_s}{\xi^{bc} E_p}} \cdot \frac{l}{r_o} \right) + 1.0 \quad (15)$$

Eq. (15) was used to compute the variation of the elastic compression settlement:base settlement ratio in the function of pile dimension and stiffness ratio and results were compared with the experimental results of Brandl on Figs 10 and 11. The similitude between the measured and calculated curves is remarkable.

3. Conclusions

The aim of the discussion presented herein was to reveal the possible reasons of the inability of the plasticity approach to determine the ultimate shaft bearing capacity of piles. These reasons are as follows:

3.1 The physical equation of the side load transfer can be expressed in the function of the relative displacement between the shaft and the adjacent soil.

3.2 The ultimate side resistance is time dependent and the long term value can be approximated by the yield value. Its time dependent nature is caused partly by the time dependent soil parameters partly by the fact that the relative displacement between pile and soil is time dependent.

3.3 Soil deformations under newly applied load results in skin friction variation because deep foundations are statically undetermined structures. According to Section 1.3 an interrelationship exists among the skin friction, soil deformation and the vertical normal stress of soil. The final value of the skin friction is limited by the vertical yield stress of the soil around pile.

3.4 The hypothesis that the yield of skin resistance coincides with a small and dimension independent base settlement was supported in the case of five statically loaded piles. Point settlements associated with the yield of skin resistance were back-calculated from load test results. They have been found as negligibly small.

3.5 Dimension and property dependence of the elastic settlement-base settlement ratio determined by a parametric analysis has been found as very similar to the well known dimension and property dependence of the unit skin resistance experienced in loading tests. This similitude is the corollary of the above mentioned hypothesis.

REFERENCES

1. Baligh, M.M., Torrence Martin, R., Azzouz, A.S., Morrison, M.J.: The Piezo-Lateral Stress Cell. Proc. of the XI. ICSMFE, San Francisco, Vol. 2. (1985), 841-844.
2. Brandl, H.: Bearing capacity of piers and piles with large diameters. Proc. of the XI. ICSMFE, San Francisco: Balkema, Vol. 3. (1985), 1525-1530.
3. Carvalho, O.S., Kovári, K.: The measurement of strain distribution in large diameter steel piles. Proc. of the Int. Symp. on Measurements in Geomechanics. Zurich, (1983), 361-371.
4. Ellison, R.D., D'Appolonia, E., Thiers, G.R.: Load-deformation mechanism for bored piles. Journal of the Soil Mech. and Found. Div. ASCE Vol. 97, SM4. (1971), 661-678.
5. Francis, A.J., Savory, N.R., Stevens, L.K., Trollope, D.H.: The behaviour of slender point bearing piles in soft soils. Symp. on Design of Tall Buildings, Univ. of Hong Kong (1961), 25-50.
6. Imre, E.: Skin bearing capacity of piles in layered soil. Mélyépítéstudományi Szemle XXXVII. 2. (1987), 71-84. (in Hungarian).
7. Imre, E.: Skin bearing capacity of piles. Proc. of Seminar on Deep Found. on Bored and Auger Piles. Ghent 7-10 June 1988, 421-429.
8. Kézdi, Á.: Talajmechanika II. Tankönyvkiadó Budapest, (1979), 515 pp.
9. Luker, I.: Prediction of the load-settlement characteristics of bored piles. Proc. of the 1st Int. Geot. Seminar on Deep Found. on Bored and Piles. Ghent, (1988), 229-239.

10. Meyerhof, G.G., Sastry, V.V.R.N.: Bearing capacity of piles in layered soil. Part 2. Sand overlying clay. *Canadian Geotechnical Journal* Vol. 15, 2, (1978), 183-189.
11. O'Neill, M.W., Reese, L.C.: Behaviour of bored piles in Beaumont Clay. *Journal of the Soil Mech. and Found. Div. ASCE* Vol. 98, SM2, (1972), 195-213.
12. Petrasovits, G.: Theoretical and experimental investigations of factors influencing the bearing capacity of tube piles. *Cand. Thesis, Technical University of Budapest* (1963), (in Hungarian).
13. Poulos, H.G., Davis, E.H.: The settlement behaviour of single axially loaded incompressible piles and piers. *Geotechnique* XVIII. (1968), 351-371.
14. Prodinger, W.: Measurement of the redistribution of stress around deep foundation. *Proc. of Int. Symp. on Field Measurements in Geomechanics* (1983), 543-551.
15. Randolph, M., Wroth, C.P.: Analysis of Deformation of Vertically Loaded Piles. *Journal of the Geot. Eng. Div. ASCE* Vol. 104, GT. 12. (1978), 1465-1489.
16. Robinsky, E.J., Cragg, C.B.H.: Volume Displacement Effects on Pile Capacity in Loose Sand, *Canadian Geotechnical Journal*, Vol. 10. (1973), 645-647.
17. Seed, H.B., Reese, L.C.: The action of soft clay along friction piles. *Trans. ASCE* (1957), 731-764.
18. Scott, R.F.: *Foundation Analysis*, Prentice Hall Englewood Cliffs, N.J. (1981).
19. Trochanis, A.M.: On a Friction Layer Model for Contact Problems. *M.Sc. Thesis, Carnegie-Mellon University, Pittsburgh* (1985).
20. Trochanis, A.M., Bielak, J., Christiano, P.P.: Hysteretic Dissipation of Piles under Cyclic Axial Load. *ASCE Journ. of Geotechn. Eng.* 113. No. 4. (1987), 335-351.
21. Van Impe, W.F.: Considerations on the auger pile design. *Proc. of the 1st Geotechnical Seminar: Deep Foundations on Bored and Auger Piles, Ghent June 7-10, (1988), 193-217.*
22. Vesic, A.S.: Ultimate Loads and Settlements of Deep Found. in Sand. *Bearing Capacity and Settlement of Foundations, Proc. of the Symp. Duke University, (1965), 53-58.*
23. Vesic, A.S.: *Design of Pile Foundations*. Transportation Research Board. Nat. Res. Council. Washington, D.C. (1977).

EXPERT SYSTEM FOR GEOTECHNICAL TESTING OF DAMAGED BUILDINGS

RÉDEY, G.* - PAÁL, T.**

(Received: 5 November 1987)

A new software type, expert systems (ES), is swamping the world quickly nowadays, that is proved to be useful for many application instances of several fields in Hungary, too. As for the applications to the field of engineering, or more precisely that of architectural engineering, they have been increasing in number and varying unboundedly in subject in the recent few years. Only in the Hungarian Institute of Building Science there are two systems which we started to develop last year. One of them is an ES based on the knowledge of the Hungarian Building Regulations and supporting decision making in the building authorization process; the other one, discussed below, is a rule based prototype system written in MPROLOG trying to cover the knowledge of an experienced human expert who deals with finding out possible reasons of building failures.

1. The expert knowledge of the system

When a building is damaged, it may be useful to find out the possible reasons of the damage for later restorations. Usually the owner of the building asks an expert to perform this job. The expert makes his examinations on the spot, collects building, soil mechanical, environmental etc. data, and he also makes interviews with people living there if it is necessary.

This kind of work requires great experience, caution and expertness, many standpoints are supposed to be weighed simultaneously. So some details which seem to be unessential at first sight can escape human attention and early prejudice can surpass certain routine analyses. This is the reason why human expert's working style based on 'soft' memory and 'associative' reasoning method is to be supported by the 'hard' memory and 'deductive' reasoning method of ESs.

*Rédey, G., SzKI Intelligens Software Rt., H-1015 Budapest, Donáti u. 35-45, Hungary

**Paál, T., Municipal Institute for Civil Engineering Design, H-1014 Budapest, Úri u. 64-66, Hungary

We present here some parts of the expert knowledge from the engineer's point of view which is systematized on the base of the following principles/1/:

1) To start with, we evaluate the environmental data including e.g. the ground conditions, the position of the building related to its surroundings, the neighbouring mining activities or waterflows if there are any etc.

2) It is followed by the building data, partly the bearing capacity of the structure, partly the data of the foundation concerning mostly the case under discussion (the uniformity of the foundation etc.).

3) The next step is to take into consideration the external effects on the building: dynamic effects (earthquake, damage caused by war, pile driving etc.), external objects or events having effect on the ground below the foundation (neighbouring building activities, ground water drain etc.), previous changes on the building (adding a new storey to it, change of ceiling etc.).

4) Then it is followed by the description of the damage: the number and position of the damaged buildings, the classification of the cracks, the dynamics of the damage process, water conduit defects, foundation damage etc.

5) Finally these data are completed by the classification, qualification and conditional characterization of the soil according to soil mechanical standards.

Now we present some representative part of the expert knowledge, namely the connection between the data associated with the environment, the building etc., and the types or the phenomena of the damage.

During the analysis the so-called primary characteristics have always particular importance with respect to the determination of the damage. Because of its complexity, the reason of the damage is not always clear, so we have to take into consideration the so-called necessary but alternative and the possible characteristics, too. Besides, we have to sort out the cases when damage can be definitely or almost definitely excluded.

The above-mentioned relations can be characterized by the following categories:

- ∅ primary sign,
- I necessary but alternative sign,
- ∴ possible,
- ⊗ almost excluded,
- x excluded.

The damage types are the following:

- i water gets to the foundation,
- ii ground water level changes,
- iii heat effects on the ground,
- iv soil compression,
- v ground movements,
- vi the damage is not in connection with soil data.

The damage phenomena related to the damage types are as follows:

- i/1 compaction,
- i/2 subsidence,
- i/3 erosion,
- i/4 swelling,
- i/5 loss of consistency,
- i/6 chemical effects,
- ii/1-6 the same as above, because of ground water conditions,
- iii/1 freezing,
- iii/2 shrinking,
- iii/3 burning out,
- iv/1 compaction,
- iv/2 subsidence,
- v/1 sliding,
- v/2 earthquake,
- v/3 underground hollow/cellar,
- v/4 underground mining/metro building,
- vi the damage can not be traced back to soil characteristics.

Some representative parts of the expert knowledge are shown in Tables 1-5. The detailed description of the expert knowledge can be found in /3/.

2. The formalization of the expert knowledge

In this paragraph we try to demonstrate the formalization process of the previously presented expert knowledge parts. However, considering the size of the knowledge base and the difficulties arising as soon as more than informal information is to be given about this process, we can only try to illustrate it with an example having rules from almost every level of the knowledge base.

Table 1 Environmental data

| | i | ii | iii | iv | v | vi |
|------------------------------------|---|----|-----|----|---|----|
| the ground under the building | | | | | | |
| is { nearly horizontal | | | | | ! | |
| { inclined | | | | | ! | |
| { steep | | | | | 0 | |
| the building stands | | | | | | |
| { partly } in cutting | | | | | | ! |
| { totally } | | | | | | ! |
| exposed to erosion | | | | | ! | |
| sliding area | | | | | 0 | |
| mining activities { underneath | | | | | 0 | |
| { nearby | | | | | 0 | |
| | | | | | | |
| <u>old beds/dead stream beds</u> | | | | | | |
| { underneath | | ! | | 0 | | |
| { nearby | | ! | | | | |
| <u>water flows to the building</u> | 0 | | | | | |
| { gathers in | ! | | | | | |
| { depressions | | | | | | |
| { near to | | | | | | |

Table 2 Building data

| | i | ii | iii | iv | v | vi |
|-------------------------------|---|----|-----|----|---|----|
| the storey number is { one | | | 0 | | ! | |
| { two | | | ! | | ! | |
| a cellar is made { | | | | | | |
| { partly under | | | ! | ! | | |
| { the building | | | | | | |
| no cellar underneath | | | ! | ! | | |
| the load bearing structure is | | | | | | |
| { pier | | | | ! | | |
| { mixed | ! | | | ! | ! | |
| | | | | | | |

Table 3 External effects on the building

| | i | ii | iii | iv | v | vi |
|---|---|----|-----|----|---|----|
| dynamic effects | | | | | Ø | |
| earthquake | | | | | | |
| damage caused by war | | | | | | Ø |
| explosion | | | | | | |
| pile driving/sheet | | | | | | |
| piling | | | | | | |
| traffic diversion | | | | | | |
| something else | | | | | | |
| special heat effects cold-storage plant | | | | | | |
| boiler | | | Ø | | | |
| foundry | | | Ø | | | |
| | | | | | | |

Table 4 The description of the damage

| | i | ii | iii | iv | v | vi |
|------------------------------|---|----|-----|----|---|----|
| the damage is individual | | | | | | |
| some buildings | | | | | | |
| standing separately | | | | | | |
| are included | | | | | | |
| in a group | | | | | | |
| the damage occurrence varies | | | | | | |
| depending on direction | | | | | | |
| | | | | | | |
| <u>there were</u> | | | | | | |
| gutter and drainpipe | | | | | | |
| defects | | | | | | |
| wall dampening | | | | | | |
| cellar watering | | | | | | |
| preceding the damage | | | | | | |
| Ø | | Ø | | | | |
| | | | | | | |

Table 5 The classification, qualification and conditional characterization of the soil under the building

| | | i | | | | | ii | | | | | iii | | | | | iv | | v | | | |
|--|--------|---|---|---|---|---|----|---|---|---|---|-----|---|---|---|---|----|---|---|---|---|---|
| | | 1 | 2 | 3 | 4 | 5 | 6 | 1 | 2 | 3 | 4 | 5 | 6 | 1 | 2 | 3 | 1 | 2 | 1 | 2 | 3 | 4 |
| classification according to the grain size distribution ¹ | | | | | | | | | | | | | | | | | | | | | | |
| gravel (G) over 2mm | | : | x | x | x | x | | : | x | x | x | x | | x | x | x | | x | x | | | |
| sand (S) 0.1+2mm | | | : | ∅ | x | x | | | : | ∅ | x | x | | x | x | | | : | x | | | |
| mo (M) 0.02+0.1mm | | | | ∅ | x | | | | | ∅ | x | | | | x | | | | | | | |
| silt (Si) 0.002+0.02mm | | : | | : | x | | | : | | : | x | | | | x | | : | | | | | |
| clay (C) under 0.002mm | | | : | | | | | | : | | | | | | | | | : | | | | |
| uniformity coefficient (U) ² | | | | | | | | | | | | | | | | | | | | | | |
| gravel well | sorted | x | x | x | x | x | | x | x | x | x | x | | x | x | x | x | x | x | | | |
| medium | | | x | x | x | x | | | x | x | x | x | | x | x | x | | x | x | | | |
| badly | | : | x | x | x | x | | : | x | x | x | x | | x | x | x | : | x | x | | | |
| sand well | sorted | | | | x | x | | | | | x | x | | x | x | | | | x | | | |
| medium | | | | : | x | x | | | | : | x | x | | x | x | | | | x | | | |
| badly | | | : | : | x | x | | | : | : | x | x | | x | x | | : | | x | | | |
| mo well | sorted | | | | x | | | | | | x | | | | x | | | | | | | |
| medium | | | | | x | | | | | | x | | | | x | | | | | | | |
| badly | | | | | x | | | | | | x | | | : | x | | | | | | | |

¹ Classification according to the name of the component having the greatest share. If (Si + C) > 10% and the soil is not cohesive then its adjective is 'silty'. If the adjective can not be determined in accordance with the previous rule, then the most distant component plays this role.

²
$$\left. \begin{array}{l} U > 10 \\ 3 < U \leq 10 \\ U \leq 3 \end{array} \right\} \begin{array}{l} \text{well} \\ \text{medium} \\ \text{badly} \end{array} \text{ sorted}$$

Table 5 (continued) The classification, qualification and conditional characterization of the soil under the building

| | | i | | | | | ii | | | | | iii | | | | | iv | | | v | | | |
|--------------------------------|------------|---|---|---|---|---|----|---|---|---|---|-----|---|---|---|---|----|---|---|---|---|---|--|
| | | 1 | 2 | 3 | 4 | 5 | 6 | 1 | 2 | 3 | 4 | 5 | 6 | 1 | 2 | 3 | 1 | 2 | 1 | 2 | 3 | 4 | |
| degree of saturation (S_r) | | | | | | | | | | | | | | | | | | | | | | | |
| damp | under 0.3 | | | | | | | | | | | | | | | | | | | | | | |
| wet | 0.3+0.8 | | | | | | | | | | | | | | | | | | | | | | |
| nearly saturated | 0.8+0.99 | | | | | | | | | | | | | | | | | | | | | | |
| saturated | 1.00 | | x | | | | | | x | | | | | | | | | | | | | | |
| plasticity index (I_p) | | | | | | | | | | | | | | | | | | | | | | | |
| mo | under 5% | | | | x | | | | | | x | | | | x | | | | | | | | |
| silty mo | 5+10% | | | | x | | | | | | x | | | ∅ | x | | | | | | | | |
| silt | 10+15% | | | | x | | | | | | x | | | ∅ | x | | | | | | | | |
| lean clay | 15+20% | | | | | | | | | | | | | | | | | | | | | | |
| medium clay | 20+30% | | | x | | | | | x | | | | | | | | | | | | | | |
| fat clay | over 30% | | x | x | ∅ | | | | x | x | ∅ | | | ∅ | | | x | | | | | | |
| consistency index (I_c) | | | | | | | | | | | | | | | | | | | | | | | |
| very soft | under 0.25 | ∅ | x | | x | | | ∅ | x | | x | | | | x | x | ∅ | x | ∅ | | | | |
| soft | 0.25+0.50 | ∅ | x | | x | | | ∅ | x | | x | | | | x | x | ∅ | x | ∅ | | | | |
| close to plastic | 0.50+0.75 | | | | x | | | | | | x | | | | | | | | | | | | |
| plastic | 0.75+1.00 | | | | | | | | | | | | | | | | | | | | | | |
| hard | 1.00+1.50 | | | x | | | | | | x | | | | | | | | | | | | | |
| very hard | over 1.50 | x | | x | | | | x | | x | | | | | | | x | | | | | | |
| compactness | | | | | | | | | | | | | | | | | | | | | | | |
| natural granular soil | | | | | | | | | | | | | | | | | | | | | | | |
| void ratio (e) | | | | | | | | | | | | | | | | | | | | | | | |
| very dense | under 0.6 | x | x | x | | | | x | x | x | | | | | | | x | x | | | | | |
| medium dense | 0.6+0.7 | | | | | | | | | | | | | | | | | | | | | | |
| loose | over 0.7 | ∅ | ∅ | | | | | ∅ | ∅ | | | | | | | | ∅ | ∅ | | | | | |

Table 5 (continued) The classification, qualification and conditional characterization of the soil under the building

| | | | i | | | | | | ii | | | | | | iii | | | | | | iv | | | v | | | | |
|--------------------------------------|--------------|------------------|------|---|---|---|---|---|----|---|---|---|---|---|-----|---|---|---|---|---|----|---|---|---|--|--|--|--|
| | | | 1 | 2 | 3 | 4 | 5 | 6 | 1 | 2 | 3 | 4 | 5 | 6 | 1 | 2 | 3 | 1 | 2 | 3 | 1 | 2 | 3 | 4 | | | | |
| natural cohesive soil | | | | | | | | | | | | | | | | | | | | | | | | | | | | |
| $I_p = 5\%$ | | | | | | | | | | | | | | | | | | | | | | | | | | | | |
| $I_p = 25\%$ | | | | | | | | | | | | | | | | | | | | | | | | | | | | |
| $I_p = 45\%$ | | | | | | | | | | | | | | | | | | | | | | | | | | | | |
| $e = 0.5$ | very dense | | x | x | x | | | | x | x | x | | | | | | | x | x | | | | | | | | | |
| | dense | | x | x | x | | | | x | x | x | | | | | | | x | x | | | | | | | | | |
| | 0.62 | 0.62 | 0.78 | | | | | | | | | | | | | | | | | | | | | | | | | |
| | medium dense | | : | : | : | : | | | : | : | : | : | | | : | : | : | : | : | : | | | | | | | | |
| | 0.69 | 0.75 | 0.98 | | | | | | | | | | | | | | | | | | | | | | | | | |
| <u>loose</u> | | | Ø | Ø | | | | | Ø | Ø | | | | | | | | Ø | Ø | | | | | | | | | |
| 0.78 | 0.92 | 1.22 | | | | | | | | | | | | | | | | | | | | | | | | | | |
| <u>very loose</u> | | | Ø | Ø | | | | | Ø | Ø | | | | | | | | Ø | Ø | | | | | | | | | |
| | | | | | | | | | | | | | | | | | | | | | | | | | | | | |
| fill | | | | | | | | | | | | | | | | | | | | | | | | | | | | |
| degree of compaction ($T_{r\phi}$) | | | | | | | | | | | | | | | | | | | | | | | | | | | | |
| <u>very loose</u> | | <u>under 0.8</u> | Ø | Ø | | | | | Ø | Ø | | | | | | | | Ø | Ø | | | | | | | | | |
| <u>loose</u> | | <u>0.80+0.85</u> | Ø | Ø | | | | | Ø | Ø | | | | | | | | Ø | Ø | | | | | | | | | |
| medium dense | | 0.85+0.90 | : | : | : | : | | | : | : | : | : | | | : | : | : | : | : | : | | | | | | | | |
| dense | | 0.90+0.95 | x | x | x | | | | x | x | x | | | | | | | x | x | | | | | | | | | |
| very dense | | over 0.95 | x | x | x | | | | x | x | x | | | | | | | x | x | | | | | | | | | |
| | | | | | | | | | | | | | | | | | | | | | | | | | | | | |

The expert knowledge can roughly be divided into two parts: one of them processes verbal input data (Tables 1-4), and the other one converts numerical input data into non-numerical information (Table 5). The ES asks for these data and passes them to the knowledge base for further processing.

The system is prepared for dealing with the knowledge associated with the primary characteristics having signed by Ø in the tables of the 2nd paragraph. Dealing with uncertain knowledge requires further preparations which exceeds the limits of this preliminary research, however, we are planning to extend the system in this way at the next stage.

An example set of rules which can be extracted from the tables above, namely from the lines underlined, is the following:

'Compaction' is the reason of the damage

if (water gets to the foundation

or ground water level changes in a dangerous degree

or soil compression arises
and (the consistency of the soil (I_c) is less than or equal to 'soft'
or the compactness of the soil is less than or equal to 'loose').

Water gets to the foundation

if water flows to the building
or gutter/drainpipe defects preceeded the damage
or

Ground water level changes in a dangerous degree

if cellar watering preceeded the damage
or

Soil compression arises

if old beds/dead stream beds are underneath
or

The consistency of the soil is 'very soft'

if I_c is less than 0.25.

The consistency of the soil is 'soft'

if I_c is between 0.25 and 0.50.

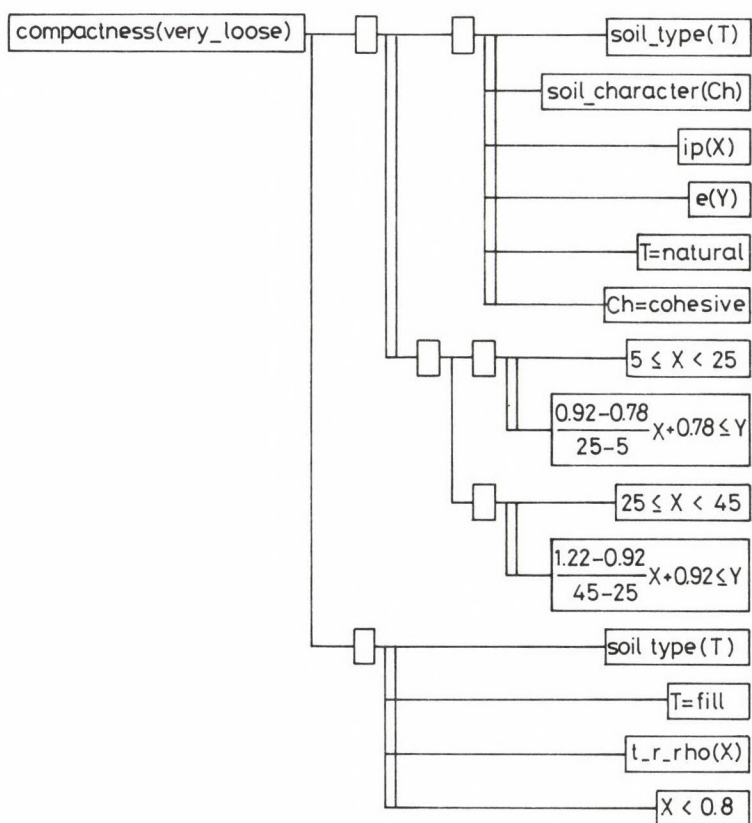
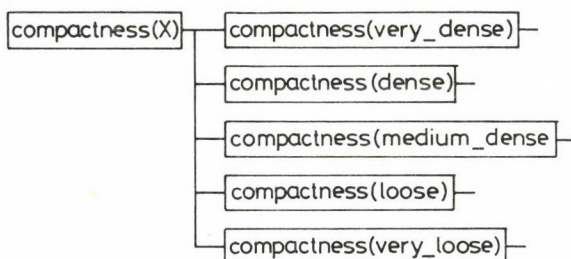
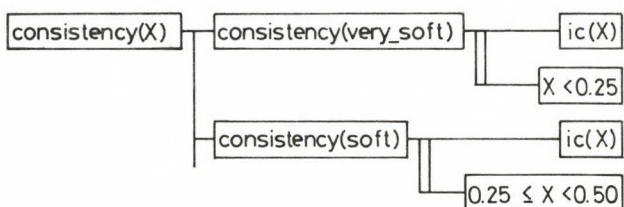
The compactness of the soil is 'loose'

if its type is 'natural',
and its character is 'granular'
and its void ratio (e) is over 0.7.

.....

The compactness of the soil is 'very loose'

if {(its type is 'natural'
and [its character is 'cohesive']
and (its plasticity (I_p) is between 5 and 25%
and its void ratio (e) is greater than or
equal to $\frac{(0.92-0.78)I_p}{25-5} + 0.78$
or (its plasticity (I_p) is between 25 and 45%
and its void ratio (e) is greater than or
equal to $\frac{(1.22-0.92)I_p}{45-25} + 0.92$]]}
or its type is 'fill'
and its degree of compaction (I_{rg}) is below 0.8.



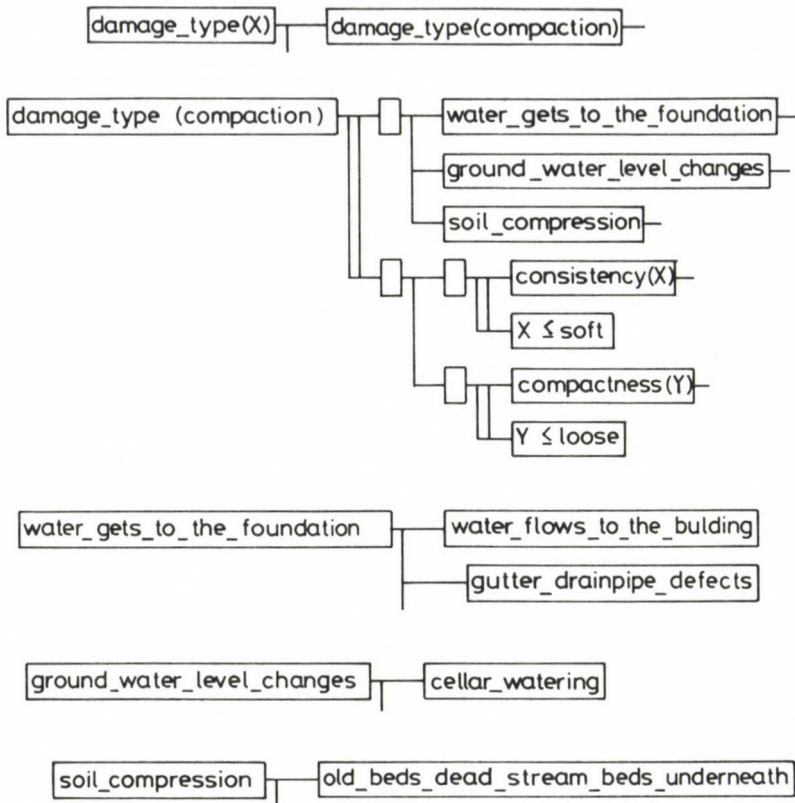


Fig. 1. The 'and-or' tree of the set of example rules

The list of rules above is certainly not complete, some definitions like 'something is less than something' etc. are missing, and it is also obvious that the formalized description may not miss a lot of similar definitions of other evident concepts which can not be discussed here in detail.

We present now a part of the 'and-or' tree (Fig. 1) corresponding to the rules of the same example, which is a useful device for representing the logic structure of this knowledge part. (Here \square corresponds to an 'and' node, \square to an 'or' one.) A proposition appearing at any non-terminal node of the tree represents a consequence reasoned by its antecedents which are to be at the successor nodes of the former one. The leaf nodes represent data input or some other basic procedure which do not have any particular importance. The rules are represented in MPROLOG, a modular

implementation of the logic programming language Prolog, developed by the Computer Research and Innovation Center (SzKI), Hungary /2/, /5/, /6/.

3. The shell of the system

An ES shell is a kind of programming tool that helps the expert develop his own knowledge base. It is a "domain independent" framework for constructing and running consultation programs with the facilities for defining data types and rules according to some set of conventions, which the user is supposed to keep when codifying the knowledge of his domain /4/.

We have used an experimental ES shell developed by Zsuzsa FARKAS (SzKI) having the following features.

It is an APES like shell, or more precisely it performs two of its functions:

- explanation trace (reasons for the achieved conclusion),
- user query (to collect missing information).

The main advantage of this system is that it performs only one level interpretation of the rules making optimum use of the MPROLOG interpreter. It talks in English to the user and the system has some useful devices to make the conversation more fluent. It puts the questions either in menu lists or one by one, in this latter case the valid answers are also available. The explanation trace starts if needed and follows the rule activations level by level.

4. A simple example session

The dialogue of a simple example session showing how our system actually gets to conclusion and gives its explanations is presented below. ("*", marking the user's answers, is the prompt of the shell. Our comments are emphasized in the text.).

For which object X is it true that water gets_to_the_foundation (X)?

- 1 water_flows_to_the_building
- 2 cracks_of_the_walls_are_at the_water_block
- 3 cracks_of_the_walls_are_at the_drainpipe
- 4 cracks_of_the_walls_are_at the_drain_gutter_defects
- 5 cracks_of_the_walls_are_at the_gutter_or_water_conduit_leading
through_the_wall
- 6 known_gutter_or_water_conduit_defects

```

7 water_consumption_raise
8 gutter_and_drainpipe_defects
9 corrosion_of_the_foundation
10 water_delivery_pressure_pipe_defect_discovered_at_the_foundation
11 gutter_break_discovered_at_the_foundation
12 drainpipe_break_discovered_at_the_foundation
13 water_of_unknown_origin_discovered_at_the_foundation

```

(We have chosen the first option.)

*1

For which object X is it true that ic(X)?

*0.1

(Let $I_c = 0.1$.)

damage_type(compaction) can be deduced

Do you need explanation?

*yes

(Here starts the explanation trace that describes how the conclusion could be or has been made using the facts and rules in the knowledge base.)

damage_type(compaction) \Leftarrow is deduced using the rule:

```

=====
damage_type(compaction) if
    (water_gets_to_the_foundation or ground_water_level_changes or soil_
     compression) and
    (consistency(X) and_greater_than_or_equal_to(soft, X) or compactness
     (Y) and_greater_than_or_equal_to(loose, Y)).
=====

```

showing the following conditions

- (1) water_gets_to_the_foundation(water_flows_to_the_building)
 - and
- (2) consistency(very_soft)
 - and
- (3) greater_than_or_equal_to(soft, very_soft)

(The rule printed in prolog format above is the same as the first member of the example set of rules presented in the 2nd section. The menu list following it contains the fulfilled conditions and the corresponding variable assignments of the rule that were sufficient to draw the conclusion.)

Continue?

*1

water_gets_to_the_foundation(water_flows_to_the_building) \Leftarrow was told by the user

(The previous answer of the system referring to a fact given by the user indicates the end of this branch of the deduction tree (see Fig. 1), so we continue on our explanation trace by backtracking to the preceeding level.)

Continue?

*parent

damage_type(compaction) \Leftarrow is deduced using the rule:

```
=====
damage_type(compaction) if
    (water_gets_to_the_foundation or ground_water_level_changes or soil_
     compression) and
    (consistency(X) and greater_than_or_equal_to(soft,X)
     or compactness(Y) and greater_than_or_equal_to(loose,Y)).
=====
```

showing the following conditions

- (1) water_gets_to_the_foundation(water_flows_to_the_building)
 - and
- (2) consistency(very_soft)
 - and
- (3) greater_than_or_equal_to(soft, very_soft)

Continue?

*2

consistency(very_soft) \Leftarrow is deduced using the rule:

```
=====
consistency(very_soft) if
    ic(X) and  $X < 0.25$ .
=====
```

(See example set of rules.)

showing the following conditions

- (1) ic(0.1)

Continue?

*1

ic(0.1) \Leftarrow was told by the user

Continue?

*parent

consistency(very_soft) \Leftarrow is deduced using the rule:

```
=====
consistency(very_soft) if
    ic(X) and  $X < 0.25$ .
=====
```

showing the following conditions

- (1) ic(0.1)

Continue?

*parent

damage_type(compaction) \Leftarrow is deduced using the rule:

```
=====
damage_type(compaction) if
  (water_gets_to_the_foundation or ground_water_level_changes or soil_
   compression) and
  (consistency(X) and greater_than_or_equal_to(soft, X)
   or compactness(Y) and greater_than_or_equal_to(loose,Y)).
=====
```

showing the following conditions

- (1) water_gets_to_the_foundation(water_flows_to_the_building)
 - and
- (2) consistency(very_soft)
 - and
- (3) greater_than_or_equal_to(soft, very_soft)

Continue?

*3

greater_than_or_equal_to(soft, very_soft) \Leftarrow is deduced using the rule:

```
=====
greater_than_or_equal_to(X,Y) if
  X  $\gg$  Z and greater_than_or_equal_to(Z,Y).
=====
```

(This is the definition of 'something is greater than or equal to something' to compare non-numerical objects.)

showing the following conditions

- (1) soft \gg very_soft
 - and
- (2) greater_than_or_equal_to(very_soft, very_soft)

Continue?

*1

soft \gg very_soft \Leftarrow is a fact

Continue?

*parent

greater_than_or_equal_to(soft, very_soft) \Leftarrow is deduced using the rule:

```
=====
greater_than_or_equal_to(X,Y) if
  X  $\gg$  Z and greater_than_or_equal_to(Z,Y).
=====
```

showing the following conditions

- (1) soft \gg very_soft
 - and
- (2) greater_than_or_equal_to(very_soft, very_soft)

Continue?

*2

greater_than_or_equal_to(very_soft, very_soft) \Leftarrow is a fact

Continue?

*parent

greater_than_or_equal_to(soft, very_soft) \Leftarrow is deduced using the rule:

```
=====
greater_than_or_equal_to(X,Y) if
    X  $\gg$  Z and greater_than_or_equal_to (Z,Y).
=====
```

showing the following conditions

- (1) soft \gg very_soft
 and
- (2) greater_than_or_equal_to(very_soft, very_soft)

Continue?

*parent

damage_type(compaction) \Leftarrow is deduced using the rule:

```
=====
damage_type(compaction) if
    (water_gets_to_the_foundation or ground_water_level_changes or soil_
    compression) and
    (consistency(X) and greater_than_or_equal_to(soft, X)
    or compactness(Y) and greater_than_or_equal_to(loose, Y)).
=====
```

showing the following conditions

- (1) water_gets_to_the_foundation(water_flows_to_the_building)
 and
- (2) consistency(very_soft)
 and
- (3) greater_than_or_equal_to(soft, very_soft)

Continue?

*end

 X = compaction

Continue (y/n)? .n

OK

:

REFERENCES

1. Rétháti, L.: "Building Failures of Soil Origin", (in Hungarian), Akadémiai Kiadó, Budapest 1977.
2. MPROLOG documentation Release 2.1, Logicware - SzKI, Sept. 1985.
3. Rédey, G., Holnapy, D., Zsidóné, Georgieva, P.: "Expert system Samples", (in Hungarian), Építéstudományi Intézet, Budapest 1986.
4. Jackson, P.: Introduction to Expert Systems, Addison - Wesley, Publishing Company, Wokingham, England, 1986.
5. Clocksin, W.F., Mellish, C.S.: Programming in Prolog, Springer-Verlag, Berlin-Heidelberg-New York, 1981.
6. ES Projects in Hungary in MPROLOG, Computer Research and Innovation Center (SzKI), Budapest 1986.

CALCULATION OF HYPERBOLIC PARABOLOID SEGMENTAL SHELL WITH PROTRUDING UNSUPPORTED EDGE

SAJTOS, I.*

(Received: 5 November 1987)

Membrane forces of a hyperbolic paraboloid segmental shell with protruding unsupported edge are given in a closed form in this work. Calculations have been made on the basis of Pucher's equilibrium differential equation defined in oblique co-ordinate system. A numerical example is given to compare the result of calculations with the solution resulting from the difference method.

Introduction

Among aesthetically attractive segmental shells (Fig. 1a), the most daring design is a shell with protruding unsupported edge and segments bent in two directions (Fig. 1b).

The membrane forces of such shells have been dealt with, among other authors, by Csonka /1/ who has found two solutions, one where the surface is determined for given load and given stress function and another where the solution applies to a shell segment designed as given translation surface (e.g. hyperbolic paraboloid shell) the force system being determined by use of the difference method.

Based on solution of the equilibrium differential equation system, a segmental shell with hyperbolic paraboloid mid surface has been built by Candela /7/. He used successive approximation to meet the boundary conditions.

This work deals with determination of the membrane forces of a hyperbolic paraboloid segmental shell with protruding unsupported edge. Calculations are made on the basis of Pucher's equilibrium differential equation defined in oblique co-ordinate system. A numerical example is used to compare the result obtained and the solution obtainable by means of the difference method.

*Sajtos, István, H-1035 Budapest, Vörösvári u. 27. X. 29.

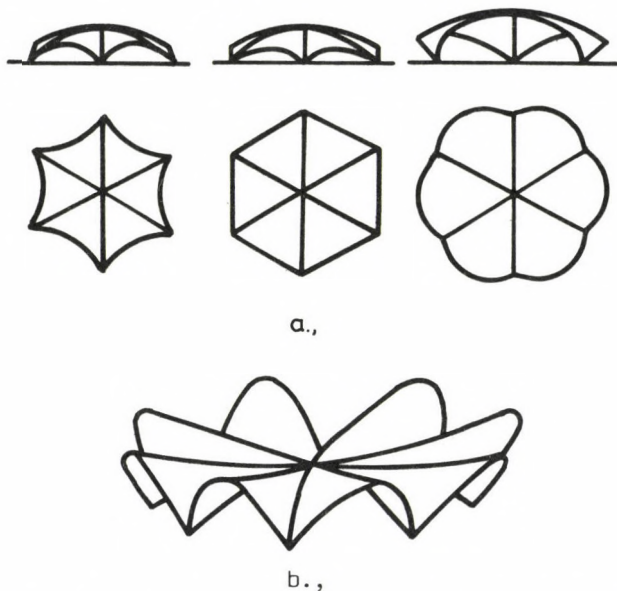


Fig. 1. a) Segmental shells; b) Segmental shell with segments bent in two directions and with a protruding unsupported edge

Assumptions, conditions

The basic assumptions of the membrane theory have been adopted in calculations [1/, [2/, [3/.

The mid surface of the shell is a hyperbolic paraboloid described in Cartesian co-ordinate system xyz by equation (Fig. 2)

$$z = Ax^2 - By^2 \quad (1)$$

where

$$A = \frac{f_1}{a^2}, \quad B = \frac{f_2}{b^2} \quad (2a,b)$$

The geometry of the projection of a shell segment is determined by two radial straight lines and a parabolic arc at the unsupported edge (Fig. 2).

The segment is supported rigidly along the straight edges while unsupported along the parabolic arc. Equation of the projection of the unsupported edge:

$$y = D - Ex^2, \quad (3)$$

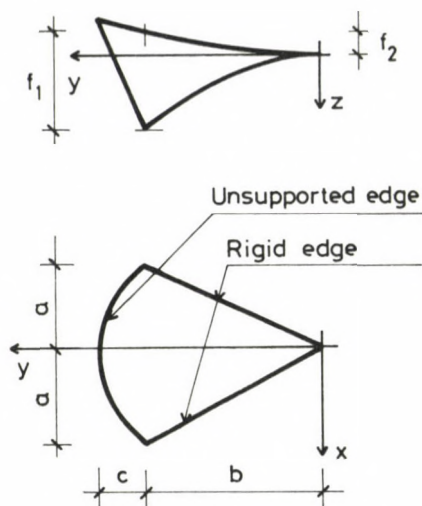


Fig. 2. Geometrical specifications of a shell segment

where

$$D = b + c, \quad E = \frac{c}{a^2}. \quad (4a,b)$$

Only vertical loads (in the direction of axis z) have been taken into consideration in calculations.

Possible solutions

The sectional forces can be obtained by solution of Pucher's equilibrium differential equation.

Shape of the equilibrium differential equation in the Cartesian coordinate system:

$$\frac{\partial^2 z}{\partial y^2} \frac{\partial^2 F}{\partial x^2} - 2 \frac{\partial^2 z}{\partial x \partial y} \frac{\partial^2 F}{\partial x \partial y} + \frac{\partial^2 z}{\partial x^2} \frac{\partial^2 F}{\partial y^2} = -g \quad (5)$$

where $z = z(x, y)$ equation of the mid surface

$F = F(x, y)$ stress function

$g = g(x, y)$ intensity of vertical loads relative to the baseplane.

Simple integration can be used to resolve the differential equation provided (5) can be transformed into

$$\frac{\partial^2 F}{\partial u \partial v} = -Z/u, v/ \quad (6)$$

by co-ordinate transformation,

where u and v are new variables while

$Z(u,v)$ is the load function obtained after transformation.

Transformation is possible in two ways.

1) As is well known, it is possible to assign to a two-variable quasi-linear partial differential equation of the second order according to (5) an ordinary differential equation /8/, /9/

$$\frac{\partial^2 z}{\partial y^2} dy^2 - 2 \frac{\partial^2 z}{\partial x \partial y} dx dy + \frac{\partial^2 z}{\partial x^2} dx^2 = 0, \quad (7)$$

the solutions of which giving the characteristics of the equation.

In case of a hyperbolic differential equation, there exist two real groups of characteristics. (In case of a hyperbolic paraboloid mid surface, partial differential equation (5) is hyperbolic.)

By means of the characteristics, it is possible to write the differential equation (5) in a canonical form. In the hyperbolic case this will be e.g.

$$\frac{\partial^2 F}{\partial u \partial v} = -Z(u,v), \quad (8)$$

obtained by introduction of new variable u and v .

2) Another possible method is to define the mid surface of the shell in an oblique co-ordinate system uvz resulting in

$$\frac{\partial^2 z}{\partial u^2} = 0, \quad \frac{\partial^2 z}{\partial v^2} = 0. \quad (9a,b)$$

Now also the Pucher equilibrium differential equation shall be defined in this oblique co-ordinate system. The equation will then be /5/, /6/, /7/ (Fig. 3):

$$\frac{\partial^2 z}{\partial u^2} \frac{\partial^2 F}{\partial v^2} - 2 \frac{\partial^2 z}{\partial u \partial v} \frac{\partial^2 F}{\partial u \partial v} + \frac{\partial^2 z}{\partial v^2} \frac{\partial^2 F}{\partial u^2} = -g \cdot \sin \omega, \quad (10)$$

where $z = z(u,v)$ equation of the mid surface in co-ordinate system uvz
 ω angle included by axes u and v
 $F = F(u,v)$ unknown stress function

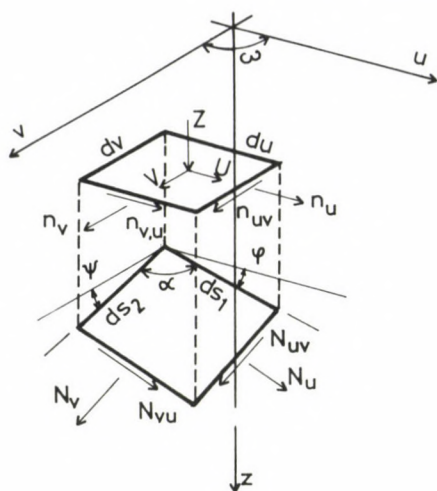


Fig. 3. Definition of sectional forces in oblique co-ordinate system uvz

$g = g(u, v)$ vertical load intensity function parallel to axis z in co-ordinate system uvz , relative to the baseplane.

Because of conditions (9a,b), equation (10) will take the following shape:

$$-2 \frac{\partial^2 z}{\partial u \partial v} \frac{\partial^2 F}{\partial u \partial v} = -g \sin \omega. \quad (11)$$

The second way is adopted in this work.

Transformation of the mid surface of the shell

Transformation includes rotation of axes x, y in their own plane around the origin through angle φ and change of the angle included by them (90°) into angle ω ($\omega \neq 90^\circ$) (Fig. 4).

The relationship between co-ordinate systems uv and xy is described by the following equations:

$$x = u' \cos \varphi - v' \sin \varphi, \quad (12a)$$

$$y = u' \sin \varphi + v' \cos \varphi, \quad (12b)$$

where

$$u' = u + v \cos \omega, \quad (13a)$$

$$v' = v \sin \omega. \quad (13b)$$

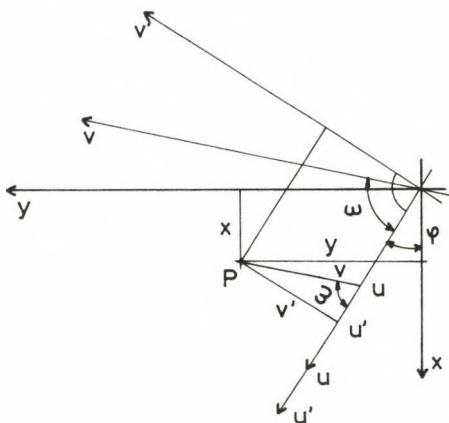


Fig. 4. Relationship between co-ordinate systems uv and xy

Substituting this into (1) by use of conditions (9a,b),

$$\operatorname{tg} \varphi = \sqrt{\frac{A}{B}} \quad (14)$$

and

$$\omega = \pi - 2\varphi \quad (15)$$

are obtained (only one of the possible values of angle φ has been taken into consideration).

Then, with (12), (13), (14), (15) substituted into (1), the equation of the mid surface of the shell will be obtained in the new co-ordinate system uvz as

$$z = r \cdot uv \quad (16)$$

where

$$r = -2(A \cos^2 \varphi + B \sin^2 \varphi) \quad (17)$$

In the new co-ordinate system, the equation of the unsupported edge is obtained by substitution of (12), (13), (14), (15) into (3):

$$u_b = \frac{(2vE \cos^2 \varphi - \sin \varphi) \pm \sqrt{(\sin \varphi - 2vE \cos^2 \varphi)^2 - 4E \cos^2 \varphi (v \sin \varphi + v^2 E \cos^2 \varphi - D)}}{2E \cos^2 \varphi}, \quad (18a)$$

$$v_b = \frac{(2uE \cos^2 \varphi - \sin \varphi) \pm \sqrt{(\sin \varphi - 2uE \cos^2 \varphi)^2 - 4E \cos^2 \varphi (u \sin \varphi + u^2 E \cos^2 \varphi - D)}}{2E \cos^2 \varphi}. \quad (18b)$$

It is only the positive (+) sign that has a meaning in the above expressions if $\varphi > \alpha$ (Fig. 5).

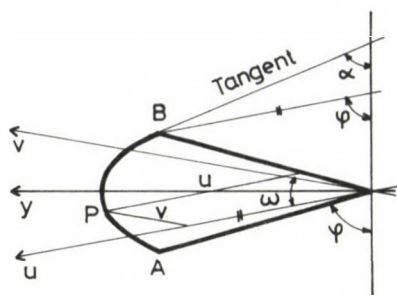


Fig. 5.

In this case, only one value v is associated with each value u because straight lines $v = \text{const.}$ and the parabola have one intersection along arc \widehat{AB} if the value of v varies between v_A and v_B . The same applies also to variable u .

Condition $\varphi > \alpha$ shall be satisfied so that the membrane state of the shell segment will be existing and unanimous [4], [8].

The unsupported edge shall be such as to intersect each characteristic at only one point as otherwise no membrane state of the shell could exist (Fig. 6).

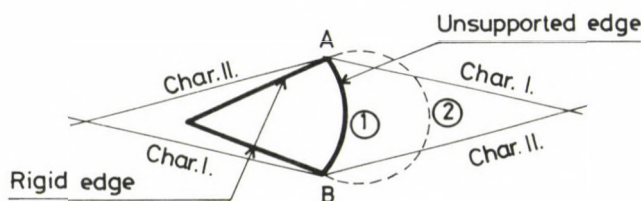


Fig. 6. Rule of plotting of the geometry of the unsupported edge

Relation between sectional forces in oblique and Cartesian co-ordinate system

The relationships between sectional forces in oblique and Cartesian co-ordinate system are well known [2], [6], [7] and the same relationships are applied to reduced sectional forces in the present case (Fig. 7).

The following results are obtained:

$$n_x = \frac{1}{2 \operatorname{tg} \varphi} (n_u + n_v - 2 n_{uv}) , \quad (19a)$$

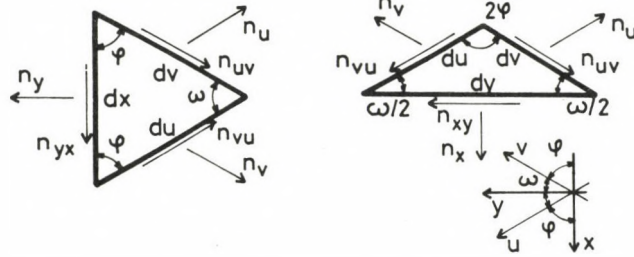


Fig. 7. Relation between sectional forces in oblique and Cartesian co-ordinate system

$$n_y = \frac{\operatorname{tg} \varphi}{2} (n_u + n_v + 2 n_{uv}) \quad , \quad (19b)$$

$$n_{xy} = \frac{n_u - n_v}{2} \quad . \quad (19c)$$

Determination of sectional forces

Taking into consideration (11) and (16), Pucher's differential equation can be written, as follows:

$$- 2r \frac{\partial^2 F}{\partial u \partial v} = - g(u, v) \sin \omega \quad . \quad (20)$$

Of this equation, the stress function can be obtained by integration:

$$F = - \frac{1}{2r} \sin \omega \iint (- g(u, v)) du dv + C_1(u) + C_2(v) \quad . \quad (21)$$

The reduced sectional forces can be calculated in the knowledge of the stress function /1/, /2/, /3/, /5/, /6/:

$$n_{uv} = - \frac{\partial^2 F}{\partial u \partial v} = \frac{1}{2r} (- g(u, v)) \sin \omega \quad , \quad (22a)$$

$$n_u = \frac{\partial^2 F}{\partial v^2} \quad , \quad (22b)$$

$$n_v = \frac{\partial^2 F}{\partial u^2} \quad (22c)$$

Boundary conditions can be stipulated along the unsupported edge /1/. After their transformation, conditions

$$\frac{\partial F}{\partial u} = 0 \quad , \quad \text{if} \quad v = v_b(u) \quad , \quad (23a)$$

and

$$\frac{\partial F}{\partial v} = 0 \quad , \quad \text{if} \quad u = u_b(v) \quad . \quad (23b)$$

are obtained.

Required for calculation are also the derivatives of functions (18a), (18b) describing the unsupported edge:

$$u'_b = \frac{du_b}{dv} = 1 - \frac{2 \sin \varphi}{\sqrt{(\sin \varphi - 2vE\cos^2 \varphi)^2 - 4E\cos^2 \varphi (v\sin \varphi + v^2E\cos^2 \varphi - D)}} \quad , \quad (24a)$$

$$v'_b = \frac{dv_b}{du} = 1 - \frac{2 \sin \varphi}{\sqrt{(\sin \varphi - 2uE\cos^2 \varphi)^2 - 4E\cos^2 \varphi (u\sin \varphi + u^2E\cos^2 \varphi - D)}} \quad . \quad (24b)$$

The actual sectional forces can be calculated in the known way after both oblique and, as a result of transformation, Cartesian co-ordinate system /1/, /2/, /3/, /5/, /6/.

To produce stress function (21) directly would be a rather tiresome job while the reduced sectional forces can be relatively simply calculated.

Stress function (21) takes the following shape:

$$F = F_{1(u,v)} + C_{1(u)} + C_{2(v)} \quad . \quad (25)$$

Quantities $\partial C_1 / \partial u$ and $\partial C_2 / \partial v$ can be calculated from conditions (23),

$$\frac{\partial F_{1(u,v_b)}}{\partial u} + \frac{\partial C_{1(u)}}{\partial u} = 0 \quad , \quad (26a)$$

$$\frac{\partial F_{1(u_b,v)}}{\partial v} + \frac{\partial C_{2(v)}}{\partial v} = 0 \quad , \quad (26b)$$

and by means of these quantities, also expressions $\partial^2 c_1 / \partial u^2$ and $\partial^2 c_2 / \partial v^2$ can be obtained. In the knowledge of the derivatives of integration constants, the reduced sectional forces can be calculated on the basis of (22):

$$n_u = \frac{\partial^2 F_{1(u,v)}}{\partial v^2} + \frac{\partial^2 c_{2(v)}}{\partial v^2} \quad , \quad (27a)$$

$$n_v = \frac{\partial^2 F_{1(u,v)}}{\partial u^2} + \frac{\partial^2 c_{1(u)}}{\partial u^2} \quad (27b)$$

n_{uv} being obtainable on the basis of (22a).

Sectional forces

1. In case of uniformly distributed load

Load function:

$$g(x,y) = g(u,v) = p = \text{const.} \quad (28a)$$

Using (21), (22), (27), the reduced sectional forces are obtained as

$$n_{uv} = -\frac{1}{2r} p \sin 2\varphi \quad , \quad (28b)$$

$$n_u = -\frac{1}{2r} p \sin 2\varphi \cdot u'_b \quad , \quad (28c)$$

$$n_v = -\frac{1}{2r} p \sin 2\varphi \cdot v'_b \quad (28d)$$

2. In case of arbitrary load

A polynomial is used to approximate the load function. In the Cartesian co-ordinate system, the polynomial takes the following shape:

$$\begin{aligned} g(x,y) = & p + p_1 x + p_2 y + p_3 x^2 + p_4 xy + p_5 y^2 + p_6 x^3 + p_7 x^2 y + p_8 xy^2 + \\ & + p_9 y^3 + p_{10} x^4 + p_{11} x^3 y + p_{12} x^2 y^2 + p_{13} xy^3 + p_{14} y^4 + \dots \end{aligned} \quad (29)$$

Transformation of the load function is carried out term by term, the sectional forces associated with the different terms of the load function being obtained in the following way, making use of (21), (22), (27):

$$g_1(x, y) = p_1 x, \quad g_1(u, v) = p_1 \cos \varphi (u - v), \quad (30a)$$

$$n_{uv} = -\frac{1}{2r} p_1 \cos \varphi \sin 2\varphi (u - v), \quad (30b)$$

$$n_u = \frac{1}{2r} p_1 \cos \varphi \sin 2\varphi [-u - (u_b u'_b - u'_b v - u_b)] , \quad (30c)$$

$$n_v = \frac{1}{2r} p_1 \cos \varphi \sin 2\varphi [v - (v_b + uv'_b - v_b v'_b)] . \quad (30d)$$

$$g_2(x, y) = p_2 y, \quad g_2(u, v) = p_2 \sin \varphi (u + v), \quad (31a)$$

$$n_{uv} = -\frac{1}{2r} p_2 \sin \varphi \sin 2\varphi (u + v), \quad (31b)$$

$$n_u = \frac{1}{2r} p_2 \sin \varphi \sin 2\varphi [u - (u_b u'_b + u'_b v + u_b)] , \quad (31c)$$

$$n_v = \frac{1}{2r} p_2 \sin \varphi \sin 2\varphi [v - (v_b + uv'_b + v_b v'_b)] . \quad (31d)$$

$$g_3(x, y) = p_3 x^2, \quad g_3(u, v) = p_3 \cos^2 \varphi (u^2 - 2uv + v^2), \quad (32a)$$

$$n_{uv} = -\frac{1}{2r} p_3 \cos^2 \varphi \sin 2\varphi (u^2 - 2uv + v^2), \quad (32b)$$

$$n_u = \frac{1}{2r} p_3 \cos^2 \varphi \sin 2\varphi \left\{ -u^2 + 2uv - [3u_b^2 u'_b - (2u_b u'_b v + u_b^2) + u'_b v^2 + 2u_b v] \right\}, \quad (32c)$$

$$n_v = \frac{1}{2r} p_3 \cos^2 \varphi \sin 2\varphi \left\{ -v^2 + 2uv - [2uv_b + u^2 v'_b - (v_b^2 + 2uv_b v'_b) + 3v_b^2 v'_b] \right\}. \quad (32d)$$

$$g_4(x, y) = p_4 xy, \quad g_4(u, v) = p_4 \sin \varphi \cos \varphi (u^2 - v^2), \quad (33a)$$

$$n_{uv} = -\frac{1}{2r} p_4 \sin \varphi \cos \varphi \sin 2\varphi (u^2 - v^2), \quad (33b)$$

$$n_u = \frac{1}{2r} p_4 \sin \varphi \cos \varphi \sin 2\varphi [-2uv - (u_b^2 u'_b - u'_b v^2 - 2u_b v)] , \quad (33c)$$

$$n_v = \frac{1}{2r} p_4 \sin \varphi \cos \varphi \sin 2\varphi [2uv - (2uv_b + u^2 v'_b - v_b^2 v'_b)] . \quad (33d)$$

$$g_5(x, y) = p_5 y^2, \quad g_5(u, v) = p_5 \sin^2 \varphi (u^2 + 2uv + v^2), \quad (34a)$$

$$\eta_{uv} = -\frac{1}{2r} p_5 \sin^2 \varphi \sin 2\varphi (u^2 + 2uv + v^2), \quad (34b)$$

$$\eta_u = \frac{1}{2r} p_5 \sin^2 \varphi \sin 2\varphi \left[u^2 + 2uv - (3u_b^2 u_b' + 2u_b u_b' v + u_b^2 + u_b' v^2 + 2u_b v) \right], \quad (34c)$$

$$\eta_v = \frac{1}{2r} p_5 \sin^2 \varphi \sin 2\varphi \left[v^2 + 2uv - (2uv_b + u_b^2 v_b' + v_b^2 + 2uv_b v_b' + 3v_b^2 v_b') \right]. \quad (34d)$$

$$g_6(x, y) = p_6 x^3, \quad g_6(u, v) = p_6 \cos^3 \varphi (u-v)^3, \quad (35a)$$

$$\eta_{uv} = -\frac{1}{2r} p_6 \cos^3 \varphi \sin 2\varphi (u-v)^3, \quad (35b)$$

$$\eta_u = \frac{1}{2r} p_6 \cos^3 \varphi \sin 2\varphi \left\{ -u^3 + 3u^2 v - 3uv^2 - [u_b^3 u_b' - (3u_b^2 u_b' v + u_b^3) + 3(u_b u_b' v^2 + u_b^2 v) - (u_b' v^3 + 3u_b v^2)] \right\}, \quad (35c)$$

$$\eta_v = \frac{1}{2r} p_6 \cos^3 \varphi \sin 2\varphi \left\{ 3u^2 v - 3uv^2 + v^3 - [3u^2 v_b + u_b^3 v_b' - 3(uv_b^2 + u^2 v_b v_b') + v_b^3 + 3uv_b^2 v_b' - v_b^3 v_b'] \right\}. \quad (35d)$$

$$g_7(x, y) = p_7 x^2 y, \quad g_7(u, v) = p_7 \sin \varphi \cos^2 \varphi (u^3 - uv^2 - u^2 v + v^3), \quad (36a)$$

$$\eta_{uv} = -\frac{1}{2r} p_7 \sin \varphi \cos^2 \varphi \sin 2\varphi (u^3 - uv^2 - u^2 v + v^3), \quad (36b)$$

$$\eta_u = \frac{1}{2r} p_7 \sin \varphi \cos^2 \varphi \sin 2\varphi \left\{ -u^2 v - \frac{u^3}{3} + 3uv^2 - [u_b^3 u_b' - u_b u_b' v^2 + u_b^2 v - \frac{1}{3} (3u_b^2 u_b' v + u_b^3) + u_b' v^3 + 3u_b v^2] \right\}, \quad (36c)$$

$$\eta_v = \frac{1}{2r} p_7 \sin \varphi \cos^2 \varphi \sin 2\varphi \left\{ 3u^2 v - \frac{v^3}{3} - uv^2 - [3u^2 v_b + u_b^3 v_b' - \frac{1}{3} (uv_b^3 + 3uv_b^2 v_b') - uv_b^2 - u_b^2 v_b v_b' + v_b^3 v_b'] \right\}. \quad (36d)$$

$$g_8(x, y) = p_8 xy^2, \quad g_8(u, v) = p_8 \sin^2 \varphi \cos \varphi (u^3 - uv^2 + u^2 v - v^3), \quad (37a)$$

$$\eta_{uv} = -\frac{1}{2r} p_8 \sin^2 \varphi \cos \varphi \sin 2\varphi (u^3 - uv^2 + u^2 v - v^3), \quad (37b)$$

$$\eta_u = \frac{1}{2r} p_8 \sin^2 \varphi \cos \varphi \sin 2\varphi \left\{ -u^2 v + \frac{u^3}{3} - 3uv^2 - [u_b^3 u_b' - u_b u_b' v^2 - u_b^2 v + \frac{1}{3} (3u_b^2 u_b' v + u_b^3) - u_b' v^3 - 3u_b v^2] \right\}, \quad (37c)$$

$$n_v = \frac{1}{2r} p_8 \sin^2 \varphi \cos \varphi \sin 2\varphi \left\{ 3u^2 v - \frac{v^3}{3} + uv^2 - [3u^2 v_b + u^3 v_b' - \right. \\ \left. - \frac{1}{3} (uv_b^3 + 3uv_b^2 v_b') + uv_b^2 + u^2 v_b v_b' - v_b^3 v_b'] \right\} . \quad (37d)$$

$$g_9(x, y) = p_9 y^3 , \quad g_9(u, v) = p_9 \sin^3 \varphi (u+v)^3 \quad (38a)$$

$$n_{uv} = -\frac{1}{2r} p_9 \sin^3 \varphi \sin 2\varphi (u+v)^3 , \quad (38b)$$

$$n_u = \frac{1}{2r} p_9 \sin^3 \varphi \sin 2\varphi \left\{ u^3 + 3u^2 v + 3uv^2 - [u_b^3 u_b' + (3u_b^2 u_b' v + u_b^3) + \right. \\ \left. + 3(u_b u_b' v^2 + u_b^2 v) + (u_b' v^3 + 3u_b v^2)] \right\} , \quad (38c)$$

$$n_v = \frac{1}{2r} p_9 \sin^3 \varphi \sin 2\varphi \left\{ 3u^2 v + 3uv^2 + v^3 - [3u^2 v_b + u^3 v_b' + 3(uv_b^2 + u^2 v_b v_b') + \right. \\ \left. + v_b^3 + 3uv_b^2 v_b' + v_b^3 v_b'] \right\} . \quad (38d)$$

$$g_{10}(x, y) = p_{10} x^4 , \quad g_{10}(u, v) = p_{10} \cos^4 \varphi (u-v)^4 , \quad (39a)$$

$$n_{uv} = -\frac{1}{2r} p_{10} \cos^4 \varphi \sin 2\varphi (u-v)^4 , \quad (39b)$$

$$n_u = \frac{1}{2r} p_{10} \cos^4 \varphi \sin 2\varphi \left\{ -u^4 + 4u^3 v - 6u^2 v^2 + 4uv^3 - [u_b^4 u_b' - 4u_b^3 u_b' v - u_b^4 + \right. \\ \left. + 2(3u_b^3 u_b' v^2 + 2u_b^3 v) - 2(2u_b u_b' v^3 + 3u_b^2 v^2) + u_b' v^4 + 4u_b v^3] \right\} , \quad (39c)$$

$$n_v = \frac{1}{2r} p_{10} \cos^4 \varphi \sin 2\varphi \left\{ 4u^3 v - 6u^2 v^2 + 4uv^3 - v^4 - [4u^3 v_b + u^4 v_b' - \right. \\ \left. - 2(3u^2 v_b^2 + 2u^3 v_b v_b') + 2(2uv_b^3 + 3u^2 v_b^2 v_b') - (v_b^4 + 4uv_b^3 v_b') + v_b^4 v_b'] \right\} . \quad (39d)$$

$$g_{11}(x, y) = p_{11} x^3 y , \quad g_{11}(u, v) = p_{11} \sin \varphi \cos^3 \varphi (u-v)^3 (u+v) , \quad (40a)$$

$$n_{uv} = -\frac{1}{2r} p_{11} \sin \varphi \cos^3 \varphi \sin 2\varphi (u-v)^3 (u+v) , \quad (40b)$$

$$n_u = \frac{1}{2r} p_{11} \sin \varphi \cos^3 \varphi \sin 2\varphi \left\{ -\frac{1}{2} u^4 + 3u^2 v^2 - 4uv^3 - [u_b^4 u_b' - \right. \\ \left. - \frac{1}{2} (4u_b^3 u_b' v + u_b^4) + 2u_b u_b' v^3 + 3u_b^2 v^2 - (u_b' v^4 + 4u_b v^3)] \right\} , \quad (40c)$$

$$\begin{aligned} n_v = \frac{1}{2r} p_{11} \sin \varphi \cos^3 \varphi \sin 2\varphi \left\{ 4u^3 v - 3u^2 v^2 + \frac{1}{2} v^4 - [4u^3 v_b + u^4 v_b' - \right. \\ \left. - (3u^2 v_b^2 + 2u^3 v_b v_b') + \frac{1}{2} (v_b^4 + 4uv_b^3 v_b') - v_b^4 v_b'] \right\}. \end{aligned} \quad (40d)$$

$$g_{12}(x, y) = p_{12} x^2 y^2, \quad g_{12}(u, v) = p_{12} \sin^2 \varphi \cos^2 \varphi (u-v)^2 (u+v)^2, \quad (41a)$$

$$n_{uv} = -\frac{1}{2r} p_{12} \sin^2 \varphi \cos^2 \varphi \sin 2\varphi (u-v)^2 (u+v)^2, \quad (41b)$$

$$\begin{aligned} n_u = \frac{1}{2r} p_{12} \sin^2 \varphi \cos^2 \varphi \sin 2\varphi \left\{ -\frac{4}{3} u^3 v + 4v^3 u - [u_b^4 u_b' - \right. \\ \left. - \frac{2}{3} (3u_b^2 u_b' v^2 + 2u_b^3 v) + 4u_b v^3 + u_b' v^4] \right\}, \end{aligned} \quad (41c)$$

$$\begin{aligned} n_v = \frac{1}{2r} p_{12} \sin^2 \varphi \cos^2 \varphi \sin 2\varphi \left\{ 4u^3 v - \frac{4}{3} uv^3 - [4u^3 v_b + u^4 v_b' - \right. \\ \left. - \frac{2}{3} (2uv_b^3 + 3u^2 v_b^2 v_b') + v_b^4 v_b'] \right\}. \end{aligned} \quad (41d)$$

$$g_{13}(x, y) = p_{13} xy^3, \quad g_{13}(u, v) = p_{13} \sin^3 \varphi \cos \varphi (u-v)(u+v)^3, \quad (42a)$$

$$n_{uv} = -\frac{1}{2r} p_{13} \sin^3 \varphi \cos \varphi \sin 2\varphi (u-v)(u+v)^3, \quad (42b)$$

$$\begin{aligned} n_u = \frac{1}{2r} p_{13} \sin^3 \varphi \cos \varphi \sin 2\varphi \left\{ \frac{u^4}{2} - 3u^2 v^2 - 4uv^3 - [u_b^4 u_b' + \frac{1}{2} (4u_b^3 u_b' v + u_b^4) - \right. \\ \left. - 2u_b u_b' v^3 - 3u_b^2 v^2 - u_b' v^4 - 4u_b v^3] \right\}, \end{aligned} \quad (42c)$$

$$\begin{aligned} n_v = \frac{1}{2r} p_{13} \sin^3 \varphi \cos \varphi \sin 2\varphi \left\{ 4u^3 v + 3u^2 v^2 - \frac{v^4}{2} - [4u^3 v_b + u^4 v_b' + 3u^2 v_b^2 + \right. \\ \left. + 2u^3 v_b v_b' - \frac{1}{2} (v_b^4 + 4uv_b^3 v_b') - v_b^4 v_b'] \right\}. \end{aligned} \quad (42d)$$

$$g_{14}(x, y) = p_{14} y^4, \quad g_{14}(u, v) = p_{14} \sin^4 \varphi (u+v)^4, \quad (43a)$$

$$n_{uv} = -\frac{1}{2r} p_{14} \sin^4 \varphi \sin 2\varphi (u+v)^4, \quad (43b)$$

$$\begin{aligned} n_u = \frac{1}{2r} p_{14} \sin^4 \varphi \sin 2\varphi \left\{ u^4 + 4u^3 v + 6u^2 v^2 + 4uv^3 - [u_b^4 u_b' + 4u_b^3 u_b' v + u_b^4 + \right. \\ \left. + 2(3u_b^2 u_b' v^2 + 2u_b^3 v) + 2(2u_b u_b' v^3 + 3u_b^2 v^2) + u_b' v^4 + 4u_b v^3] \right\}, \end{aligned} \quad (43c)$$

$$n_v = \frac{1}{2r} p_{14} \sin^4 \varphi \sin 2\varphi \left\{ 4u^3 v + 6u^2 v^2 + 4uv^3 + v^4 - [4u^3 v_b + u^4 v_b' + \right. \\ \left. + 2(3u^2 v_b^2 + 2u^3 v_b v_b') + 2(2uv_b^3 + 3u^2 v_b^2 v_b') + v_b^4 + 4uv_b^3 v_b' + v_b^4 v_b'] \right\} . \quad (43d)$$

Numerical example

Let the equation of the surface be (Fig. 8)

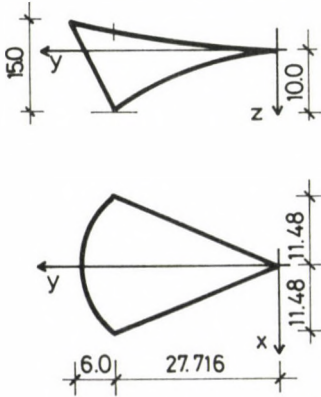


Fig. 8. Numerical example

$$z = 0.1015 x^2 - 4.3984 \cdot 10^{-3} y^2$$

while the equation of the projection of the unsupported edge

$$y = 33.716 - 0.0455 x^2 ,$$

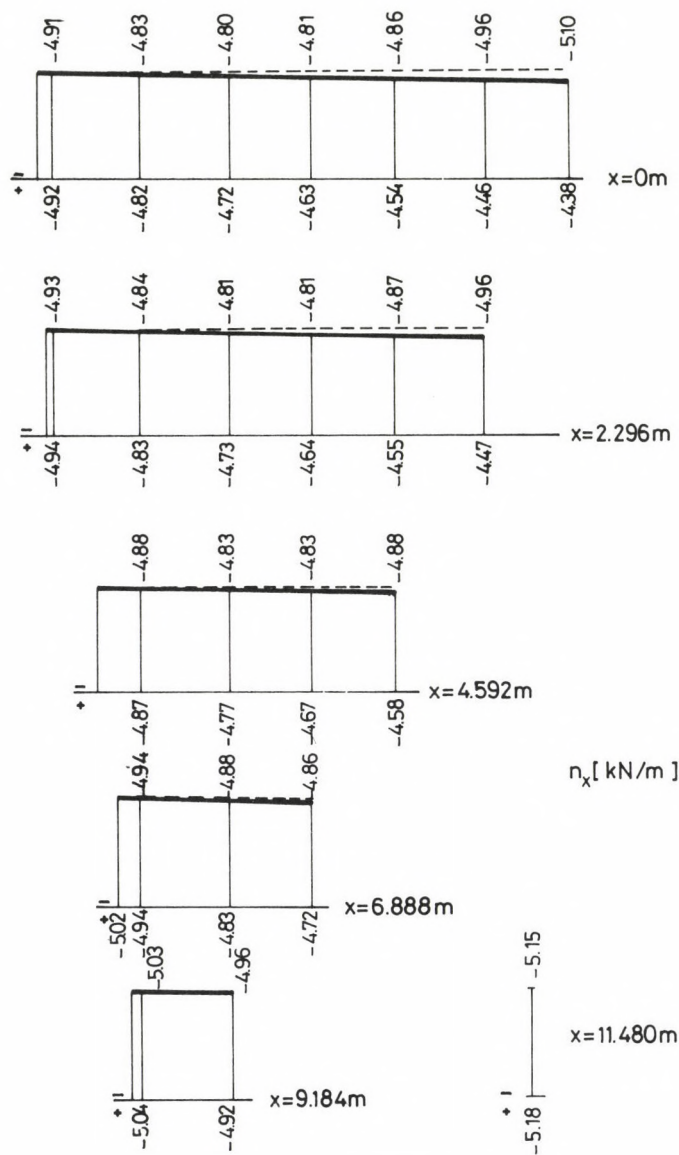
the load being uniformly distributed:

$$p = 1.0 \text{ kN/m}^2 .$$

Quantities required for calculation:

$$\begin{aligned} A &= 0.1015, \\ B &= 4.3984 \cdot 10^{-3}, \\ D &= 33.716 \text{ m}, \\ E &= 0.0455 \text{ m}^{-1}, \\ \varphi &= 1.3655 \text{ rad}, \\ r &= -0.01686 . \end{aligned}$$

The reduced sectional forces can be seen in Figs 9a, b, c.



a.,

Fig. 9a.

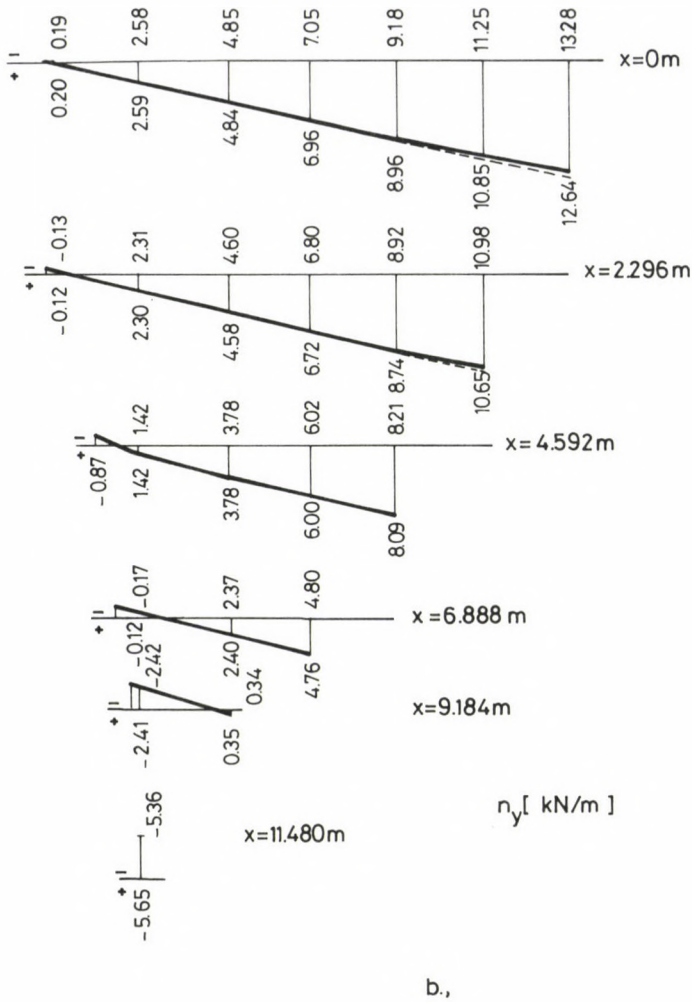


Fig. 9b.

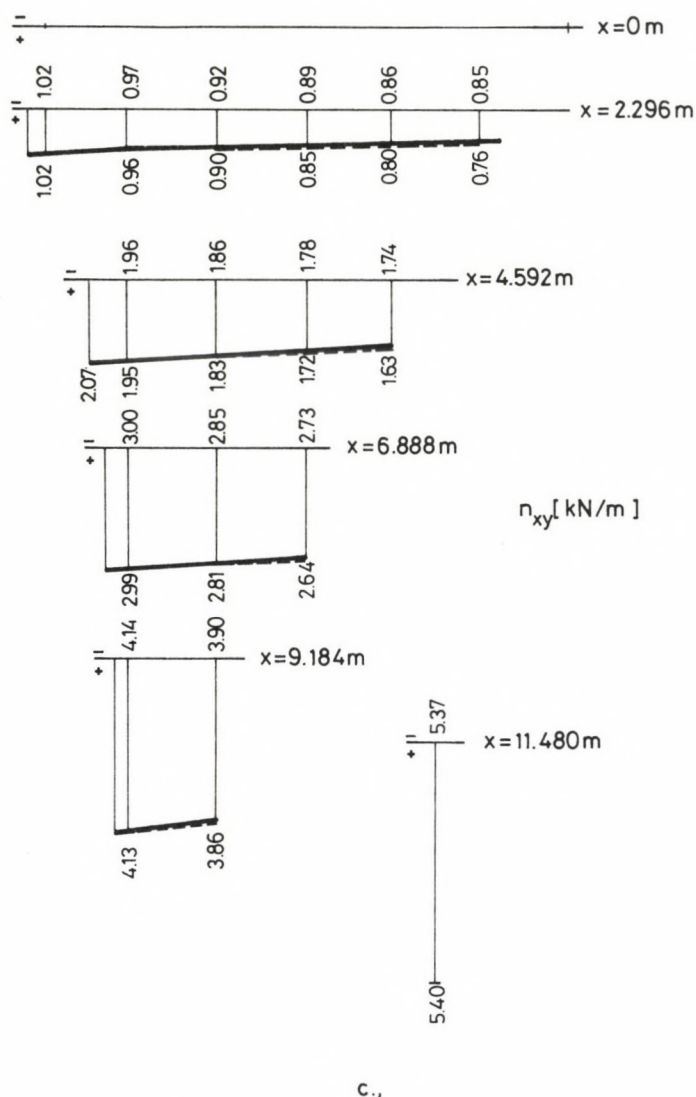


Fig. 9. Reduced sectional forces of the shell

— analytical method
 - - - - - difference method

Let the calculated sectional forces be compared with sectional forces determined on the basis of the difference method according to /1/.

Agreement between the difference method and the analytical method can be clearly seen in Figs 9a, b, c.

A deviation between both methods becomes appreciable towards the centre of the shell. This can be attributed to the fact that, in the difference method, the values calculated previously have been taken as a basis for determination of the sectional forces at the different points from the edge towards the centre and thus the inaccuracy of calculation is cumulative.

Inaccuracy may result also from interpolation to be used to determine the values of the stress function along the edge in case of the difference method as the points of division and the edge are not always coincident.

Let a point of the edge be investigated to see whether or not the boundary condition is satisfied.

Let the co-ordinates of the selected point of the edge be $x = 5.74$ m and $y = 32.217$ m. At this point, the reduced sectional forces are $n_x = -4.99$ kN/m, $n_y = -1.37$ kN/m, $n_{xy} = 2.6$ kN/m, the reduced principal sectional forces and their direction being

$$n_{1,2} = \frac{n_x + n_y}{2} \pm \sqrt{\left(\frac{n_x - n_y}{2}\right)^2 + n_{xy}^2},$$

$$\operatorname{tg} 2 \alpha_0 = \frac{2n_{xy}}{n_x - n_y},$$

$$n_{1,2} = \frac{-4.99 - 1.37}{2} \pm \sqrt{\left(\frac{-4.99 + 1.37}{2}\right)^2 + 2.6^2},$$

$$n_1 = 0,$$

$$n_2 = -6.34 \text{ kN/m},$$

$$\operatorname{tg} 2 \alpha_0 = \frac{2 \cdot 2.6}{-4.99 + 1.37} = -1.4364,$$

$$\alpha_0 = 62.422^\circ.$$

Angle of inclination of the tangent of the edge:

$$y' = -0.0910 \quad x = -0.0910 \cdot 5.74 = -0.52234$$

$$\beta = -27.578^{\circ}$$

$$\beta = \alpha_0 - 90^{\circ} = 62.422^{\circ} - 90^{\circ} = -27.578^{\circ} .$$

The boundary conditions are satisfied because n_1 is normal to the tangent of the edge and $n_1 = 0$, $n_{12} = 0$.

REFERENCES

1. Csonka, P.: Shell Structures (in Hungarian). Akadémiai Kiadó, Budapest, 1981
2. Flügge, W.: Stresses in Shells. Springer-Verlag, Göttingen, 1960
3. Bölcskei, E. - Orosz, A.: Reinforced Concrete Structures. Shells (in Hungarian). Tankönyvkiadó, Budapest, 1983
4. Tarnai, T.: On Existence and Uniqueness Conditions of the Membrane State of Shells. I. Hyperbolic Shells (in Hungarian). Műszaki Tudomány, 56 (1978), 19-47.
5. Kollár, L.: Beton Kalender 1984. Schalenkonstruktionen. Ernst & Sohn, Berlin, 1984
6. Polonyi, S.: Berechnung von hyperbolischen Paraboloidschalen über beliebigen Viereck Grundrissen. Beton und Stahlbetonbau, 9 (1962), 213-220.
7. Faber, C.: Candela The Shell Builder. Reinhold, New York, 1963
8. Korn, G.A. - Korn, T.M.: Mathematical Handbook for Engineers (in Hungarian). Műszaki Könyvkiadó, Budapest, 1975
9. Czách, L.: Partial Differential Equations (in Hungarian). Association of Hungarian Geophysicists, Budapest, 1969

KINEMATICAL INDETERMINACY OF A PAIR OF TETRAHEDRAL FRAMES

TARNAI, T.^{*} - MAKAI, E.^{**}

(Received: 12 January 1989)

In this paper the lack of structural rigidity, that is, the free infinitesimal movability of a both statically and kinematically indeterminate structure consisting of two equal regular tetrahedral frames is investigated. The structure is, in fact, a finite mechanism and its behaviour depends on the relative positions of the tetrahedra. Degrees of kinematic indeterminacy are determined and it is obtained that their value is changing during motion. A change in the degrees of kinematic indeterminacy refers to the existence of a bifurcation phenomenon in compatibility.

1. Introduction

To equilibrate given forces in space by six forces of given line of action, or what is the same, to determine reactions of a rigid body supported by six pin-ended bars, subjected to forces in space is one of the basic problems of elementary statics /1/. As is well-known it is, in general, uniquely soluble but there are "pathological" cases where this problem has no solution or has an infinity of solutions. In such a case the constraint (the structure) is both statically and kinematically indeterminate.

This paper presents a structure defining such a "pathological" case which, in spite of its simplicity, shows some additional properties which are not at all elementary.

The structure in question was invented by L. Tompos Jr, a second year undergraduate of the Hungarian Academy of Craft and Design in 1982. Its physical model consists of two equal regular tetrahedral frames which are fitted together in such a way that the bars of one of the frames touch from the outside those of the other. The six contacts constitute six bar-

^{*}Tarnai, Tibor, Hungarian Institute for Building Science, H-1113 Budapest, Dávid F. u. 6, Hungary

^{**}Makai, Endre, Mathematical Institute of the Hungarian Academy of Sciences, H-1364 Pf. 127 Budapest, Reáltanoda u. 13/15, Hungary

like constraints of degree one which are usually sufficient for preventing relative motions between two rigid bodies in space. Therefore, we would expect the pair of tetrahedral frames to be rigid. However, holding the physical model in our hands we may easily move one tetrahedron relative to the other, with the crossing bars sliding over each other. But we also find that during this motion the bars bend a little, because the cross sections of the bars have a finite diameter.

In order to avoid the effect of the thickness of the bars we consider an ideal structure whose bars have no thickness and draw all the diagonals of all the faces of a cube. In this way the edges of two regular tetrahedra are obtained (Fig. 1). This position of the tetrahedra is called

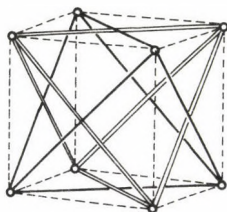


Fig. 1. Tompos' pair of tetrahedra

basic position. One of these tetrahedra is kept fixed and allow the other one to move. The only restriction is that

- (*) each pair of edges of both tetrahedra which were originally diagonals of the same face of the cube should still remain coplanar (i.e., intersect, are parallel or coincide).

The question is whether such motions are possible.

The motions admitted by the physical model - that is, where all the points of intersection of the corresponding edges of the tetrahedra are internal points of the edges - are called physically admissible motions. The motions not admitted by the physical model - that is, where some or all of the points of intersection of the straight lines of the corresponding edges of the tetrahedra are not internal points of the edges - are called physically inadmissible motions.

The aim of this paper is to describe the physically admissible infinitesimal motions of the pair of tetrahedra and to show what specific features they have in different positions. The physically inadmissible infinitesimal motions of the tetrahedra are investigated in a separate paper /2/, but the finite motions (both physically admissible and inadmissible) of the pair of tetrahedra are discussed in /3/. In this study the kinematic

analysis is executed in a statical way, but in Section 4 a direct kinematical investigation concerning infinitesimal motions is also presented. The primary aim is to determine the infinitesimal degrees of freedom, or with other words, degrees of kinematic indeterminacy.

2. Principle of the statical method

In order to distinguish the two tetrahedra let one of them be denoted by P and the other by Q. The edges of tetrahedra P and Q are drawn in the figures by double thin lines and single heavy lines, respectively. If tetrahedron P is rigidly attached to a foundation then tetrahedron P constitutes a constraint for tetrahedron Q. The constraint is such that the edges of P support the corresponding edges of Q, and the direction of any associated force (reaction) is perpendicular to the corresponding intersecting edges. Since a tetrahedron has six edges, the statical problem that can be formulated for the tetrahedron Q is one that is mentioned in the Introduction: to equilibrate given forces in space by six forces of given line of action.

Equilibrium of tetrahedron Q can be written by a system of linear equations whose coefficient matrix (which is denoted by \tilde{G}^T) is a square matrix of order 6. (\tilde{G} is the geometric or compatibility matrix and \tilde{G}^T is known as the equilibrium matrix where superscript T is the symbol of transposition.) It is known /4,5/ that if \tilde{G} is a square matrix then the degree of kinematic indeterminacy, i.e., the infinitesimal degree of freedom (which is denoted by f) is equal to the degree of static indeterminacy, i.e., the number of independent states of self-stress; and

$$f = \nu(\tilde{G}) = \nu(\tilde{G}^T)$$

where ν denotes the nullity of the matrix. (Nullity is defined as the difference between the order and the rank of the matrix.)

In this way the existence of kinematic indeterminacy and the infinitesimal degree of freedom itself can be established by means of a statical analysis.

3. Infinitesimal motions in different positions

In this section the infinitesimal movability will be investigated in a statical way, and in special positions the infinitesimal degrees of freedom of Tompos' pair of tetrahedra will be determined. Without restricting generality we suppose the edge length of the tetrahedra to be equal to $2\sqrt{2}$.

3.1 The basic position

Let \underline{s}_i be the vector of the reaction arising at the i -th support of tetrahedron Q , \underline{e}_i the corresponding unit vector parallel to the axis of the i -th support and s_i the algebraic magnitude of the i -th reaction ($i=1,2,\dots,6$). Then, $\underline{s}_i = s_i \underline{e}_i$.

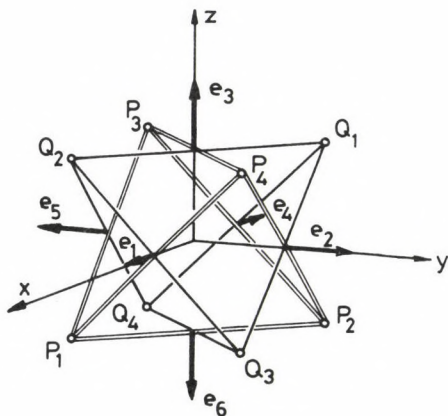


Fig. 2. Directions of the forces in the basic position

In the basic position, let the direction of unit vectors \underline{e}_i be considered in accordance with Fig. 2. Then, the equilibrium equations concerning the projections of the forces on the coordinate axes x , y , z and moments of the forces with respect to the coordinate axes x , y , z take the form

$$\begin{bmatrix} 1 & & & & & \\ & 1 & & & & \\ & & 1 & & & \\ & & & 1 & & \\ & & & & 1 & \\ & & & & & 1 \end{bmatrix} \begin{bmatrix} s_1 \\ s_2 \\ s_3 \\ s_4 \\ s_5 \\ s_6 \end{bmatrix} + \begin{bmatrix} \sum F_x \\ \sum F_y \\ \sum F_z \\ \sum M_x \\ \sum M_y \\ \sum M_z \end{bmatrix} = \underline{0} \quad (1)$$

where F_x , F_y , F_z and M_x , M_y , M_z are the projections and moments of a single external force F with respect to axes x , y , z , respectively, and the non-printed elements of the coefficient matrix are zeros. It is apparent that in this case

$$f = \nu(\tilde{G}) = 3 \quad .$$

The fact, that the last three rows of the equilibrium matrix in (1) are zeros, means that the structure is not able to equilibrate the moments of external forces about axes x , y , z , so infinitesimal rotations about axes x , y , z can freely develop. Let us denote the vectors of the respective rotations by φ_1 , φ_2 , φ_3 . By linear combinations of these three rotation vectors we can define three linearly independent free infinitesimal rotations about the axes passing through the opposite face midpoints (Fig. 3/a), the opposite edge midpoints (Fig. 3/b) and the opposite vertices (Fig. 3/c) of the cube, which are called motions of the first kind, of the second kind and of the third kind, respectively. In [3] it has been proved that these three infinitesimal motions are actually the derivatives of three finite motions, also called of the first, second and third kind, respectively. In the case of motions of the first kind, also the finite motion has only a rotation part, however in the case of motions of the second and third kinds, the finite motion has a non-zero translation part, as well.

Let φ_{10} , φ_{20} , φ_{30} denote the positive unit vectors of φ_1 , φ_2 , φ_3 , and let φ denote the vector of rotations of different kinds. The unit vector of φ , denoted by φ_0 , represents the direction of the axis of rotation; and the algebraic magnitude of φ , denoted by φ , represents the value of the angle of rotation.

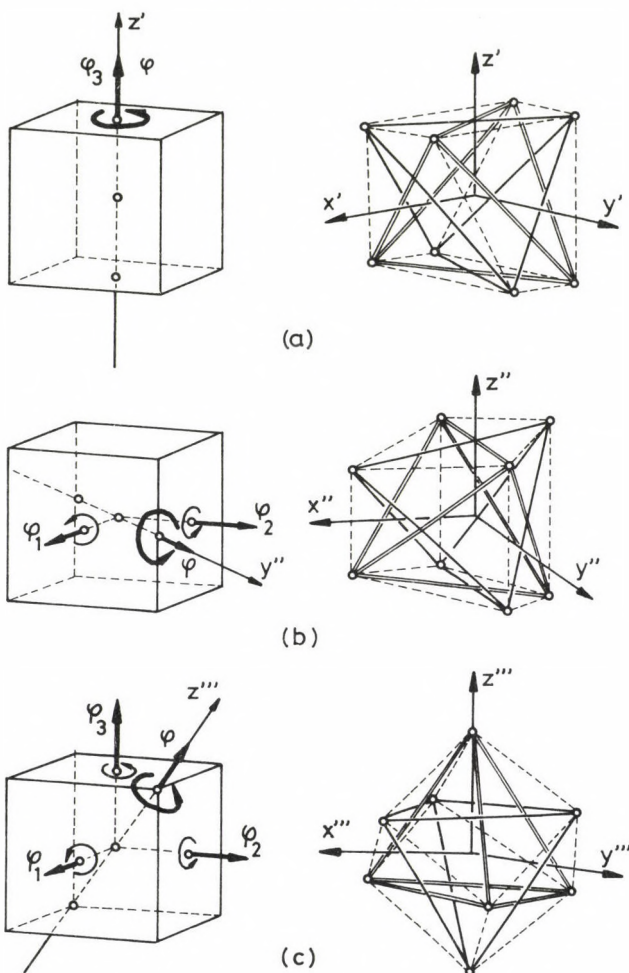


Fig. 3. Different kinds of motion of the pair of tetrahedra: (a) motion of the first kind, (b) motion of the second kind, (c) motion of the third kind

In the positions obtained by different kinds of motion the pair of tetrahedra has got certain symmetries. Taking these symmetries into consideration we choose new coordinate systems advantageous for further action. In Fig. 3 these new coordinate systems for positions of the first, second, third kind are marked by single, double, triple prime, respectively. The coordinate systems of single and double prime are cartesian but in that of triple prime the axes x''' and y''' are both orthogonal to the z''' axis, and they are inclined at 120° to each other.

3.2 Positions obtained by motion of the first kind

In a position produced by a motion of the first kind, and with the force directions according to Fig. 4, the equilibrium equations obtained by resolving along and taking moments of the forces about the x' , y' , z' axes result in the following coefficient matrix:

$$\tilde{G}^T = \begin{bmatrix} B & 0 & 0 & -B & 0 & 0 \\ 0 & B & 0 & 0 & -B & 0 \\ -A & A & 1 & -A & A & -1 \\ 0 & kB & 0 & 0 & -kB & 0 \\ kB & 0 & 0 & -kB & 0 & 0 \\ 0 & 0 & 0 & 0 & 0 & 0 \end{bmatrix} \quad (2)$$

where $A = \sin \beta$, $B = \cos \beta$.

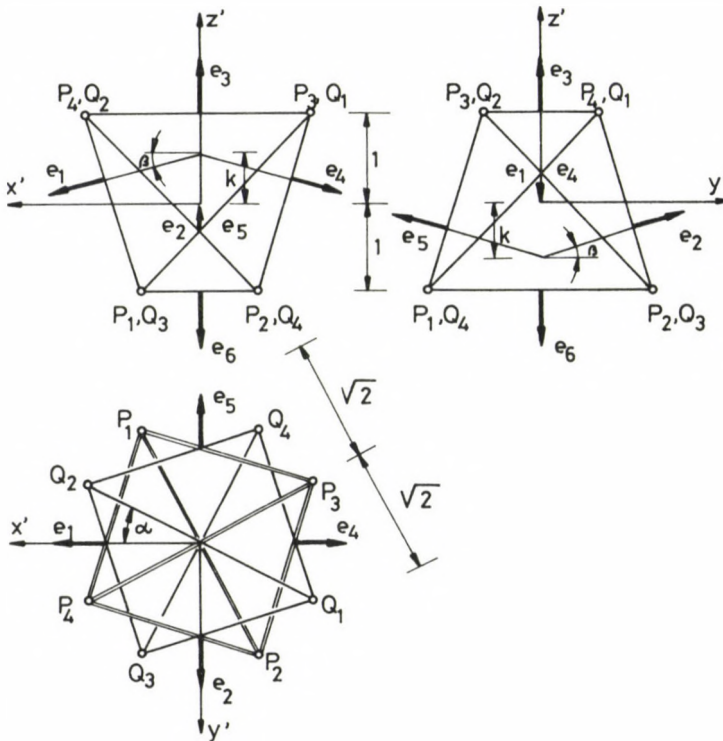


Fig. 4. Directions of the forces in a position obtained by motion of the first kind

Symbols β and k are defined in Fig. 4. Both β and k are functions of the angle α . (We remark that angle of rotation φ in Fig. 3/a is given, in the present notation, by $\varphi = 90^\circ - 2\alpha$.) It can be seen that the first and fifth rows as well as the second and fourth rows of matrix \tilde{G}^T is (2) are proportional, and the sixth row of \tilde{G}^T is identically zero; but the first, second and third rows are linearly independent. Therefore, the nullity of \tilde{G}^T , and thus the infinitesimal degree of freedom of the structure, is equal to three:

$$f = \nu(\tilde{G}) = 3.$$

The fact that the elements of the last row of \tilde{G}^T are zeros means that the structure is not able to equilibrate the moment of external forces about axis z' . Therefore, infinitesimal rotation about axis z' can develop freely, and its angle may be regarded as an increment of angle α since the sides of angle α are perpendicular to this axis. This property is valid for any value of α ; in accordance with the fact that really there exists a free finite rotation about axis z' .

The above statement concerning the infinitesimal degree of freedom is valid for general positions in the motion of the first kind. However, the question arises whether there are any particular positions of the pair of tetrahedra in this kind of motion for which the infinitesimal degree of freedom is greater than 3. It may be shown that the infinitesimal degree of freedom would increase from 3 (to 5) only if $|\beta| = 90^\circ$. Now β is the angle between the axis z' and a tangent plane of the hyperboloid of revolution generated by rotation of the edges of the tetrahedron which are not perpendicular to axis z' . Since this angle cannot be greater than the angle between axis z' and the asymptotes of the generating hyperbola of the hyperboloid of revolution (which is 45°), it follows that $|\beta|$ cannot be equal to 90° . Consequently, the infinitesimal degree of freedom cannot be greater than 3, unless some corresponding edges are parallel or coincident (i.e., for $\varphi \neq \pm 90^\circ, 180^\circ$).

3.3 Positions obtained by motion of the second kind

In a position produced by motion of the second kind, and with the force directions according to Fig. 5, the equilibrium equations obtained by resolving along and taking moments of the forces about the x'' , y'' , z'' axes result in the following coefficient matrix:

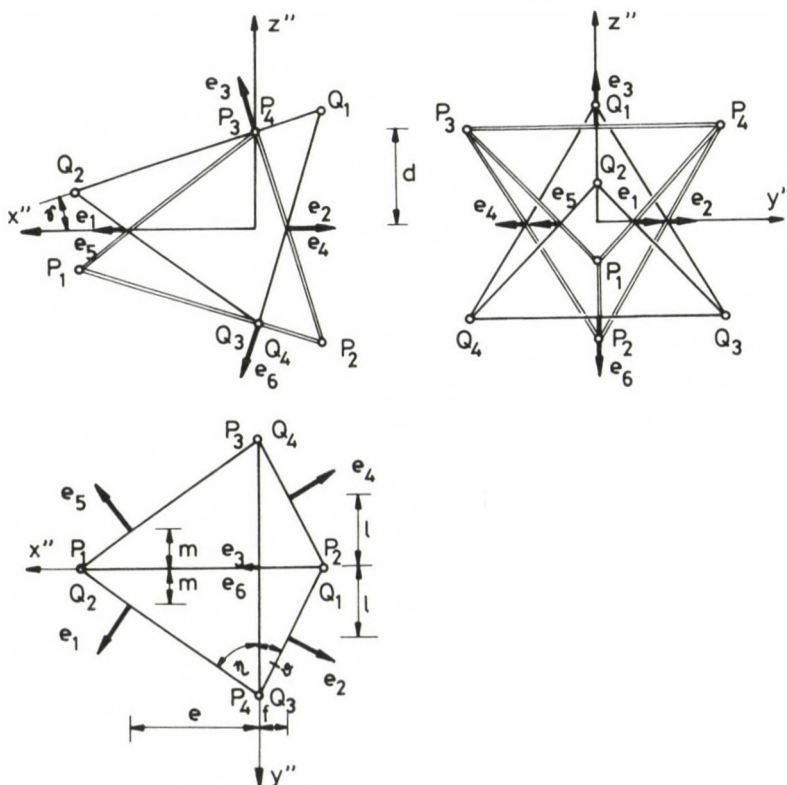


Fig. 5. Directions of the forces in a position obtained by motion of the second kind

$$\tilde{G}^T = \begin{bmatrix} F & -D & A & F & -D & A \\ E & C & 0 & -E & -C & 0 \\ 0 & 0 & B & 0 & 0 & -B \\ 0 & 0 & 0 & 0 & 0 & 0 \\ 0 & 0 & dA & 0 & 0 & -dA \\ G & H & 0 & -G & -H & 0 \end{bmatrix} \quad (3)$$

where

$$\begin{aligned} A &= \sin \gamma, & B &= \cos \gamma, \\ C &= \sin \vartheta, & D &= \cos \vartheta, \\ E &= \sin \eta, & F &= \cos \eta, \\ G &= -mF + eE, & H &= lD - fC. \end{aligned}$$

Angles γ, η, ϑ and distances d, e, f, l, m are defined in Fig. 5. All of these angles and distances are functions of the angle γ . (We remark that the angle of rotation φ in Fig. 3/b is given, in the present notation, by $\varphi = 2\gamma$.) It can be seen that the third and fifth rows of matrix \underline{G}^T in (3) are linearly dependent, and that the fourth row of \underline{G}^T is identically zero; but the other rows of \underline{G}^T are, in general, linearly independent. Therefore, the nullity of \underline{G}^T , and thus the infinitesimal degree of freedom of the structure, is, in general, equal to two:

$$f = \nu(\underline{G}) = 2.$$

The linear dependence of the third and fifth rows of \underline{G}^T means that the structure is not able to equilibrate external forces whose moment about axis y'' and projection on axis z'' are linearly independent. So infinitesimal rotation about axis y'' and a coupled infinitesimal translation parallel to axis z'' can freely develop. The angle of infinitesimal rotation may be considered as an increment of angle γ since the sides of angle γ are perpendicular to axis y'' . This property holds for arbitrary values of $\gamma (\neq \pm 90^\circ)$; in accordance with the fact that really there exists a free finite motion depending on γ .

The question also arises here whether there are any particular positions of the pair of tetrahedra in this kind of motion for which the infinitesimal degree of freedom is greater than 2. In order to answer this question let us transform matrix \underline{G}^T in (3) by standard manipulations of rows and columns to a band matrix (block-diagonal matrix) which contains the following 2x2 submatrices in its principal diagonal:

$$\begin{bmatrix} B & 0 \\ 0 & F \end{bmatrix}, \quad \begin{bmatrix} E & C \\ G & H \end{bmatrix}, \quad \begin{bmatrix} 0 & 0 \\ 0 & 0 \end{bmatrix}.$$

Let the determinant of the second submatrix be denoted by L : $L = EH - CG$. The nullity of \underline{G}^T is equal to the sum of nullities of these three submatrices.

Since B and F are not equal to zero at any points of the domain under consideration, the nullity of the matrix (3) (and hence the infinitesimal degree of freedom) increases (by 1); and so it will be equal to 3, when

$$L = EH - CG = 0 \quad . \quad (4)$$

We have computed the values of function L for different values of γ in the domain of the physically admissible motions of the second kind, and we give them in Table 1. The results in Table 1 show that L is an even function and the only value of γ (among the listed ones), for which equality (4) is satisfied, is zero; which corresponds to the basic position of the pair of tetrahedra. These considerations intuitively convince us that, apart from the basic position, no other positions exist among the physically admissible positions in this kind of motion, in which the infinitesimal degree of freedom is greater than 2.

Table 1 Values of function L

| $\gamma \frac{10}{\arctan \sqrt{2}}$ | 0 | ± 1 | ± 2 | ± 3 | ± 4 | ± 5 |
|--------------------------------------|---|---------------------------|---------------------------|---------------------------|---------------------------|---------------------------|
| L | 0 | 1.796699×10^{-4} | 3.021204×10^{-3} | 1.659941×10^{-3} | 5.872989×10^{-2} | 1.656306×10^{-1} |

3.4 Positions intermediate between those obtained by motions of the first and second kinds

In any position produced by motion of the second kind, every element of the fourth row of equilibrium matrix (3) of the structure is identically zero. This means that there exists free infinitesimal rotation about the x'' axis for an arbitrary value of γ . However, as has been shown in [3], not only free infinitesimal but also finite rotation may take place about this axis. In the case of rotation about the x'' axis, just as in the case of a rotation about the y'' axis, translations are coupled with the rotation. From a position of the second kind obtained by rotation of a given magnitude about the y'' axis, the pair of tetrahedra can be taken into a position of the first kind by a definite rotation about the x'' axis. Thus, this motion constitutes a transition between the motions of the first and second kinds.

In a position produced by motion intermediate between the first and the second kinds, we choose a new Cartesian coordinate system x'' , y'' , z''

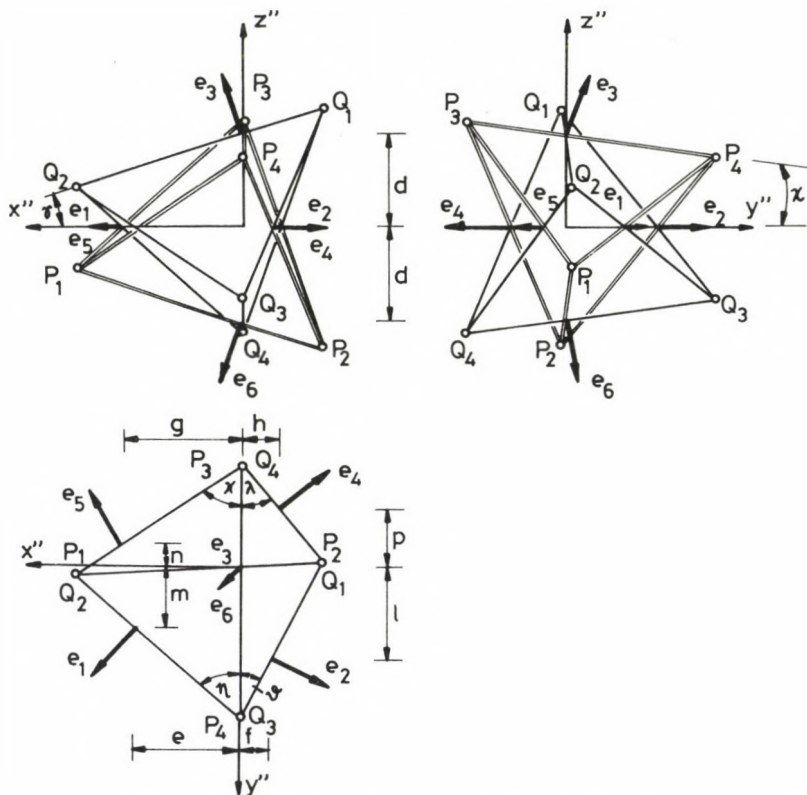


Fig. 6. Directions of the forces in a position intermediate between those obtained by motions of the first and second kinds

(Fig. 6). In this coordinate system, and with the force directions according to Fig. 6, the equilibrium equations obtained by resolving along and taking moments of the forces about the x'' , y'' , z'' axes result in the following coefficient matrix:

$$\underline{G}^T = \begin{bmatrix} F & -D & X & T & -R & X \\ E & C & Y & -S & -P & Y \\ 0 & 0 & Z & 0 & 0 & -Z \\ 0 & 0 & -dY & 0 & 0 & dY \\ 0 & 0 & dX & 0 & 0 & -dX \\ G & H & 0 & U & V & 0 \end{bmatrix} \quad (5)$$

where

$$\begin{aligned}
 C &= \sin \vartheta, & D &= \cos \vartheta, \\
 E &= \sin \eta, & F &= \cos \eta, \\
 G &= -mF + eE, & H &= \ell D - fC, \\
 P &= \sin \lambda, & R &= \cos \lambda, \\
 S &= \sin \kappa, & T &= \cos \kappa, \\
 U &= nT - gS, & V &= -pR + hP,
 \end{aligned}$$

and X, Y, Z are the direction cosines of the unit vector \underline{e}_3 . Angles $\vartheta, \eta, \lambda, \kappa$ and distances $d, e, f, g, h, \ell, m, n, p$ are defined in Fig. 6. All of these angles and distances as well as direction cosines of \underline{e}_3 are functions of the angles γ and χ . We find that the third and fourth as well as the third and fifth rows of the equilibrium matrix \underline{G}^T in (5) are linearly dependent; but the other rows, in general, are linearly independent. Therefore, the nullity of \underline{G}^T , and thus the infinitesimal degree of freedom of the structure is, in general, equal to two:

$$f = \nu(\underline{G}) = 2.$$

This indicates that infinitesimal rotations about the x'' and y'' axes and a coupled infinitesimal translation parallel to the z'' axis can develop freely. The angles of infinitesimal rotations may be considered as increments of the angles χ and γ . This property holds for an arbitrary intermediate position (i.e., for arbitrary admissible values of the angles χ and γ) in accordance with the fact that really there exists a free finite motion involving the rotations about axes x'' and y'' .

Although we have not made a detailed analysis, it seems that among the physically admissible positions the infinitesimal degree of freedom increases from 2 (to 3) only if the intermediate position is identical to a position of the first kind.

3.5 Positions obtained by motion of the third kind

In a position produced by motion of the third kind, with the force directions according to Fig. 7, the equilibrium equations obtained by resolving along and taking moments of the forces about the x''' , y''' , z''' axes result in the following coefficient matrix:

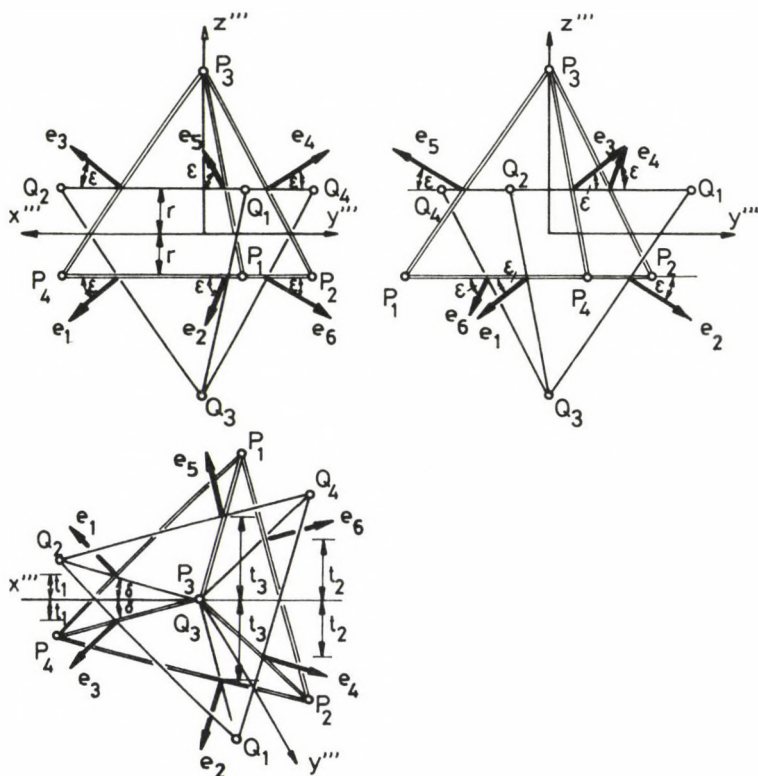


Fig. 7. Directions of the forces in a position obtained by motion of the third kind

$$\underline{G}^T = \begin{bmatrix} BH & -BD & BF & BH & -BD & BF \\ BF & BH & -BD & -BD & BF & BH \\ A & A & A & -A & -A & -A \\ T_1 & T_2 & -T_3 & T_1 & T_2 & -T_3 \\ -T_3 & T_1 & T_2 & T_2 & -T_3 & T_1 \\ BI & BI & BI & -BI & -BI & -BI \end{bmatrix} \quad (6)$$

where

$$\begin{aligned} A &= \sin \varepsilon, & B &= \cos \varepsilon, \\ C &= \sin \delta, & D &= \cos \delta, \\ E &= \sin(60^\circ + \delta), & F &= \cos(60^\circ + \delta), \\ G &= \sin(60^\circ - \delta), & H &= \cos(60^\circ - \delta), \\ I &= \sin(60^\circ - 2\delta), & T_1 &= t_1 A - rBG, \\ T_2 &= t_2 A - rBC, & T_3 &= t_3 A - rBE. \end{aligned}$$

Angles δ, ε and distances r, t_1, t_2, t_3 are defined in Fig. 7 where ε denotes the angle between vector \underline{e}_i ($i=1,2,\dots,6$) and the $x''' y'''$ plane. All of the distances r, t_1, t_2, t_3 and the angle ε are functions of the angle δ . (We remark that angle of rotation φ in Fig. 3/c is given, in the present notation, by $\varphi = 60^\circ - 2\delta$.) It can be seen that the third and sixth rows of matrix \underline{G}^T in (6) are linearly dependent for any value of the angle δ ; but the other rows of \underline{G}^T are, in general, linearly independent. Thus, the nullity of \underline{G}^T , and hence the infinitesimal degree of freedom of the structure is, in general, equal to one:

$$f = \nu(\underline{G}) = 1.$$

The fact that the third and sixth rows of \underline{G}^T are linearly dependent means that the structure is not able to equilibrate external forces whose projection and moments with respect to the z''' axis are linearly independent. So infinitesimal rotation about axis z''' and a coupled infinitesimal translation parallel to the axis z''' can develop freely. The angle of infinitesimal rotation may be considered as an increment of the angle δ , since the sides of angle δ are perpendicular to the z''' axis. This property holds for arbitrary values of δ ($\neq -15^\circ, 75^\circ$), in accordance with the fact that really there exists a free finite rotation about the z''' axis, together with a coupled translation parallel to the same axis z''' : a helical, or screw motion.

A question also arises here: are there particular positions of the pair of tetrahedra in this kind of motion, for which the infinitesimal degree of freedom is greater than 1? In order to answer this question we shall apply a process similar to that used in Section 3.3. Let us transform the matrix \underline{G}^T in (6) by standard manipulations of rows and columns to a band matrix (block-diagonal matrix) which contains the following 2x2 submatrices in its principal diagonal:

$$\begin{bmatrix} D+F & F-H \\ T_2+T_3 & T_1+T_3 \end{bmatrix}, \quad \begin{bmatrix} D & F \\ T_2 & T_3 \end{bmatrix}, \quad \begin{bmatrix} B & 0 \\ 0 & 0 \end{bmatrix}.$$

Let the determinant of the first submatrix be denoted by M : $M=(D+F)(T_1+T_3)-(F-H)(T_2+T_3)$, and let the determinant of the second submatrix be denoted by N : $N=DT_3-FT_2$. The nullity of \underline{G}^T is equal to the sum of nullities of

these three submatrices. Since B is not equal to zero in any points of the domain under consideration, the nullity of matrix (6) increases by 1 if either

$$M = (D+F) (T_1 + T_3) - (F-H)(T_2 + T_3) = 0 \quad (7)$$

or

$$N = DT_3 \quad FT_2 = 0 \quad . \quad (8)$$

But the nullity of matrix (6) increases by 2 if both equalities (7) and (8) hold simultaneously. We have computed the values of functions M and N for different values of δ in the domain of the physically admissible motions of the third kind and we give them in Table 2. (Values of δ are in degrees.) The results in Table 2 suggest that both M and N are even functions with respect to the variable $\delta - 30^\circ$. Further, for $\delta = 30^\circ$ M and N simultaneously fulfil equalities (7) and (8), respectively, and it seems that neither M nor N has other zeros in the domain of interest apart from $\delta = 30^\circ$, which corresponds to the basic position of the pair of tetrahedra. These considerations intuitively convince us that, apart from the basic position, no other positions exist in this kind of motion, in the physically admissible domain, in which the infinitesimal degree of freedom is greater than 1.

Table 2 Values of functions M and N

| $\frac{\delta}{6^\circ} - 5$ | 0 | ± 1 | ± 2 | ± 3 | ± 4 | ± 5 |
|------------------------------|---|---------------------------|---------------------------|---------------------------|---------------------------|---------------------------|
| M | 0 | 6.022794×10^{-4} | 1.030882×10^{-2} | 5.870108×10^{-2} | 2.218331×10^{-1} | 7.071068×10^{-1} |
| N | 0 | 2.007597×10^{-4} | 3.436274×10^{-3} | 1.956703×10^{-2} | 7.394436×10^{-2} | 2.357023×10^{-1} |

4. Characterization of infinitesimal motions by means of direct kinematic relationships using the theory of small displacements

In this section we present another approach to the results obtained above in a statical way, independent of the above one and of course confirming the above results, namely a direct kinematic analysis using the theory of small displacements. Here the applied technique will be outlined briefly, and some examples of its application will be presented.

Rigid motions of the three-dimensional space are of the form $\tilde{\Phi}(\underline{x}) = \underline{A}\underline{x} + \underline{b}$ where \underline{A} is an orthogonal matrix with determinant +1 representing a rotation, and \underline{b} is a vector representing a translation. Motions of the tetrahedron Q are rigid motions under the constraint $(*)$. (Notation $(*)$ is explained in the Introduction.) Note that the different kinds of motions investigated above, apart from those of the third kind with $|\varphi| > 90^\circ$, can be obtained from the basic position by continuous deformation, always satisfying $(*)$. Also the different kinds of motions depend analytically on some parameters. (They constitute analytic submanifolds of the manifold of all motions $\tilde{\Phi}(\underline{x})$.)

Let Q_i, P_k ($i, k=1, 2, 3, 4$) denote the vertices of the tetrahedra according to Fig. 2. With their coordinates we can write them in the form $Q_i(x_{Qi}, y_{Qi}, z_{Qi})$, $P_k(x_{Pk}, y_{Pk}, z_{Pk})$ ($i, k=1, 2, 3, 4$). Condition $(*)$ means that the volume of the tetrahedra spanned by the end points of the originally intersecting edges $Q_i Q_j, P_k P_\ell$ has to be equal to zero, that is

$$\begin{vmatrix} x_{Qi} & y_{Qi} & z_{Qi} & 1 \\ x_{Qj} & y_{Qj} & z_{Qj} & 1 \\ x_{Pk} & y_{Pk} & z_{Pk} & 1 \\ x_{Pl} & y_{Pl} & z_{Pl} & 1 \end{vmatrix} = 0, \quad i, j, k, \ell = 1, 2, 3, 4; \quad (9)$$

$$\begin{matrix} i \neq j; & k \neq \ell; & k \neq i, j; \\ \ell \neq i, j, \end{matrix}$$

which define six constraints.

Let tetrahedron P be fixed with vertices $P_1(1, -1, -1)$, $P_2(-1, 1, -1)$, $P_3(-1, -1, 1)$, $P_4(1, 1, 1)$. We consider the different kinds of motions, and for each of them we investigate the following. We take some particular position, say, Q^0 of the moving tetrahedron Q , obtained by a motion of the respective kind, and then consider all positions of Q satisfying $(*)$, near this fixed position Q^0 . We will use the fact that the variable position of Q , satisfying $(*)$, can be obtained from the fixed position Q^0 of Q by a motion,

i.e., a transformation $\Phi(x) = Ax + b$, with A an orthogonal matrix with determinant +1, where $A = [a_{ij}]$ is near the identity matrix I , and $b = [b_i]$ is near 0.

Let $A = I + [\varepsilon_{ij}]$. The orthogonality of A means that the scalar product of the vectors in the i -th and j -th column is δ_{ij} ($\delta_{ij} = 1$ for $i=j$ but $=0$ otherwise); that means $\varepsilon_{ii} = 0$, $\varepsilon_{ij} + \varepsilon_{ji} = 0$ (up to quantities of second degree). Thus we will write $A = [\delta_{ij} + \varepsilon_{ij}]$, where $[\varepsilon_{ij}]$, as described above, is skew-symmetric and has small elements. (We note that $\det A = -1$ cannot occur for A near I .)

We will substitute the coordinates of the vertices of the moving tetrahedron Q (these vertices are obtained from the vertices of the fixed position Q^0 of Q by the application of the transformation $\Phi(x) = Ax + b$) in equations (9), thereby obtaining six equations for the unknowns ε_{12} , ε_{23} , ε_{31} , b_1 , b_2 , b_3 . Omitting the quantities of second degree in these variables we will obtain a system of six homogeneous linear equations for the six variables ε_{ij} and b_i . We will determine in each case (i.e., for each kind of motion and for a suitable Q^0 obtained by that kind of motion) the nullity of the matrix of this system of equations, i.e., the dimension of the linear manifold of the solutions. Thus we will find how many parameters are required to describe the small motions in a neighbourhood of the fixed position Q^0 , up to quantities of second degree, in our above sense.

This determination of the nullity will be performed only for a single position Q^0 for each kind of motion. In general the nullity will not be greater than the value, say k , obtained in this way. Moreover, the nullity can be greater than k only for a small set of special values of the (analytic) parameters determining the position in the motion of the respective kind. In fact, in the fixed position Q^0 we have a non-vanishing minor of rank $6-k$, which also is an analytic function of the parameters, which vanishes on the set of zeros of an analytic function of one variable (in the case of motions of first, second and third kinds), or of two variables (for the intermediate kind).

We note here that we will determine the nullity of the matrix by performing operations on the columns and rows (as with determinants), in order to obtain a diagonal matrix in which the number of the zero elements in the diagonal is equal to the nullity. Details of the calculations will not be given. Our results will be in agreement with the results of Section 3.

4.1 Motion of the first kind

We consider the position Q^0 with angle of rotation $\varphi = 90^\circ$ about the axis φ_{30} (orientation on the orthogonal plane seen by looking backwards from the vector of rotation). Then the matrix of the system of equations in question is

$$\begin{bmatrix} 0 & 0 & 0 & 0 & 0 & 0 \\ 0 & 2 & -2 & 1 & 1 & -1 \\ 0 & -2 & -2 & -1 & 1 & 1 \\ 0 & 2 & -2 & 1 & 1 & 1 \\ 0 & 2 & 2 & 1 & 1 & 1 \\ 0 & 0 & 0 & 0 & 0 & 0 \end{bmatrix}$$

which has nullity 3.

4.2 Motion of the second and intermediate kind

We consider the position Q^0 in the motion of the second kind with angle of rotation $\varphi = \arctan \sqrt{2}$ about the axis $(\varphi_{10} + \varphi_{20})/\sqrt{2}$ (with the associated translation). Then we obtain the corresponding matrix

$$\begin{bmatrix} 0 & 1 & 1 & -1 & 1 & 1 \\ 3\sqrt{3}-1 & 2\sqrt{3}-4 & -\sqrt{3}+5 & 3+2\sqrt{3} & -2-\sqrt{3} & 2+\sqrt{3} \\ 2\sqrt{3} & -2 & -2+2\sqrt{3} & -1+\sqrt{3} & 1+\sqrt{3} & 1-\sqrt{3} \\ 2\sqrt{3} & 2-2\sqrt{3} & 2 & 1+\sqrt{3} & -1+\sqrt{3} & -1+\sqrt{3} \\ 3\sqrt{3}-1 & \sqrt{3}-5 & 4-2\sqrt{3} & -\sqrt{3}-2 & 2\sqrt{3}+3 & -\sqrt{3}-2 \\ 0 & 1-\sqrt{3} & 1-\sqrt{3} & 0 & 0 & -1 \end{bmatrix}$$

which has nullity 2. Since a position obtained by a motion of the second kind is also an intermediate position between positions obtained by motions of the first and second kinds, we see that also for the intermediate positions, in general, the nullity is not greater than 2.

4.3 Motion of the third kind

Observe that in this case we have two manifolds: one for $|\varphi| < 90^\circ$, the other for $|\varphi| > 90^\circ$. In the first case we consider the position Q^0 with angle of rotation $\varphi = 60^\circ$ about the axis $(\varphi_{10} + \varphi_{20} + \varphi_{30})/\sqrt{3}$ (with the associated translation).

Then the corresponding matrix is

$$\begin{bmatrix} 2 & 2 & 0 & -1 & 1 & 1 \\ 0 & 2 & 2 & 1 & -1 & 1 \\ 2 & 0 & 2 & 1 & 1 & -1 \\ 4 & 2 & 6 & 5 & -1 & -1 \\ 6 & 4 & 2 & -1 & 5 & -1 \\ 2 & 6 & 4 & -1 & -1 & 5 \end{bmatrix}$$

which has nullity 1. In the second case we consider the position Q^0 with angle of rotation $\varphi = 180^\circ$ about the axis $(\varphi_{10} + \varphi_{20} + \varphi_{30})/\sqrt{3}$ (with the associated translation). Then the corresponding matrix is

$$\begin{bmatrix} 0 & -2 & 2 & 0 & 0 & 1 \\ 2 & 0 & -2 & 1 & 0 & 0 \\ -2 & 2 & 0 & 0 & 1 & 0 \\ 2 & 0 & -2 & -1 & 2 & 2 \\ -2 & 2 & 0 & 2 & -1 & 2 \\ 0 & -2 & 2 & 2 & 2 & -1 \end{bmatrix}$$

which also has nullity 1.

5. Conclusions

5.1 Tompos' pair of tetrahedra is a true sliding mechanism. In /3/ it has been shown that the physically admissible finite motions of the pair of tetrahedra constitute one- and two-dimensional manifolds in the six-dimensional space of rigid motions and these manifolds may be given uniquely by their projections on the three-dimensional space of rotations (i.e., the translation parts of the motions are uniquely determined by the rotation parts), as visualized in Fig. 8. The circles in the figure represent the two-dimensional manifolds of the motions intermediate between the motions of the first and the second kinds, and the diagonal straight lines represent the one-dimensional manifolds of motions of the third kind. This

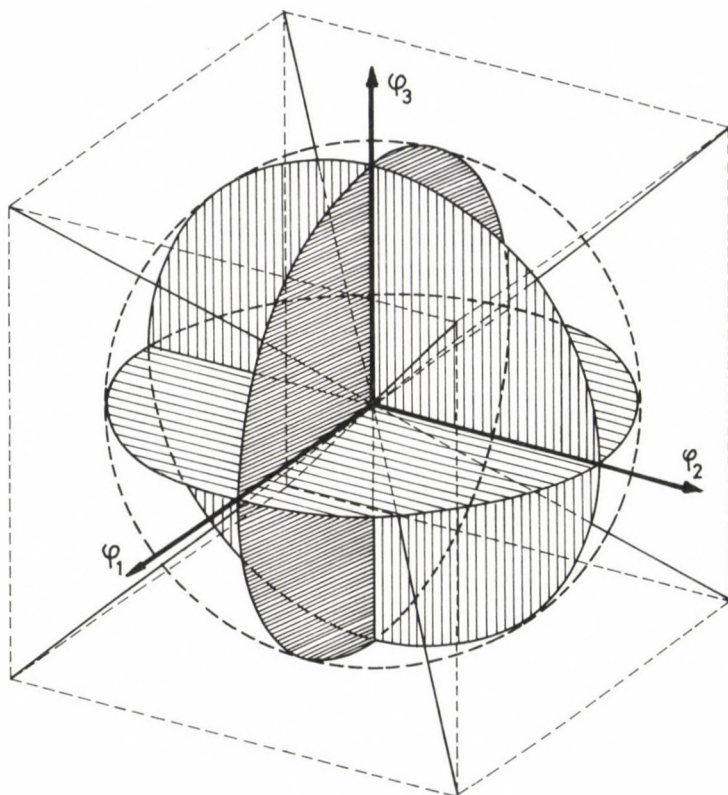


Fig. 8. Manifolds of the physically admissible motions of the pair of tetrahedra in a projection on the three-dimensional space of rotations

figure, however, does not characterize the manifolds of motions metrically but only topologically.

5.2. As follows from the proof of Theorem 1 of /2/, for any rotation \underline{A} near the identity, equations (9) are satisfied up to quantities of fifth degree of smallness, for a suitable translation \underline{b} (depending on \underline{A}) which is unique up to quantities of fifth degree of smallness. That means that near the basic position we have a three-parameter set of solutions, up to quantities of fifth degree of smallness. This is also supported by the calculations made in this paper. Tables 1 and 2 show that the functions characterizing the motions of the corresponding kind tend to zero approximately in the fourth order. Thus the nullity of the matrices in Sections 3.3 and 3.5 becomes three if we neglect terms of order ≈ 4 . These explain our apparent feeling, when we hold the physical model in our hands, that the pair of

tetrahedra has a 3-parameter finite motion in a neighbourhood of the basic position although, as proved in /3/, such a finite motion does not exist.

5.3. In Section 3 kinematic indeterminacy has been shown via static indeterminacy. This latter can also be explained directly by the geometry of the lines of action of the six reactive forces. In the basic position these lines of action are concurrent in space, so the constraint is 3 times statically indeterminate. In a position of the first kind two lines of action are coincident and constitute the axis of rotation, the four other lines of action intersect this axis. Considering the resultants of the reactive forces symmetrical to this axis we have four collinear forces, which form a 3 times statically indeterminate system. In a position of the intermediate kind (the second kind included) the pair of tetrahedra and the reactions have a plane of symmetry. Four of the lines of action of the reactive forces are lying in this plane. Considering the resultant of the two reactive forces symmetrical to this plane we have five coplanar forces, which form a 2 times statically indeterminate system. In a position of the third kind the configuration has an axis of rotation. Considering the resultant of each of the reactive force triplets rotationally symmetrical to this axis we have two collinear wrenches (whose force part and couple part are dependent), which form a 1 times statically indeterminate system.

5.4. Movability with free finite motion itself is an unexpected property of the pair of tetrahedra, but its most surprising property is that the infinitesimal degree of freedom (i.e., degree of kinematic indeterminacy) changes during motion. For instance, in Fig. 8, at general points on the circular discs the infinitesimal degree of freedom is 2; but along the line of their intersection corresponding to motion of the first kind the infinitesimal degree of freedom is 3. Along the diagonal straight lines the infinitesimal degree of freedom is, in general, 1; but at the point of intersection of these lines and the circular discs the infinitesimal degree of freedom is 3.

The lines and points of intersection of the manifolds of motions are places of singularity, since there the infinitesimal degree of freedom increases. The manifolds of motions can be considered as compatibility surfaces, since they consist of all the points corresponding to positions in which the structure is compatible. Their intersection is in fact a bifurcation. Thus, an explanation of the change of infinitesimal degree of freedom can be given in terms of bifurcation of the compatibility surfaces. This

phenomenon is analogous to the bifurcation of equilibrium surfaces of structures subjected to multiparameter loads.

ACKNOWLEDGEMENTS

We thank Prof. C.R. Calladine for his many valuable comments and suggestions. We are grateful to Dr. I. Hegedűs and Dr. S. Pellegrino for helpful discussions. Research reported here was supported by ATA Grant No. 07-060 and OTKA Grant No. 744 awarded by the Basic Research Foundation and by the Hungarian Scientific Research Foundation, respectively.

REFERENCES

1. Timoshenko, S.P. - Young, D.H.: Theory of Structures, 2nd Edn. McGraw-Hill, New York, (1965), 176-183.
2. Tarnai, T. - Makai, E.: Physically inadmissible motions of a movable pair of tetrahedra. Proc. 3rd Int. Conf. on Engineering Graphics and Descriptive Geometry, Vienna, Vol. 2, (1988), 264-271.
3. Tarnai, T. - Makai, E.: A movable pair of tetrahedra. Proc. Roy. Soc. London, Ser. A 423, (1989).
4. Szabó, J.: The equation of state-change of structures. Periodica Polytechnica, Mech. Eng. 17, (1973), 55-71.
5. Calladine, C.R.: Buckminster Fuller's "Tensegrity" structures and Clerk Maxwell's rules for the construction of stiff frames. Int. J. Solids Structures 14, (1978), 161-172.

ACCURACY TEST OF SIMPLIFIED CONTINUUM CALCULATIONS OF TWO-LAYER SPACE GRIDS

TÜRKÖSSY, A.*

(Received: 9 December 1986)

In the recent twenty years, three-dimensional lattice structures have found worldwide use.

Accurate computer calculations for three-dimensional lattices is today a routine job. However, a disadvantage of such calculations is that they are not demonstrative enough and not suited to be taken as a basis for preliminary strength calculations of the structure, moreover, the designer has to make sure that the data set obtained as a result of computer calculation is correct.

The so-called 'continuum method' of space grid calculation is a help to the designer in coping with the problem.

This work is designed to test the accuracy of simplified continuum calculation as compared with the accurate values obtained by computer calculation for two-layer space grids using numerical calculation and to draw the necessary conclusions for applicability of the continuum method in practical design.

The internal forces of two-layer space grids can be determined simply and within a relatively short time by means of the simplified continuum method to an accuracy shown in the tables, and according to experience, the accuracy of the method is sufficient for preliminary design or for the accuracy test of data obtained in computer calculation.

1. Introduction

Static calculations of engineering structures include essentially investigation by means of a model containing the characteristics of the structures to be designed. Depending on the model to be used, the structures can be divided in two major groups, such as

- structures to be designed on the basis of a finite model like lattices and frames,
- structures to be designed on the basis of a continuum model like plates, discs and shells.

A special group is that of so-called lattice-surface structures (space grids). Both models can be used for calculation for these structures.

Accurate calculation of space grids is based on the finite model.

*Türköszy, Attila H-6722 Szeged, Londoni krt. 18, Hungary

With the structure consisting of discrete elements itself considered to be the model, the equilibrium and displacement equations are written for each bar and node.

The number of unknown static quantities in the calculations is very large because of the large number of discrete elements constituting the structure. Therefore, the required calculation is practically impossible without the use of a computer.

Today the computer calculation is a routine job but it is not demonstrative enough for a prompt evaluation of the force action and for selection, or possibly necessary modification, of the structure on the basis of consideration of the advantages and disadvantages.

Data acquisition for the computer calculation is difficult (especially for the cross section of bars). Moreover, the static designer using the data set obtained in computer calculation needs an independent calculation process to make sure at random that the data to be used are correct. This demand is met by approximate calculation based on the continuum model.

2. Description of the continuum method

Essentially, the continuum method uses the elastic continuum of an anisotropic or in certain cases isotropic or orthotropic plate to substitute for the space lattice consisting of discrete elements with hinged joint between them, equivalent to the space grid from a statical point of view but mainly in respect of rigidity. The stresses of this continuum are calculated making use of the known, tabulated results of the theory of plates and, finally, the stresses are converted into bar forces of the lattice structure.

2.1 The case of chord layers of identical rigidity

The space grid can be substituted for with an isotropic or orthotropic plate if the rigidity characteristics of its top and bottom chord layers are identical or proportional, the static behaviour of the plate being described by one single partial differential equation of the fourth order with a bend deflection function w in it.

2.2 The case of chord layers of different rigidity

Should the two chord layers of the space grid investigated differ from each other in rigidity characteristics qualitatively, then a plate with one side ribbed in both directions can be assumed as a substituting continuum /1/.

The static behaviour of this ribbed plate as a plate under bending and forces within the plane of the plate is described by a partial non-linear differential equation system of the fourth order the unknowns of which being bend deflection function w and the stress function describing the membrane stresses arising in the top plate /2/.

$$\frac{B}{h} \nabla^2 \nabla^2 w = \frac{p}{h} + \frac{\partial^2 \Phi}{\partial y^2} \cdot \frac{\partial^2 w}{\partial x^2} + \frac{\partial^2 \Phi}{\partial x^2} \cdot \frac{\partial^2 w}{\partial y^2} - 2 \frac{\partial^2 \Phi}{\partial x \partial y} \cdot \frac{\partial^2 w}{\partial x \partial y} \quad (1)$$

$$\nabla^2 \nabla^2 \Phi = E \left[\left(\frac{\partial^2 w}{\partial x \partial y} \right)^2 - \frac{\partial^2 w}{\partial x^2} \cdot \frac{\partial^2 w}{\partial y^2} \right] \quad (2)$$

Complex as it is, the equation system can not be solved explicitly while a numerical solution is unnecessary as in this case, it would be more reasonable to take into consideration the space lattice itself, consisting of discrete elements, as a computation model.

3. Calculation of the simplified continuum

An additional approach, the so-called simplified continuum calculation, can be used in such cases /1/.

Taking the ribbed plate as an example, this approach neglects the shearing rigidity existing in the plane of the top plate and thus stress function Φ is omitted with only one partial differential equation of the fourth order remaining for bend deflection w , which complies with the Huber differential equation of a normal orthotropic plate /3/:

$$B_x \cdot w'''' + B_y \cdot w'''' + 2H \cdot w'''' = -p \quad (3)$$

This approach is applied to two-layer grids by neglecting the excess rigidity of the 'more rigid' chord layer containing different types of rigidity as compared with the rigidity of the other ('softer') chord layer.

It is usually the shearing rigidity existing in one of the chord layers which appears as an excess rigidity. With this excess rigidity neglected, also the accessory stress and strain state of the space grid falls away together with stress function ϕ describing it. A pure bending force and strain state are brought about in this way, which can be described by bend deflection function w and accordingly, a single partial differential equation of the fourth order is left as a result for bend deflection w also in case of the space grid.

In accordance with its function, stress function ϕ can be eliminated in two different ways such as

- by the simplified equilibrium method and
- by the simplified compatibility method.

Another approximation, e.g. adaptation of Giencke's theory to two-layer grids /4/ is also possible.

3.1 Use of the simplified equilibrium method to investigate two-layer grids

If the rigidities of two chord layers of the space lattice are of different magnitude, the neutral planes of bending or torsional moments will not coincide. There will be no coincidence either if the rigidity of the entire system is ensured by so-called 'closed lattice-type tubes'. The case where one of the chord layers contains a certain kind of stiffness while the other one doesn't contains it at all is a special case of non-proportional rigidities with the neutral plane falling within the chord layer containing the rigidity in question.

Under the circumstances, the stress function is designed to ensure compatibility of the strains by developing one single common neutral plane for every bending and torsional effect. Hence, compatibility of the strains can not be satisfied if the stress function is eliminated from the calculation but the equilibrium condition is satisfied. Since only rigidities existing in the 'softer' chord layer are taken into consideration, the entire structure is being 'softened' with every rigidity having a counterpart in the other chord layer.

3.2 Use of the simplified compatibility method to investigate two-layer lattices

The stress function can be eliminated also by determining of a common neutral plane for all the bending and torsional effects to ensure compatibility of the strains without, however, satisfying the equilibrium condition.

Namely, the neutral plane defined will not coincide with the centre of gravity of some pairs of rigidities and therefore the forces arising in the chord layers will not be equal in magnitude. Hence, not only paired forces will arise but horizontal forces are acting as well.

Under the circumstances, the stress function ought to have provided for equilibrium by means of the accessory stress state. If it is neglected, the mentioned resultant horizontal forces shall be left out of consideration as well.

The common neutral plane shall be determined within the actual common neutral plane of more rigidities or in case the space grid includes 'closed lattice-type tubes', in the torsional neutral axis of the 'tubes'.

Then the rigidities of the more rigid chord layer shall be divided in two parts. The rigidity of part I shall be assumed to be 'k' times as much as the rigidities of the softer chord layer which is taken as a basis.

Factor 'k' shall be assumed in such a way that the neutral plane determined will coincide with the centre of gravity of the total or partial rigidities of both chord layers.

Part II of the rigidity of the more rigid chord layer contains the excess rigidities supplying those resultant horizontal forces which have no counterpart in the softer chord layer. The structure is 'stiffened' by this procedure.

3.3 Adaptation of Giencke's theory /4/ to investigate two-layer lattices

Giencke's theory can be adapted to space grids where the rigidity of one of the chord layers complies with that of the top plate of the ribbed plate, while the 'closed lattice-type tubes' of the space grid comply with the ribs of the ribbed plate.

Essentially, the theory is adapted by superimposing the rigidity of the 'ribs' upon the 'top plate' by calculating a substitutional torsional rigidity H^* in place of torsional rigidity H included in differential equation (3).

4. Objective of the study

This study is designed to investigate the accuracy that can be achieved in simplified continuum calculation in case of two-layer space grids. It examines whether or not the use of the simplified equilibrium model and compatibility model results in values approximating the lower or upper limit of accurate values calculated by computer on the basis of the finite model in case of space grid of different geometry and with chord layers of different rigidity /8/.

Efforts are made to draw conclusions for use of the simplified continuum model in practical design work.

By accuracy of simplified continuum calculation we understand the extent of compliance of the values determined for bar forces by means of continuum calculation with the values obtained by computer calculation on the basis of the finite computation model, considered to be accurate.

5. Possible uses of the continuum method in case of two-layer space grids

Bars constituting the different chord layers can be arranged in different ways. They may run in three directions or parallel with more than three directions or parallel with less than three directions.

The geometry determines on the one hand the isotropic or orthotropic or, possibly, aeolotropic character of the substitutional continuum and on the other hand, it decides whether the bar forces are statically determinate or statically indeterminate.

5.1 Continuum equations of space grids with chord layers of identical or proportional rigidity

The substitutional continuum of such structures is an isotropic or orthotropic plate with stress function ϕ non-included in its accurate differential equation. Thus this equation can be considered to be at the same time the differential equation of the simplified method /1/.

5.2 Continuum equations of space grids with chord layers of different rigidity

The substitutional continuum of such structures is a ribbed plate. Hence, to write the simplified differential equations of the structures, it is necessary that stress function ϕ be eliminated.

The accuracy of simplified continuum calculation has been tested for space grids falling within this group, the chord layers of which being flat surfaces parallel to each other:

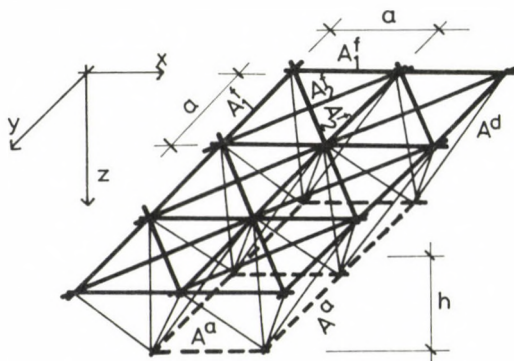


Fig. 1. 'Square with diagonals on square offset' /1/

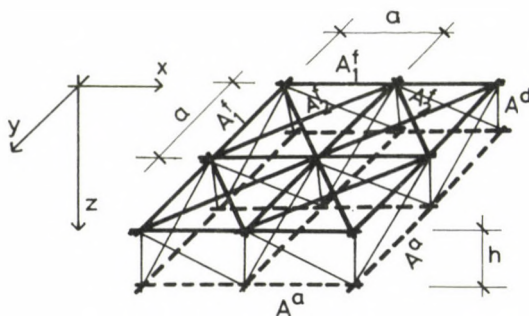


Fig. 2. 'Square with diagonals on square' /1/

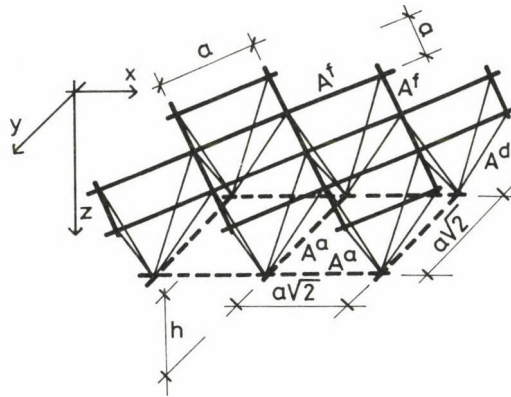


Fig. 3. 'Diagonal on square' /1/

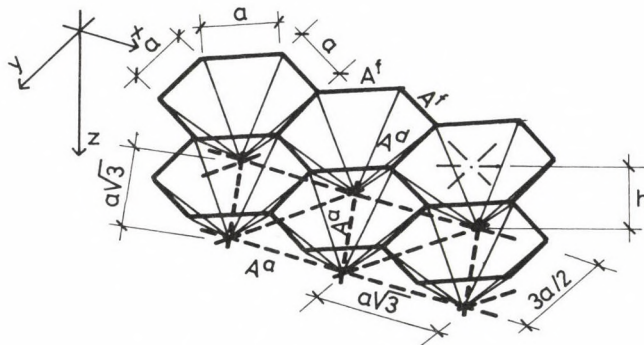


Fig. 4. 'Hexagonal on triangular' /1/

5.2.1 Use of the simplified equilibrium method to write continuum equations

5.2.1.1 'Square with diagonals on square offset' /1/, /9/

As seen in Fig. 1, the top chord of this grid constitutes together with the connecting bracing 'closed tubes of triangular cross section' which are suited to take up shear forces and as a result of the geometric arrangement, a lattice type 'set of tubes' is obtained.

Transversal elongation rigidity T_{12}^t in the top chord plane has no counterpart in the bottom chord plane. Moreover, the neutral planes of bending and torsion are found at different places for each stress.

T_{12}^t is neglected but the shearing rigidity of the top chord plane is kept because it is present in the entire system due to the 'closed lattice-type tubes'.

Value of bending rigidity:

$$B = \frac{E}{a} h^2 \frac{\left(A_1^t + \frac{A_2^t}{2} \right) A^b}{\left(A_1^t + \frac{A_2^t}{2} \right) + A^b} \quad (4)$$

Value of torsional rigidity:

$$H = \frac{E \cdot h^2}{2a} \frac{A_2^t}{\sqrt{2} + 4 \frac{A_2^t}{A^{\text{brac}}} \left(\frac{h^2}{a^2} + \frac{1}{2} \right)^{3/2}} \quad (5)$$

In the knowledge of the above rigidity factors, the differential equation of the substitutional orthotropic plate can be written, as follows:

$$B \cdot w'''' + B \cdot w'' + 2H \cdot w'' = -p \quad (6)$$

5.2.1.2 'Square with diagonals on square' /1/

As seen in Fig. 2, this grid has no actual torsional rigidity because of the vertical strut bracing but only swelling rigidity due to the shearing rigidity of the top chord plane. Statically, its behaviour complies with that of the ribbed plate.

Let shearing rigidity

$$T_{33}^t = \frac{E}{a} \cdot \frac{A_2^t}{\sqrt{2}} \quad (7)$$

and transversal elongation rigidity

$$T_{12}^t = T_{33}^t \quad (8)$$

of the top chord plane be neglected. A 'torsionless' substitutional orthotropic plate is obtained in this way, where $H = 0$ and the bending rigidity in the direction of the x and y axis complies with (4).

Differential equation of the plate:

$$B(w'''' + w'') = -p \quad (9)$$

5.2.1.3 'Diagonal square over square' /1/

A particular feature of the structure illustrated in Fig. 3 is that it undergoes strain $\epsilon_x = -\epsilon_y$ without any resistance:



Fig. 5.

Accordingly, the top chord plane is capable of taking up only waist forces of identical magnitude in the direction of the x and y axes:

$$N = n_x \cdot \sqrt{2} \cdot a = n_y \cdot \sqrt{2} \cdot a$$

The elongation rigidity of the top chord plane can be determined only for a force system of this type:

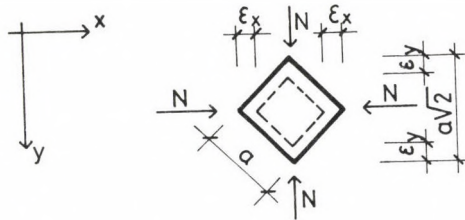


Fig. 6.

Tensile rigidity:

$$T_{11}^t = T_{22}^t = \frac{E \cdot A^t}{a} \quad (10)$$

The top chord plane has also shearing rigidity as it resists the following shearing force system:

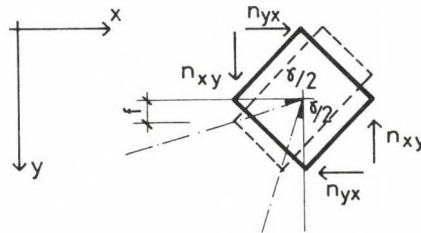


Fig. 7.

This shearing rigidity shall be neglected because the bottom chord plane has only elongation rigidity in the direction of the x and y axis:

$$T_{11}^b = T_{22}^b = E \cdot A^b / \sqrt{2} \cdot a \quad (11)$$

Elongation rigidity matrix of the two chord planes:

$$\underline{T}_{\text{hydrost.}}^t = \frac{E \cdot A^t}{a} \begin{bmatrix} 1 & 1 & 0 \\ 1 & 1 & 0 \\ 0 & 0 & \boxed{1/2} \end{bmatrix} \quad (12)$$

$$\underline{T}_{\text{hydrost.}}^b = \frac{E \cdot A^b}{\sqrt{2} \cdot a} \begin{bmatrix} 1/2 & 1/2 & 0 \\ 1/2 & 1/2 & 0 \\ 0 & 0 & \boxed{0} \end{bmatrix} \quad (13)$$

Hence, with T_{33}^t neglected, the remaining rigidities can be rendered proportional to each other.

The top chord plane is capable of taking up only waist forces of identical magnitude in the direction of the x and y axis. That means that a hydrostatic stress state is prevailing. Therefore, also the bending moments and the section waist forces must be identical in these two directions and accordingly, the same applies also to the bottom chord plane.

Any stress state can be divided in a hydrostatic part and a deviatoric part and similarly, the strain state associated with a stress state can be divided in two parts, the principal elongation ϵ_0 of one part being equal to the average principal elongation, or to the octahedral specific elongation, while the other part being of deviatoric character.

Matrix (13) satisfies the above conditions. Hydrostatic rigidities can be defined as the hydrostatic part of strain state ϵ_x , ϵ_y :

$$\epsilon_x^{\text{hydr.}} = \epsilon_y^{\text{hydr.}} = \frac{\epsilon_y + \epsilon_x}{2} \quad (14)$$

The bending rigidity of the space lattice is given by the moment of inertia of the rigidities of both flange planes for the common axis of gravity:

$$B_{11} = B_{22} = B^{\text{grid}} \frac{E \cdot h^2}{a} \cdot \frac{A^t}{1 + \sqrt{2} \frac{A^t}{A^b}} \quad (15)$$

The space lattice has no torsional rigidity and thus the load is carried by bending in the direction of the x and y axes /3/:

$$m_x'' + m_y'' = -p \quad (16)$$

Waist forces $n_x = n_y$ are equal to the waist forces determined by the actual rigidities of the flange planes.

Since the upper flange plane undergoes strain $\epsilon_x = -\epsilon_y$ without resistance, curvatures

$$w'' = w'' = \frac{\epsilon_x}{h}$$

result from it without bending moments. Therefore, the relationship between the average of the curvatures and the bending moments can be written, as follows:

$$m_x = m_y = -B^{\text{grid}} \frac{w'' + w''}{2} = -B^{\text{grid}} \nabla^2 \cdot w \quad (17)$$

The simplified differential equation of the space is obtained by substituting equation (17) into (15):

$$\frac{B^{\text{grid}}}{2} w'''' + \frac{B^{\text{grid}}}{2} w'' + B^{\text{grid}} w'' = 2 \cdot 2 \cdot w \cdot \frac{B^{\text{grid}}}{2} = -p \quad (18)$$

Hence, the equivalent continuum is an isotropic plate the bending rigidity of which being half of the bending rigidities of the original grid. 'Hexagonal on triangular'

5.2.1.4 'Hexagon over triangle' /1/, /10/

The bottom chord plane of the grid illustrated in Fig. 4 has a definite substitutional elongation and shearing rigidity:

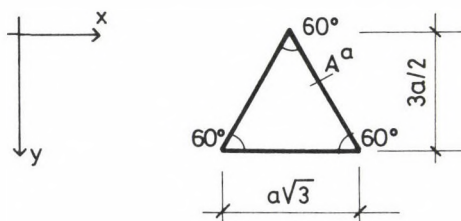


Fig. 8.

$$T_{11}^b = T_{22}^b = \frac{3E \cdot A^b}{4a} \quad (19)$$

$$T_{12}^b = T_{21}^b = \frac{E \cdot A^b}{4a} \quad (20)$$

$$T_{33}^b = \frac{E \cdot A^b}{4a} \quad (21)$$

Elongation rigidity matrix of the bottom chord plane:

$$\underline{I}^b = \frac{E \cdot A^b}{4a} \begin{bmatrix} 3 & 1 & 0 \\ 1 & 3 & 0 \\ 0 & 0 & 1 \end{bmatrix} \quad (22)$$

The entire structure contains the shearing rigidity of the bottom chord plane owing to three sets of 'closed lattice-type tubes' intersecting at angles of 120° .

The top chord is unstable, moving in the way illustrated below without resistance:

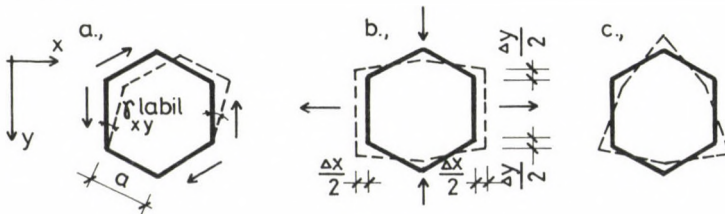


Fig. 9.

The strain according to Fig. 9/a corresponds to angular distortion $\gamma_{xy}^{\text{labil}}$ resulting from pure shear. Hence, the top chord is incapable of taking up shear forces.

The strain according to Fig. 9/b is described by relationship

$$\epsilon_x^{\text{labil}} = -\epsilon_y^{\text{labil}} \quad (23)$$

Accordingly, the top chord is capable of taking up tension or pressure equivalent to hydrostatic tension or pressure only. However, it has a definite rigidity to resist such tensions and pressures:

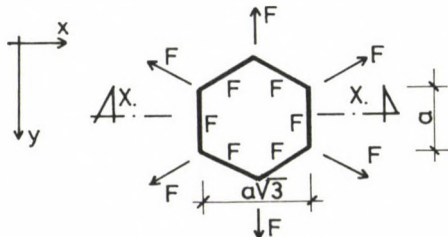


Fig. 10.

Hydrostatic tension gives rise to forces in the hexagon acting in the way illustrated in Fig. 10. That means that a force of a magnitude identical with force F acting upon the joints arises in every bar.

In the x - x section, a force F acts upon a section of a length of $a \cdot \sqrt{3}$. Thus the appropriate tensile force, $n_x = n_y$, will be

$$n_x = n_y = \frac{F}{a \cdot \sqrt{3}} \quad (24)$$

Elongation of the bars is essentially a dilatation:

$$\epsilon^{\text{bar}} = \frac{F}{E \cdot A^t} \quad (25)$$

resulting in a dilatation $\epsilon_x^{\text{dil}} = \epsilon_y^{\text{dil}} = \epsilon^{\text{bar}}$ in every bar. Therefore, the substitutional dilatation-type tensile rigidity will be

$$I_{\text{dil}}^t = \frac{n_x}{\epsilon_x^{\text{dil}}} = \frac{n_y}{\epsilon_y^{\text{dil}}} = \frac{E \cdot A^t}{a \sqrt{3}} \quad (26)$$

Elongation rigidity matrix of the top chord plane for the overall strain vector,

$$\underline{\epsilon}^t = \underline{\epsilon}_{\text{labil}}^t + \underline{\epsilon}_{\text{dil}}^t \quad (27)$$

will be

$$I_{\text{dil}}^t = \begin{bmatrix} \frac{I_{\text{dil}}^t}{2} & \frac{I_{\text{dil}}^t}{2} & 0 \\ \frac{I_{\text{dil}}^t}{2} & \frac{I_{\text{dil}}^t}{2} & 0 \\ 0 & 0 & 0 \end{bmatrix} = \frac{E \cdot A^t}{2a \sqrt{3}} \begin{bmatrix} 1 & 1 & 0 \\ 1 & 1 & 0 \\ 0 & 0 & 0 \end{bmatrix} \quad (28)$$

where requirement

$$n_x^t = n_y^t = I_{\text{dil}}^t \frac{(\epsilon_x^t + \epsilon_y^t)}{2} ; \quad n_{xy}^t = 0$$

is satisfied.

Statically, the behaviour of this grid is similar to that described in par 5.2.1.3. A difference is, however, that it shows a torsional rigidity owing to the stable bottom chord and to the 'closed lattice-type tubes'.

There is no relationship between the strain according to Fig. 9/c and section forces of any type and it sets no direct limits to the forces.

Since stress function ϕ is neglected, waist forces of identical magnitude arise in the direction of the x and y axis also in the bottom chord plane (hydrostatic stress state). Therefore, although the rigidities of the chord planes are not proportional (elongation and transversal elongation), the hydrostatic elongation rigidities of the bottom chord plane can be determined which are proportional to the similar rigidities of the top chord plane!

Hydrostatic rigidity matrix of the bottom chord plane:

$$I_{\text{hydr}}^b = \frac{E \cdot A^b}{2a} \begin{bmatrix} 1 & 1 & 0 \\ 1 & 1 & 0 \\ 0 & 0 & \boxed{1} \end{bmatrix} \quad (29)$$

From the matrix, the coefficient of shearing rigidity is omitted because it is included in 'closed lattice-type tubes'.

The bending rigidity and transversal bending rigidity can be calculated on the basis of elongation rigidity matrices I_{dil}^t and I_{hydr}^b , respectively.

The simplified differential equation of the space grid can be written on the basis of the general equilibrium equation of plates/3/:

$$m_x'' + m_y'' + m_{xy}' = -p \quad (30)$$

Since the top chord plane undergoes strain $\epsilon_x = -\epsilon_y$ without resistance that is

$$m_x = m_y,$$

curvatures

$$w'' = -w'' = \frac{\epsilon_x}{h} \quad (31)$$

result from it without bending moments. Therefore, a relationship between the average of the curvatures and the bending moments shall be written:

$$m_x = m_y = -B^{\text{grid}} \frac{w'' + w''}{2} = -\frac{B^{\text{grid}}}{2} \nabla^2 w \quad (32)$$

where

$$B_{11}^{\text{grid}} = B_{22}^{\text{grid}} = \frac{E \cdot h^2}{2a} \cdot \frac{\frac{A^t}{\sqrt{3}} \cdot A^b}{\frac{A^t}{\sqrt{3}} + A^b} \quad /1/; /9/ \quad (33)$$

and

Thus the hydrostatic bending rigidity matrix of the space grid, which means the bending rigidity of the chord planes, will be

$$\underline{\underline{B}}^{\text{hydr.}} = \begin{bmatrix} B^{\text{hydr.}} & B^{\text{hydr.}} & 0 \\ B^{\text{hydr.}} & B^{\text{hydr.}} & 0 \\ 0 & 0 & 0 \end{bmatrix} \quad (35)$$

Torsional rigidity of the structure:

Shear force n_{xy}^b arising in the bottom chord plane has no counterpart in the top chord plane as the top chord plane has no torsional rigidity (see Fig. 9/c).

The overall torsional rigidity of the entire structure can be attributed to 'closed lattice-type tubes', the torsional rigidity of a 'tube' being /10/

$$G \cdot J_t = \frac{M_t}{\vartheta} = \frac{2 \sqrt{3} \cdot E \cdot h^2}{\frac{1}{A^t} + \frac{2 \alpha^3}{A^{\text{brac.}}} + \frac{3 \sqrt{3}}{A^b}} \quad (36)$$

Plate-type torsional rigidity of the entire structure /9/:

$$B_{33} = \frac{G \cdot J_t}{6a} = \frac{E \cdot h^2}{2a} \cdot \frac{A^b}{\frac{\sqrt{3} \cdot A^b}{2A^t} + \sqrt{3} \left(1 + \frac{h^2}{a^2} \right) \frac{3}{2} \cdot \frac{A^b}{A^{\text{brac.}}} + \frac{9}{2}} \quad (37)$$

In addition to torsional rigidity, bending rigidity B_{33} and transversal bending rigidity - B_{33} are ensured in the direction of the x and y axis by the three 'tubes' intersecting at angles of 120° .

Bending rigidity matrix of the 'tubes' /10/:

$$\underline{\underline{B}}^{\text{tube}} = \begin{bmatrix} B_{33}^{\text{tube}} & B_{33}^{\text{tube}} & 0 \\ -B_{33}^{\text{tube}} & B_{33}^{\text{tube}} & 0 \\ 0 & 0 & B_{33}^{\text{tube}} \end{bmatrix} \quad (38)$$

Both matrix (35) and matrix (38) are isotropic and therefore also their sum that is the overall bending rigidity of the space grid will be isotropic:

$$\underline{B}^{isotr} = \underline{B}^{hydr} + \underline{B}^{tube} = \begin{bmatrix} B^{hydr} + B_{33}^{tube} & B^{hydr} - B_{33}^{tube} & 0 \\ B^{hydr} - B_{33}^{tube} & B^{hydr} + B_{33}^{tube} & 0 \\ 0 & 0 & B_{33}^{tube} \end{bmatrix} \quad (39)$$

the differential equation of which being

$$B^{isotr} \cdot W'''' + B^{isotr} \cdot W'' + 2B^{isotr} \cdot W = -p \quad (40)$$

where

$$H^{isotr} = B_{12}^{isotr} + 2B_{33}^{isotr} = B^{isotr} \quad (41)$$

5.2.2 Use of the simplified compatibility method to write continuum equations /1/

5.2.2.1 'Square with diagonals on square offset' (Fig. 1)

Let the neutral plane of torsional rigidities of 'closed lattice-type tubes' be selected as the place of the neutral plane.

$$k = 1 + 4 \sqrt{2} \frac{A_2^t}{A^{brac}} \left(\frac{h^2}{a^2} + \frac{1}{2} \right)^{3/2} \quad (42)$$

The top chord plane is more rigid. Part I of the rigidity:

$$\Gamma_{11,I}^t = \Gamma_{22,I}^t = k \cdot \Gamma_{11}^b \quad (43)$$

Part II of the rigidity includes 'excess' rigidities:

$$\Gamma_{11,II}^t = \Gamma_{22,II}^t = \Gamma_{11}^t - \Gamma_{11,I}^t \quad (44)$$

$$\Gamma_{12}^t = \frac{E}{a} \cdot \frac{A_2^t}{\sqrt{2}} \quad (45)$$

(Γ_{33}^t is included in the bending rigidity matrix)

Elongation rigidity matrices of the top and bottom chord planes:

$$\underline{\underline{I}}^t = \frac{E}{a} \begin{bmatrix} \left(A_1^t + \frac{A_2^t}{\sqrt{2}} \right) & \boxed{\frac{A_2^t}{\sqrt{2}}} & 0 \\ \boxed{\frac{A_2^t}{\sqrt{2}}} & \left(A_1^t + \frac{A_2^t}{\sqrt{2}} \right) & 0 \\ 0 & 0 & \boxed{\frac{A_2^t}{\sqrt{2}}} \end{bmatrix} \quad (46)$$

Included
in tubes!

$$\underline{\underline{I}}^b = \frac{E}{a} \begin{bmatrix} A^b & \boxed{0} & 0 \\ \boxed{0} & A^b & 0 \\ 0 & 0 & \boxed{0} \end{bmatrix} \quad (47)$$

The matrix of bending rigidities will be obtained if the framed elements in matrices (46), (47) are omitted:

$$\underline{\underline{B}} = \frac{E}{a} \begin{bmatrix} A^b \cdot h^2 \frac{k}{1+k} & 0 & 0 \\ 0 & A^b \cdot h^2 \frac{k}{1+k} & 0 \\ 0 & 0 & 0 \end{bmatrix} \quad (48)$$

The 'excess' bending rigidity factors are supplied by the following relationships:

$$B_{11}^{\text{exc}} = T_{11,II}^t \cdot (h^t)^2 \quad (49)$$

$$B_{12}^{\text{exc}} = T_{12}^t (h^t)^2 \quad (50)$$

Matrix of 'excess' bending rigidities:

$$B^{\text{exc}} = \frac{E}{a} (h^t)^2 \begin{bmatrix} \left(A_1^t + \frac{A_2^t}{\sqrt{2}} \right) (1-k) & \frac{A_2^t}{\sqrt{2}} & 0 \\ \frac{A_2^t}{\sqrt{2}} & \left(A_1^t + \frac{A_2^t}{\sqrt{2}} \right) (1-k) & 0 \\ 0 & 0 & 0 \end{bmatrix} \quad (51)$$

where

$$h^t = \frac{A^b}{A^b + \left(A_1^t + \frac{A_2^t}{\sqrt{2}} \right)} \cdot h \quad (52)$$

Matrix of bending rigidities supplied by 'closed' lattice-type 'tubes':

$$\underline{\underline{B}}^{\text{tube}} = \frac{G.J_t}{2a} \begin{bmatrix} 0 & 0 & 0 \\ 0 & 0 & 0 \\ 0 & 0 & \frac{1}{2} \end{bmatrix} \quad (53)$$

where

$$G.J_t = \frac{E h^2}{a} \frac{A_2^t}{\sqrt{2} + 4 \frac{A_2^t}{A^{\text{brac}}} \left(\frac{h^2}{a^2} + \frac{1}{2} \right)^{3/2}} \quad (54)$$

The bending rigidity matrix for writing the simplified differential equation of the continuum is supplied by the sum of matrices (48), (51), (53):

$$\Sigma \underline{\underline{B}} = \underline{\underline{B}} + \underline{\underline{B}}^{\text{exc}} + \underline{\underline{B}}^{\text{tube}} \quad (55)$$

$$\Sigma \underline{\underline{B}} = \begin{bmatrix} (B_{11}^{\text{exc}} + B_{11}) & B_{12}^{\text{exc}} & 0 \\ B_{21}^{\text{exc}} & B_{22}^{\text{exc}} + B_{22} & 0 \\ 0 & 0 & B_{33}^{\text{tube}} \end{bmatrix} \quad (56)$$

Simplified differential equation of the substitutional continuum:

$$(B^{\text{exc}} + B) w'''' + (B^{\text{exc}} + B) w'' + 2(B_{12}^{\text{exc}} + B_t^{\text{tube}}) w'' = -p \quad (57)$$

The above equation complies with equation of orthotropic plates.

$$B w'''' + B w'' + B H w'' = -p$$

5.2.2.2 'Square with diagonals on square' /1/ (Fig. 2)

Let the centre of gravity of elongation rigidities of the chord planes be selected as the place of the neutral plane.

The elongation rigidity matrix of the top chord bottom plane complies with (46) while that of the chord plane with (47).

Since there are no 'closed lattice-type tubes' in this space grid

$$T_{12}^t = \frac{E}{a} \cdot \frac{A_2^t}{\sqrt{2}} ; \quad T_{33}^t = \frac{E}{a} \cdot \frac{A_2^t}{\sqrt{2}}$$

are obtained as excess rigidity and these rigidities can be used to calculate for the elements of the excess rigidity matrix:

$$B_{12}^{\text{exc}} = T_{12}^t (h^t)^2 \quad (58)$$

$$B_t^{\text{exc}} = 2B_{33}^{\text{exc}} = 2T_{33}^t (h^t)^2 \quad (59)$$

where h^t is identical with (52).

Matrix of bending rigidities:

$$\underline{\underline{B}} = \frac{E}{a} h^t{}^2 \begin{bmatrix} \left(A_1^t + \frac{A_2^t}{\sqrt{2}} \right) A^b & 0 & 0 \\ \left(A_1^t + \frac{A_2^t}{\sqrt{2}} \right) A^b & \left(A_1^t + \frac{A_2^t}{\sqrt{2}} \right) A^b & 0 \\ 0 & \left(A_1^t + \frac{A_2^t}{\sqrt{2}} \right) A^b & 0 \\ 0 & 0 & 0 \end{bmatrix} \quad (60)$$

$$\underline{\underline{B}}^{\text{exc}} = \frac{E}{a} (h^t)^2 \begin{bmatrix} 0 & \frac{A_2^t}{\sqrt{2}} & 0 \\ \frac{A_2^t}{\sqrt{2}} & 0 & 0 \\ 0 & 0 & 2 \frac{A_2^t}{\sqrt{2}} \end{bmatrix} \quad (61)$$

The bending rigidity matrix for writing of the simplified differential equation of the continuum is supplied by the sum of matrices (60), (61): $\Sigma \underline{B} = \underline{B} + \underline{B}^{exc}$ (62)

$$\Sigma \underline{B} = \begin{bmatrix} B_{11} & B_{12}^{exc} & 0 \\ B_{12}^{exc} & B_{22} & 0 \\ 0 & 0 & B_{33}^{exc} \end{bmatrix} \quad (63)$$

where $B_{11} = B_{22} = B$.

The equivalent continuum is an orthotropic plate. Simplified differential equation of the structure:

$$B \cdot w'''' + B \cdot w'' + 2(B_{12}^{exc} + B_t^{exc}) w'' = -p \quad (64)$$

5.2.2.3 'Diagonal on square' (Fig. 3)

Let the centre of gravity of elongation rigidities of the chord planes be selected as the place of the neutral plane.

Considering rigidity matrices (12), (13) of the chord planes, T_{33}^t is obtained as an additional rigidity. With this, the 'excess' bending rigidity will be

$$B_{33}^{exc} = \frac{E \cdot A^t}{2a} (h^t)^2 \quad (65)$$

where

$$h^t = \frac{\frac{A^b}{\sqrt{2}}}{\frac{A^b}{\sqrt{2}} + A^t} h \quad (66)$$

Using the bending rigidity matrix (14):

$$\underline{B} = \frac{E}{a} (h^t)^2 \begin{bmatrix} \frac{A^t}{1 + \sqrt{2} \frac{A^t}{A^b}} & \frac{A^t}{1 + \sqrt{2} \frac{A^t}{A^b}} & 0 \\ \frac{A^t}{1 + \sqrt{2} \frac{A^t}{A^b}} & \frac{A^t}{1 + \sqrt{2} \frac{A^t}{A^b}} & 0 \\ 0 & 0 & 0 \end{bmatrix} \quad (67)$$

The 'excess' bending rigidity matrix:

$$\underline{B}^{\text{exc}} = \frac{E}{a} (h^t)^2 \begin{bmatrix} 0 & 0 & 0 \\ 0 & 0 & 0 \\ 0 & 0 & \frac{A^t}{2} \end{bmatrix} \quad (68)$$

where

$$B_t^{\text{exc}} = 2B_{33}^{\text{exc}} = \frac{E \cdot A^t}{a} (h^t)^2 \quad (69)$$

For writing the simplified continuum equation of the continuum, the bending rigidity matrix is supplied by the sum of matrices (67), (68):

$$\Sigma \underline{B} = \underline{B} + \underline{B}^{\text{exc}} = \frac{E(h^t)^2}{a} \begin{bmatrix} \frac{A^t}{1 + \sqrt{2} \frac{A^t}{A^b}} & \frac{A^t}{1 + \sqrt{2} \frac{A^t}{A^b}} & 0 \\ \frac{A^t}{1 + \sqrt{2} \frac{A^t}{A^b}} & \frac{A^t}{1 + \sqrt{2} \frac{A^t}{A^b}} & 0 \\ 0 & 0 & \frac{A^t}{2} \end{bmatrix} \quad (70)$$

The equivalent continuum is an orthotropic plate. Simplified differential equation of the structure:

$$B \cdot w'''' + B \cdot w'' + 2(B + B_t^{\text{exc}}) w'' = -p \quad (71)$$

where

$$B = \frac{B^{\text{grid}}}{2} \quad \text{see (18)} \quad (72)$$

Here the statically equivalent orthotropic plate has a torsional rigidity $(B + B_t^{\text{exc}})$, rather unusually in the theory of orthotropic plates.

5.2.2.4 'Hexagon over triangle' (Fig. 4)

Let the place of the neutral plane be selected in the neutral plane of torsional rigidities of 'closed lattice-type tubes'.

It is the top chord plane that shall be considered to be the basis in this case while the rigidity of the bottom chord plane shall be divided in part I and part II using a proportionality factor k^* :

$$k^* = \frac{1}{2\sqrt{3}} \cdot \frac{A^b}{A^t} + \frac{\alpha^3}{\sqrt{3}} \cdot \frac{A^b}{A^{brac}} \pm \frac{1}{2} \quad (73)$$

where

$$\alpha = \sqrt{\frac{h^2}{a^2} + 1} \quad (74)$$

Matrix of rigidity part I:

$$k^* \cdot \underline{\underline{I}}^t = \underline{\underline{I}}_{hydr}^b \quad \underline{\underline{I}} = k^* \cdot \frac{E \cdot A^t}{2 \sqrt{3} \cdot a} \begin{bmatrix} 1 & 1 & 0 \\ 1 & 1 & 0 \\ 0 & 0 & 0 \end{bmatrix} \quad (75)$$

The matrix of bending rigidities can be calculated on the basis of the above matrix:

$$\underline{\underline{B}} = h^2 \frac{k^*}{1+k^*} \cdot \frac{E \cdot A^t}{2 \sqrt{3} \cdot a} \begin{bmatrix} 1 & 1 & 0 \\ 1 & 1 & 0 \\ 0 & 0 & 0 \end{bmatrix} \quad (76)$$

With the shearing rigidity neglected, the matrix of the remaining 'excess' elongation rigidities of the lower flange plane will be

$$\underline{\underline{I}}_{hydr,II}^b = \underline{\underline{I}}_{hydr}^b - \underline{\underline{I}}_{hydr,I}^b \quad (77)$$

$$\underline{\underline{I}}_{hydr,II}^b = \frac{E \cdot A^b}{4a} \begin{bmatrix} 3 & 1 & 0 \\ 1 & 3 & 0 \\ 0 & 0 & \boxed{1} \end{bmatrix} - k^* \frac{E \cdot A^t}{2 \sqrt{3} \cdot a} \begin{bmatrix} 1 & 1 & 0 \\ 1 & 1 & 0 \\ 0 & 0 & 0 \end{bmatrix} \quad (78)$$

included in tubes!

Coefficients of elongation rigidity required to determine the 'excess' bending rigidity matrix:

$$T_{11,II}^b = \frac{E}{2a} \left(3 \cdot A^b - k^* \frac{A^t}{\sqrt{3}} \right) \quad (79)$$

$$T_{12,II}^b = \frac{E}{2a} \left(\frac{A^b}{2} - k^* \frac{A^t}{\sqrt{3}} \right) \quad (80)$$

Coefficients of 'excess' bending rigidity:

$$B_{11}^{exc} = T_{11,II}^b (h^b)^2 \quad (81)$$

$$B_{12}^{exc} = T_{12,II}^b (h^b)^2 \quad (82)$$

$$h^b = \frac{C}{h \cdot E \cdot A^b} \quad (83)$$

$C = G \cdot J_t$ shall be calculated according to (36).

Matrix of bending rigidities supplied by the 'tubes':

$$\underline{\underline{B}}^{tube} = \begin{bmatrix} B_t^{tube} & -B_t^{tube} & 0 \\ -B_t^{tube} & B_t^{tube} & 0 \\ 0 & 0 & B_t^{tube} \end{bmatrix} \quad (84)$$

Matrix of 'excess' bending rigidities:

$$\underline{\underline{B}}^{exc} = \frac{E}{2a} (h^b)^2 \begin{bmatrix} \left(3A^b - k^* \frac{A^t}{\sqrt{3}}\right) \left(\frac{A^b}{2} - k^* \frac{A^t}{\sqrt{3}}\right) & 0 \\ \left(\frac{A^b}{2} - k^* \frac{A^t}{\sqrt{3}}\right) & 3A^b - k^* \frac{A^t}{\sqrt{3}} \\ 0 & 0 & 0 \end{bmatrix} \quad (85)$$

The bending rigidity matrix required for writing of the simplified differential equation of the equivalent continuum is supplied by the sum of matrices (76), (84), (85): $\underline{\underline{\Sigma B}} = \underline{\underline{B}} + \underline{\underline{B}}^{tubes} + \underline{\underline{B}}^{exc}$ (86)

$$\underline{\underline{\Sigma B}} = \begin{bmatrix} (B_{11}^{11} + B_t^{tubes} + B_{11}^{exc}) & (B_{12} - B_t^{tubes} + B_{12}^{exc}) & 0 \\ (B_{21} - B_t^{tubes} + B_{21}^{exc}) & (B_{22} + B_t^{tubes} + B_{22}^{exc}) & 0 \\ 0 & 0 & B_t^{tube} \end{bmatrix} \quad (87)$$

The continuum of the space grid is an orthotropic plate, the simplified differential equation of the structure being

$$(B + B_t^{tube} + B^{exc}) w'''' + (B + B_t^{tube} + B^{exc}) w'' + 2(B_{12} - B_t^{tube} + 2B_t^{tube} + B_{12}^{exc}) w'' = -p \quad (88)$$

5.2.3 Adaptation of Giencke's theory to two-layer space grids /4/

According to Giencke, the differential equation of smooth orthotropic plates (3) will apply to ribbed plates if the longitudinal and transversal reinforcing ribs are arranged symmetrically in two directions normal to each other (Fig. 11).

An asymmetry of longitudinal and transversal ribs will result in torsional moments and shear forces in the eccentric top plate in case of a twist of the ribbed plate (Fig. 12).

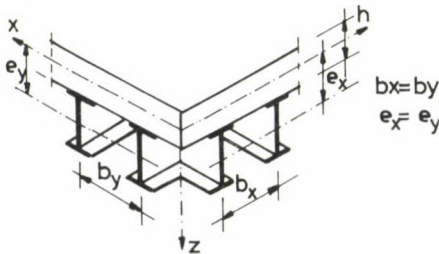


Fig. 11.

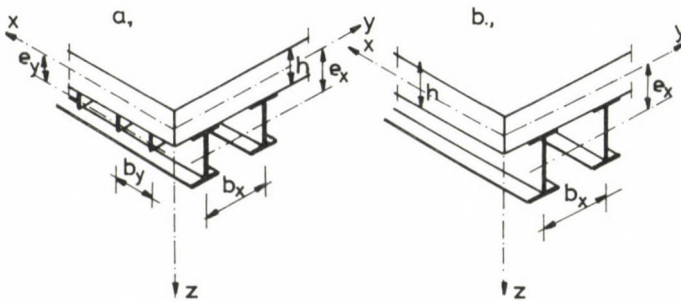


Fig. 12.

On an equilibrium basis, normal forces are also associated with the shear forces. That means that normal forces arise in the midplane.

Based on the usual assumptions of the plate theory and neglecting the effect of elongations of the centroid axes upon deflection of the plate, the equation of eccentrically ribbed plates has been derived by Giencke:

$$B_x \cdot w'''' + B_y \cdot w'''' + 2H^x \cdot w'''' = -p \quad (89)$$

This equation is essentially identical with equation (3), a difference lying only in the torsional rigidity.

$$H^* = C + \nu \cdot e_x \cdot e_y D + (e_x + e_y)^2 \frac{(1-\nu) D}{4} \quad (90)$$

where the definition of e_x and e_y is given in Fig. 12,

$$C = B + \frac{B_{xy} + B_{yx}}{2}$$

(bending rigidity of the ribbed plate, taking into consideration the torsional rigidity of the ribs),

$$D = \frac{E \cdot h}{1-\nu^2}$$

(membrane part of the rigidity of the ribbed plate), ν = transversal contraction factor.

According to Kollár's calculations which have not been published so far,

$$H^* = (h^t)^2 \cdot (T_{12}^t + T_{33}^t) \quad (91)$$

in case of space lattices of 'cross-brace type square shifted over square' and 'cross-brace type square over square' type, where, according to h^t in (52), T_{12}^t can be calculated only on the basis of the top chord plane.

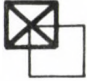



An important result of Giencke's theory is the substitutional rigidity according to (90) the use of which permits the theory to be applied to two-layer lattices provided the bending part and membrane part of the rigidity of the space lattice is similar to the rigidities of the ribbed plate.

6. Practical application of the simplified continuum method

The internal forces of the space grid are determined on the basis of the internal forces of the equivalent continuum by converting the section forces into bar forces.

Using the simplified continuum method, differential equations of isotropic plates or orthotropic plates where the bending rigidities in the direction of the x and y axis are identical can be written in case of a geometrically homogenous network of bars or bars of identical section within a group of bars. Hence, the statically equivalent continua of space grids of this type differ from each other only in the ratio of torsional rigidity H and bending rigidity $B/1/$.

Table 1 Simplified differential equations based on the simplified equilibrium method

| grid type symbol | Reference | Differential equation | Equivalent continuum |
|---|-----------|---|----------------------|
|  | (6) | $B \cdot w'''' + B \cdot w'''' + 2H \cdot w'''' = -p$ given H/B ratio | orthotropic |
|  | (9) | $B(w'''' + w''') = -p$ H=0, H/B=0 | orthotropic |
|  | (18) | $\frac{B^{grid}}{2} \cdot w'''' + \frac{B^{grid}}{2} \cdot w'''' + B^{grid} \cdot w'''' = -p$ H=B, H/B=1 | isotropic |
|  | (40) | $B^{isotr} \cdot w'''' + B^{isotr} \cdot w'''' + 2B^{isotr} \cdot w'''' = -p$ | isotropic |

As seen in the Tables,

| | |
|---------------------------|---------------------------|
| H/B = 0 | for 'torsionless plates', |
| H/B = 1 | for isotropic plates, |
| 0 < H/B < 1 or H/B > 1 | for orthotropic plates. |

Table 2 Simplified differential equations based on the simplified compatibility method

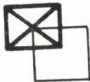



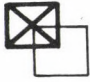

| grid type symbol | Reference | Differential equation | Equivalent continuum |
|--|-----------|---|----------------------|
|  | (57) | $(B+B^{exc})w''''+(B+B^{exc})w'''+2(B_{12}^{exc}+B_t^{tubes})w'''' = -p$ <p>given H/B ratio</p> | orthotropic |
|  | (64) | $Bw''''+Bw'''+2(B_{12}^{exc}+B_t^{exc})w'''' = -p$ <p>given H/B ratio</p> | orthotropic |
|  | (71) | $Bw''''+Bw'''+2(B+B_t^{exc})w'''' = -p$ <p>H > B, given H/B ratio</p> | orthotropic |
|  | (81) | $(B+B^{exc}+B_t^{tubes})w''''+(B+B^{exc}+B_t^{tubes})w'''+2(B_{12}^{exc}-B_{12}^{tubes}+2B_t^{tubes})w'''' = -p$ <p>given H/B ratio</p> | orthotropic |

Table 3 Simplified differential equation based on adaptation of Giencke's theory

| grid type symbol | Reference | Differential equation | Equivalent continuum |
|---|-----------|---|----------------------|
|  | (89) | $B_x.w''''+B_y.w'''+2H^*.w'''' = -p$ <p>given H/B ratio</p> | orthotropic |
|  | (89) | $B_x.w''''+B_y.w'''+2H^*.w'''' = -p$ <p>given H/B ratio</p> | orthotropic |

Simplified differential equations are advantageous not only in that they can be solved in a simpler way as compared with the coupled differential equations of the fourth order but also because for some bending and torsional moments, values ready for use are found in the literature /3/, /5/, /6/, /7/.

Also, diagrams supplying the mentioned values between ratios $H/B=0$ and $H/B=1$ are found in /1/ and /9/ for maximum bending and torsional moments of rectangular plates of different ratio between the sides in case of different supports.

The use of available solutions permits the calculation of moment by solution of the plate equation with respect to w to be avoided:

$$m_x^{\text{grid}} = -Bw'' - B_{12} w'' \quad /3/ \quad (92)$$

$$m_y^{\text{grid}} = -Bw'' - B_{12} w'' \quad /3/ \quad (93)$$

$$m_{xy}^{\text{grid}} = -B_t w' \quad /3/ \quad (94)$$

6.1 Decomposition of moments in accordance with the types of rigidity

To be stressed are some important points. Symbols 'H' and 'B' in the equation of the orthotropic plate may contain three types of rigidity such as

- rigidity of the chord planes,
- additional rigidities in the simplified compatibility method (see superscript 'exc.'),
- rigidity of 'closed lattice-type tubes' (see superscript 'tubes').

Hence, moments m_x , m_y , m_{xy} shall be decomposed in accordance with the types of rigidity occurring in the following way:

If there are no 'tube-type' rigidities /1/, the moments shall be simply decomposed in accordance with the ratio between rigidity of the chord plane and 'excess' rigidity as both rigidities are of identical character:

$$\underline{m}^{\text{chord planes}} = \underline{B}(\underline{B} + \underline{B}^{\text{exc}})^{-1} \cdot \underline{m}^{\text{grid}} \quad (95)$$

$$\underline{m}^{\text{exc}} = \underline{B}^{\text{exc}}(\underline{B} + \underline{B}^{\text{exc}})^{-1} \cdot \underline{m}^{\text{grid}} \quad (96)$$

Formula

$$n = \frac{m}{h} \text{ chord planes} \quad (97)$$

shall be used to calculate membrane forces resulting from the part of moment associated with the bending rigidity of the chord planes

Formulae

$$n_{exc.}^t = \frac{m^{exc}}{h^t} \quad (\text{pressure}) \quad (98)$$

and

$$n_{exc.}^b = \frac{m^{exc}}{h^b} \quad (\text{tension}) \quad (99)$$

shall be used to calculate membrane forces resulting from part $m^{exc.}$ of the moment in relation with 'excess' rigidities, depending on whether the 'excess' membrane force has arisen in the upper chord plane or in the lower chord plane.

The bar forces of the chord planes can be calculated on the basis of membrane forces according to (97), (98), (99).

If also 'tube-type' rigidities are present /1/, torsional moments m_{ti} occurring in 'closed lattice-type tubes' shall be determined as well.

In case of a 'Square with diagonals on square offset' space grid, the bending moments are borne by the chord planes while the torsional moments by the 'closed lattice-type tubes'.

In case of a 'hexagonal on triangular' space grid, torsional moments m_{ti} can not be calculated on the basis of part m^{tube} of the decomposed plate moments but only on the basis of overall plate moments m . Namely, matrix B^{exc} is of the same character as matrix B and the sum of both matrices can be considered to be bending rigidity matrix B of the flange planes.

Therefore, the following formula shall be used to calculate moments arising in the chord planes, associated with bending rigidity matrix B :

$$m_{\text{chord planes}} = B(B + B^{exc} + B^{tube})^{-1} \cdot m_{\text{grid}} \quad (100)$$

Formula for calculation of torsional moments arising in 'closed lattice-type tubes':

$$m_t = -\frac{c}{2b} \left(\begin{matrix} 1 & \beta \end{matrix} \right)^{-1} \cdot \begin{matrix} 1 \\ \beta \end{matrix} \cdot B(B + B^{exc} + B^{tube})^{-1} \cdot m_{\text{grid}} \quad (101)$$

where $C = G \cdot I_t$,

b = width of the 'tube',

$$\left(\hat{\underline{L}} \hat{\underline{\beta}} \right)^{-1} = \begin{bmatrix} 2/3 & 0 & 1/3 \\ 0 & 2/3 & 1/3 \\ -2/3 & -2/3 & 1/3 \end{bmatrix} \quad (102)$$

$$\hat{\underline{L}} \hat{\underline{\beta}} = \begin{bmatrix} 0 & 0 & 1 \\ -\frac{\sqrt{3}}{2} & \frac{\sqrt{3}}{2} & -\frac{1}{2} \\ 0 & 0 & 0 \end{bmatrix} \quad (103)$$

In case of the simplified equilibrium method, the following formulae can be used to decompose the moments:

— in the centre of the space grid:

$$m_x^{\text{chords}} = m_y^{\text{chords}} = \frac{m_x^{\text{grid}} + m_y^{\text{grid}}}{2} \quad (104)$$

$$m_{xy}^{\text{chords}} = 0 \quad (105)$$

— in the corner of the space grid

$$m_x^{\text{chords}} = m_y^{\text{chords}} = 0 \quad (106)$$

The torsional moment shall be decomposed into components resulting in twist of the three pipes running in three directions.

$$m_{t1} = \frac{4}{3} m_{xy}^{\text{grid}} \quad (107)$$

$$m_{t2} = -\frac{1}{\sqrt{3}} \left(m_x^{\text{grid}} - m_y^{\text{grid}} \right) - \frac{2}{3} m_{xy}^{\text{grid}} \quad (108)$$

$$m_{t3} = \frac{1}{\sqrt{3}} \left(m_x^{\text{grid}} - m_y^{\text{grid}} \right) - \frac{2}{3} m_{xy}^{\text{grid}} \quad (109)$$

In case of the simplified compatibility method, equations (100) and (101) shall most reasonably be calculated numerically.

6.2 Some problems in relation to the use of solutions available in the literature on plate theory /6/

Although a solution ready for use as mentioned in par 6 may be found for the plate of a H/B ratio corresponding to the space grid investigated, it is still possible that the B_{12} to B_t ratio in torsional rigidity H of the equivalent plate differs from the B_{12} , B_t ratio in torsional rigidity H of

the investigated space lattice that is Poisson number

$$\nu^e = \frac{B_{12}}{B}$$

of the equivalent continuum differs from that of the space grid in question. (Note that all types of bending rigidity shall be taken into consideration when calculating for ν^e .)

The solutions of statically equivalent isotropic or orthotropic plates with a different ν^e as compared with the space grid are identical for bending deflection (w) that is the Poisson number is not ranging among the boundary conditions. This applies to the case of

- clamped edges and
- edges bearing up freely

but it does not apply to the case of free edges because the expressions of bending force and shear force disappearing there contain ν .

Let ν^{grid} be the Poisson number of the space grid investigated while ν^e that of the equivalent plate.

Equations (92), (93), (94) can be rewritten, as follows:

$$m_x = -B (w'' + w^{'''}) \quad (110)$$

$$m_y = -B (w^{'''} + w'') \quad (111)$$

$$m_{xy} = -B_t \cdot w' \quad (112)$$

With the partial derivatives of bending deflection function 'w' determined and expressed as the moments (m^e) of the equivalent plate, using relationships (110), (111), (112) we obtain

$$w'' = - \frac{m_x^e - \nu^e \cdot m_y^e}{B^e [1 - (\nu^e)^2]} \quad (113)$$

$$w^{'''} = - \frac{m_y^e - \nu^e \cdot m_x^e}{B^e [1 - (\nu^e)^2]} \quad (114)$$

$$w' = - \frac{m_{xy}^e}{B_t^e} \quad (115)$$

Values (113), (114), (115), shall than be substituted again into (92), (93), (94), respectively to obtain the moments of the space grid on the basis of the moments of the equivalent plate:

$$m_x^{\text{grid}} = m_x^e \frac{1 - \nu^e \cdot \nu^{\text{grid}}}{1 - (\nu^e)^2} + \nu^{\text{grid}} \cdot m_y^e \frac{1 - \frac{\nu^e}{\nu^{\text{grid}}}}{1 - (\nu^e)^2} \quad (116)$$

$$m_y^{\text{grid}} = m_y^e \frac{1 - \nu^e \cdot \nu^{\text{grid}}}{1 - (\nu^e)^2} + \nu^{\text{grid}} \cdot m_x^e \frac{1 - \frac{\nu^e}{\nu^{\text{grid}}}}{1 - (\nu^e)^2} \quad (117)$$

$$m_{xy}^{\text{grid}} = \frac{B_t^{\text{grid}}}{B_t^e} m_{xy}^e \quad (118)$$

In case of $\nu^e = 0$ (that is $B_{12}^e = 0$), equations (116), (117), (118) will reduce themselves to

$$m_x^{\text{grid}} = m_x^e + \nu^{\text{grid}} \cdot m_y^e \quad (119)$$

$$m_y^{\text{grid}} = m_y^e + \nu^{\text{grid}} \cdot m_x^e \quad (120)$$

$$m_{xy}^{\text{grid}} = \frac{B_t^{\text{grid}}}{H^e} \cdot m_{xy}^e \quad (121)$$

respectively.

In case of a 'diagonal on square' type space grid:

$$\nu^{\text{grid}} = \frac{B_{12}^{\text{grid}}}{B^{\text{grid}}} = 1 ; \quad B_t^{\text{grid}} = 0 \quad (122)$$

$$m_x^{\text{grid}} = m_y^{\text{grid}} = \frac{m_x^e + m_y^e}{1 + \nu^e} \quad (123)$$

$$m_{xy}^{\text{grid}} = 0$$

6.3 Calculation of internal forces of the space grids investigated.
Comparison of the results of approximate calculation with accurate results
calculated by computer

Approximate calculations using solutions according to /1/, /3/, /9/ apply to square space grids with different length of the sides from among which

- 'square with diagonals on square' type space grids (see Figs 14 and 15 and Table 5) and
- 'diagonal on square' type space grids (see Figs 16, 17 and Table 6) have top and bottom chord planes with different rigidity while
- 'hexagonal on triangular' type space grids (see Figs 20, 21 and Table 8) are reinforced against twist by so-called 'closed lattice-type' tube.

Table 4 Recommended computation models





| grid type symbol | top chord | | bottom chord | |
|---|-------------|---------------|--------------|---------------|
| | equilibrium | compatibility | equilibrium | compatibility |
|  | x +27% | | | x + 3% |
|  | | x + 6% | x + 7% | |
|  | | x + 10% | x - 7% | |
|  | x + 0% | | x + 9% | |

Table 5 Bar forces of 'cross-brace type square over square' type space

| | BAR | EQUI kN | ELT % | SZG. kN | COMP kN | ELT % | GIENCKE % | ELT % |
|------------------------------|-------|------------|----------|------------|------------|----------|--------------|----------|
| In centre | 53-65 | -4.65 | +48 | -3.11 | -3.28 | +6 | -3.34 | +7 |
| top | 53-66 | -3.23 | +48 | -2.18 | -2.31 | +6 | -2.19 | 0 |
| chord | 54-65 | -3.23 | +41 | -2.29 | -2.28 | 0 | -2.48 | +8 |
| | 65-66 | -4.61 | +41 | -3.26 | -3.28 | +1 | -3.34 | +3 |
| bottom | 59-71 | +9.17 | + 7 | +8.61 | +6.52 | -24 | +6.64 | -23 |
| chord | 71-72 | +9.17 | + 3 | +8.94 | +6.52 | -27 | +6.64 | -26 |
| bracing | 53-59 | -1.70 | +12 | -1.52 | -1.45 | -5 | | |
| | 53-71 | +0.44 | +10 | +0.40 | +0.48 | +20 | | |
| | 65-71 | -1.22 | - 2 | -1.25 | -0.75 | -40 | -0.75 | -40 |
| | 65-72 | +0.48 | +20 | +0.39 | +0.41 | + 5 | +0.41 | +3 |
| | 66-72 | -1.00 | 0 | -1.00 | -1.00 | 0 | -1.00 | 0 |
| middle of | 49-50 | -0.88 | -50 | -1.75 | -0.63 | | | |
| the edge | 49-61 | -0.88 | -43 | -1.54 | -0.63 | | | |
| top chord | 49-62 | -0.62 | -33 | -0.92 | -0.27 | | | |
| | 50-61 | -0.62 | | -1.42 | -0.61 | | | |
| | 61-62 | -0.88 | | -2.07 | -0.63 | | | |
| bottom | 55-56 | 0.00 | | 0.00 | 0.00 | | | |
| chord | 55-67 | 0.00 | | -2.47 | 0.00 | | | |
| | 67-68 | 0.00 | | 0.00 | 0.00 | | | |
| bracing | 49-55 | 0.00 | | +0.53 | +0.53 | 0 | | |
| | 59-65 | +4.43 | -5 | +4.69 | +4.24 | -10 | | |
| | 49-67 | +0.28 | | -0.60 | +0.20 | | | |
| | 61-67 | 0.00 | | -0.76 | +0.44 | -42 | | |
| corner | 61-68 | +4.87 | -8 | +5.31 | +4.10 | -23 | | |
| top | 1-13 | -0.17 | | +0.06 | -0.12 | | | |
| chord | 1-14 | -0.12 | | +0.65 | -1.41 | | | |
| | 2-13 | -0.12 | | -1.11 | -1.41 | +27 | | |
| bottom chord | 7-19 | 0.00 | | 0.00 | 0.00 | | | |
| bracing | 1-7 | 0.00 | | 0.00 | 0.00 | | | |
| | 1-19 | 0.00 | | -0.68 | 0.00 | | | |
| Deflection in the centre (m) | | | | | | | | |
| | | 0.0056 | -14 | 0.0065 | 0.0035 | -45 | | |

Table 6 Bar forces of 'diagonal on square' type space

| | BAR | EQUI kN | ELT % | SZG kN | COMP kN | ELT % |
|---------------------------------|-------|------------|----------|-----------|------------|----------|
| In centre top chord | 65-70 | -10.06 | +42 | -7.07 | -7.78 | +10 |
| bottom chord | 24-28 | +14.20 | - 7 | +15.27 | +11.00 | -28 |
| | 21-24 | +14.20 | - 3 | +14.66 | +11.00 | -25 |
| bracing | 24-65 | - 0.62 | +17 | - 0.53 | - 0.56 | + 6 |
| | 24-70 | + 0.62 | +19 | + 0.52 | + 0.56 | + 8 |
| middle of the edge top chord | 31-39 | - 2.14 | | +0.0002 | - 1.65 | |
| | 33-39 | - 2.14 | | + 0.82 | - 1.65 | |
| bottom chord | 12-13 | + 3.02 | -17 | + 3.65 | + 2.33 | -36 |
| bracing corner | 13-39 | - 5.52 | -13 | - 6.34 | - 5.02 | -21 |
| top chord | 37-43 | - 0.85 | -41 | + 1.45 | - 0.66 | |
| bottom chord | 4-7 | + 1.20 | | - 0.99 | + 0.93 | |
| | 4-17 | + 1.20 | -17 | + 1.45 | + 0.93 | -36 |
| bracing | 4-43 | - 2.20 | -12 | - 2.51 | - 2.46 | - 2 |

Deflection in the centre (m)

| | | | | |
|-------|-----|-------|-------|-----|
| 0.043 | - 4 | 0.045 | 0.035 | -22 |
|-------|-----|-------|-------|-----|

Table 7 Bar forces of 'square with diagonals on square offset' type space grid

| | BAR | EQUI kN | ELT % | SZG kN | COMP kN | ELT % | GIENCKE kN | ELT % |
|-----------------------|-------|------------|----------|-----------|------------|----------|---------------|----------|
| In centre | 53-69 | -4.20 | +27 | -3.30 | -4.44 | +35 | -3.15 | - 4 |
| top chord | 53-71 | -2.93 | +27 | -2.31 | -3.11 | +35 | -2.19 | - 5 |
| | 54-69 | -2.94 | +22 | -2.41 | -3.11 | +29 | -2.23 | - 8 |
| | 69-71 | -4.20 | +21 | -3.46 | -4.44 | +28 | -3.16 | - 9 |
| bottom chord | 58-59 | +8.35 | - 2 | +8.56 | +8.83 | + 3 | +6.28 | -27 |
| | 59-70 | +8.35 | - 6 | +8.85 | +8.83 | 0 | +6.28 | -29 |
| bracing | 53-59 | +0.16 | -48 | +0.31 | +0.20 | -36 | +0.07 | |
| | 59-69 | +0.02 | | +0.01 | 0.00 | | +0.07 | |
| | 59-71 | -0.20 | -39 | -0.33 | -0.20 | -39 | -0.21 | -36 |
| middle of the edge | 49-50 | -0.80 | +48 | -0.54 | -0.85 | | | |
| | 49-61 | -0.80 | | -1.64 | -0.85 | | | |
| top chord | 49-63 | -0.51 | -12 | -0.58 | -0.58 | 0 | | |
| | 50-61 | -0.61 | -39 | -1.00 | -0.61 | -39 | | |
| | 61-63 | -0.80 | +43 | -0.56 | -0.85 | | | |
| bottom chord | 43-55 | +1.60 | | -0.22 | +1.69 | | | |
| | 55-62 | +1.60 | | -0.29 | +1.69 | | | |
| bracing | 49-55 | +0.68 | | +1.74 | +0.85 | | | |
| | 50-55 | -0.64 | | -1.82 | -0.81 | | | |
| | 55-61 | +0.96 | | +2.15 | +0.89 | | | |
| | 55-63 | -1.00 | | -2.08 | -0.93 | | | |
| corner | 1-13 | -0.15 | | -0.02 | -0.16 | | | |
| top chord | 1-14 | -0.34 | | +0.93 | -0.06 | | | |
| | 2-14 | -0.15 | | -1.17 | -0.15 | | | |
| bottom chord | 7-19 | +0.31 | +15 | +0.27 | +0.32 | +18 | | |
| bracing | 1-7 | -1.08 | -23 | -1.40 | -0.18 | | | |
| | 7-13 | +1.40 | -17 | +1.69 | +0.52 | | | |
| | 7-14 | -1.72 | -13 | -1.98 | -0.86 | | | |

Deflection in the centre (m)

0.00513 - 9 0.00560 0.00229 -61

Table 8 Bar forces of 'hexagonal on triangular' type space

| | BAR | EQUI kN | ELT % | SZG kN | COMP kN | ELT % |
|--|---------|------------|----------|-----------|------------|----------|
| In centre top chord | 89-94 | -17.37 | 0 | -17.29 | -18.26 | + 6 |
| | 94-103 | -17.37 | 0 | -17.41 | -18.26 | + 5 |
| bottom chord | 82-104 | +10.04 | + 8 | + 9.28 | +10.55 | +14 |
| | 102-104 | +10.04 | + 9 | + 9.18 | +10.50 | +15 |
| bracing | 89-104 | 0.00 | | - 0.03 | 0.00 | |
| | 94-103 | 0.00 | | - 0.03 | 0.00 | |
| middle of the one side top chord | 67-72 | - 3.48 | -14 | - 4.05 | - 2.23 | -17 |
| | 67-73 | - 2.86 | -38 | - 4.65 | - 3.34 | -28 |
| | 72-84 | - 3.17 | -21 | - 4.04 | - 3.34 | -17 |
| | 84-90 | - 2.86 | -29 | - 4.05 | - 3.34 | -17 |
| bottom chord | 62-78 | + 2.36 | | + 6.94 | + 2.03 | |
| bracing | 67-78 | + 0.15 | | - 2.77 | + 0.02 | |
| | 72-78 | + 4.02 | | + 9.03 | + 3.51 | |
| | 73-78 | - 3.88 | | - 6.51 | - 3.48 | |
| | 78-84 | + 2.72 | | + 9.03 | + 3.57 | |
| | 78-85 | - 2.86 | | - 5.44 | - 3.60 | |
| | 78-90 | - 0.15 | | - 3.32 | - 0.02 | |
| middle of the other side top chord | 5-10 | - 3.81 | -19 | - 4.73 | - 4.00 | -15 |
| | 5-11 | - 3.81 | -19 | - 4.71 | - 4.00 | -15 |
| | 10-22 | - 3.85 | -12 | - 4.36 | - 4.00 | - 8 |
| | 11-23 | - 3.77 | -16 | - 4.48 | - 4.00 | -11 |
| | 22-28 | - 3.66 | -38 | - 5.90 | - 3.99 | -32 |
| | 23-28 | - 3.96 | -38 | - 6.39 | - 4.01 | -37 |
| bottom chord | 15-16 | + 2.14 | | + 6.06 | + 2.30 | |
| | 16-17 | + 2.26 | | + 6.33 | + 2.32 | |
| | 16-32 | + 2.45 | | + 5.08 | + 2.33 | |
| | 16-33 | + 1.95 | | + 4.18 | + 2.29 | |
| bracing | 5-16 | + 8.13 | -23 | +10.57 | + 8.55 | -19 |
| | 10-16 | + 0.09 | | - 0.16 | + 0.01 | |
| | 11-16 | - 0.09 | | - 0.48 | - 0.01 | |
| | 16-22 | - 2.12 | -19 | - 2.63 | - 1.99 | -24 |
| | 16-23 | - 1.90 | + 3 | - 1.85 | - 2.25 | +22 |
| | 16-28 | - 4.03 | -26 | - 5.45 | - 4.24 | -22 |
| Corner top chord | 1-6 | - 0.73 | -17 | - 0.88 | - 0.76 | -14 |
| | 1-7 | - 0.73 | -17 | - 0.88 | - 0.76 | -14 |
| | 6-18 | - 0.73 | -17 | - 0.88 | - 0.76 | -14 |
| | 7-19 | - 0.73 | | - 1.49 | - 0.76 | -49 |
| | 18-24 | - 0.73 | -17 | - 0.88 | - 0.76 | -14 |
| | 19-24 | - 2.28 | +10 | - 2.07 | - 1.03 | |
| bottom chord | 12-19 | + 0.42 | | + 1.03 | + 0.97 | - 6 |
| | 12-29 | - 2.26 | | + 2.39 | - 0.09 | |

Table 8 (continued)

| | BAR | EQUI kN | ELT % | SZG kN | COMP kN | ELT % |
|---------|-------|------------|----------|-----------|------------|----------|
| bracing | 1-12 | + 1.02 | -48 | + 1.98 | + 1.77 | -11 |
| | 6-12 | + 1.73 | -12 | + 1.97 | + 0.69 | |
| | 7-12 | - 0.97 | | - 2.34 | - 0.43 | |
| | 12-18 | + 1.00 | | + 1.97 | + 0.88 | |
| | 12-19 | + 0.64 | +18 | + 0.54 | - 1.83 | |
| | 12-24 | + 0.39 | | - 4.11 | - 0.26 | |

Deflection in the centre (m)

| | | | | |
|--------|---|--------|--------|-----|
| 0.0024 | 0 | 0.0024 | 0.0016 | -33 |
|--------|---|--------|--------|-----|

Uniformly distributed vertical load $p = 1.0 \text{ kN/m}^2$ is acting upon any of the four space grid types and each space grid is supported by bearing up freely along the periphery of the top chord plane (the supports being illustrated by circles in the layout plane of the space grid). Thus the boundary conditions along the supported edges /1/:

$y = \text{constant}$

$w = 0$ (zero deflection)

$m_y = 0$ (zero bending moment at right angles to the edge)

$\Phi'' = 0$ (zero supplementary horizontal membrane force at right angles to the edge in the upper plane)

$\Phi' = 0$ (zero supplementary shearing membrane force in the top chord plane).

Dark areas in the top plan of the space grid are bar groups for which the bar forces arising have been calculated. From among these bar groups, three important groups have been selected for each space grid, one in the centre of the space grid, a second in the centre of the supported edge while a third in the corner of the space grid that is at point where the value of bending moment, shear force and torisonal moment is maximum.

The bar forces arising in the selected bar groups have been tabulated and compared with the accurate values of bar forces obtained by computer calculation (Department of Engineering Computation, SZÁMGÉP, ÉGSZI). Abbreviations 'equil and 'COMP' in the Tables indicate the results obtained in kN by the simplified equilibrium and simplified compatibility method, respectively.

'SZG' indicates the accurate result in kN obtained by computer calculation while 'ELT' is used in any case for the difference in load

(+ or -) in % as compared with the accurate result. Deviations above 50% or those meaningless because of the low values of bar force have not been indicated.

The values of deflection in the centre of the space grid, including also deflection due to transversal shear, have been tabulated.

The values obtained for chord bar forces by approximate calculation as well as the accurate values are illustrated also diagrammatically in the axes of symmetry parallel to axis x of the space grid, at the boundary and along the boundary.

7. Summary and evaluation of the results of the accuracy test

Two curves are obtained in illustrating the values obtained for bar forces using the two different approximate methods, these curves lying in some cases below or above the curve of accurate values of bar forces they flank the curve of accurate values in other cases.

In case of chord bars lying in the axis of symmetry parallel to axis x , the curve of accurate values lies actually between the curves of approximate values along some sections while in case of bars lying at, or near, the boundary, the accurate values lie usually beyond the curves of approximate values because the supports and the introduction of forces (e.g. introduction of maximum torsional force arising in the corner to the 'lattice-type tube' which has not been a geometrically 'fully closed tube' yet result in effects that can not be taken into consideration in the approximate continuum method.

7.1 Effect of approach used in calculation of bending moments on accuracy

Solutions ready for use in the literature give the maximum bending moment arising in the centre of the plate and the maximum torsional moment arising in the corner of the plate.

To calculate the value of bending moments arising at different points of the substituting continuum on the basis of maximum bending moments, a parabol of the second degree was used as an approximation while double linear reduction was used to calculate the torsional moment on the basis of maximum torsional moment.

The effect of approximation used in calculating for bending moments on the accuracy of the values of moment is illustrated below:

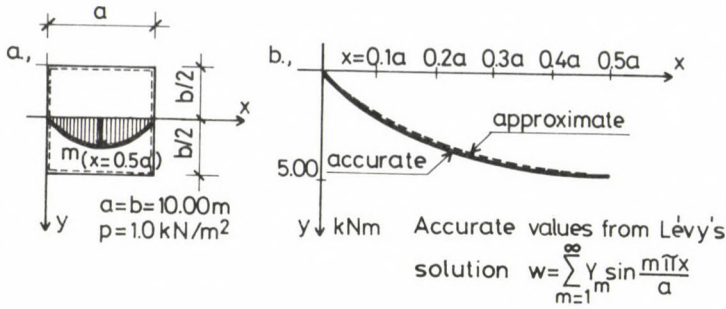


Fig. 13.

The accuracy of calculation of moments can be improved by taking into consideration the error committed. This is a better approximation of the accurate solution of the computation model. The effect of correction in case of the 'hexagonal on triangular' type space grid is illustrated diagrammatically for the chord bar forces of the top chord plane.

7.2 Problems of applicability of the simplified continuum methods

Concerning applicability of the simplified continuum method, a significant amount of deviation from accurate bar force values (error) was found to result from the neglect of supplementary plane stress and strain state arising in the 'more rigid' chord plane containing more types of rigidities. Namely, bar forces that can not be neglected are brought about by the supplementary plane stress and strain state in this chord plane, in particular

tension in the centre and compression near the edges of the space grid in the top chord plane in case of 'square with diagonals on square offset', 'square with diagonals on square', and 'diagonal on square' type space grids

while

compression in the centre of the space grid and tension in the vicinity of the edges in the bottom chord plane of a 'hexagonal on triangular' type space grid

with, however, little effect on the values of bar force of the other chord plane.

It follows from what has been said that acceptable bar forces are usually supplied by the simplified equilibrium model in the chord plane

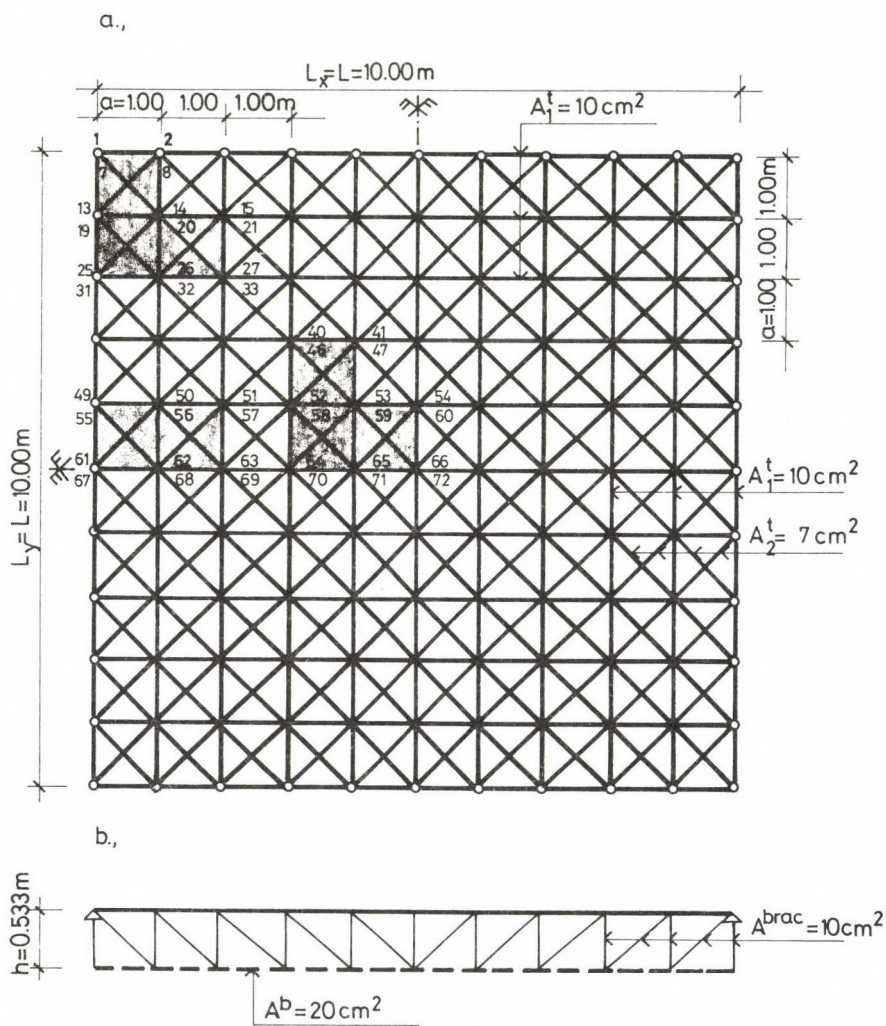


Fig. 14. 'Square with diagonals on square'

a) Top view; b) Cross section

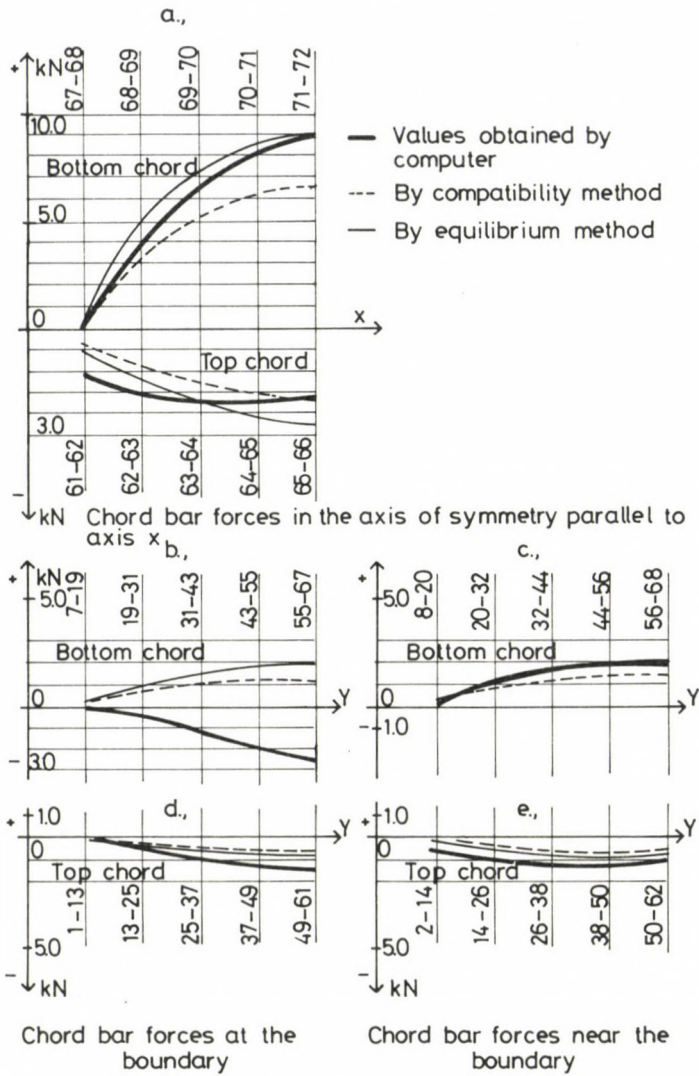


Fig. 15. 'Square with diagonals on square' grid

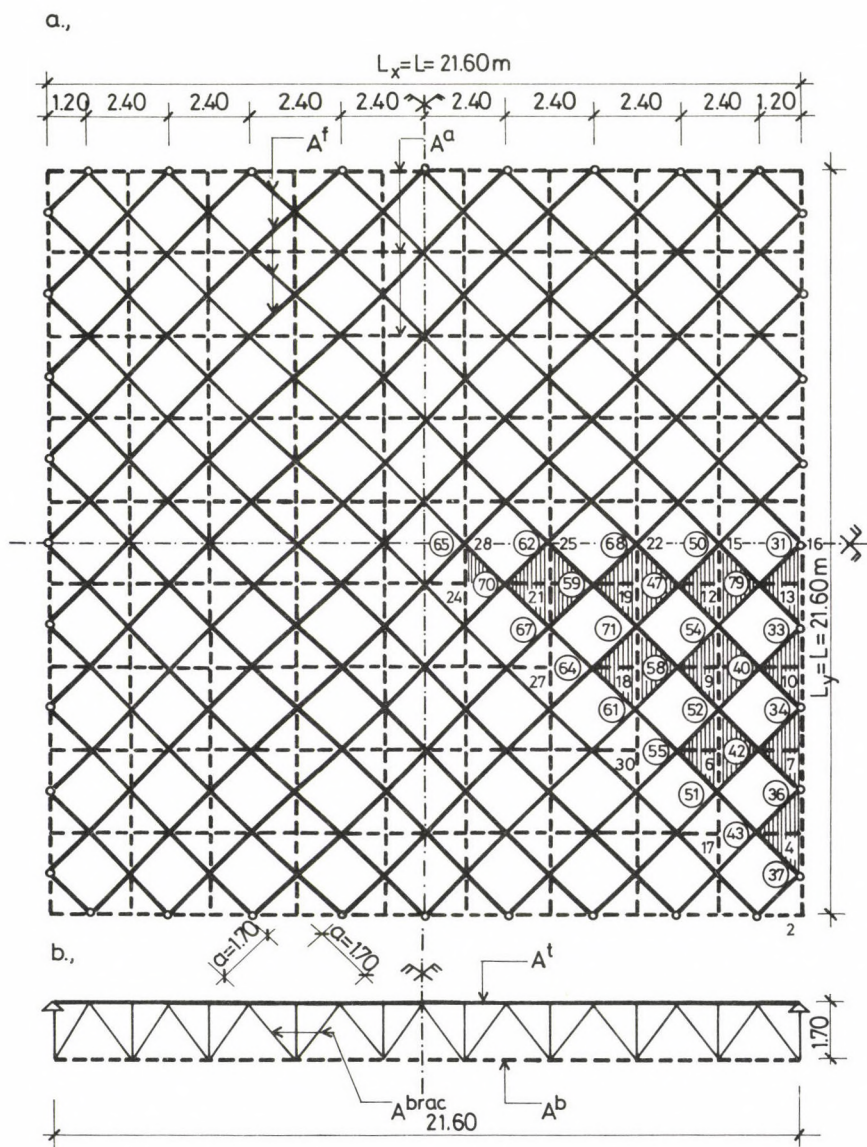


Fig. 16. 'Diagonal on square'
a) Top view; b) Cross section

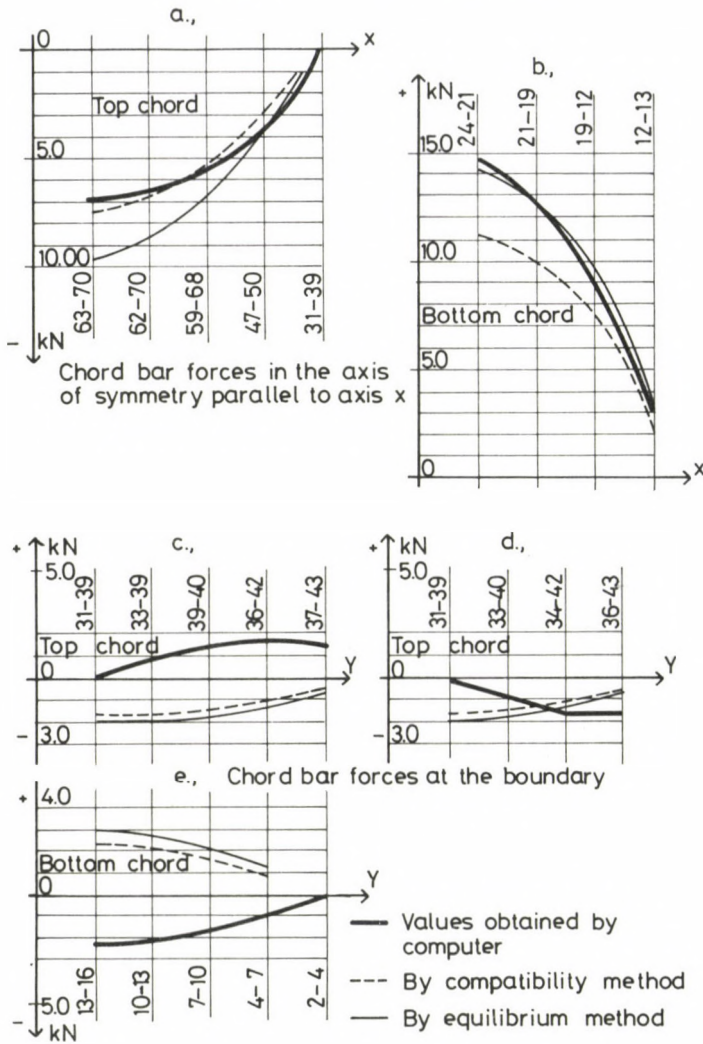


Fig. 17.

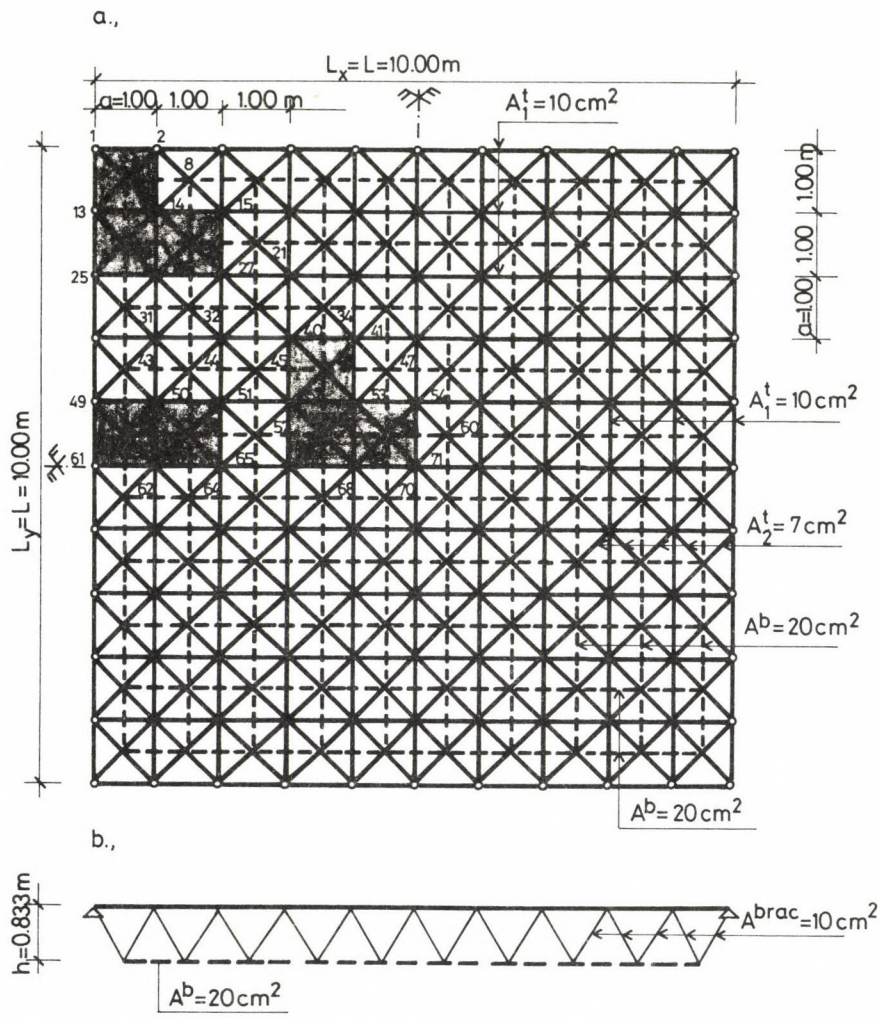


Fig. 18. 'Square with diagonals on square offset'
a) Top view; b) Cross section

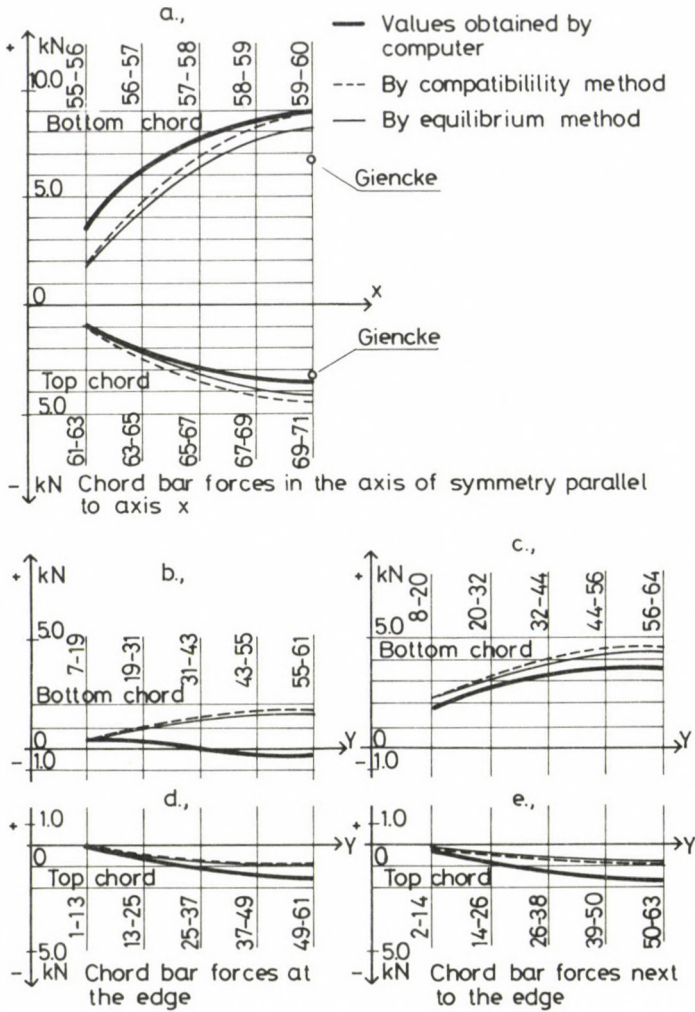


Fig. 19. 'Square with diagonals on square offset' space grid

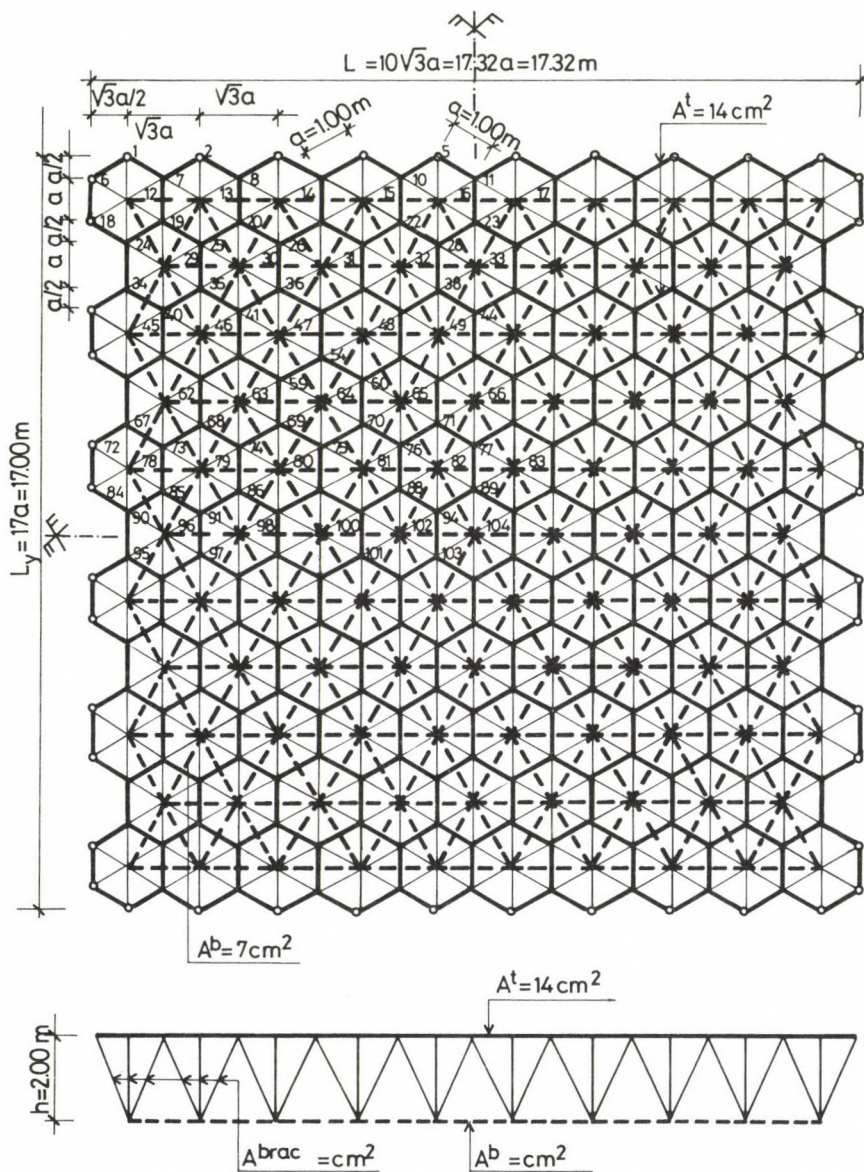
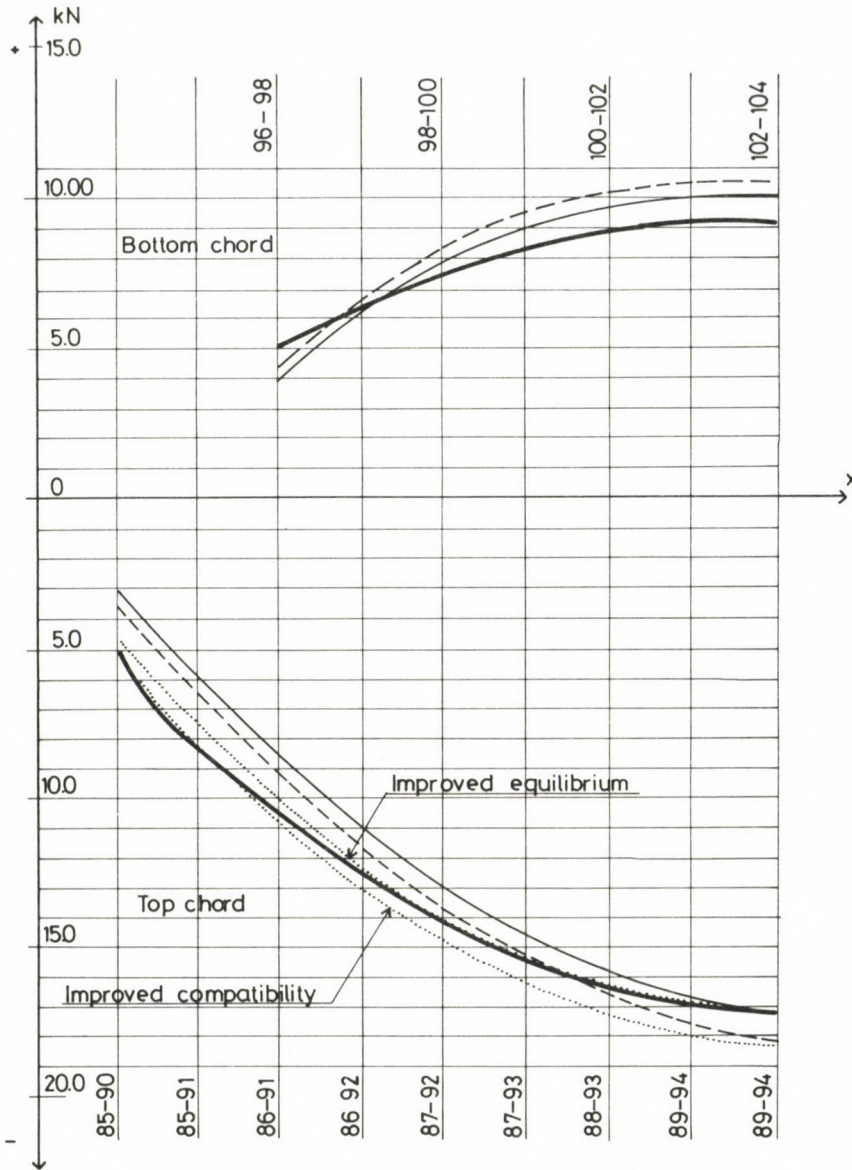


Fig. 20. 'Hexagonal on triangular'

a) Top view; b) Cross section



- Values obtained by computer
- By compatibility method
- By equilibrium method
- Improved valued

Fig. 21. 'Hexagonal on triangular'

containing less types of rigidity ('softer chord plane') and thus no rigidity need be neglected. At the same time, in the chord plane where a rigidity is neglected (e.g. in case of a 'hexagonal on triangular' type space grid), the error in the values of bar force supplied by the method is considerable.

Calculation on the basis of the simplified compatibility model supplies values for bar forces to a good approximation in the chord plane containing more types of rigidity ('more rigid' chord plane). This can be attributed to the fact that all types of rigidity present in the chord plane are taken into consideration by this model and thus the calculation comprises the disturbance of the accessory plane stress and strain state over the entire chord plane although it is not calculated numerically.

Significant deviations may result from the difference between actual and assumed support at, and near, the boundaries, first of all in case of minor bar forces which are, however, insignificant in design.

Bar forces neglected along with the plane stress and strain state may also result in a significant error in some cases because chord bar forces resulting from bending in the vicinity of the boundaries are extremely small as compared with the neglected bar forces.

In case of a 'cross-brace type square over square' type space grid, the neglected swelling rigidity of the structure is similar to torsional rigidity. With the swelling rigidity neglected, the bending stress increases and as a result, also the chord bar forces calculated on the basis of the bending stress increase. Major deviations from the accurate values result presumably from the asymmetry of the grid of columns. Nodes of the lower and upper chord planes for which the moments are written for calculation of the bar force arising in the bars in the other chord plane are significantly shifted as compared with the mid cross section of the bars in question.

Deflections calculated using the equilibrium model lie significantly closer to the accurate values than those based on the compatibility model. An explanation is that the deflection of the structure is practically unaffected by the accessory plane stress and strain state and thus neglect will not result in an appreciable error either.

Although including the accessory plane stress and strain state, the compatibility model converts all the relevant rigidities into an imaginary inertial moment and reduces thus the calculated deflection without reason.

Bar forces lying closer to the accurate values are supplied by

adaptation of Giencke's theory to the 'more rigid' chord plane containing more types of rigidity and, owing to superposition of the ribs on the 'cover plate' (cf. 4.3), also the rigidity of the ribs where the accessory plane stress and strain state takes place.

Giencke calculated bending on the basis of actual bending and torsional rigidities but he assumed swelling rigidity to take place where the average of bending centres of gravity was found. Giencke's method reminds us therefore of the simplified equilibrium method as far as bending while of the simplified compatibility method as far as torsion is concerned but it is not identical with either method but rather a hybrid computation process.

7.3 Summary

To the accuracy of calculated bar forces, the internal forces of two-layer grids can be calculated simply and demonstratively within a relatively short time on the basis of stresses of orthotropic plates of different torsional rigidity using the simplified continuum method.

The process is sufficiently accurate for use in preliminary design, in determination of the cross section of the bars or in testing a data set obtained by machine computation.

Values best approximating the accurate values of bar forces are expectable in the centre of the space grid, in case of chord bars.

A simplified computation model to be reasonably used for determination of values best approximating the accurate values of bar forces arising in the top or bottom chord plane in the centre of the space grid in case of the different types of space grids is illustrated below.

In the Table, the values of maximum deviation from the accurate values of bar force are given in per cents.

A reasonable method to calculate the expectable deflections is the simplified equilibrium model. In this case, there is a deviation of $\pm 0\% - 14\%$ between the calculated and accurate values of deflection.

REFERENCES

1. Kollár, L. - Hegedűs, I.: Analysis and Design of Space Frames by the Continuum Method. Akadémiai Kiadó, Budapest 1985.

2. Szilárd, R.: Theory and Analysis of Plates. Prentice-Hall Inc. New Jersey 1974.
3. Timoshenko - Woinowsky - Krieger: Theory of plates and shells (Hungarian edition). Műszaki Könyvkiadó, Budapest 1966.
4. Giencke, E.: Die Grundgleichungen für die orthotrope Platte mit exzentrischen Steifen. Der Stahlbau, 1955.
5. Bares, R.: Berechnungstabellen für Platten und Wandscheiben. Bauverlag, Wiesbaden 1971.
6. Czerny, F.: Tafeln für vierseitig und dreiseitig gelagerte Rechteckplatten. Beton-Kalender, Part I. W. Ernst und Sohn, Berlin 1976.
7. Krug, S. - Stein, P.: Einflussfelder orthogonal anisotroper Platten. Springer, Berlin 1969.
8. Melosh: Basis for Derivation of Matrices for the Direct Stiffness Method. Journal of AIAA, July 1963
9. Kollár, L.: Calculation for the dimensions of two-layer lattices using the simplified continuum method (in Hungarian). Mélyépítéstudományi Szemle, Vol. 27, 1977.
10. Kollár, L.: Investigation of a 'hexagonal on triangular' type two-layer grid by the continuum method. Műszaki Tudomány 53, 1977.

BOOK REVIEWS

Iványi, M. ed.: Stability of steel structures, volumes I and II.
Akadémiai Kiadó, Budapest 1988. 1106 pages.

This work of two books contains the contributions to a conference on Stability of Steel Structures held in Tihany (Hungary), September 25-26, 1986 as one of a series of international meetings from among which meetings in Hungary had been suggested and organized by the late Ottó Halász, Professor and Corresponding Member of the Hungarian Academy of Science, Head of Department of Steel Structures of the Technical University Budapest, until he died in 1986. Therefore this conference, the second one held in Hungary, has been dedicated to the memory of Ottó Halász by Professor Miklós Iványi, his successor.

In this work, first you can read a biography of Ottó Halász and a description of his scientific achievements, including a list of his publications. Then 125 papers submitted by 146 authors from four continents of the world are presented.

As an introduction, you find a 'state-of-the art' type general report at first place in each chapter to give an overview of the recent results of research in given field and to act as a bridge between the different papers. Comments on the papers and discussion are given at the end of each chapter. Included among the extremely valuable contributions of quite a number are papers presenting new dimensioning processes or inventive experimental test methods or recommendations concerning development and increasing of the accuracy of standards and the like.

The two books contain nine chapters to present papers from nine fields within the science of stability of steel structures:

I Design concepts and codes

Here you can read papers giving a valuable summary of standards and recommendations used in the field of stability of steel structures like LRFD (Load and Resistance Factor Design) for U.S.A. or EUROCODE and DIN for Europe.

II Columns and beam columns

This chapter deals with the dimensioning problems and strength calculation for columns under centric and eccentric axial load. The methods of statistical mechanics are often used to support theoretical and practical considerations. Recommendations of quite a number can be read for buckling curves.

III Lateral buckling

Most of the papers deal with methods to study the lateral buckling of multispan continuous steel beams and with the stability of beam columns on the basis of a non-elastic or even elastoplastic model. A comprehensive international picture of the results of research into the stability test of bars is given, distinctions being made between problems solved and those to be solved.

IV Frames

The new trends lay increasing emphasis on the effect of joints upon the behaviour of the entire structure. In general, semi-rigid joints in combination with imperfect models are considered to be the key to improvement of the design methods.

V Trusses

The stability test and optimum design of trusses of different types are discussed in the papers of this chapter.

VI Plate and box girders

You can read about the stability problems of plated structures, load capacity tests of girders under static and dynamic load, economic dimensioning of longitudinally stiffened steel plates, elastoplastic behaviour of box girders and their optimum design etc. in this chapter.

VII Shells

Discussed in this chapter are the design and stability problems of the most important and widely used types of shells (cylindric, conic, spherical and toroidal ones) as well as thin-walled cylindric steel silos etc.

VIII Thin-walled structures

Treated by the papers here are the stability analysis of thin-walled structures, methods to test beams resisting shear, bending and torsion as well as problems in relation to sandwich structures.

IX Special problems

Presented in this chapter are special unique problems in relation to elements of different structures as well as methods of calculation and measurement in this special field.

Although the official language of the conference has been English and Russian, the language of the book is English and thus even papers written originally in Russian are presented in English language in the book. An authors' register including name and address of the participants of the conference is given in the book to facilitate communication with the authors and a subject index contributes to orientation in the text.

The book has been intended first of all for scientists of the field to add to their knowledge but it may be a valuable aid also for engineers of the practical world who can find ideas to be realized in practice or relationships they seldom encounter with in everyday work.

Gy. Czeglédi

Kézdi, Á. - Rétháti, L.: Soil mechanics of earthworks, foundations and highway engineering. Akadémiai Kiadó, Budapest 1988, 361 pages.

The book is the third volume of a serial Handbook of Soil Mechanics. It presents the conventional and advanced models used in engineering practice. Six chapters cover

- soil mechanics of earthwork,
- load-bearing capacity and settlement of shallow foundations,
- bearing capacity and settlement of pile foundations,
- soil mechanics in road construction,
- improvement of the physical properties of soils,
- soil dynamics

comprehensively.

The merit of the book lies first of all in the clear presentation of practical problems, both conventional and new ones (like reinforced earth or dynamic behaviour of road pavements). Outlining the procedures used in conservative engineering practice, the authors draw attention to the numerous effects, circumstances and approximations influencing the validity and adequacy of mechanical models. This carefulness is of vital importance in geotechnics - the book combines practical and theoretical considerations proportionately.

The computational models are fitted to the assumption of linear elastic or ideally plastic material behaviour. The untimely death of the senior author, Professor Kézdi, resulted in some predominance of conservative calculational approaches. Tables of influence factors and nomograms help to solve numerical problems but no reference is made to the results brought by age of computers. From this point of view, the book is a synthesis of classic knowledge and its value is not only scientific but also historical.

Some non-linear models or computational approaches are missing but important contributions (not very common in this kind of textbooks) are found in the book to probabilistic treatment of problems. The second author, Professor Rétháti, added his achievements without interfering with the original material. Therefore, the book is a valuable aid of civil engineers working in a practical field.

P. Scharle

Rétháti, L.: Probabilistic solutions in geotechnics. Akadémiai Kiadó Budapest, 1988, 451 pages.

The author of this volume, 46th in the series of "Developments in Geotechnical Engineering" (Elsevier - Akadémiai Kiadó, joint edition, 1988), Professor L. Rétháti is a well-known scientist and, what is more, acknowledged expert of practical geotechnical problems. The book reflects these capabilities: it covers all those fields where the practical use of old (or younger) thumbrules, relationships and models can be improved by introducing statistic and probabilistic considerations and methods.

The author starts with three very transparent introductory chapters, presenting the fundamental concepts and theorems relevant to practical use in mathematical statistics and theory of probability. Clear and simple examples convince the reader that the effort needed for mastering the less known concepts and approaches pays well. The precise mathematical treatment and the clear comments stimulate the reader to use the presented methods for his particular problems. The reviewer ventures the remark this was the primary ambition of the author.

The particular domains of geotechnics are set forth in self-contained Chapters as follows:

- determination of the site and the number of soil tests,
- determination of the qualifying characteristics of the soil,
- comparison of tests performed with the same soil,
- evaluation of the test data before planning,
- determination of the bearing capacity of the soil,
- settlement forecasting,
- stability of free standing and supported slopes,
- quality control of earthworks.

The practising engineer finds his keywords mostly in the contents, while the subject index lists mainly the terms of statistics. The references (some 250) are taken mostly from literature written in English, nevertheless the treatment reflects properly the results of outstanding Russian Schools and those of the author himself, too. Therefore, the book serves as a reference as well: the explanation of the essential knowledge is followed by reliable references for further study.

The attentive reader may find a special pleasure in the 8th Chapter, where the basic principles of planning based on the theory of probability are analyzed in detail. Beyond the uncertainty involved in the computational models, the consideration of the lifetime and the safety margin, the author pays attention to strategic decision making, dealing simultaneously both with the technical and economic factors.

A sarcastic dictum (referred to by M. Tribus) says that "research is reading more than one book". In the age of publication boom this statement may incline anybody to meditate about the research problem of finding those books definitely worthy of reading. The reviewer thinks Professor Rétháti's work must be classified as one of those few to be studied and kept handy in the years to come.

P. Scharle

PRINTED IN HUNGARY

Akadémiai Kiadó és Nyomda Vállalat, Budapest

NOTICE TO CONTRIBUTORS

Papers in English* are accepted condition that they have not been previously published or accepted for publication.

Manuscripts in two copies (the original type-written copy plus a clear duplicate one) complete with figures, tables, and references should be sent to

Acta Technica
Nádor u. 7. I. 118
Budapest, Hungary
H-1051

Although every effort will be made to guard against loss, it is advised that authors retain copies of all material which they submit. The editorial board reserves the right to make editorial changes.

Manuscripts should be typed double-spaced on one side of good quality paper with proper margins and bear the title of the paper and the name(s) of the author(s). The full postal address(es) of the author(s) should be given in a footnote on the first page. An abstract of 50 to 100 words should precede the text of the paper. The approximate locations of the tables and figures should be indicated on the margin. An additional copy of the abstract is needed. Russian words and names should be transliterated into English.

References. Only papers closely related to the author's work should be referred to. The citations should include the name of the author and/or the reference number in brackets. A list of numbered references should follow the end of the manuscript.

References to periodicals should mention: (1) name(s) and initials of the author(s); (2) title of the paper; (3) name of the periodical; (4) volume; (5) year of publication in parentheses; (6) numbers of the first and last pages. Thus: 5. Winokur, A., Gluck, J.: Ultimate strength analysis of coupled shear walls. American Concrete Institute Journal 65 (1968) 1029-1035

References to books should include: (1) author(s)' name; (2) title; (3) publisher; (4) place and year of publication. Thus: Timoshenko, S., Gere, J.: Theory of Elastic Stability. McGraw-Hill Company, New York, London 1961.

Illustrations should be selected carefully and only up to the necessary quantity. Black-and-white photographs should be in the form of glossy prints. The author's name and the title of the paper together with the serial number of the figure should be written on the back of each print. Legends should be brief and attached on a separate sheet. Tables, each bearing a title, should be self-explanatory and numbered consecutively.

Authors will receive proofs which must be sent back by return mail.

Authors will receive 50 reprints free of charge.

*Hungarian authors can submit their papers also in Hungarian.

Periodicals of the Hungarian Academy of Sciences are obtainable
at the following addresses:

AUSTRALIA

C.B.D. LIBRARY AND SUBSCRIPTION SERVICE
Box 4886, G.P.O., Sydney N.S.W. 2001
COSMOS BOOKSHOP, 145 Ackland Street
St. Kilda (Melbourne), Victoria 3182

AUSTRIA

GLOBUS, Höchstadtplatz 3, 1206 Wien XX

BELGIUM

OFFICE INTERNATIONAL DES PERIODIQUES
Avenue Louise, 485, 1050 Bruxelles
E. STORY-SCIENTIA P.V.B.A.
P. van Duyseplein 8, 9000 Gent

BULGARIA

HEMUS, Bulvar Ruszki 6, Sofia

CANADA

PANNONIA BOOKS, P.O. Box 1017
Postal Station "B", Toronto, Ont. M5T 2T8

CHINA

CNPICOR, Periodical Department, P.O. Box 50
Peking

CZECHOSLOVAKIA

MAD'ARSKA KULTURA, Národní třída 22
115 66 Praha
PNS DOVOZ TISKU, Vinohradská 46, Praha 2
PNS DOVOZ TLACE, Bratislava 2

DENMARK

EJNAR MUNKSGAARD, 35, Nørre Søgade
1370 Copenhagen K

FEDERAL REPUBLIC OF GERMANY

KUNST UND WISSEN ERICH BIBER
Postfach 46, 7000 Stuttgart 1

FINLAND

AKATEMINEN KIRJAKAUPPA, P.O. Box 128
00101 Helsinki 10

FRANCE

DAWSON-FRANCE S.A., B.P. 40, 91121 Palaiseau
OFFICE INTERNATIONAL DE DOCUMENTATION ET
LIBRAIRIE, 48 rue Gay-Lussac
75240 Paris, Cedex 05

GERMAN DEMOCRATIC REPUBLIC

HAUS DER UNGARISCHEN KULTUR
Karl Liebknecht-Straße 9, DDR-102 Berlin

GREAT BRITAIN

BLACKWELL'S PERIODICALS DIVISION
Hythe Bridge Street, Oxford OX1 2ET
BUMPUS, HALDANE AND MAXWELL LTD.
Cowper Works, Olney, Bucks MK46 4BN
COLLET'S HOLDINGS LTD., Denington Estate,
Wellingborough, Northants NN8 2QT
WM DAWSON AND SONS LTD., Cannon House
Folkstone, Kent CT19 5EE
H. K. LEWIS AND CO., 136 Gower Street
London WC1E 6BS

GREECE

KOSTARAKIS BROTHERS INTERNATIONAL
BOOKSELLERS, 2 Hippokratous Street, Athens-143

HOLLAND

FAXON EUROPE, P.O. Box 167
1000 AD Amsterdam
MARTINUS NIJHOFF B. V.

Lange Voorhout 9-11, Den Haag
SWETS SUBSCRIPTION SERVICE
P.O. Box 830, 2160 Sz Lisse

INDIA

ALLIED PUBLISHING PVT. LTD.
750 Mount Road, Madras 600002
CENTRAL NEWS AGENCY PVT. LTD.
Connaught Circus, New Delhi 110001
INTERNATIONAL BOOK HOUSE PVT. LTD.
Madame Cama Road, Bombay 400039

ITALY

D. E. A., Via Lima 28, 00198 Roma
INTERSCIENTIA, Via Mazzé 28, 10149 Torino
LIBRERIA COMMISSIONARIA SANSONI
Via Lamarmora 45, 50121 Firenze
SANTO VANASIA, Via M. Macchi 58
20124 Milano

JAPAN

KINOKUNIYA COMPANY LTD.
Journal Department, P.O. Box 55
Chitose, Tokyo 156
MARUZEN COMPANY LTD., Book Department
P.O. Box 5050 Tokyo International, Tokyo 100-31
NAUKA LTD., Import Department
2-30-19 Minami Ikebukuro, Toshima-ku, Tokyo 171

KOREA

CHULPANMUL, Phenjan

NORWAY

TANUM-TIDSKRIFT-SENTRALEN A.S.
Karl Johansgata 43, 1000 Oslo

POLAND

WĘGIERSKI INSTYTUT KULTURY
Marszałkowska 80, 00-517 Warszawa
CKP I W, ul. Towarowa 28, 00-958 Warszawa

ROUMANIA

D. E. P., Bucuresti
ILEXIM, Calea Grivitei 64-66, Bucuresti

SOVIET UNION

SOYUZPECHAT — IMPORT, Moscow
and the post offices in each town
MEZHDUNARODNAYA KNIGA, Moscow G-200

SPAIN

DIAZ DE SANTOS Lagasca 95, Madrid 6

SWEDEN

ESSELTE TIDSKRIFTSSENTRALEN
Box 62, 101 20 Stockholm

SWITZERLAND

KARGER LIBRI AG, Petersgraben 31, 4011 Basel

USA

EBSCO SUBSCRIPTION SERVICES
P.O. Box 1943, Birmingham, Alabama 35201
F. W. FAXON COMPANY, INC.
15 Southwest Park, Westwood Mass. 02090
MAJOR SCIENTIFIC SUBSCRIPTIONS
1851 Diplomat, P.O. Box 819074,
Pallas, Tx. 75381-9074
READ-MORE PUBLICATIONS, INC.
140 Cedar Street, New York, N. Y. 10006

YUGOSLAVIA

JUGOSLOVENSKA KNJIGA, Terazije 27, Beograd
FORUM, Vojvode Mišića 1, 21000 Novi Sad

ACTA TECHNICA

ACADEMIAE SCIENTIARUM HUNGARICAE

EDITOR-IN-CHIEF: P. MICHELBERGER

VOLUME 102
NUMBERS 3—4

CIVIL ENGINEERING — C/3



AKADÉMIAI KIADÓ, BUDAPEST 1989

ACTA TECHN. HUNG.

ACTA TECHNICA

A JOURNAL OF THE HUNGARIAN ACADEMY OF SCIENCES

CENTRAL EDITORIAL BOARD

T. CZIBERE, K. GÉHER, L. KOLLÁR, P. MICHELBERGER (EDITOR-IN-CHIEF),
A. LÉVAI, J. PROHÁSZKA, K. REMÉNYI, J. SZABÓ,
GY. CZEGLÉDI (MANAGING EDITOR)

EDITORIAL COMMITTEE FOR CIVIL ENGINEERING (SERIES C.)

A. BÉNYEI, ZS. GÁSPÁR, L. KOLLÁR (CHAIRMAN), L. RÉTHÁTI,
L. SOMLYÓDY

Acta Technica publishes original papers, preliminary reports and reviews in English, which contribute to the advancement of engineering sciences.

Acta Technica is published by

AKADÉMIAI KIADÓ

Publishing House of the Hungarian Academy of Sciences
H-1117 Budapest, Prielle K. u. 19—35.

Subscription information

Orders should be addressed to

KULTURA Foreign Trading Company
H-1389 Budapest P.O. Box 149

or to its representatives abroad

Acta Technica is abstracted/indexed in Applied Mechanics Reviews, Current Contents—Engineering, Technology and Applied Sciences, GeoRef Information System, Science Abstracts.

Dedicated
to
Professor
János SZABÓ
on his
70th birthday

CONTENTS

| | |
|--|-----|
| <u>Bojtár, I. - Bagi, K.:</u> Micromechanical model for numerical analysis of granular materials | 207 |
| <u>Gáspár, Zs. - Domokos, G.:</u> Global investigation of discrete models of the Euler buckling problem | 227 |
| <u>Györgyi, J.:</u> Production of dynamic stiffness matrix in case of other than rigid joints and rigid elements | 239 |
| <u>Iványi, M.:</u> Failure tests with steel frameworks | 247 |
| <u>Kaliskzy, S. - Lógó, J.:</u> Optimal design of dynamically loaded reinforced concrete frames under single displacement constraint | 267 |
| <u>Kollár, L.:</u> Space structures: static relationships, structural forms | 281 |
| <u>Kurutz, M.:</u> Stability of simple structures with non-smooth energy functionals in the one-dimensional case | 291 |
| <u>Páczelt, I. - Szabó, T.:</u> A bandwidth reduction process for substructural element method . | 315 |
| <u>Popper, Gy.:</u> Identification of damping parameters in linear vibration systems | 327 |
| <u>Roller, B.:</u> The general state change equation of bar structures | 339 |
| <u>Scharle, P.:</u> Attractions and risks of the analogies | 355 |
| <u>Tarnai, T.:</u> Higher-order infinitesimal mechanisms | 363 |
| <u>Vásárhelyi, A. - Lógó, J.:</u> Analysis of the structures for dynamic effects with mathematical programming | 379 |
| <u>Vértés, Gy.:</u> Investigation of nonlinear behaviour of building structures under dynamic load | 391 |
| BOOK REVIEW | |
| <u>Kaliskzy, S.:</u> Plasticity (Mrs. P. Elter) | 405 |



The authors of this volume are former students, university colleagues and coauthors of **János SZABÓ**, member of the Hungarian Academy of Sciences. By this joint publication they would like to express their thanks, respect and good wishes towards their master, colleague and friend on the occasion of his 70th birthday.

MICROMECHANICAL MODEL FOR NUMERICAL ANALYSIS OF GRANULAR MATERIALS

BOJTÁR, I.* - BAGI, K.**

(Received: 27 November 1989)

A numerical method has been developed for the analysis of the internal behaviour of granular materials. State-changing processes of microstructure can be followed; the final aim is to find state variables that can reliably describe these processes.

Introduction

The constitutive equations generally used to describe granular materials are based on the traditional continuum-mechanical variables like stress and strain. Since the material is replaced with a continuous model, these variables cannot properly describe the fundamental behaviour of granular materials i.e. the internal structure and its changing.

The usual way of taking into account this effect is to define the 'material properties' as functions of the state variables (with new parameters introduced, of course). To improve the constitutive equations, more and more parameters are introduced until the equations become 'overcrowded' - especially those parts containing the material properties.

It seems to be a much better approach to find totally new variables beside, or instead of, the traditional ones. These new variables should reflect the fact that the material has a characteristic internal structure changing as a result of external effects.

There are several theoretical proposals concerning these variables but the difficulty is to prove that they are really efficient.

A numerical model is presented in this paper by which the efficiency of the suggested variables can be analysed by numerical experiments. The model is able to follow the state-changing process of the material under external load while the values of the analysed variables are continuously calculated.

*Bojtár, Imre, H-1221 Budapest, Arany J. u. 96/A, Hungary

**Bagi, Katalin, H-1052 Budapest, Váci u. 7, Hungary

The first chapter includes the best known approaches to more efficient description of granular assemblies.

In the second chapter, the numerical model proposed for their analysis is presented.

The third chapter gives two numerical examples.

1. Suggested variables for the description of internal behaviour of granular assemblies

Given state of a granular assembly could exactly be described only if all geometrical characteristics like shape, position, material properties of the grains and of the contacts between them, and the contact forces and relative displacements at all contacts were known. The response of the assembly to changes in external effects could exactly be predicted in this case ('average' deformation, change of porosity, loss of stability etc.). This 'response' is derived from three basic effects: first, the change in shape and size of grains (usually negligibly small); second, the relative motion of adjoining grains at the contacts without loosing connections; third, the rearrangement of the internal structure, change of topology (joining and disjoining).

It is impossible to follow these effects by means of traditional continuum-mechanical state variables. - Therefore, as early as in the 1960s, more and more ideas were born about how to define more efficient state variables, how to find new ways of description of the behaviour of granular materials.

The most evident attempt was to re-define the stress and strain tensors so that they will be able to describe a granular assembly with discrete nature instead of a continuous material (good summary is given by Nemat-Nasser in /1/).

Besides this traditional approach, totally new ideas were also born. Pioneering work was done by Takeo Mogami in 1965 (see /2/, /3/) who was the first to use statistical entropy for finding the most probable state of granular assembly. This route was followed by many others (Moroto, /4/; Brown, /5/; etc.). They suggested that the effort to find the least biased state of the assembly be treated as a constrained optimization problem: maximization of entropy with given constraining conditions satisfied (average porosity or coordination number specified, equilibrium equations satisfied etc.).

Another approach was born in the 1970s: geometrical analysis of the microstructure (angular distribution of contact normals or of long axes of grains; effect of initial anisotropy; role of sliding and rolling of grains in deformation etc.; see for instance /6/ and /7/). The basic variable called fabric tensor shall be introduced here; its well known definition is

$$H_{ij} = \frac{1}{M} \sum_{c=1}^M n_i^c n_j^c \quad (1.1)$$

where $n^c = (n_i^c)$ is the unit vector normal to the surfaces of touching grains at contact 'c'; M is the total number of contacts of the analysed assembly. This variable was suggested for characterisation of anisotropy of the internal structure. (In the recent few years, it has already been suspected that at least a fourth-rank fabric tensor is required for proper description; see /8/).

The most promising ideas were born in the early 1980s. The first one was developed by M. Satake (see /9/ and /10/) who introduced a graph representation of granular assemblies and defined several variables based on the micro-level analysis of geometrical structures. The second one comes from P.A. Cundall (see /11/) who separated the different physical effects upon the material by dividing the stress tensor in four partitions, each expressing a different aspect of behaviour. Let's have a closer look at these suggestions.

1.1. The Satake-variables

In a two-dimensional assembly of discs ('grains') let's define two graphs. The first one called replaced graph is obtained by connecting the central points of discs in contact with each other; the second one called dual graph is derived from the common tangents of adjoining grains (see Fig. 1.1).

Using this graph representation, the variable fabric tensor can be defined as

$$\varphi_{ij} = \frac{\sum_{p=1}^N \left(\sum_{c=1}^m n_i^c n_j^c \right)}{\sum_{p=1}^N m} \quad (1.2)$$

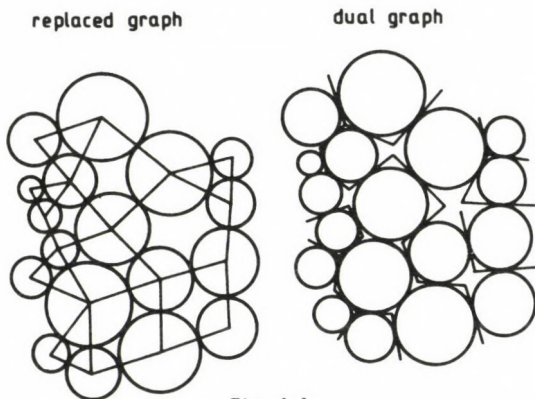


Fig. 1.1.

Here N is the number of grains in the analysed domain; m is the number of contacts of particle p ; n_i^c is the unit normal vector at contact c of particle p .

The $n_i^c n_j^c$ term can be weighted by the replaced graph branch lengths of the contacts ('branch tensor' gained); or by the dual graph branch lengths ('contact tensor' given); by the elastic energy stored in the contacts ('energy tensor' defined in this way). Other physical quantities can also be used for weighting.

1.2. Cundall's stress analysis

Cundall proposed to separate physical effects upon the material in the following way:

From the original two-dimensional domain R , an area A can be separated, which is not disturbed by boundary conditions (external loads acting directly on a grain, kinematical constraints etc.). For area A , the average stress tensor ($\bar{\sigma}_{ij}$) can be defined for circular grains as

$$\bar{\sigma}_{ij} = \frac{1}{A} \sum_{p=1}^N (R^p \sum_{c=1}^m n_i^c F_j^c) \quad (1.3)$$

Here R^p is the radius of particle p , m the number of contact points of particle p , F_j^c is the total contact force vector and n_i^c the unit vector normal to the grain surface at contact c .

Cundall separated this stress tensor in four partitions:

$$\bar{\sigma}_{ij} = \bar{\sigma}_{ij}^{(s)} + \bar{\sigma}_{ij}^{(f)} + \bar{\sigma}_{ij}^{(v)} + \bar{\sigma}_{ij}^{(i)} \quad (1.4)$$

where the four partitions are:

$\bar{\sigma}_{ij}^{(s)}$ shear stress tensor

$\bar{\sigma}_{ij}^{(v)}$ normal variation stress tensor

$\bar{\sigma}_{ij}^{(f)}$ fabric stress tensor

$\bar{\sigma}_{ij}^{(i)}$ isotropic stress tensor

First, the total contact force acting upon given contact point of a grain is split into normal and tangential components. The shear stress is calculated from the tangential forces:

$$\bar{\sigma}_{ij}^{(s)} = \frac{1}{A} \sum_{p=1}^N R^p \sum_{c=1}^m \left[n_i^c F_j^c - (F_k^c n_k^c) n_i^c n_j^c \right] \quad (1.5)$$

The Einstein summation rule is applied. This partition corresponds to the mobilised shear forces; it is related to the tendency of the contacts to slide and thus to the dissipation of energy during the state-changing process.

In the second step, the average normal force associated with the grain is separated from each normal force acting on the grain. From the remaining part, the normal variation stress component is calculated:

$$\bar{\sigma}_{ij}^{(v)} = \frac{1}{A} \sum_{p=1}^N R^p \sum_{c=1}^m \left[(F_k^c n_k^c) n_i^c n_j^c - \left[\frac{1}{m} \sum_{c=1}^m (F_k^c n_k^c) \right] n_i^c n_j^c \right] \quad (1.6)$$

This partition corresponds to variation in the magnitude of normal forces with angular changes, reflects the eccentricity of forces acting on the grains, similarly to the classic buckling problems.

The remaining part of the stress tensor may be split into the isotropic component:

$$\bar{\sigma}_{ij}^{(i)} = \delta_{ij} \bar{\sigma}_0 - \frac{\delta_{ij}}{A \delta_{kk}} \sum_{p=1}^N R^p \sum_{c=1}^m (F_k^c n_k^c) \quad (1.7)$$

and into the fabric component:

$$\bar{\sigma}_{ij}^{(f)} = \left[\frac{1}{A} \sum_{p=1}^N R^p \sum_{c=1}^m F^{p(av)} n_i^c n_j^c \right] - \bar{\sigma}_0 \delta_{ij} \quad (1.8)$$

that corresponds to the angular distribution over contact points related thus to the anisotropy of the microstructure. In this expression δ_{ij} is the Kronecker symbol and $F^{p(av)}$ the average of normal forces acting on particle p .

We want to find a method to analyse these - or perhaps other - suggested variables during loading processes.

2. The numerical model

Our analysis is restricted to 2D only. Displacements of each grain of the assembly are followed; relative displacements and contact forces between the grains are calculated under external loads. The suggested variables can then be calculated from these data.

Since the deformation of individual grains is negligibly small, the material is modelled as a random assembly of perfectly rigid circular discs with deformable contacts between them.

The initial data of the assembly are the position and radius of each grain and the properties of the contacts (the so-called micro-material-law, stiffnesses, strength etc.).

Loads are acting directly on the grains or on the 'walls' confirming the assembly. The loading process is a series of load steps; an equilibrium state shall be found for each load step until the assembly is totally destroyed. - Hence, the state-changing process is assumed to be a series of equilibrium states. Calculations for finding the equilibrium states are based on the displacement method. The values of the suggested variables are calculated in the equilibrium states and thus their change can be followed during the entire state-changing process.

2.1. Geometrical model

The geometry of the assembly is modelled by means of random number generator. Input data are the size of the rectangular domain under consideration and the minimum and maximum grain radius. The program generates grains with a radius changing at random between given minimum and maximum values.

The random number generator applied to the present program is capable of following any probability density function, hence any sieve curve can be simulated. It can be indispensable when the grain radius varies in a wide range.

Starting at the bottom, the domain is filled upwards by dropping the grains (see Fig. 2.1). Every grain must be supported by the others or by the edges of the domain so that this process will lead to a stable structure.

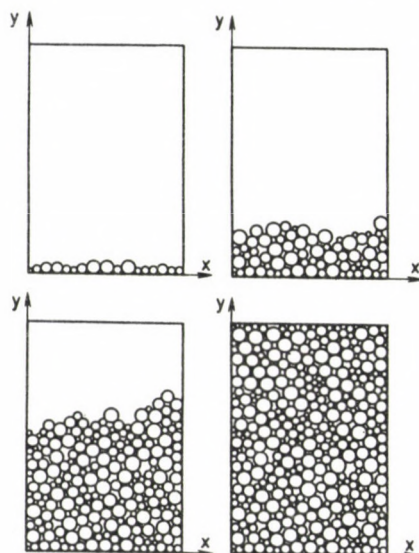


Fig. 2.1.

2.2. Connections between the grains

One of the fundamental problems in the analysis is to define the properties of the connections. Our knowledge of the micro-material-law of the contacts is based on assumptions only; two types of connections are used experimentally in the model at present but other types can be used as well.

In the first case, the contacts are assumed to be rigid; they resist tension or compression, shear force and bending moment (see Fig. 2.2). The shearing stiffness depends on the average normal stress acting between the grains.

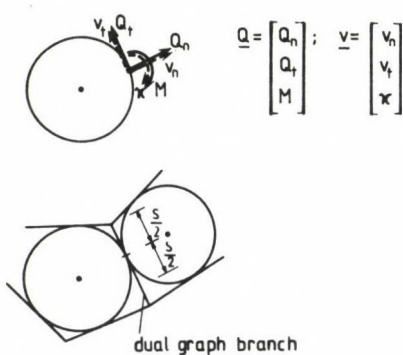


Fig. 2.2.

The relationship between contact forces \underline{Q} (see figure 2.2 for exact meaning) and relative displacement vector \underline{v} is given by equation $\underline{Q} = \underline{k} \underline{v}$ where \underline{k} is the contact stiffness matrix

$$\underline{k} = \begin{bmatrix} Es & 0 & 0 \\ 0 & Gs & 0 \\ 0 & 0 & \frac{Es^3}{12} \end{bmatrix}, \quad (2.1)$$

the shear stiffness depending on the normal stress acting upon the contact:

$$G = G_0 - \frac{\mu v_n E}{s} \quad (2.2)$$

Here E is the normal elastic modulus, G_0 the initial shear modulus, s the symmetric section of the dual graph edge belonging to the contact, and μ is a 'frictional' factor.

The micro-material-law of this contact type is illustrated in Fig. 2.3 where the fracture criteria are also shown.

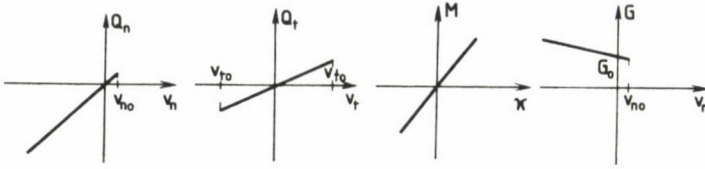


Fig. 2.3.

In the second case, the contacts resist only compression and 'frictional' shear force (see Fig. 2.4)

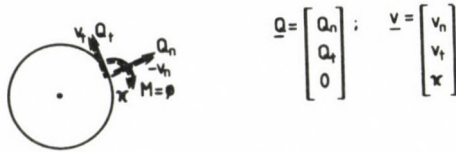


Fig. 2.4.

so \underline{k} has a simpler form:

$$\underline{k} = \begin{bmatrix} E_s & 0 & 0 \\ 0 & \bar{G}_s & 0 \\ 0 & 0 & 0 \end{bmatrix} \quad (2.3)$$

where

$$\bar{G} = \bar{G}_0 - \frac{\mu v_n E}{s} \quad (2.4)$$

\bar{G}_0 is assumed to be much smaller than G_0 used in the first case. Fig. 2.5 illustrates the micro-material-law.

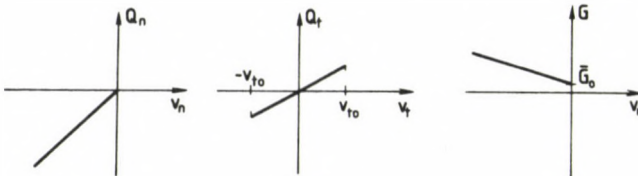


Fig. 2.5.

2.3. The equilibrium equations

Our unknowns are the displacements of all grains as shown in Fig. 2.6; the equilibrium equations of the assembly are set up to find them.

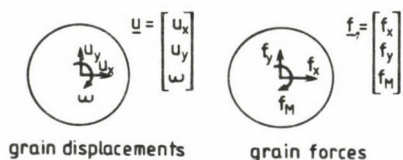


Fig. 2.6.

The relative displacements at contact 'c' of grains 'i' and 'j' can be written as

$$\underline{v}^c = \underline{I}^c(j) \underline{u}^{(j)} - \underline{I}^c(i) \underline{u}^{(i)} \quad (2.5)$$

where the displacement vector of grain 'i' is

$$\underline{u}^{(i)} = \begin{bmatrix} u_x^{(i)} \\ u_y^{(i)} \\ \omega(i) \end{bmatrix} \quad (2.6)$$

and the transformation matrices are

$$\underline{I}^c(j) = \begin{bmatrix} \cos \alpha^c & \sin \alpha^c & 0 \\ -\sin \alpha^c & \cos \alpha^c & R^{(j)} \\ 0 & 0 & 1 \end{bmatrix} \quad (2.7)$$

$$\underline{I}^c(i) = \begin{bmatrix} \cos \alpha^c & \sin \alpha^c & 0 \\ -\sin \alpha^c & \cos \alpha^c & -R^{(i)} \\ 0 & 0 & 1 \end{bmatrix} \quad (2.8)$$

(see Fig. 2.7).

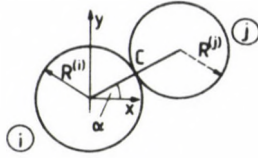


Fig. 2.7.

The resultant force of the contact forces acting on grain 'i':

$$\underline{f}^{(i)} = \begin{bmatrix} f_x^{(i)} \\ f_y^{(i)} \\ f_M^{(i)} \end{bmatrix} = \sum_{c=1}^m \underline{T}^{c(i)T} \underline{Q}^c \quad (2.9)$$

With this calculation made for every grain, the global system of equilibrium equations can be set up where the boundary conditions are also considered:

$$\underline{F} = \underline{K}_{glob} \underline{u} \quad (2.10)$$

2.4. Effect of geometrical non-linearity

It can be rightly assumed that 'rigid' contacts break even in the range of small displacements. Therefore, assemblies with frictional contacts are considered only in the analysis of the effect of geometrical non-linearity.

Let's consider two adjoining grains as shown in Fig. 2.8:

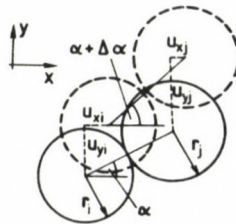


Fig. 2.8.

Here α belongs to the state before relative displacement and $\alpha + \Delta\alpha$ belongs to the state after deformation. Using the notation of finite element descriptions the relation between the local and global variables:

$$\begin{aligned}\underline{u}_g &= \underline{I}^T \underline{u}_1 \\ \underline{k}_g &= \underline{I}^T \underline{k}_1 \underline{I} \\ \underline{q}_g &= \underline{I}^T \underline{q}_1\end{aligned}\quad (2.11)$$

Here 1 indicates that the effects are described in the local coordinate system and g refers to the global basis; \underline{u} is the displacement of given 'node' (grain center); \underline{k} the stiffness matrix of given 'finite element' (given contact); \underline{q} forces acting on the 'node' and \underline{I} the transformation matrix:

$$\underline{I} = \begin{bmatrix} -\cos \alpha & -\sin \alpha & 0 & \cos \alpha & \sin \alpha & 0 \\ \sin \alpha & -\cos \alpha & r_i & -\sin \alpha & \cos \alpha & r_j \\ 0 & 0 & -1 & 0 & 0 & 1 \end{bmatrix}\quad (2.12)$$

Geometrical non-linearity means that \underline{I} depends on \underline{u} :

$$\underline{I} = \underline{I}(\underline{u})\quad (2.13)$$

The last equation of (2.11) can be written in incremental form neglecting the second order term:

$$\underline{q}_g + \Delta \underline{q}_g = (\underline{I}^T + \Delta \underline{I}^T) (\underline{q}_1 + \Delta \underline{q}_1)\quad (2.14)$$

and arranged as

$$\Delta \underline{q}_g = \underline{I}^T \Delta \underline{q}_1 + \Delta \underline{I}^T \underline{q}_1 = \underline{k}_g \Delta \underline{u}_g + \Delta \underline{I}^T \underline{q}_1\quad (2.15)$$

The last term can be expressed as

$$\Delta \underline{I}^T \underline{q}_1 = \sum_{i=1}^3 \underline{q}_{1i} \Delta \underline{I}_{i1}^T = \underbrace{\sum_{i=1}^3 \underline{q}_{1i} \left[\frac{\partial \underline{I}_{i1}^T}{\partial u_{g1}}, \frac{\partial \underline{I}_{i1}^T}{\partial u_{g2}}, \dots, \frac{\partial \underline{I}_{i1}^T}{\partial u_{g3}} \right]}_{\underline{k}_g} \Delta \underline{u}_g\quad (2.16)$$

Matrix \underline{k}_g on the right side of the equation is called geometrical stiffness matrix. Using this form in eq. (2.15):

$$(\underline{k} + \underline{k}_g) \Delta \underline{u}_g = \Delta \underline{q}_g \quad (2.17)$$

Matrix \underline{k}_g can be easily produced from

$$\underline{k}_g = \sum_{i=1}^3 \underline{q}_{1i} \underline{G}_i \quad (2.18)$$

where matrix \underline{G}_i consists of the partial derivatives of columns of \underline{T}^T with respect to displacement increments. Since

$$\underline{q}_{1i} = \begin{bmatrix} N \\ T \\ 0 \end{bmatrix}, \quad (2.19)$$

only matrices \underline{G}_1 and \underline{G}_2 have to be constructed. On the basis of expressions (2.19), all values are known for construction of matrix \underline{k}_g . However, eq. (2.17) satisfies only the equilibrium equations while the compatibility conditions remain unsatisfied. Therefore, let the increments of internal forces derived from $\Delta \underline{q}_g$ on the basis of the geometry of the 'previous' state be evaluated first. By 'previous state' we understand the geometry given by the previous load step ($k-1$, if k denotes the load step index) or by the previous iteration step.

Increments of internal forces:

$$\Delta \underline{S}_i = \underline{D}_i \Delta \underline{u}_{1i} - \Delta \underline{S}''_{1(i-1)} \quad (2.20)$$

Here i is the iteration step index in given load step; \underline{D}_i is the matrix of micro-constitutive-law (also a variable); $\Delta \underline{S}''_{1(i-1)}$ denotes the kinematic load increment calculated in the previous iteration step. Its value is zero at the beginning of each load step.

The total internal load is simply obtained from the increments of internal forces

$$\underline{S} = \underline{S}_{k-1} + \sum_{i=1}^{k-1} \Delta \underline{S}_i \quad (2.21)$$

Here \underline{S}_{k-1} is the internal force vector of the previous load steps. On the basis of the value of \underline{S} we can determine nodal equilibrium error vector Δq_{gi} .

Internal normal forces are calculated from the new position of grain centers in the following way:

$$N = \frac{(l_{\text{new}} - (r_i + r_j)) (EA)_i}{r_i + r_j} = \Delta u_{li}'' \quad (2.22)$$

Global kinematic load vector $\Delta q_{gi}''$ is determined from this force by means of the transformation matrix. The new displacement increment vector is calculated by using the sum ($\Delta q_{gi}' + \Delta q_{gi}''$) as a load vector. The above procedure shall be repeated in an internal iteration cycle until the error vectors decrease below the specified limit.

2.5. State-changing analysis

If the geometry of the assembly and the contact properties are uniquely defined, the equilibrium state associated with given load step can be determined using the displacement method. First the program calculates the contact stiffness matrices for every contact in the assembly. The value of shear stiffness at given contact is estimated on the basis of the value of relative normal displacement after the previous load step. In the first load step, the initial G_0 value is used.

The contact stiffness matrices are transformed into global basis and the unknown displacements of the grains are calculated by the frontal solver technique. Then the contact forces are determined. A state obtained in this way will be possible only if the stresses do not exceed the corresponding strengths at any contact.

If there are broken contacts, the geometrical structure shall be modified: broken contacts are omitted and grains which lost stability are moved in the direction of the external forces directly acting on them (or downwards in lack of directly acting forces) until they find a new stable position for themselves where they are supported by stable grains. Grains which cannot find a stable position are omitted. Now this modified structure has to carry the total load; and the calculations shall be repeated for total load until a stable state is found.

In the stable state, the shear stiffnesses are checked; and the geometrical non-linearity is taken into consideration by modifying the positions of grains.

Finally, if a stable and compatible equilibrium state is found, the values of the suggested variables shall be calculated.

3. Numerical examples

Our first example illustrates the behaviour of an assembly with rigid contacts. The initial configuration, the loads and the strength characteristics are shown in Fig. 3.1:

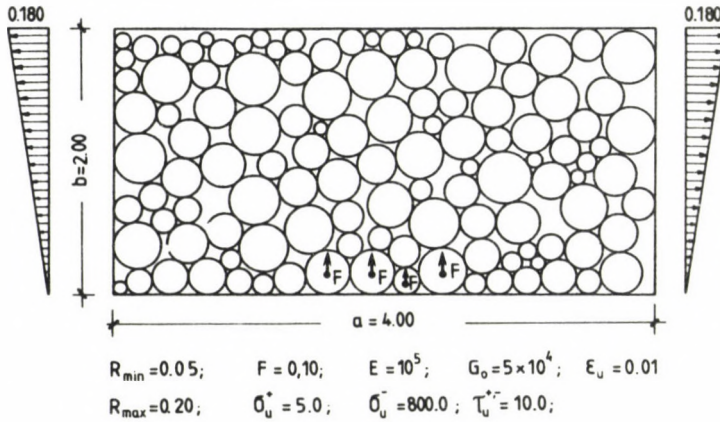


Fig. 3.1.

With the load factor increased, the contacts break one after the other; the change of the replaced graph can be seen in Fig. 3.2.

a,

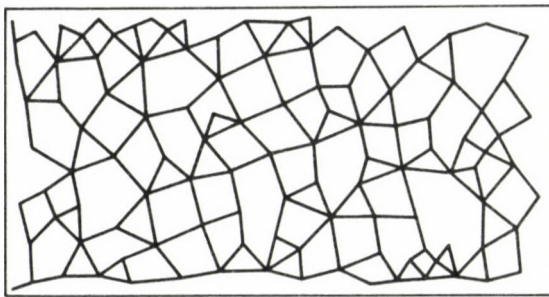
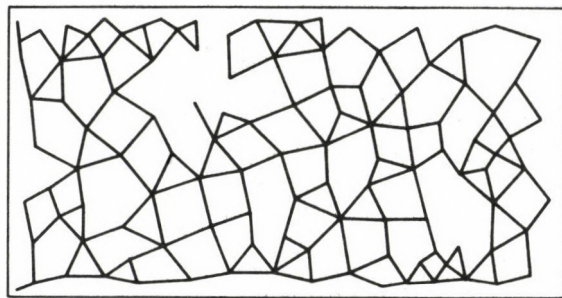
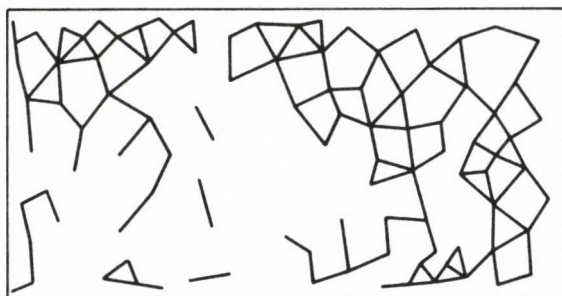


Fig. 3.2a.

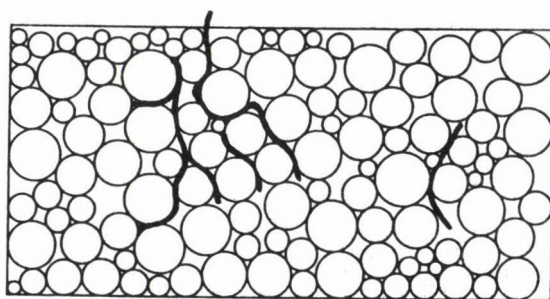
b,

Fig. 3.2b.

c,

Fig. 3.2c.

d,

Fig. 3.2d.

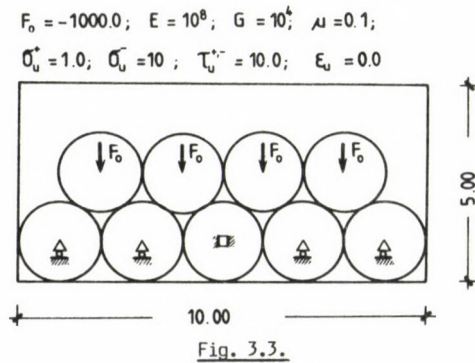
Finally, the Cundall-tensors are tabulated for the first, an intermediate and the last load step in Table 1.

Table 1

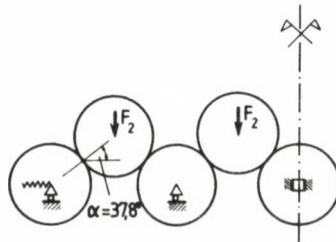
| Load factor | $\bar{\sigma}$ (s) | $\bar{\sigma}$ (N) | $\bar{\sigma}$ (f) | $\bar{\sigma}_0$ |
|-------------|--|---|--|------------------|
| 1.00 | $\begin{bmatrix} 0.447 & -0.220 \\ & -0.045 \end{bmatrix}$ | $\begin{bmatrix} 0.049 & 0.022 \\ & -0.049 \end{bmatrix}$ | $\begin{bmatrix} -0.005 & 0.0005 \\ & 0.005 \end{bmatrix}$ | 0.0667 |
| 1.40 | $\begin{bmatrix} 0.066 & -0.03 \\ & -0.066 \end{bmatrix}$ | $\begin{bmatrix} 0.065 & 0.03 \\ & -0.065 \end{bmatrix}$ | $\begin{bmatrix} -0.007 & 0.0005 \\ & 0.007 \end{bmatrix}$ | 0.116 |
| 1.8 | $\begin{bmatrix} 0.035 & -0.06 \\ & -0.034 \end{bmatrix}$ | $\begin{bmatrix} 0.011 & -0.005 \\ & -0.01 \end{bmatrix}$ | $\begin{bmatrix} 0.079 & 0.005 \\ & 0.079 \end{bmatrix}$ | 0.143 |

CUNDALL - stresses

Our second example shows an assembly with frictional contacts only. The initial state can be seen in Fig. 3.3:



The internal structure is strongly changing during the loading process as illustrated in Fig. 3.4 until stability is lost.



The fabric tensor describing the anisotropy of the replaced graph shows a significant change; the initial and final state being shown in Table 2:

Table 2

| Load factor | φ_{ij} |
|-------------|--|
| 1.00 | $\begin{bmatrix} 0.292 & -8 \times 10^{-17} \\ & 0.708 \end{bmatrix}$ |
| 3.6 | $\begin{bmatrix} 0.625 & -2.7 \times 10^{18} \\ & 0.375 \end{bmatrix}$ |

Conclusions

The present paper described a possible method for numerical modelling of granular assemblies. Efforts were made to find variables that can be used also in macro-level constitutive equations. The examples illustrated the efficiency of the numerical model. A detailed analysis of the selected variables became possible in this way.

REFERENCES

1. Nemat-Nasser, S.: Overall Stresses and Strains in Solids with Microstructures, in Modelling Small Deformations of Polycrystals, ed. J. Gittus, J. Zarka; Elsevier, 1986, 41-64
2. Mogami, T.: A Statistical Approach to the Mechanics of Granular Materials. Soils and Foundations, Vol. 5, No. 2, (March 1965)
3. Mogami, T.: On the Deformation of Granular Materials. Trans. of Japan Society of Civil Engineers, No. 129, (May 1966)
4. Moroto, N.: Parameters for Shear Deformation. Proceedings of US-Japan Seminar on Continuum-Mechanical and Statistical Approaches in the Mechanics of Granular Materials, 1978, Tokyo, 110-113
5. Brown, C.B.: The Use of Maximum Entropy in the Characterisation of Granular Media. Proceedings of US-Japan Seminar on Continuum-Mechanical and Statistical Approaches in the Mechanics of Granular Materials, 1978, Tokyo, 98-108
6. Oda, M.: Initial Fabric and Their Relations to Mechanical Properties of Granular Material. Soils and Foundations, Vol. 12, No. 1, (March 1972)
7. Oda, M. et al.: Experimental Micromechanical Evaluation of the Strength of Granular Materials: Effects of Particle Rolling. Mechanics of Granular Materials: New Models and Constitutive Equations, ed. J.T. Jenkins, M. Satake; 1983, Elsevier, 21-30

8. Mehrabadi, M.M. et al.: Some Basic Theoretical and Experimental Results on Micromechanics of Granular Flow. *Micromechanics of Granular Materials*, ed. M. Satake, J.T. Jenkins; 1988, Elsevier, 253-262
9. Satake, M.: Constitution of Mechanics of Granular Materials Through the Graph Theory, *Proceedings of US-Japan Seminar on Continuum-Mechanical and Statistical Approaches in the Mechanics of Granular Materials*, 1978, Tokyo, 47-62
10. Satake, M. - Kishino, Y.: A New Simulation Method for Granular Materials. *Acta Stereol*, 1987, 6/III. 365-370
11. Cundall, P.A. - Strack, O.D.L.: Modelling of Microscopic Mechanisms in Granular Material. *Mechanics of Granular Materials: New Models and Constitutive Equations*, ed. J.T. Jenkins, M. Satake; 1983, Elsevier, 137-149

GLOBAL INVESTIGATION OF DISCRETE MODELS OF THE EULER BUCKLING PROBLEM

ZS. GÁSPÁR* - G. DOMOKOS**

(Received: 15 December 1989)

Mathematical tools for the global description of discretized line continua are presented. These tools are applied to the analysis of the planar buckling of elastic bars under static loading. The results of the computer experiments display an essential difference between discrete models consisting of even and odd number of rigid bars. Propositions are presented referring to the mathematical background of the aforementioned paradoxes.

1. Introduction

Our aim is to investigate discrete models of the well-known buckling problem of the perfect, simply supported planar rod, described first by Euler (1744). In his work Euler demonstrates several qualitatively different equilibrium shapes of the "linea elastica". The first thorough numerical treatment of the problem is delivered by Saalschütz (1880). The complete mathematical classification of the solution curves (including "looping" solutions) is due to Love (1927). Reference to these last mentioned solutions can be found in Timoshenko & Gere (1961), as well. The present paper is devoted partly to the problem, whether the solutions of the discretized model can be classified in a similar way, or there is a qualitative difference. The continuous structure has unstressed length L , bending stiffness EJ and axial stiffness $EA = \infty$. The discrete model, consisting of n rigid bars connected by $n-1$ linear rotational springs is illustrated in Fig. 1. The spring constants s_i of the discrete model are derived from the bending stiffness of the continuous beam: $s_i = 2EI/(L_i + L_{i+1})$ ($i = 1, 2, \dots, n-1$), where L_i is the length of the i th rigid bar ($\sum L_i = L$). The structure is assumed to be straight at zero loading.

*Gáspár, Zsolt, H-1025 Budapest, Kapy u. 40/b, Hungary

**Domokos, Gábor, H-1056 Budapest, Váci u. 44, Hungary

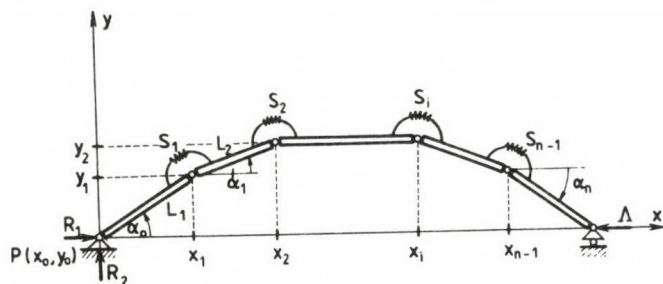


Fig. 1.

The shape of the discrete model can be described by the configuration vector C with components $C_i = \alpha_{i-1}$ ($i = 1, 2, \dots, n$). At the initial point there is no spring, i.e. only $\alpha_0 \in I$, $I = (-\pi, \pi]$ will be discussed. By considering this restriction, the shape of the structure supported only at initial point can be mutually uniquely identified by an element of $G = I \times R^{n-1}$. The configurations with $y_n = 0$ (two supports) form a proper subset $G_B \subset G$. If $x_n = y_n = 0$ is required, then we arrive at $G_C \subset G_B$. According to our assumptions, the structure is loaded only at the endpoints, i.e. by fixing the reaction forces $R_1 = \Lambda$ and R_2 the elements α_i of the configuration vector can be derived from α_0 by the following recursion formula:

$$\begin{aligned} x_j &= x_{j-1} + L_j \cos \alpha_{j-1} \\ y_j &= y_{j-1} + L_j \sin \alpha_{j-1} \end{aligned} \quad (1)$$

$$\alpha_i = \alpha_{i-1} - \frac{R_1}{s_i} (y_{i-1} + L_i \sin \alpha_{i-1}) + \frac{R_2}{s_i} (x_{i-1} + L_i \cos \alpha_{i-1})$$

$$(i = 1, 2, \dots, n-1; \quad j = 1, 2, \dots, n)$$

since $x_0 = y_0 = 0$ are constants. The elements of the equilibrium set can be identified by a configuration vector C and the corresponding load parameters R_1 and R_2 . The equilibrium set of the structure supported only at the initial point will be denoted by E ($E \subset G \times R^2$). The equilibrium positions satisfying $y_n = 0$ as well form the set E_B ($E_B \subset G_B \times R^2$). If $x_n \neq 0$, then the global equilibrium for the structure yields $R_2 = 0$, i.e. the equilibrium positions satisfying $x_n \neq 0$, $y_n = 0$ can be identified by the elements of $E_D \subset (G_B - G_C) \times R$. Our aim is to reduce the dimension of the

equilibrium set, i.e. to find the space with minimal dimension, onto a subset of which E_B or E_D can be mapped in a mutually one to one way.

Definition: E_B is called unique in R^t iff there exists a mapping $M: E_B \rightarrow R^t$, that M gives a mutually one to one mapping between E_B and $M(E_B) \subset R^t$. (Similar formulation holds for E_D .)

Dimension Reduction Lemma: In the case of the investigated discrete structure (Fig. 1) E_B is unique in R^3 , E_D is unique in R^2 .

Remark, that $M(E_B) \subset I \times R^2$, $M(E_D) \subset I \times R$.

Proof of Lemma

The equilibrium positions can be mutually uniquely identified by the corresponding number triple $(\alpha_0, R_1, R_2) \in R^3$, since, on the one hand, any element of $I \times R^2$ is mapped onto one and only one element of $G \times R^2$ by eq. (1) and, on the other hand, the numbers α_0, R_1 and R_2 are coordinates of the elements of E_B , i.e. to each element of E_B one and only one number triple corresponds. By similar argumentation the equilibrium positions satisfying $x_n \neq 0$ ($R_2 = 0$) are uniquely identified by (α_0, R_1) . Q.e.d.

This Lemma implies, that the equilibrium paths plotted in $I \times R^2$ ($I \times R^3$) can only intersect, if there is a bifurcation point. Similar lemmas for other types of discretized line continuums can be derived in an analogous way. It may be of interest, that dimension reduction of the equilibrium path is possible for continuous structures, as well. Theorems on this problem are demonstrated by Domokos (1989).

2. Computer experiments

Based on the dimension reduction lemma and recursion formula (1) a computer program has been developed to detect all possible equilibrium positions. To make visualization easier the case $x_n = 0$ has been excluded from the computation, i.e. all equilibrium paths could be plotted in the (ω_0, λ) plane. At $x_n = 0$ a bifurcation occurs, which can be interpreted as a rigid body rotation around $P(0, 0)$. This phenomenon was first discussed by Domokos (1989) for the continuous beam. Stability analysis is delivered by Gáspár & Domokos (1990) for the discrete model $n = 2$ with finite axial stiffness. The equilibrium paths corresponding to this bifurcation can not be plotted in the (ω_0, λ) plane without intersecting other paths, therefore the bifurcation points are marked by small circles. These bifurcation points have been extra computed, but only for paths where n/k is integer,

n denoting the number of bars, k denoting the serial number of buckling mode. In the computer experiments only models with equal elements ($L_1 = L/n$) have been investigated. The equilibrium path P can be subdivided into a connected (P_C) and a disconnected (P_D) part. P_C contains all equilibrium positions which can be reached on a continuous path from the trivial one. In Fig. 2.a-k the connected parts (P_C) for $n = 2$ to 12 are plotted in the interval $\alpha_0 \in (0, \pi)$. The numerical and qualitative data gained from the computer experiments is partly summarized in the forthcoming Tables.

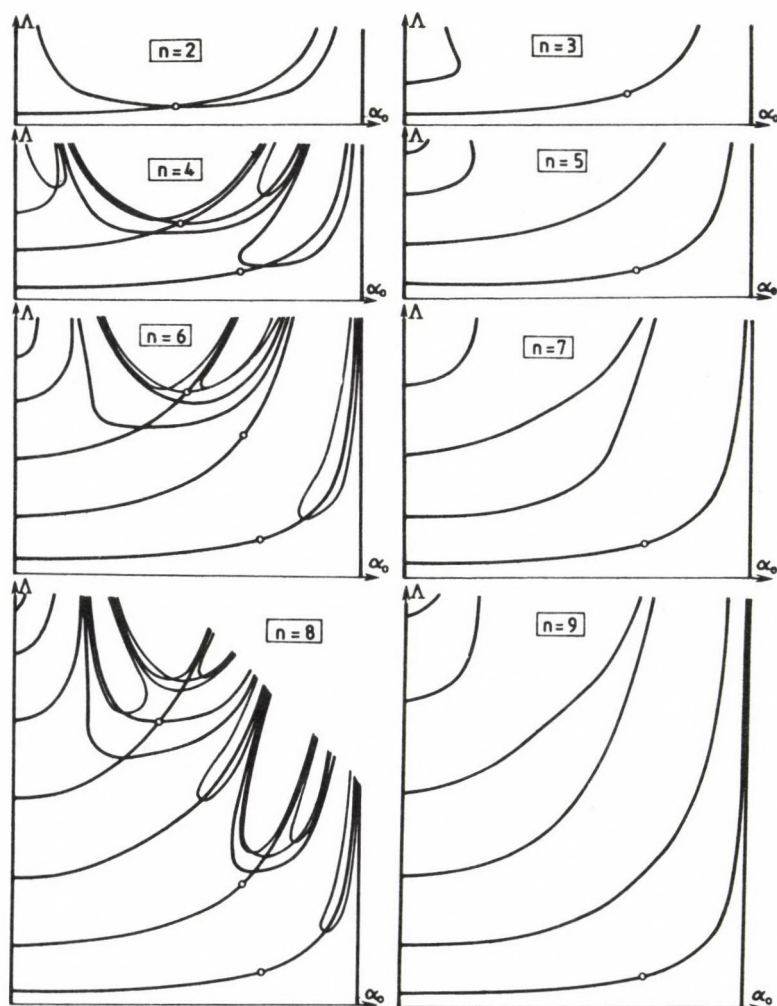


Fig. 2.a-h.

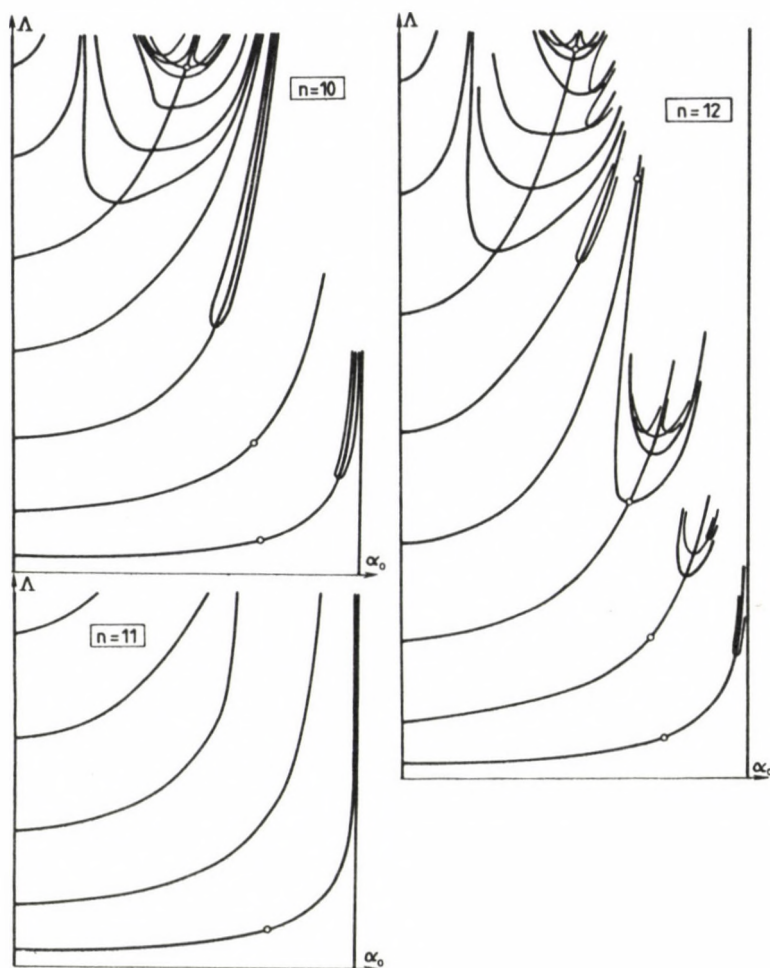


Fig. 2.i-k.

Table 1

| n | F_1^n/F_1^∞ | F_2^n/F_1^∞ | F_2^n/F_2^∞ | $\alpha_{0,2}^n$ |
|----------|--------------------|--------------------|--------------------|------------------|
| 2 | 0.811 | 1.266 | 0.579 | 1.571 |
| 3 | 0.912 | 2.205 | 1.011 | 2.102 |
| 4 | 0.949 | 1.960 | 0.895 | 2.092 |
| 5 | 0.967 | 2.089 | 0.957 | 2.171 |
| 6 | 0.977 | 2.107 | 0.965 | 2.204 |
| 7 | 0.983 | 2.131 | 0.976 | 2.223 |
| 8 | 0.987 | 2.142 | 0.981 | 2.242 |
| 9 | 0.989 | 2.144 | 0.982 | 2.251 |
| 10 | 0.990 | 2.153 | 0.986 | 2.262 |
| 11 | 0.991 | 2.162 | 0.990 | 2.266 |
| 12 | 0.992 | 2.165 | 0.992 | 2.271 |
| ∞ | 1.000 | 2.183 | 1.000 | 2.289 |

F_1^n denotes the first buckling load of the discrete structure with n equal bars;

F_2^n denotes the load parameter at $x_n = 0$ in the first buckling mode of the n -bar structure;

α^n denotes the value of α_0 corresponding to F_2^n .

Index ∞ refers to the continuous structure. If no analytical results were available, then the approximation $n = 200$ has been accepted for this case.

The integer a_{jn} in the j th row of Table 2 gives the number of secondary bifurcations in the j th buckling mode of the discrete structure. The variable a_{nj} is only interpreted if j is a divisor of n .

Table 2

| n | 2 | 3 | 4 | 5 | 6 | 7 | 8 | 9 | 10 | 11 | 12 | ∞ |
|----------|---|---|---|---|---|---|---|---|----|----|----|----------|
| 1st mode | 2 | 1 | 2 | 1 | 2 | 1 | 2 | 1 | 2 | 1 | 2 | ? |
| 2nd mode | | | 3 | - | 1 | - | 3 | - | 1 | - | 3 | |
| 3rd mode | | | | | 4 | - | - | 1 | - | - | 4 | |
| 4th mode | | | | | | | 5 | - | - | - | - | |
| 5th mode | | | | | | | | | 6 | - | - | |
| 6th mode | | | | | | | | | | | 7 | |

Based on the data contained in Table 2 we formulate the following
Conjecture 1: In the case of $L_i = L/n$

$$a_{jn} = \begin{cases} 1 & \text{if } n/j \bmod 2 = 1 \\ j+1 & \text{if } n/j \bmod 2 = 0 \end{cases}$$

Conjecture 1 is a simple extrapolation of Table 2 to an arbitrary finite model, but it does not give explanation to the basic difference between the behaviour of "even" and "odd" models. In the forthcoming sections we will attempt to give at least particular explanation.

3. Mechanical explanation

The aim of this section is to give a plausible mechanical explanation to the $j+1$ secondary bifurcation observed in even models ($n/j \bmod 2=0$). The 3rd buckling mode ($j=3$) of the model consisting of 12 elements ($n=12$) is illustrated in Fig. 3/a. The buckled chain can now be substituted by a straight virtual chain with finite axial stiffness. A single element of the virtual chain consists of $12/3=4$ elements of the original chain. The virtual chain is illustrated in Fig. 3/b. In general, the virtual chain substituting the j th buckling mode of a chain of n elements will be denoted by V_{nj} . V_{nj} consists of j virtual elements, i.e. V_{nj} has $j-1$ buckling modes explaining $j-1$ out of the observed and predicted $j+1$ bifurcations. The buckling modes of V_{nj} occur in the reverse order, i.e. the lowest load corresponds to the highest mode. Remark, that the k th mode of V_{nj} can be expected to be a symmetric bifurcation if $[n/(j.k)] \bmod 2=0$ otherwise it is an asymmetric one.

One of the still not explained bifurcations is the already discussed rotation around $x_n=0$, marked with small circles on the equilibrium path. The last bifurcation to be explained corresponds to the individual, simul-

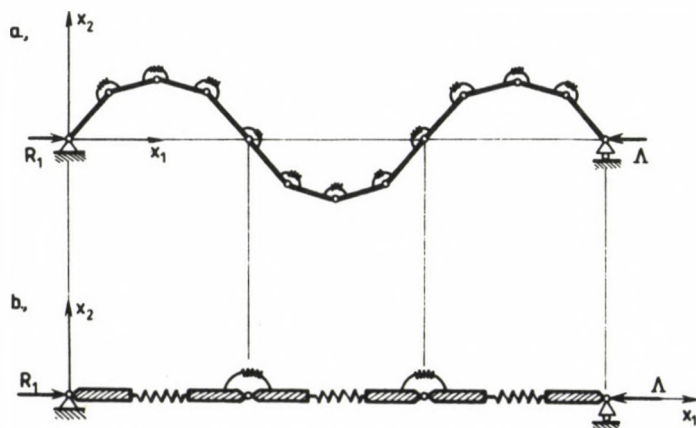


Fig. 3.

a.,

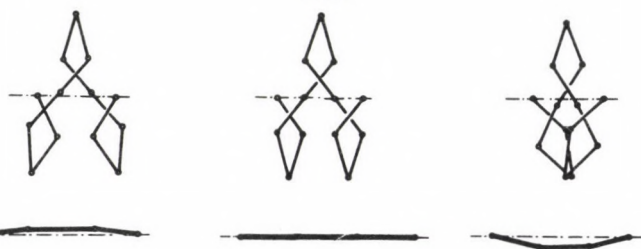
Real chain:



Virtual chain (Enlarged 10:1)



b.,

 $B_{12,3,3}$ 

c.,

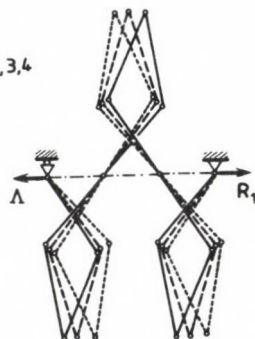
 $B_{12,3,4}$ 

Fig. 4.

taneous buckling of the virtual elements in V_{nj} . These elements are arches consisting of n/j bars. The virtual chain remains straight at this buckling, only the individual arches have a bifurcation point. This buckling can be expected to be symmetric, if j is even. Let us denote the k th buckling of V_{nj} by B_{njk} . (The first buckling corresponds to the lowest load parameter.) The secondary bucklings $B_{12,3,1}$, $B_{12,3,3}$ and $B_{12,3,4}$ are illustrated in Fig. 4. The theory just described explains only the behaviour of the even models to some extent. Up to now no reasonable mechanical clue has been found to explain, why do not "odd" models behave like this. The basic difference between the two sets of models will be discussed in the next section from the mathematical point of view.

4. Mathematical explanation

Let us return from the special discrete models treated in the computer experiments to the more general ones, consisting (typically) of non-equal bars (Fig. 1). Even this model will be further generalized, however only in a mathematical sense. Let us introduce the symbol M_j^n denoting the set of models consisting of n bars out of which exactly j bars have non-zero length ($1 \leq j \leq n$), and let us introduce the set

$$M^n = \bigcup_{j=1}^n M_j^n \quad (2)$$

The set M_j^n is a subset of the $(n-1)$ dimensional hyperplane H defined by $\sum L_i = L$ in R^n . The distance of two models is defined by the Euclidean norm, and is interpreted only for elements of sets with identical superscripts.

We are going to give a simple illustration for some M_j^n s in the hyperplane H and to make some propositions about them. These propositions are mainly based on geometrical intuition, no exact proof is delivered in this paper.

Let us begin with M^1 containing the single subset M_1^1 , which contains again a single element (Bar with unit length). This set is zero-dimensional (point). Such sets will be illustrated by circles, containing the number of non-zero bars (Fig. 5/a). M^2 (Fig. 5/b) contains the subsets M_1^2 and M_2^2 . M_1^2 has two zero-dimensional elements, since either the first, or the second

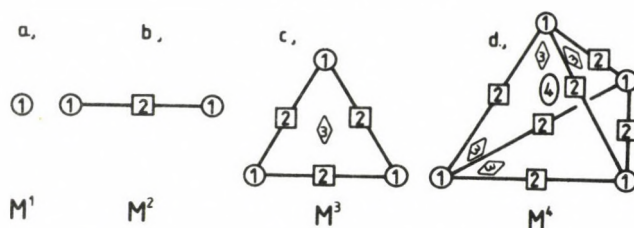


Fig. 5.

bar can have zero length. These points are the missing end-points of M_2^2 , which is an open interval. This latter type of set will be illustrated by an interval interrupted by a square, containing j . Fig. 5/c and Fig. 5/d, illustrating M^3 and M^4 respectively, are constructed in a similar way, and are (hopefully) self-explanatory. Regarding Fig. 5 the following propositions seem to be plausible.

Proposition 1. M^n is an open set iff $n > 1$.

2. M^n is a closed set.

3. M^n is a simplex.

4. The closure of M^n is M^n .

5. M_j^n is not empty. ($n \geq 1$, $1 \leq j \leq n$).

6. $\dim(M^n) = n-1$.

(Definitions of unknown terms see in Bourbaki, 1966.)

Propositions 1.-6. give some interesting mathematical hints, but do not disclose any difference between the behaviour of "even" and "odd" models. Neither does the examination of the models $E_j^n \subset M_j^n$ in which the lengths of the non-zero bars are equal. E_j^n consists of $\binom{n}{n-j}$ zero dimensional elements. The set E_2^4 is illustrated by dots as a subset of M^4 in Fig. 6.

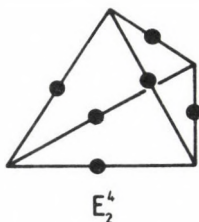


Fig. 6.

Let us now turn our attention to sets $S_j^n \subset M_j^n$, consisting of models with symmetry axis $y = x_n/2$ (Fig. 1). The notation S^n is introduced as an analogue of M^n (see (2)). It seems to be remarkable, that propositions 1-4 are true for the symmetrical models, as well ("substitution" $M \equiv S$). However, this similarity is very deceiving. There exist principal differences between sets S^n , depending on whether n is odd or even. These differences will be summarized in the next propositions:

Proposition 5'. S_j^n is empty, iff n is even and j is odd. ($n \geq 1, 1 \leq j \leq n$).

$$6'. \dim(S^n) = \begin{cases} n/2 - 1 & \text{if } n \text{ is even} \\ (n-1)/2 & \text{if } n \text{ is odd.} \end{cases}$$

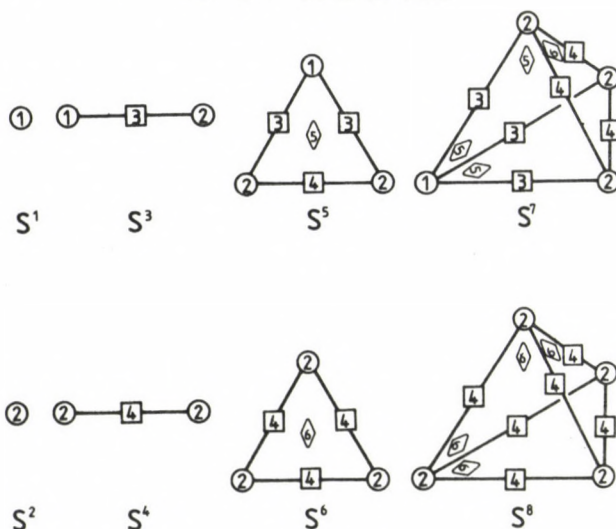


Fig. 7.

The difference can be formulated in mechanical terms, as well. It is always possible by small perturbation of the model (i.e. by adding small bars or changing slightly existing bar lengths in a symmetrical way) to transform an "even" model into an "odd" one, but not vice versa. The sets S^n ($n = 1, 2, \dots, 8$) are illustrated in Fig. 7 with the convention introduced in Fig. 5. The detected mathematical differences between "odd" and "even" models might be partly the clue to the difference of their mechanical behaviour.

REFERENCES

1. Bourbaki, N.: General topology. Paris (1966)
2. Domokos, G.: Kikötött árbocok nagy elmozdulásai. (Large deflections of guyed masts.) Thesis, Hung. Acad. of Sci., Budapest (1989)
3. Euler, L.: Methodus inveniendi lineas curvas maximi minimive proprietate gaudentes, Lausanne-Genf (1744)
4. Gáspár, Zs. - Domokos, G.: Global description of a simple mechanical model, Proc. Conf. Stab. Steel. Struc. (ed. M. Iványi). Akadémiai Kiadó, Budapest (1990) (in press)
5. Love, A.E.H.: Mathematical theory of elasticity, Dover Publications, New York (1927)
6. Saalschütz, L.: Der belastete Stab, Leipzig (1880)
7. Timoshenko, S.P. - Gere, J.M.: Theory of elastic stability McGraw-Hill, New York (1961)

PRODUCTION OF DYNAMIC STIFFNESS MATRIX IN CASE OF OTHER THAN RIGID JOINTS AND RIGID ELEMENTS

GYÖRGYI, J.*

(Received: 27 December 1989)

In calculating for real structures, the structure may contain elements connected to each other in a special way depending on the layout of the structure. Such cases are e.g. structures made of prefabricated elements. Again due to the layout, structural parts that can be considered rigid are often used between flexible elements. In order to avoid numerical problems, it is necessary that this fact be taken into consideration when the stiffness matrix of the structure is produced. This paper presents the way to cope with the above problems.

Introduction

For the elementary dynamic stiffness matrix according to the method of finite elements, it is usually assumed that the ends of the elements are connected in a rigid way to the nodes while at the same time the different nodes are interconnected by flexible elements. This paper shows how the elementary dynamic stiffness matrices can be produced in case of other than rigid joints and how the effect of rigid elements can be taken into consideration without any change in the layout of the stiffness matrix of a structure.

1. Stiffness matrix of elements with other than rigid joint between them

In calculating for structures, the elementary stiffness matrix describes the relationship between displacements and forces of the ends of the elements. The elementary matrices in combination are the stiffness matrix of the set of elements (K_h), a diagonal hypermatrix with the stiffness matrices of the different elements arranged along the diagonal. In case of a structure, the ends of the elements are interconnected with certain displacements of the ends corresponding to each other, the number

*Györgyi, József, H-1221 Budapest, Arany J. u. 96/b, Hungary

of independent displacements (n_i) being less than the number of end-of-element displacements (n_e). The relationship between the two displacement vectors can be described by means of combination matrix \underline{P} /1/. Element $k\ell$ of matrix \underline{P} will be unit if end-of-element displacement k corresponds to independent displacement ℓ ; otherwise matrix element $k\ell$ will be zero.

Thus the stiffness matrix of the interconnected elements is

$$\underline{K}_P = \underline{P}^* \underline{K}_h \underline{P} \quad (1)$$

Matrix \underline{K}_P is produced in accordance with expression /1/ but in a way other than matrix multiplication. To produce element $k\ell$ of the matrix, it shall be tested which of the end-of-element displacements corresponds to independent component displacement ℓ and the element containing the force component of direction k shall be taken from given elementary stiffness matrix accordingly.

It is a rather complicated job to produce matrix \underline{K}_P element by element in the way described above. In a simpler case, the ends of the structural elements are connected in a rigid way to the so-called structural nodes. In this case, the independent displacements can be treated in combination in nodal displacement vectors and matrix \underline{P} gives the relationship between end-of-element displacement vectors and nodal displacement vectors. Matrix \underline{P} can be defined as a hypermatrix with a unit matrix in its block $k\ell$ if the end of element associated with the displacement vector in block k in case of end-of-element displacements is connected to node ℓ .

In this case, matrix \underline{K}_P can be produced block by block in the knowledge of the block of the different elementary stiffness matrices.

How can this definitely more favourable process be applied to the case of elements of other than rigid joint between them where for given nodes, the number of independent displacements is larger than the number of nodal displacement components?

The fact that given end of element can displace freely in direction s as compared with the node means at the same time that no end-of-element force is acting in given direction that is

$$\begin{bmatrix} K_1 \\ K_s \\ K_2 \end{bmatrix} \begin{bmatrix} u_1 \\ u_s \\ u_2 \end{bmatrix} = \begin{bmatrix} g_1 \\ 0 \\ g_2 \end{bmatrix} \quad (2)$$

$$\begin{bmatrix} k_{s1}^* & k_{ss} & k_{s2}^* \end{bmatrix} \begin{bmatrix} u_2 \\ u_s \\ u_2 \end{bmatrix} = 0 \quad (3)$$

$$u_s = \frac{1}{k_{ss}} (k_{s1}^* u_1 + k_{s2}^* u_2) \quad (4)$$

That means that, in the knowledge of the other end-of-element displacement components, given end-of-element displacement component can be calculated. This also means that the number of nodal displacement components need not be exceeded by the number of displacement unknowns either.

With (4) substituted into (2), a modified stiffness matrix is obtained, containing only u_1 and u_2 while column and row s corresponding to u_s consists of zero elements only:

$$K_m = K - \frac{1}{k_{ss}} k_s k_s^* \quad (5)$$

Here K is the original while K_m the modified elementary stiffness matrix, modified by the dyadic product (1).

In the general case, the dynamic stiffness matrix of one single element can be written as

$$K_{dyn} = K - \omega^2 M \quad (6)$$

where M is the so-called mass matrix,

$$M = \rho \int_{(V)} N^* N \, dV \quad , \quad (7)$$

ρ being density while the elements of matrix N are displacement functions describing the relationship between unit end-of-element displacements and displacements within the element, in the general case approximate functions (used e.g. in statical calculations) that can be calculated from the differential equation of the oscillating bar in case of bars of invariable cross section.

If relationship (5) is used to modify the dynamic stiffness matrix, the modified dynamic stiffness matrix can not be written in a form similar to (6) where the frequency independent static stiffness matrix and a mass

matrix multiplied by ω^2 but containing constants appear independently). As a solution, production of the mass matrix according to (7) shall be repeated using displacement functions that take into consideration that no end-of-element forces can arise in given direction. The success of the method in static calculations lies in that stiffness matrices complying with different boundary conditions need not be produced each independently but they are obtained simply by dyad subtraction from the stiffness matrix of the element of rigid joint. As shown below, this is possible also in calculation of the mass matrix.

Let the displacement function associated with end-of-element displacement in direction l be denoted by v_l and let s be the direction of unconstrained displacement. In case of unit end-of-element displacement in direction l , force of a magnitude of k_s will act upon the element of rigid joint in direction s . Assume that a displacement of magnitude k_{sl}/k_{ss} is taking place there in a direction opposite to the direction of the force so that this force will be zero. The displacement functions associated with the two end-of-element displacements result in a sum to which unit end-of-element displacement belongs in direction l while no force is arising in direction s . This is the modified displacement function to be used for recalculation of given element of the mass matrix.

Element kl of the modified mass matrix:

$$\begin{aligned}
 m_{m,kl} &= \oint_{(V)} \left(v_k - \frac{k_{sk}}{k_{ss}} v_s \right) \left(v_l - \frac{k_{sl}}{k_{ss}} v_s \right) dV = \\
 &= \oint_{(V)} v_k v_l dV - \int_{(V)} \frac{k_{sk}}{k_{ss}} v_s v_l dV - \\
 &\quad - \int_{(V)} \frac{k_{sl}}{k_{ss}} v_k v_s dV + \int_{(V)} \frac{k_{sk} k_{sl}}{k_{ss}^2} v_s v_s dV = \\
 &= m_{kl} - \frac{k_{sk}}{k_{ss}} m_{sl} - \frac{k_{sl}}{k_{ss}} m_{ks} + \frac{k_{sk} k_{sl}}{k_{ss}^2} m_{ss} .
 \end{aligned} \tag{8}$$

Now the modified mass matrix is:

$$\underline{M}_m = \underline{M} - \frac{1}{k_{ss}} \left(\underline{k}_s \underline{m}_s^* + \underline{m}_s \underline{k}_s^* \right) + \frac{m_{ss}}{k_{ss}^2} \underline{k}_s \underline{k}_s^* , \tag{9}$$

that is the modified mass matrix can be calculated from the rigid-joint

element mass matrix by means of dyads obtained from the vectors of rigidity and mass matrices.

Note that in dynamic studies, additional elements are added to the dynamic stiffness matrix due to consideration of the dynamic effects. E.g. if also the effect of rotational inertia is taken into consideration, the mass matrix shall be written in a form

$$\underline{\tilde{M}} = \underline{M} + \underline{M}\varphi, \quad (10)$$

where, e.g. for a bar, $\underline{M}\varphi$ can be obtained from relationship

$$\underline{M}\varphi = \mu i^2 \int_0^l \underline{N}^{*'} \underline{N}' dx \quad (11)$$

(μ being specific mass, i the radius of inertia of the cross section).

Here \underline{N}' is the matrix containing the derivatives of the displacement functions. It can be proved that derivation of the modified displacement functions in (8) results in a modified $\underline{M}\varphi$ matrix according to (9).

In calculations of bar structures, the static normal force Q can be taken into consideration by means of geometry stiffness matrix \underline{K}_G . In this case, the end-of-element forces are

$$\underline{K}_{\text{dyn}} = \underline{K} + \underline{K}_G - \omega^2 (\underline{M} + \underline{M}\varphi)$$

where

$$\underline{K}_G = Q \int_0^l \underline{N}^{*'} \underline{N}' dx.$$

The geometry stiffness matrix can be modified by analogy with the modification of matrix $\underline{M}\varphi$.

2. Structure calculations in case of infinitely rigid element

In case of a complex system, the rigidity of the different elements may differ considerably. E.g. in case of a machine base calculatable as a bar structure, certain points of the structure are interconnected by a machine frame that can be considered infinitely rigid. This means that displacements of the different nodes of the structure are not independent of

each other. In this case, numerical difficulties will arise in solution of the equation system or eigenvalue problem if the infinitely rigid element is treated in the same way as the other elements.

Theoretically, the problem becomes manageable by means of the process described in (1) where the rigidity matrix of the structure is produced by use of coupling matrices \underline{P} in the knowledge of the rigidity matrix of the set of elements. In the coupling matrix, the number of independent displacements will be less than the number of nodal displacement components. The displacements of some node j can be calculated partly or entirely (depending on the nature of connection) from the displacement of node i .

$$\underline{u}_j = \begin{bmatrix} \underline{R}_i & \underline{R}_j \end{bmatrix} \begin{bmatrix} \underline{u}_i \\ \underline{u}_j \end{bmatrix} \quad (12)$$

(matrix \underline{R}_j will be zero if every displacement component of j can be calculated from the displacements of node i).

In the course of investigation of the structure, it seems reasonable to keep the structure associated with the nodes so that certain columns of the coupling matrix will be zero columns. Block \underline{R}_i , \underline{R}_j will also appear in the coupling matrix in addition the unit matrices in such a way that in a row of blocks, matrices \underline{R}_j and \underline{R}_i replace the unit matrix in block columns j and i , respectively.

As has been mentioned, matrix \underline{P} shall not be produced in the course of practical calculations but, instead, selected blocks of the elementary stiffness matrices shall be collected in the different blocks of the rigidity matrix (selection being controlled by the necessity of multiplication by unit matrices). Forces resulting from displacements of given nodes at given ends of the element have thus been included in the blocks of the rigidity matrix.

In the present case, if block column j is produced, block \underline{K}_r of the rigidity matrices, associated with given block row r , shall be put partly or entirely into block column i . Forces at the end of given element, obtainable from the displacements of node j are

$$\underline{g}_r = \underline{K}_r \underline{u}_j = \underline{K}_r \begin{bmatrix} \underline{R}_i & \underline{R}_j \end{bmatrix} \begin{bmatrix} \underline{u}_i \\ \underline{\tilde{u}}_j \end{bmatrix} = \begin{bmatrix} \underline{K}_{ri} & \underline{K}_{rj} \end{bmatrix} \begin{bmatrix} \underline{u}_i \\ \underline{\tilde{u}}_j \end{bmatrix} \quad (13)$$

At the node interconnected with the rigid element, the end-of-element forces are not independent because also the rigid element shall be balanced.

Relationship between the forces acting upon both ends of the rigid element:

$$\begin{bmatrix} \underline{g}_i \\ \underline{g}_j \end{bmatrix} = \begin{bmatrix} \underline{R}_i^* \\ \underline{R}_j^* \end{bmatrix} \underline{\tilde{g}}_j. \quad (14)$$

Accordingly, block \underline{K}_r of the stiffness matrix, associated with given block column r , shall be put into block row i partly or entirely when block row j is set up.

$$\begin{bmatrix} \underline{g}_i \\ \underline{g}_j \end{bmatrix} = \begin{bmatrix} \underline{R}_i^* \\ \underline{R}_j^* \end{bmatrix} \underline{K}_r \underline{u}_r = \begin{bmatrix} \underline{K}_{ir} \\ \underline{K}_{jr} \end{bmatrix} \underline{u}_r \quad (15)$$

Of course, the appropriate rows and columns of the mass matrix and/or given elements of nocal loads shall be rearranged accordingly.

After rearrangement of the stiffness matrix, zero elements will get into the principal diagonal and therefore numbers other than zero shall be put into these places.

The vector elements of \underline{u}_j can be produced in the knowledge of \underline{u}_i and, in part, $\underline{\tilde{u}}_j$.

The process described above can be used also if the nodes are congruent but in this case, only the elements of a certain displacement agree (e.g. crossing bars interconnected by pin or slabs joining each other along the edge).

In this case, matrix \underline{R} has zero and unit elements only.

REFERENCES

1. Szabó, J. - Roller, B.: Anwendung der Matrizenrechnung auf Stabwerke. Akadémiai Kiadó, Budapest, 1978
2. Györgyi, J.: Process for calculation of oscillation of (bar) structures of a damping varying by elements of frequency dependent mass matrix. Doctor's thesis, Budapest, 1984

FAILURE TESTS WITH STEEL FRAMEWORKS

IVÁNYI, M.*

(Received: 5 January 1990)

According to practical needs, approximate models in stability analysis of steel structures are widely used as information given by bifurcation theory is limited. Thus the role of experimental research is of increasing importance.

Between 1974-1989, extended research was carried out in the Department of Steel Structures (TU Budapest) regarding the ultimate load of frames and buildings. The results of experimental and theoretical analysis are summarized in this work.

Experimental and theoretical investigations are shown, permitting the plastic deformation capacity of frames with due regard to interaction of strength and stability phenomena to be analyzed, including the effect of local buckling of plate elements of sections on the response of the whole structure.

1. Introduction

The structural response in the vicinity of peak load may be extremely complex. The early and very simple methods of plastic limit analysis (based on the concept of rigid-plastic materials which are in principle completely insensitive to any form of initial imperfections) are confined to a very limited class of structures, built of bulky elements. As soon as global and even more as local instability plays role in failure,

- the effect of initial geometric imperfections is enhanced,
- the residual stresses (remaining regularly latent at lower loads, interacting with growing active stresses) result in premature plastic zones, and (last but not least)

- the usual and widely accepted tools of analysis - as beam theory (based on Bernoulli-Navier hypothesis), small deflection theory of plates and so on - cannot describe exactly enough the structure's response to failure.

The simplified model is not elaborate enough to reflect real structural behaviour, so that a secondary, more detailed local model is introduced to depict the most critical part of the structures, by which more

*Iványi, Miklós, H-1111 Budapest, Kende u. 18, Hungary

realistic quality parameters can be deduced from the already known primary parameters.

Because of the interaction of local and global behaviour, this pattern cannot be followed in the case of hyperstatic structures, as the additional information gained by the secondary, local model is to be fed back to the calculation of primary parameters as well. For this purpose, if - as very often - the secondary model can be analysed by numerical methods or only experimentally, the results have either to be re-interpreted to obtain mathematically treatable, simple enough rules, or the secondary model has to be simplified to get well-usable results. In both cases the validity or accuracy has to be proved by (usually very expensive) failure tests on the whole structures.

To sum up, it seems that because of frequent uncertainties in predicting failure load, the double check of structures - at different load levels - not only reflects different aspects of structural behaviour, but contributes to a safer design procedure as well.

2. Test program

The experimental research project was carried out in the Laboratory of the Department of Steel Structures, Technical University, Budapest.


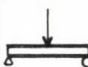

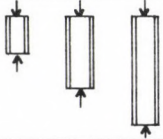
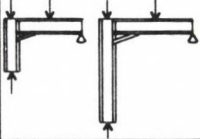



| | | | | |
|---|---|---|---|--|
|  |  |  |  |  |
| Tensile Specimens | Beam Specimens | | Axially Compressed Specimens | Subassemblages |
|  | |  | |  |
| Column Bases | | Frame Connections With Prestressed | | High-Strength Bolt's |

Fig. 1.

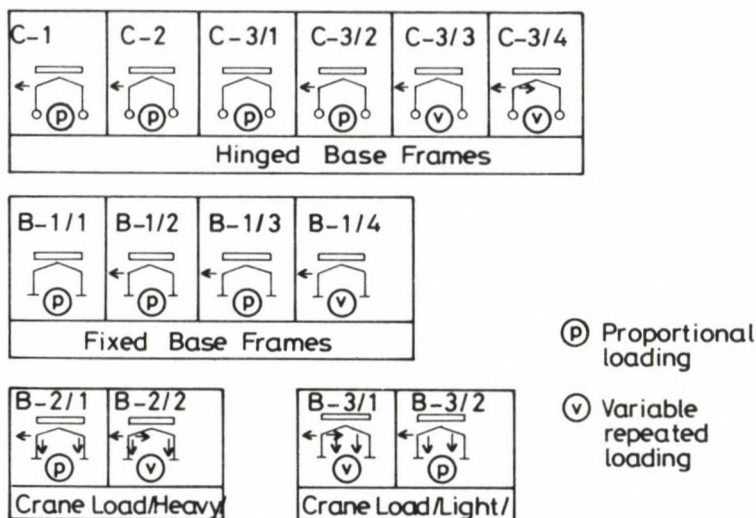


Fig. 2.

The first part of the program: Fig. 1 gives a brief summary of the additional tests on stub columns, frame corners, plates elements, simple beams (Halász, Iványi, 1979).

The second part of the program: Fig. 2 gives a brief summary of the full-scale tests and dimensions of the specimens, indicating the loads and the characteristics of the loading process.

Test frame C-3 had rafters with a slope of 30% (16.7°), welded column sections I 300-150-37 (Fig. 3.a).

Rafter-to-column and mid-span connections consisted of high-strength prestressed bolts (Fig. 3.b).

Different types of supports were applied (Fig. 4).

Vertical loads at the joining points of purlins were applied to the upper flange of rafter, so web and bottom flange were not restricted laterally. To make horizontal displacement (sidesway) unrestricted, jacks were fastened not directly to the floor-slab (Fig. 5.a), but through a so-called gravity load simulator (Fig. 5.b). This latter consisted of three elements: two bars, and a rigid triangle. The two bars had pin-joints at both ends, re-

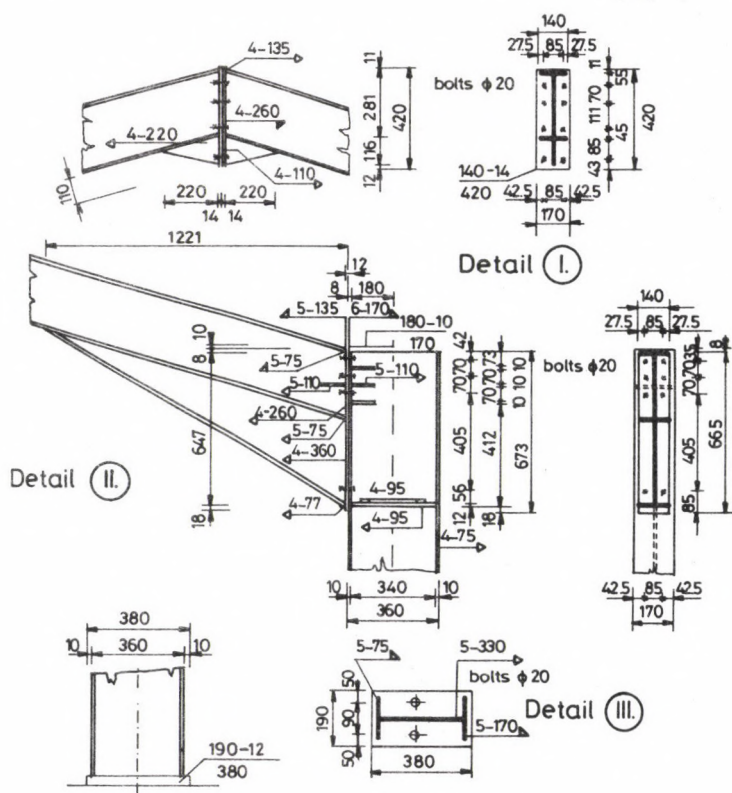
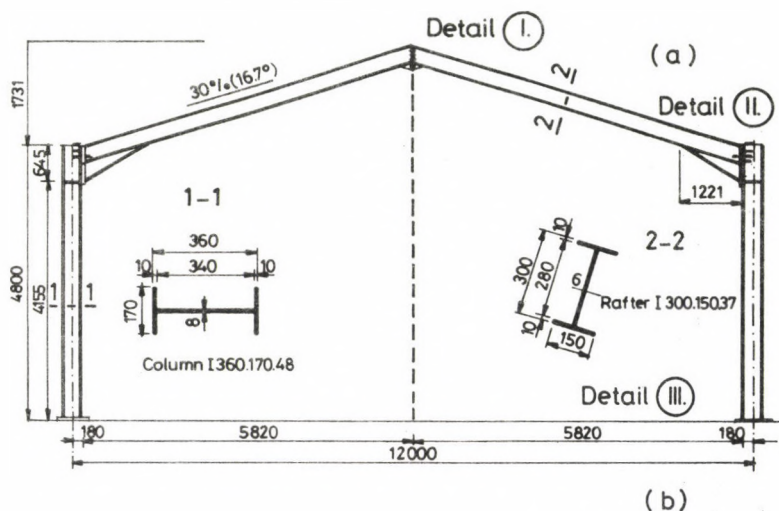


Fig. 3.

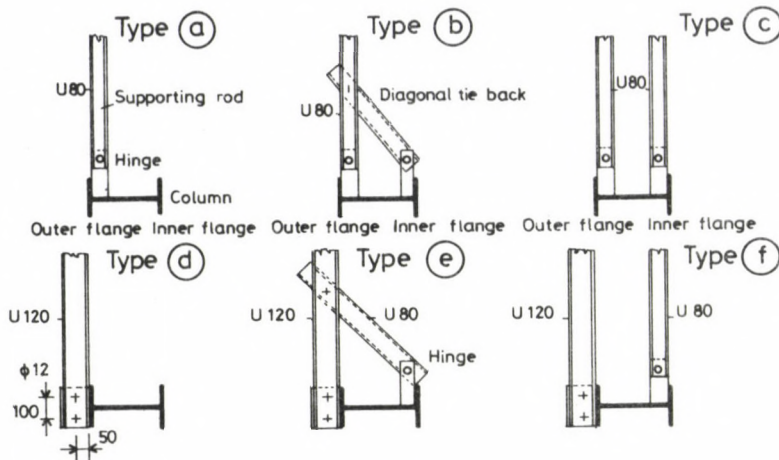


Fig. 4.

sulting in a one-degree-of-freedom mechanism. Hydraulic jacks joined the rigid triangle. This mechanism produced a vertical load acting upon the intersection of the two bar axes. Characteristics of the simulator are given in Fig. 5.c.

The third part of the program was a representative part of a multi-purpose, pinned, pitched roof industrial hall: a building section consisting of 3 frames, bracings with pinned elements, light gage purlins and wall beams with corrugated steel sheeting (Fig. 6) (Iványi, Kálló, Tomka, 1986).

Structural details of the building sections are shown on Fig. 7. The scope of investigations was threefold:

- the effect of restraint system on elastic behaviour,
- residual deformation and load bearing capacity due to cyclically repeated load,
- ultimate load of the frames.

Elastic tests were made at six different stages of erection (Fig. 6).

Non-elastic tests (cyclically repeated load, incremental collapse) were carried out on the building section corresponding to stage 6 using load combination composed from dead load and meteorological loads.

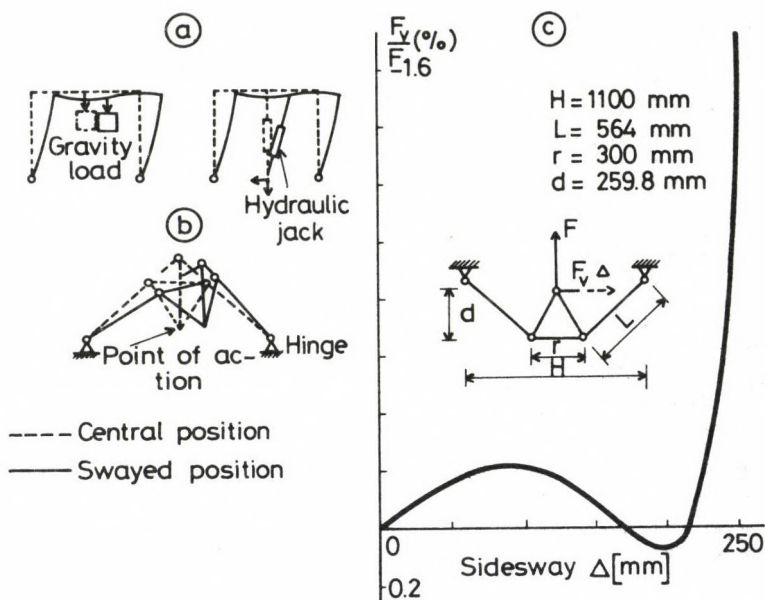


Fig. 5.

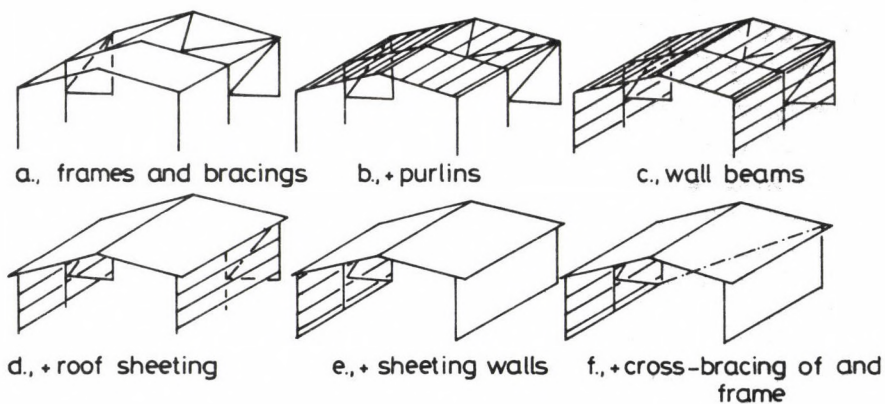


Fig. 6.

3. Computational model

The traditional concept of plastic design of steel structures is based on the assumption that, under gradually increasing static loads, plastic zones develop and grow in size and number, and eventually cause unrestricted, increasing deflections; thus loading until the onset of ultimate limit state of the structure. The concept was first introduced by Kazinczy (1914) by establishing the concept of the "plastic hinge". Some basic questions are still discussed. Among them are the effects of the difference between ideal-plastic constitutive law and actual behaviour of steel material and the consequence of local instability (plate buckling; lateral buckling). Joining in the international research in this field we tried to introduce the concept of "interactive plastic hinge", which can substitute the classic concept of plastic hinge in the traditional methods of limit design, but can reflect the effect of phenomena like strain-hardening, residual stresses, plate buckling and lateral buckling (Iványi, 1983).

The element of the bar is considered to be built up of plate elements (following the pattern of steel structures) instead of a compact section. Then the behaviour of the "plastic hinge" can be characterized by tests with simply supported beams. Based on these tests a yield-mechanism for the bar-element can be introduced (Fig. 8), giving foundations for a mechanism curve: defining thus the descending branch of the moment-rotation diagram (Fig. 9). Similar results can be obtained for the case of different loading conditions (Iványi, 1979/a, 1979/b).

This information can be used to extend the model of "equivalent cantilever" suggested by Horne (1960) including the effect of residual stresses and strain-hardening (Fig. 10), with the descending branch representing the effect of plate buckling, arriving thus to the concept of "interactive plastic hinge" (Iványi, 1983, 1985/a). In addition to the above model, a suitable yield mechanism was considered for cyclic bending, such as to correspond to the geometrical conditions and the assumed yield criterion (Fig. 11) (Gioncu, etc. 1989).

The cyclic load-deflection curve of S-3 beam is shown in Fig. 12. The interactive plastic hinge model is suitable for computer computations (Iványi, 1985/b; Baksai, etc., 1985).

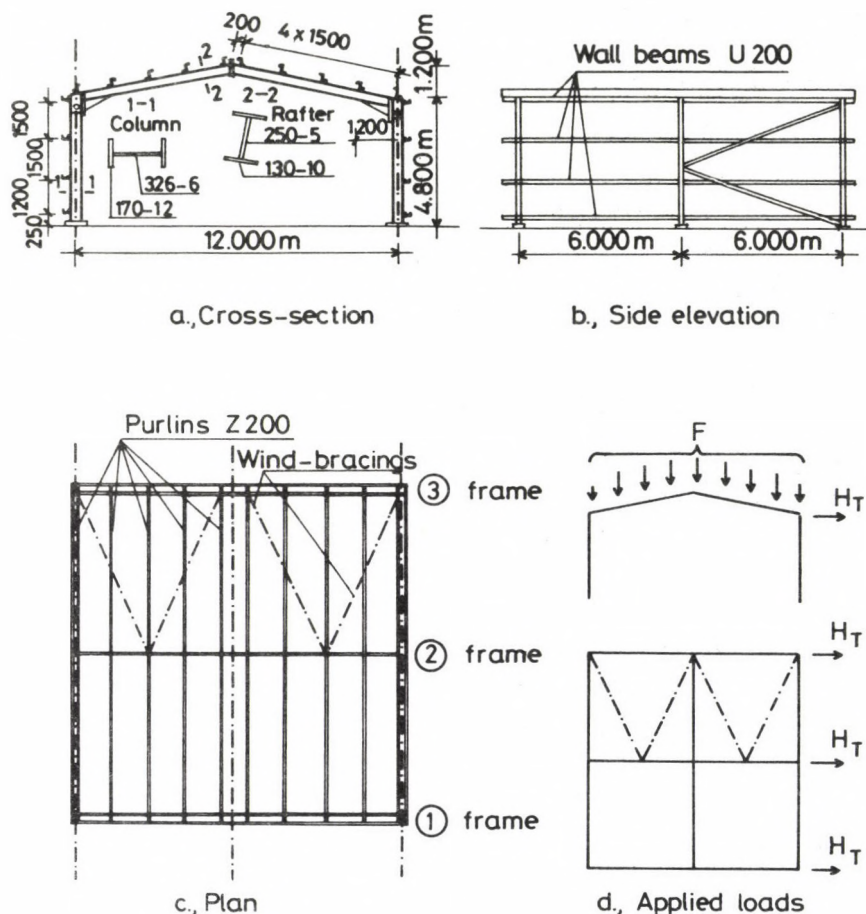


Fig. 7.

4. Results of theoretical and experimental investigations

4.1 Frame Structures under proportional loading

Concerning the experimental frame C-3/2, the relation of load-deflection curve develops according to Fig. 13. On the side of horizontal load, the first inelastic hinge develops due to the residual stresses and deformations in the cross section beneath the frame structure wedging up and this hinge develops at 52% of the maximal frame load. At 97% of the maximal load, zone L describing the effect of plate buckling develops also in this cross section, i.e. in the frame cross section an "unstable" state - a descending characteristic curve - develops.

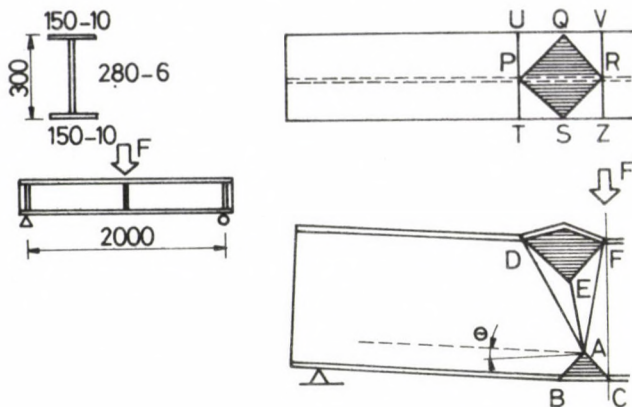


Fig. 8.

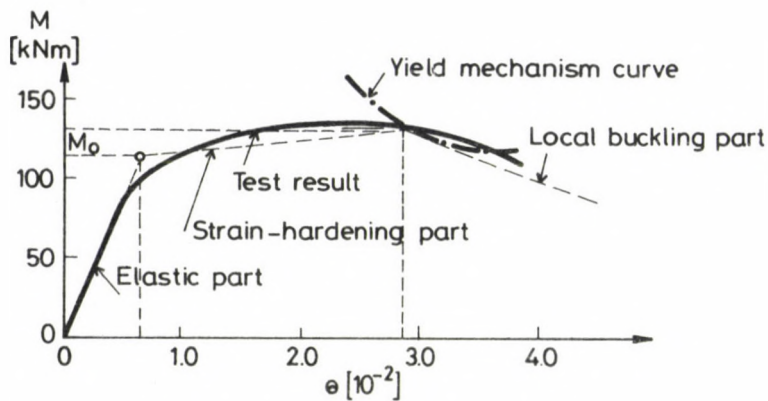


Fig. 9.

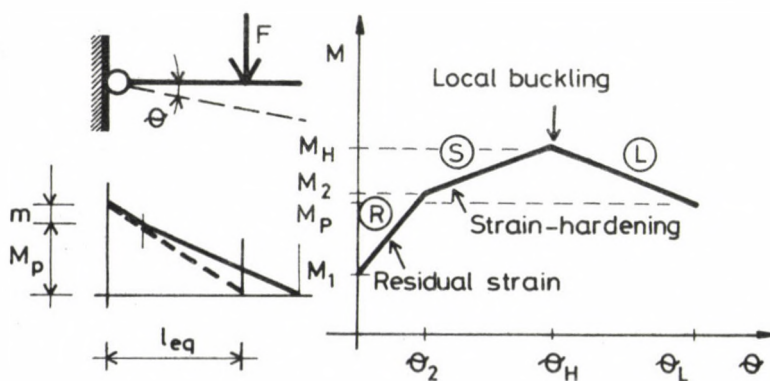


Fig. 10.

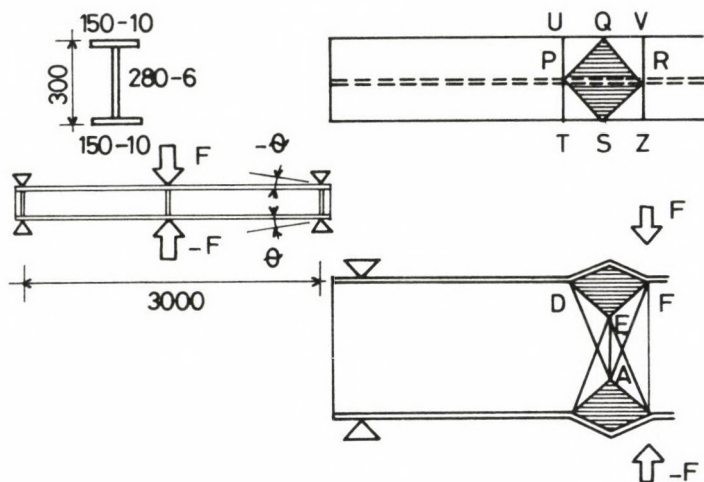


Fig. 11.

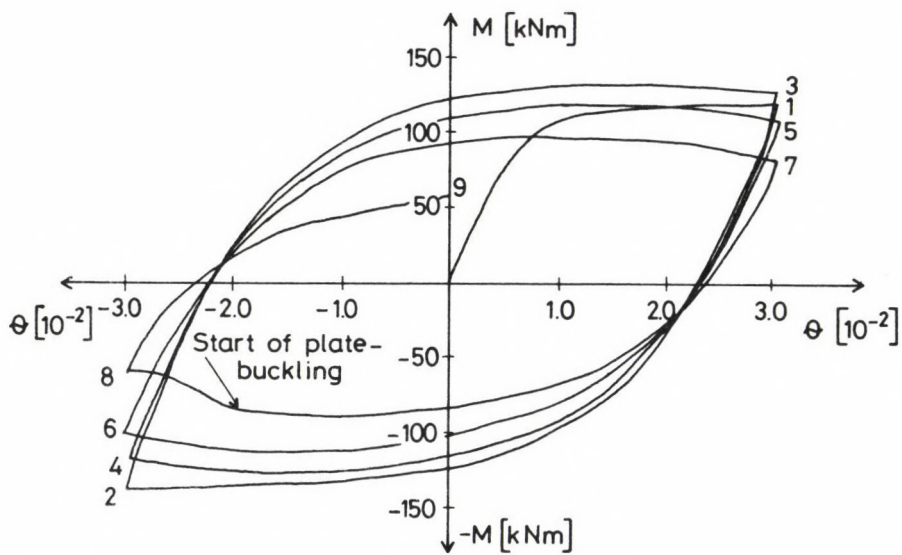


Fig. 12.

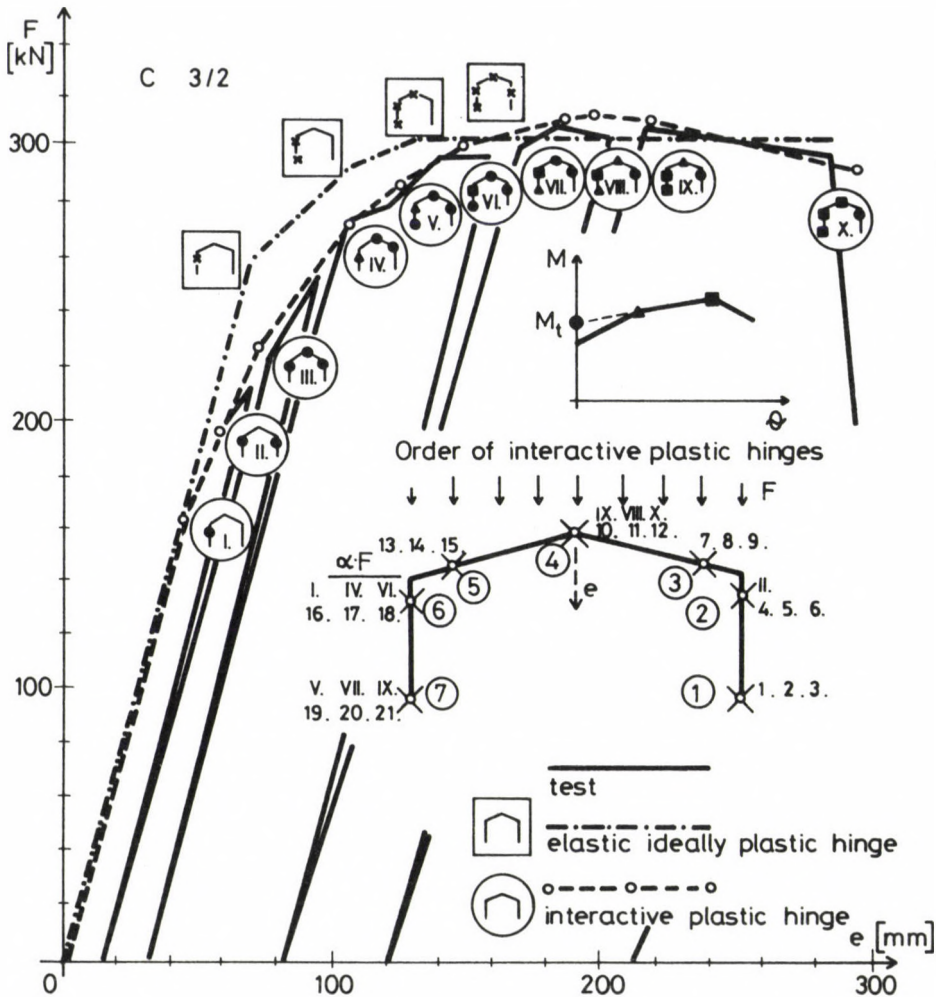


Fig. 13.

Figure 13. introduces the characteristic load-displacement curve of the frame structure in the case, too, when the basis of the computations is the traditional plastic hinge.

The results well show that the presence of residual stresses influence in a major way the range of limited plastic deformation, however, mainly because of the cross section geometry of experimental beam, the maximal load bearing values computed with the traditional (elastic-ideally plastic) hinge as well as those obtained by the interactive hinge coincide with the experimental results.

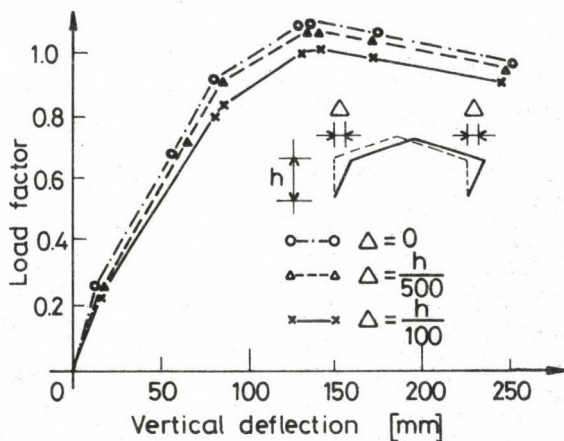


Fig. 14.

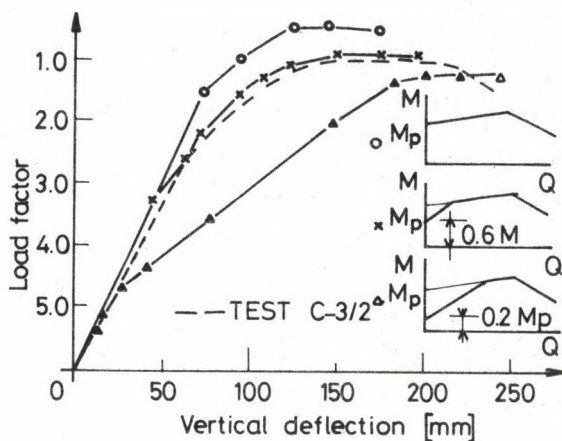


Fig. 15.

4.11 Effect of fabrication and erection

Effect of incorrect geometry was investigated by introducing different initial lateral displacements. The consequences are illustrated in Fig. 14.

The effect of the different values of residual stresses is shown in Fig. 15. The medium curve was in coincidence with test results.

The presented method for the complex analysis of frameworks takes several effects into consideration (Fig. 16).

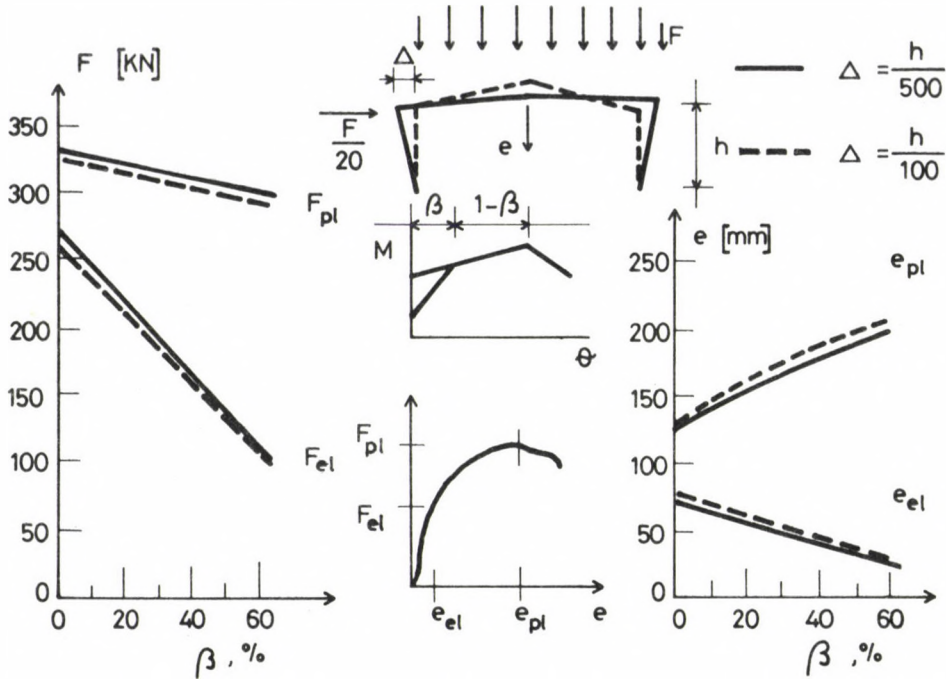
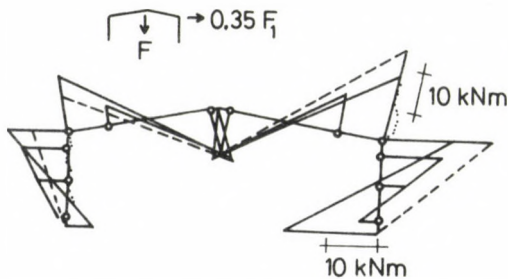


Fig. 16.



Measured and calculated bending moments

Fig. 17.

4.12 Effect of structural details

It seems worthwhile to draw attention to the occasional decisive effect of minor differences in structural details on failure as well. Some of the results are reproduced below.

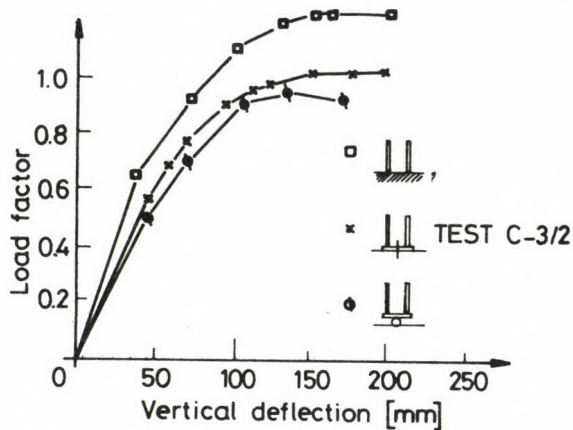


Fig. 18.

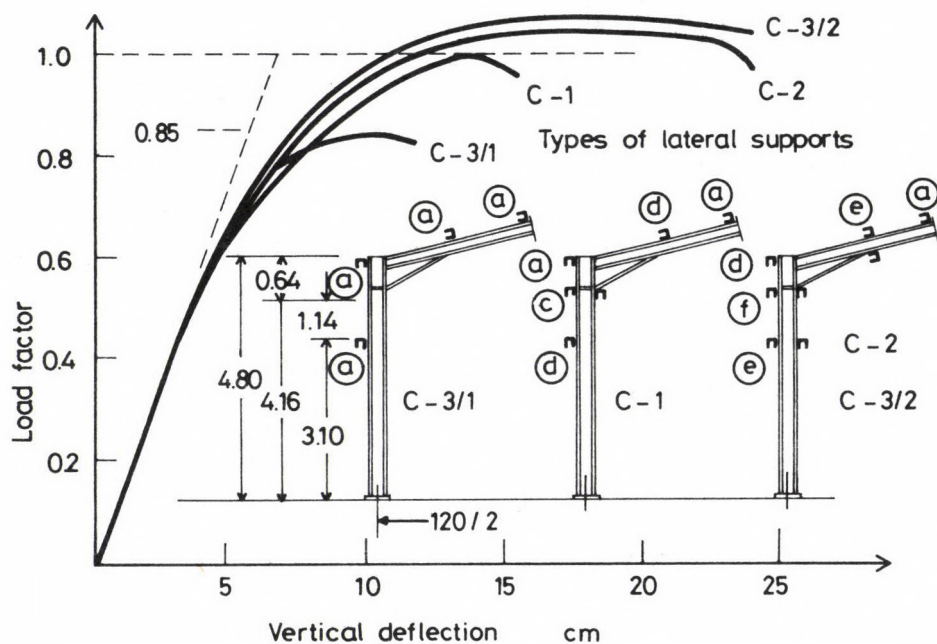


Fig. 19.

(i) Column bases

Column bases were fixed or hinged. The hinges were not ideal: columns could have been supported by larger base-plates. Figure 17 compares the measured bending moment due to vertical and horizontal load with the calculated ones assuming pinned (dashed line) and fixed (solid line) frame. The corresponding moment-rotation diagram of column base was checked experimentally, its adaption to an interactive plastic hinge indicating the load-deflection diagrams obtained by different end conditions (Fig. 18).

(ii) Lateral supports

Spacing and efficiency of lateral supports proved to be of basic importance. Their effect is illustrated in Fig. 19.

The importance of adequate spacing of lateral supports and their efficiency in preventing the rotation of cross-section around the bar-axis has to be emphasized as purlins and rails connected to tension flanges often cannot be regarded fully effective in case of thin webs. Not only the load carrying capacity can thus be substantially reduced (as by elastic lateral buckling in case of frame C-3/1 in Fig. 19), but the yield plateau in the load-deflection diagram can be too short (as in the case of frame C-1 in Fig. 19), rendering the structure sensitive against initial imperfections.

4.2 Frame Structure under variable repeated load

By repeated cycles of variable loads - for instance by those involving the subsequent application of a light crane-load D and uniformly distributed vertical load P_1 as indicated in Fig. 20, incremental collapse can be produced by a load-factor surpassing slightly the shake-down load predicted by a first-order ideally elastic-plastic analysis. The difference between test and analytical values was similar to that observed in proportional loading (due probably to strain hardening), so the gap between limit loads in proportional and cyclic loading (about 10% in the case indicated in Fig. 20) is the same in test and computation for both loading cases.

Surprising was the quick progression of residual deflections after just a few load cycles (see Fig. 20)

- to be attributed possibly to the effect of axial loads connected with remarkable changes in geometry;

- to gradual increase of imperfections (both lateral deflections of beams and curvature of plates); thus to work-softening effects overcoming the work-hardening ones.

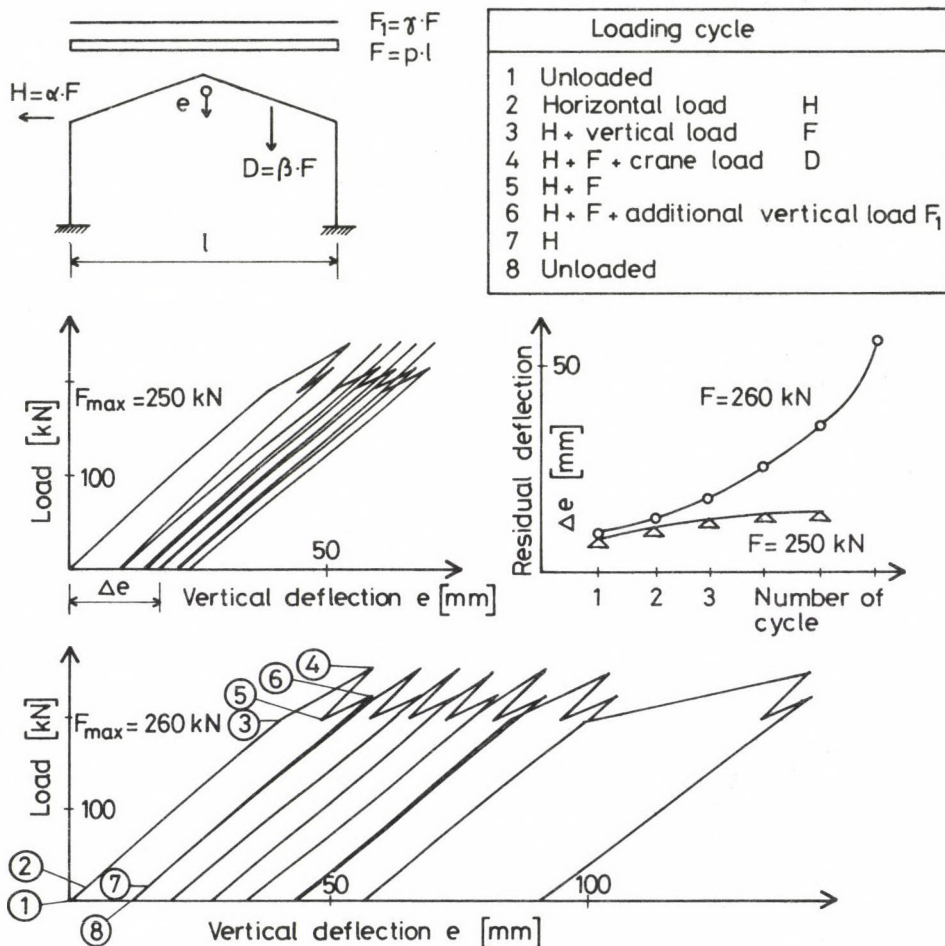


Fig. 20.

4.3 Building under proportional loading

4.31 Cross bracing of the end-frame

Measured deflections from uniform horizontal loads are shown in Fig. 21, representing the effect of both semi-rigid cross bracings of the end frame.

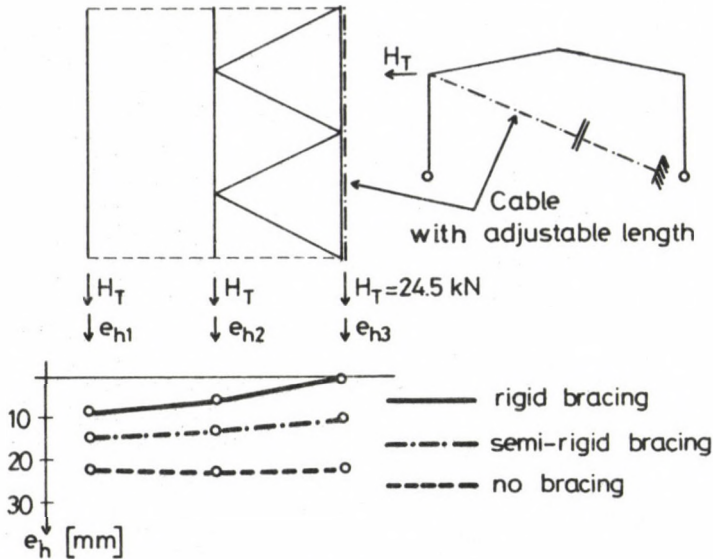


Fig. 21.

4.32 Horizontal and vertical bracing system

Load-displacement diagrams of incremental collapse tests are shown in Fig. 22. Ultimate loads are influenced by local loss of stability, previous loadings and the layout of frame-horizontal and vertical bracing connections.

4.4 Building under cyclically repeated meteorological loads

Schematic diagram of a cycle of repeated meteorological loads can be found on Fig. 23.

Analysing the results of the experiments in the different phases of construction and in the fully completed state, the following conclusions can be drawn:

The actual behaviour of hall structures is more favourable than that generally taken into consideration in design practice. In strength analysis, and in stability analysis in plane of the frame we generally neglect the effects of semi-rigid column bases, roofing sheeting, end walls.

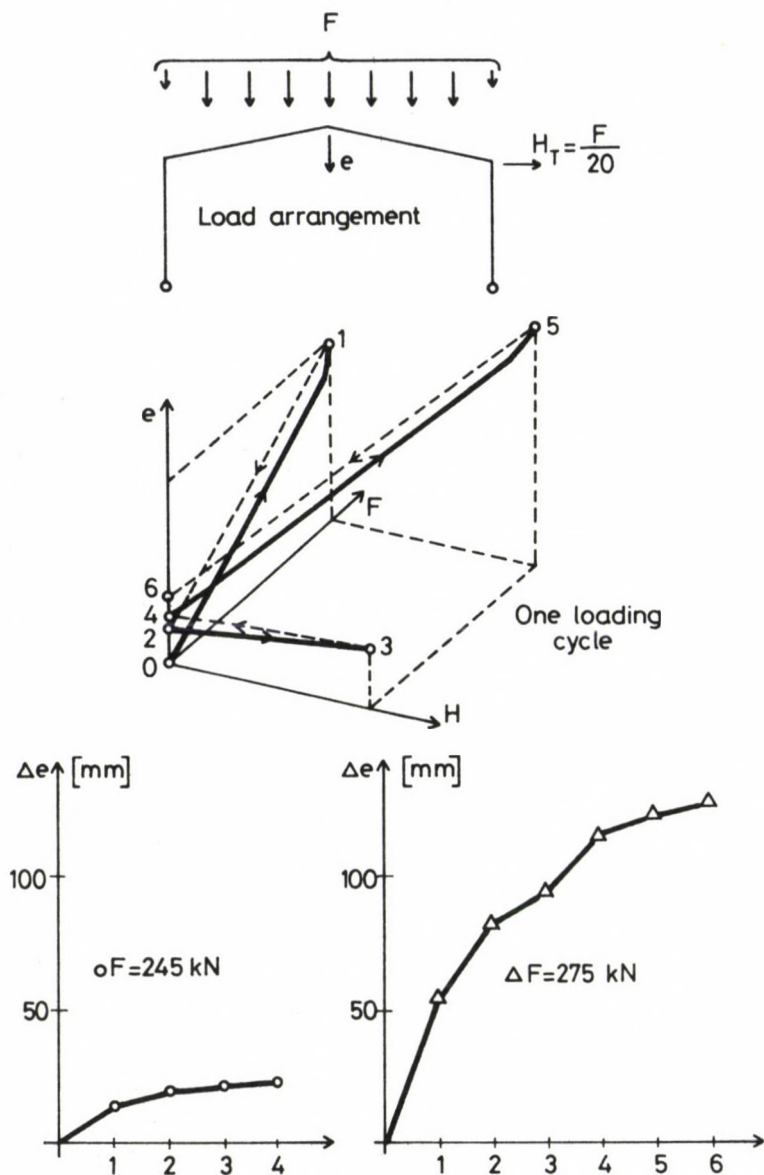


Fig. 23.

5. Conclusion

Experimental and theoretical investigations have been carried out in connection with the elastic and the plastic load-bearing study of frame and hall structures, with the steel material strain hardening, the residual stresses and plate buckling taken into account.

A method has been presented for the investigation of frame structures applying the steps of known, traditional methods so that the structure behaviour can be analyzed during the entire process of loading. Certain effects determining the structure behaviour (e.g. residual deformation, steel material strain hardening and plate buckling) have been taken into consideration with the aid of the interactive plastic hinges. The interactive hinge was incorporated into an investigation method operating with the structure matrix-calculation method. The results of the elaborated method has been compared with the experimental investigation of full-scale structures.

REFERENCES

1. Baksai, R. - Iványi, M. - Papp, F.: Computer Program for Steel Frames Taking Initial Imperfections and Local Buckling into Consideration, *Periodica Politechnica, Civil Eng.*, Vol. 29, Nos 3-4 (1985) 171-185
2. Gioncu, V. - Mateescu, G. - Drasteanu, S.: Theoretical and Experimental Research Regarding the Ductility of Welded I-sections Subjected to Bending, *Colloquium on Structural Stability*, Beijing Oct. 10-12, (1989) Proceedings, 289-298
3. Halász, O. - Iványi, M.: Tests with Simple Elastic - Plastic Frames, *Ibid*, Vol. 23, Nos 3-4 (1979) 151-182
4. Horne, M.R.: Instability and the plastic theory of structures. *Transactions of the EIC*, Vol. 4, No. 2 (1960), 31-43
5. Iványi, M.: Yield mechanism curves for local buckling of axially compressed members, *Periodica Politechnica, Civil Eng.*, Vol. 23, No. 3-4 (1979/a) 203-216
6. Iványi, M.: Moment-rotation characteristics of locally buckling beams, *Ibid*. (1979/b) 217-230
7. Iványi, M.: Interaction between strength and stability phenomena (in Hungarian), Thesis presented for the degree of Doctor of Sciences, Budapest 1983
8. Iványi, M.: A New Concept in Limit Design of Steel Structures, *Colloquium on "Stability of Metal Structures"*, Paris 16-17 nov., 1983, Final Report, 259-264
9. Iványi, M.: The Model of the "Interactive Plastic Hinge", *Periodica Politechnica, Civil Eng.*, Vol. 29, No. 3-4 (1985/a), 123-146
10. Iványi, M.: Load-Deformation Relationships for Simple Steel Frames with Unstable Elements. *Ibid*. (1985/b), 147-170
11. Iványi, M. - Kálló, M. - Tomka, P.: Experimental Investigation of Full-Scale Industrial Building Section, *Colloquium on "Stability of Steel Structures" Hungary 25-26 sept., 1986*, Final Report
12. Kazinczy, G.: Experiments with fixed-end beams (in Hungarian), *Betonszemle*, 2.68, 1914

OPTIMAL DESIGN OF DYNAMICALLY LOADED REINFORCED CONCRETE FRAMES UNDER SINGLE DISPLACEMENT CONSTRAINT

KALISZKY, S.* - LÓGÓ, J.**

(Received: 27 November 1989)

Paper deals with reinforced concrete beams and frames subjected to short-time high intensity dynamic pressure. The shape and geometry of the structure and the layout of the longitudinal reinforcement are given and the areas of reinforcement are design variables.

The determination of the plastic displacements caused by the pressure is based on the plastic hinge theory and on the assumption that during the dynamic response the structure undergoes stationary displacements. In the analysis several yield mechanisms can be taken into consideration. The problem is to minimize the total amount of reinforcement such that the plastic displacement at a given point of the structure does not exceed the allowable displacement.

The variational formulation of the problem is presented and the solution is based on the optimality criteria method which requires an iterative procedure.

1. Introduction

There are several engineering problems when in the design of a structure abnormal loading conditions as explosion, impact, earthquake etc. have to be taken into consideration. In these extreme cases the structure is usually allowed to undergo plastic deformations but must be strong enough to carry the load without excessive plastic deformations, local failure or collapse.

In the following reinforced concrete beams and frames subjected to short-time, high intensity dynamic pressure will be considered. The shape and geometry of the structure and the layout of the longitudinal reinforcements are given while the areas of the reinforcement are the design variables. The problem is to find the minimum of the total amount of longitudinal reinforcement subject to a displacement constraint determined by structural or technological consideration.

The plastic permanent displacements of the structure caused by the dynamic pressure can be determined by the use of the kinematical approxi-

*Kaliszky, Sándor, H-1089 Budapest, Delej u. 25, Hungary

**Lógó, János, H-1118 Budapest, Regös u. 7, Hungary

mation /5, 6/ based on the plastic hinge theory and on the assumption that during the dynamic response the structure undergoes only stationary displacements. This leads to closed form solution for the plastic displacements.

The relationship between the area of longitudinal reinforcements and the fully plastic moments of cross-sections will be approximated by a quadratic expression. This allows to take into consideration the minimum amount of reinforcement to be applied because of technological reasons. In the dynamic analysis, in addition to the mass of the concrete of the beam or frame, the masses attached to and moving with the structure will also be taken into account.

In the following the variational formulation of the problem will be presented and the solution is based on the optimality criteria method suggested by Berke and Khot /1, 2/. Except simple cases this requires the application of an iterative procedure well understood by structural engineers.

2. Assumptions and basic relationships

2.1. Geometry of the structure

In the following reinforced concrete beams and frames with given shape and geometry will be considered. We assume that the structure is composed of prismatic concrete members with given lengths d_s and cross-sectional dimensions b_s and h_s , as shown in Fig. 1/a. The layout of the longitudinal reinforcement is also assigned such that in given parts with fixed lengths l_i ; ($i = 1, 2, \dots, n$) the cross sectional areas A_i of the longitudinal reinforcement to be applied at the lower and/or upper surface of the cross-section are constant (Fig. 1/b). The areas A_i ; ($i = 1, 2, \dots, n$)

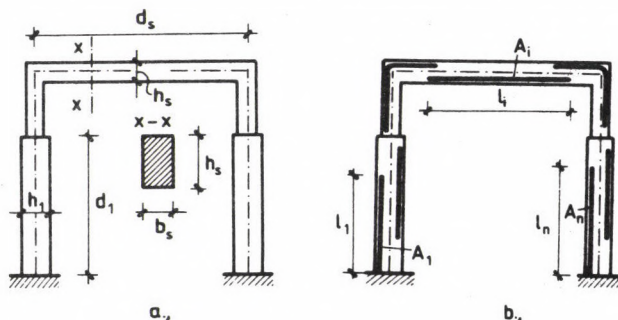


Fig. 1.

collected in the vector \underline{A} are the design variables and the volume of the total longitudinal reinforcement is expressed by the objective function

$$V = \underline{l}^T \underline{A} . \quad (1)$$

Here the vector \underline{l} collects the lengths l_1, l_2, \dots, l_n .

2.2. Loading and mass distribution

The structure is subjected to a high intensity short-time dynamic pressure $\underline{F}(x,t)$ defined in a separated variable form:

$$\underline{F}(x,t) = p(t) \underline{F}_0(x) . \quad (2)$$

Here x and t denote the coordinate measured along the axis of the structure and the time, respectively, $\underline{F}_0(x)$ defines the distribution of the dynamic pressure and $p(t)$ describes the time variation of the intensity of the pressure (Fig. 2/a-b).

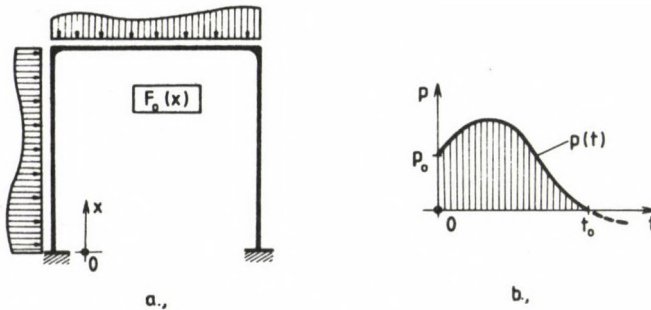


Fig. 2.

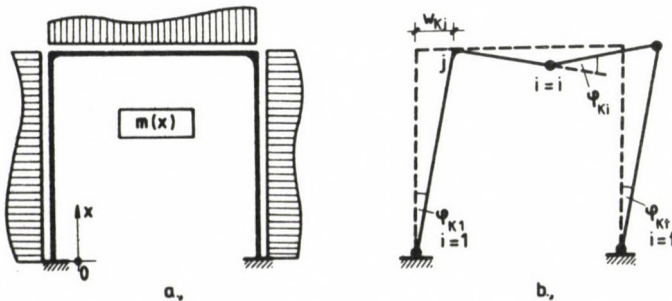


Fig. 3.

The scalar function $m(x)$ defines the mass distribution along the axis of the structure (Fig. 3/a). It contains the mass of the structure and also all the other masses (dead weights) which are attached to and move together with the structure during the dynamic response. The mass of reinforcement compared to other masses is very small therefore will be neglected in our further investigations.

2.3. Yield mechanisms and plastic moments

We assume, that the flexural behaviour of the reinforced cross-sections is rigid-plastic and apply the concept of plastic hinges. Considering the critical cross-sections where plastic hinges can develop, several yield mechanisms can be constructed at which the structure might collapse. The displacements of the "k"-th yield mechanism shown in Fig. 3/b are described by the function $w_k(x)$ while the relative rotations $\varphi_{k1}, \varphi_{k2}, \dots, \varphi_{kt}$ occurring in the plastic hinges are collected in the vektor ψ_k .

The fully plastic moments $M_1, M_2, \dots, M_i, \dots, M_n$ acting at the plastic hinges of the yield mechanisms can be expressed in terms of the areas A_i of the longitudinal reinforcement. This nonlinear relationship is usually approximated by a linear function (Fig. 4/a)

$$A_i = \alpha_i |M_i| \quad (3)$$

where the constant α_i can be assumed for $\frac{6}{5} \frac{1}{h_i \sigma_{sy}}$ where σ_{sy} is the yield stress of steel.

In practical design, however, a minimum amount of longitudinal reinforcement always has to be applied. This might be taken into account by using a quadratic function proposed in /8/ and shown in Fig. 4/b

$$A_i = A_{i0} + a_i M_i^2 \quad (4)$$

Here A_{i0} denotes the minimum amount of reinforcement to be applied and a_i is a certain constant given in /8/.

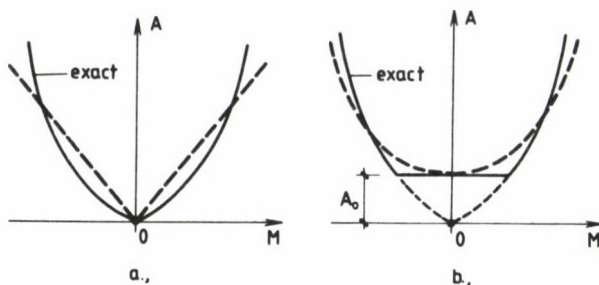


Fig. 4.

2.4. Plastic displacements

The displacements of an elasto-plastic structure subjected to dynamic pressure can be determined only by a time history analysis. To avoid the lengthy numerical calculations in the following we will apply the kinematical approximation described elsewhere /5, 6/. In this approach we assume that the structure undergoes stationary motion during the dynamic response and impose on the structure a kinematically admissible plastic displacement field expressed in a separated-variable form

$$\underline{w}_k(x, t) = w_{k0}(t) \underline{w}_k(x) . \quad (5)$$

Here $\underline{w}_k(x)$ denotes any postulated kinematically admissible plastic displacement field (yield mechanism) and $w_{k0}(t)$ is an unknown displacement parameter function. If the function $p(t)$ describing the time variation of the dynamic pressure in eq. (2) fulfils certain conditions to be given below, then $w_{k0}(t)$ is a monotonically increasing function and reaches its maximum value w_{k0}^{\max} when the structure comes to standstill. Omitting the details w_{k0}^{\max} can be expressed in the following form /6, 7/

$$w_{k0}^{\max} = K_k S_0 \left[\frac{p_e}{p_k} - 1 \right] . \quad (6)$$

Here

$$S_0 = \int_0^{t_0} t p(t) dt , \quad p_e = \frac{I_0^2}{2S_0} , \quad I_0 = \int_0^{t_0} p(t) dt \quad (7)$$

are defined by the function $p(t)$ (see Fig. 2/b) and p_k denotes the kinematically admissible load multiplier associated with the assumed displacement field $\underline{w}_k(x)$ and the quasi-static loading $F_0(x)$

$$p_k = \frac{\underline{M}^T \underline{\varphi}_k}{\int_L \underline{F}_0(x) \underline{w}_k(x) dx} \quad (8)$$

or introducing the notation

$$\underline{c}_k = \frac{\underline{\varphi}_k}{\int_L \underline{F}_0(x) \underline{w}_k(x) dx}, \quad (9)$$

$$p_k = \underline{M}^T \underline{c}_k. \quad (10)$$

Finally, K_k is a constant:

$$K_k = \frac{\int_L \underline{F}_0(x) \underline{w}_k(x) dx}{\int_L m(x) [\underline{w}_k(x)]^2 dx}. \quad (11)$$

It is to be noted that the validity of eq. (6) is restricted to the loading cases when the following conditions are fulfilled /7/:

$$\begin{aligned} p(0) &\geq p_k, & I_0 &\geq p_k t_0, \\ p(t) &= 0, & \text{if } t &> t_0. \end{aligned} \quad (12)$$

Substituting eq. (10) in eq. (6) and considering eq. (5) the plastic displacements caused by the dynamic pressure at the point j of the structure can be approximated by the expression:

$$\underline{w}_{kj}^p = \underline{w}_{kj}^{\max} \underline{w}_{kj} = \underline{w}_{kj} K_k S_0 \left[\frac{p_e}{\underline{M}^T \underline{c}_k} - 1 \right]. \quad (13)$$

Here \underline{w}_{kj} denotes the displacement at the point j of the k -th yield mechanism (see Fig. 3/b).

We note that in expression (13) S_0 and p_e depend only on the shape of function $p(t)$ and for a particular yield mechanism \underline{w}_{kj} , $\underline{\varphi}_{ki}$, K_k and \underline{c}_k are constants. Hence, in eqs (13) the plastic displacements are expressed in terms of the plastic moments \underline{M} .

Assuming several ($k = 1, 2, \dots, r$) yield mechanisms several approximate values can be obtained for the plastic displacements and then their maximum values are competent in the optimal design.

2.5. Constraints

A structure subjected to high intensity dynamic pressure must have sufficient strength and stiffness for carrying the load without excessive deformations, local failure or collapse. This design criterion can be formulated such, that at a given point j of the structure the plastic displacement should not exceed the limit (allowable) displacement, i.e.

$$\left| w_{kj}^p \right| \leq w_{j0}; \quad (k = 1, 2, \dots, r) \quad (14)$$

Here w_{kj}^p is defined by eq. (13) and the limit (allowable) displacement w_{j0} can be assigned by appropriate considerations upon the limited ductility behaviour of the reinforced concrete structure. In a particular problem w_{kj}^p and also w_{kj} in eq. (13) denote either vertical or horizontal displacements at the point j therefore in the following they will be considered as scalars.

Using the design criteria described above, next we will derive the basic relationships of the optimal design problem. For convenience, instead of the areas A_i we will introduce the plastic moments M_i ; ($i = 1, 2, \dots, n$) as new design variables. Then, using the relationship (4) the total volume of the longitudinal reinforcement is expressed in the form

$$V = \underline{\ell}^T \underline{A} = \sum_{i=1}^n \ell_i (A_{i0} + a_i M_i^2) \quad (15)$$

3. Formulation of optimal design

3.1. Solution based on a single yield mechanism

First, we will consider the simplest case when a displacement constraint is prescribed at a single point j of the structure and for the calculation of the plastic displacements only one yield mechanism is taken into consideration. Then the subscript k can be omitted in the above equations and using eqs (13), (14) and (15) the optimal design problem can be formulated as follows:

minimize

$$V = \sum_{i=1}^n \ell_i (A_{i0} + a_i M_i^2) \quad (16)$$

subject to

$$|w_j^D| = |w_j| \cdot K S_0 \left[\frac{p_e}{\underline{M}^T \underline{c}} - 1 \right] \leq w_{j0}$$

or

$$\frac{p_e}{\underline{M}^T \underline{c}} - \left[1 + \frac{w_{j0}}{K S_0 |w_j|} \right] \leq 0 \quad (17)$$

To derive the optimality criteria equations we form the Lagrangian

$$L(M_i, \lambda) = \sum_{i=1}^n \ell_i (A_{i0} + a_i M_i^2) + \lambda \left[\frac{p_e}{\underline{M}^T \underline{c}} - \left[1 + \frac{w_{j0}}{K S_0 |w_j|} \right] \right] \quad (18)$$

and require the derivatives relative to M_i vanish

$$\frac{\partial L}{\partial M_i} = 2 \ell_i a_i M_i - \lambda p_e \frac{c_i}{(\underline{M}^T \underline{c})^2} = 0 \quad ; (i = 1, 2, \dots, n) \quad (19)$$

Here λ denotes a Lagrangian multiplier.

To obtain a closed form solution we express from this equation

$$M_i = \lambda \frac{p_e}{2 \ell_i a_i} \frac{c_i}{(\underline{M}^T \underline{c})^2} \quad (20)$$

and substitute in eq. (17). Then we get

$$\lambda = \frac{2 (\underline{M}^T \underline{c})^2}{\left[1 + \frac{w_{j0}}{K S_0 |w_j|} \right] \sum_{i=1}^n \frac{c_i^2}{\ell_i a_i}} \quad (21)$$

which together with eq. (20) yields to the following result

$$M_i = \frac{p_e}{\left[1 + \frac{w_{j0}}{K S_0 |w_j|} \right]} \frac{\frac{c_i}{\ell_i a_i}}{\sum_{i=1}^n \frac{c_i^2}{\ell_i a_i}} \quad (22)$$

or

$$M_i c_i = \frac{p_e}{C_{j0}} \frac{\frac{c_i^2}{\ell_i a_i}}{\sum_{i=1}^n \frac{c_i^2}{\ell_i a_i}} \quad (23)$$

Here

$$C_{j0} = 1 + \frac{w_{j0}}{K S_0 |w_j|} \quad (24)$$

denotes a constant and the ratio $\frac{c_i^2}{\ell_i a_i}$ can be considered as the "relative efficiency" of the i -th plastic hinge.

According to eq. (9) this is proportional to the square of the relative rotation φ_i at the plastic hinge i and is in inverse ratio with the length ℓ_i and the specific cost a_i of the corresponding longitudinal reinforcement. Hence, the plastic moments which fulfil both the displacement constraint (17) and the optimality criterion (19) are determined as follows:

$$M_i c_i = \frac{p_e}{C_{j0}} \times \frac{\text{relative efficiency of the } i\text{-th plastic hinge}}{\text{sum of relative efficiencies of plastic hinges}}$$

Here the summation is extended to the plastic hinges of the assumed yield mechanism. The carrying capacity $p = \underline{M}^T \underline{c} = \sum_{i=1}^n M_i c_i$ of the structure necessary to fulfil the displacement constraint can be calculated from eq. (17). Considering the above statement to obtain the optimal solution this capacity has to be distributed in the proportion of the relative efficiencies among the plastic hinges.

3.2. Solution based on several yield mechanisms

Next, we will consider the case when in order to obtain a more accurate solution $k = 1, 2, \dots, r$ yield mechanisms are taken into consideration for the determination of the plastic displacements. Then, the displacement constraint at the point j of the structure can be written in the form:

$$\frac{p_e}{\underline{M}^T \underline{c}_k} - \left[1 + \frac{w_{j0}}{K_k S_0 |w_{kj}|} \right] \leq 0 ; \quad (k = 1, 2, \dots, r) \quad (25)$$

or

$$G_{kj} = C_k - C_{kj0} \leq 0 ; \quad (k = 1, 2, \dots, r) , \quad (26)$$

where

$$C_k = \frac{p_e}{\underline{M}^T \underline{c}_k}$$

and

$$C_{kj0} = 1 + \frac{w_{j0}}{K_k S_0 |w_{kj}|} \quad (28)$$

is the "target value" of C_k .

To derive the optimality criteria equations we form the Lagrangian:

$$L(M_i, \lambda_k) = \sum_{i=1}^n \ell_i (A_{i0} + a_i M_i^2) + \sum_{k=1}^r \lambda_k \left[\frac{p_e}{\underline{M}^T \underline{c}_k} - \left[1 + \frac{w_{j0}}{K_k S_0 |w_{kj}|} \right] \right] \quad (29)$$

and require the derivatives with respect to M_i to vanish:

$$\frac{\partial L}{\partial M_i} = 2 \ell_i a_i M_i - \sum_{k=1}^r \lambda_k p_e \frac{c_{ki}}{(\underline{M}^T \underline{c}_k)^2} = 0 ; \quad (i = 1, 2, \dots, n). \quad (30)$$

In addition, the Lagrangian multipliers λ_k have to satisfy the equations:

$$\lambda_k G_{kj} = 0 ; \quad \lambda_k \geq 0 ; \quad (k = 1, 2, \dots, r) . \quad (31)$$

From eq. (30) we can express M_i in terms of the Lagrangian multipliers λ_k :

$$M_i = \frac{p_e}{2 \ell_i a_i} \sum_{k=1}^r \lambda_k \frac{c_{ki}}{(\underline{M}^T \underline{c}_k)^2} ; \quad (i = 1, 2, \dots, n) \quad (32)$$

These equations express the optimality criterion. Substituting this expression into eqs (25) now we can not obtain a closed form solution for λ_k

therefore we follow the optimality criteria method proposed by Berke and Khot /1-4/. First, we multiply by M_i both sides of eqs (30)

$$p_e \frac{M_i c_{1i}}{(\underline{M}^T \underline{c}_1)^2} \lambda_1 + \dots + p_e \frac{M_i c_{ki}}{(\underline{M}^T \underline{c}_k)^2} \lambda_k + \dots + p_e \frac{M_i c_{ri}}{(\underline{M}^T \underline{c}_r)^2} \lambda_r = 2 \ell_i a_i M_i^2 ;$$

$$(i = 1, 2, \dots, n)$$

and accomplish the sum of these equations

$$\frac{p_e}{\underline{M}^T \underline{c}_1} \lambda_1 + \dots + \frac{p_e}{\underline{M}^T \underline{c}_k} \lambda_k + \dots + \frac{p_e}{\underline{M}^T \underline{c}_r} \lambda_r = 2 \sum_{i=1}^n \ell_i a_i M_i^2 . \quad (33)$$

Substituting eq. (27) we get

$$c_1 \lambda_1 + \dots + c_k \lambda_k + \dots + c_r \lambda_r = 2 \sum_{i=1}^n \ell_i a_i M_i^2 . \quad (34)$$

The right hand side of this equation (disregarding the constant term due to the minimum reinforcement) stands for the total volume of the reinforcement while the terms in the left hand side express the contributions of the λ_k multipliers to the volume.

In the proposed iterative solution eqs (32) are used to fulfil the optimality criterion while the constraints (26) can be satisfied by the successive change of λ_k . To obtain the most efficient way of this procedure we have to consider eq. (34).

If we find during the iteration that the k-th constraint is over-satisfied i.e. C_k is less than the target value C_{kj0} then we can decrease the participation of the k-th term in eq. (34) as the most effective component to decrease the total volume of reinforcement. This can be achieved by decreasing λ_k which at the same time, improves constraint satisfaction. On the other hand, if the k-th constraint is not satisfied i.e. C_k is greater than the target value C_{kj0} one has to increase the participation of the k-th term. This can be achieved by increasing λ_k which, at the same time, also improves constraint satisfaction.

For the appropriate updating of the Lagrangian multipliers Berke and Khot suggested several techniques /1-4/. For example the following formula can be used:

$$(\lambda_k)^{\text{new}} = \left[\lambda_k \left[\frac{C_k}{C_{kj0}} \right]^q \right]^{\text{old}} \quad (35)$$

where q is a parameter to control convergence and possibly to change as $G_{kj} \rightarrow 0$.

Deriving the above results the iterative procedure which leads to the satisfaction of the displacement constraint has the following steps:

a) select the yield mechanisms $k = (1, 2, \dots, r)$ and calculate C_{kj0} from eq. (28);

b) assume initial values for M_i and λ_k (e.g. $M_i = \text{const}$ and $\lambda_k = \text{const}$);

c) calculate C_k and $(\lambda_k)^{\text{new}}$ from eqs (27) and (35);

d) using the new values of λ_k and the old (initial) values of M_i determine the new values of M_i from eq. (32);

e) repeat steps c) and d) until the differences between C_k and C_{kj0} are sufficiently small.

4. Conclusion

The optimal design procedure described above can be extended to problems where multiple displacement constraints or at the plastic hinges plastic deformation constraints are taken into consideration. The description of these solutions and the numerical applications will be published elsewhere.

REFERENCES

1. Khot, N.S. - Berke, L. - Venkayya, V.B.: Comparison of optimality criteria algorithms for minimum weight design of structures. AIAA Journ. Vol. 17 No. 2. (1979), 182-190
2. Berke, L. - Khot, N.S.: Structural optimization using optimality criteria. In: "Computer Aided Optimal Design of Structural and Mechanical Systems" (ed. C.A. Mota Soares) Springer, Berlin 1987, 271-311
3. Rozvany, G.I.N.: Structural Design via Optimality Criteria. (The Prager approach to structural optimization.) Kluwer Academic Publishers. Dordrecht 1989
4. Rozvany, G.I.N. - Zhou, M. - Rotthaus, M. - Gollub, W. - Spengemann, F.: Continuum type optimality criteria methods for large finite systems with a displacement constraint. Structural Optimization I, 1989, 47-72.

5. Kaliszky, S.: Approximate solutions for impulsively loaded inelastic structures and continua. Int. J. Non-linear Mech. 5. (1970), 143-158
6. Kaliszky, S.: Dynamic Plastic response of structures. In: "Plasticity Today". Symposium. Udine (Ed. A. Sawczuk - G. Bianchi) Elsevier, London 1985. 787-820
7. Krajcinovic, D.: On approximate solutions for rigid-plastic structures subjected to dynamic loading. Int. J. Non-Linear Mech. 7. 1972. 571-575
8. Kaliszky, S.: Economic design by the ultimate-load method. Concrete and Constructional Engineering 1965. 365-372, 424-433, 461-467

SPACE STRUCTURES: STATIC RELATIONSHIPS, STRUCTURAL FORMS

KOLLÁR, L.*

(Received: 1 November 1989)

Space structures are mostly formed according to curved surfaces. Their overall static behaviour can be described by adequate continua, which also show the relationships between seemingly entirely different structures.

In this paper first these relationships will be presented. Second, some remarks will be made on structural forms, i.e. on shapes according to which space structures with incomplete rigidities can be built.

1. Introduction

Space structures, formed according to curved surfaces, constitute, at first sight, a great variety of different structures which have very little in common. In fact, shells, space frames, lattice shells, cable and membrane structures, folded plates are different not only with respect to their building materials and forms, but necessitate independent static theories as well.

However, if we have a closer look at their static behaviour, we can discover some basic relationships between these structures. In this paper we first try to describe these relationships.

Second, after defining structures with incomplete rigidities, we will make some remarks on structural forms, i.e. on shapes according to which these structures can be built.

2. Static relationships

When trying to establish the relationships between the various kinds of space structures, we have to start from the notion of overall static behaviour, which means the behaviour of the structure as a whole, as contrasted to local behaviour, as e.g. buckling of individual bars of space frames.

*Kollár, Lajos, H-1122 Budapest, Ráth György u. 64-66, Hungary

The overall behaviour of space structures can be adequately described by appropriate continua, on the basis of which we can establish the static relationships sought for between the various structures. To this purpose it seems appropriate to choose shell structures as a starting point.

Shell structures are, strictly speaking, continua themselves, and can be classified into two groups: bent shells and membrane shells.

Membrane shells have only "in-plane" rigidities, i.e. rigidities against tension and shear in the tangential plane of the shell surface, while bent shells have, in addition, bending and torsional rigidities, and also transverse shear stiffnesses.

There are several kinds of space structures which are related to bent shells.

Let us begin with space frames, which can be single- or double-layer. As it has been established in /Kollár and Hegedűs, 1985/, the equivalent continua of single-layer space frames with rigid joints, and of double-layer ones either with hinged or with rigid joints are bent shells. Figure 1 shows a single-layer space frame with rigid joints, and Fig. 2 a double-layer space frame (which, for simplicity, is formed according to a plane surface).

Lattice shells (Fig. 3) can be considered a special kind of single-layer space frames, in which the lattices, running in two directions, are continuous.

Let us first suppose that the lattices are connected to each other by loose bolts, i.e. these connections form hinges in the tangential plane of the surface. Comparing this lattice shell with the single-layer space frame with rigid joints (Fig. 1) we find that, on the one hand, the third row of

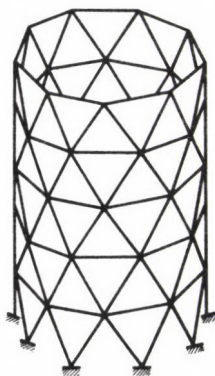
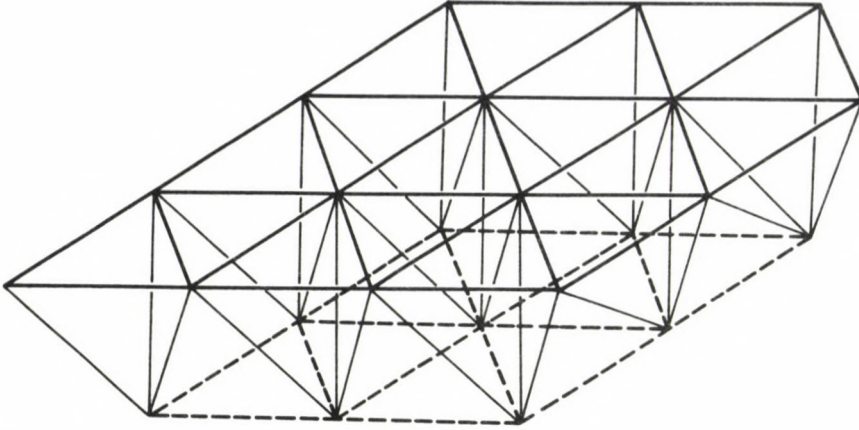
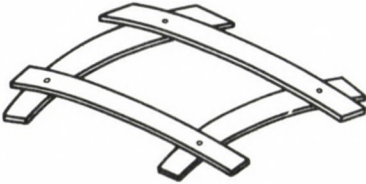


Fig. 1.

Fig. 2.Fig. 3.

bars is missing, so that the lattice shell has no shear rigidity in its tangential plane. However, on the other hand, the lattices can take bending moments in the tangential plane, thus providing an additional stiffness to the structure.

The static behaviour of the lattice shell can also be described by a continuous bent shell, but this has to be a generalized (micro-polar) one: a Cosserat-surface /Füzy, 1986/, /Füzy and Hegedűs, 1989/.

If, on the other hand, the lattices are rigidly connected to each other, then the lattice shell has an in-plane shear rigidity, but, due to the aforementioned bending moments arising in the tangential plane, the equivalent continuum has still to be a Cosserat-type surface.

Investigating the static behaviour of folded plates, we can state the following.

We can distinguish two basic types of folded plates: those with long elements (Fig. 4), and those with short elements (Fig. 5). The first type is characterized by the fact that the individual plate elements are long enough to assume a linear stress distribution in their cross sections. Con-

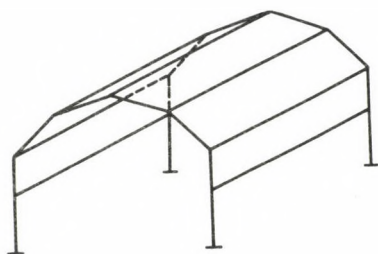


Fig. 4.

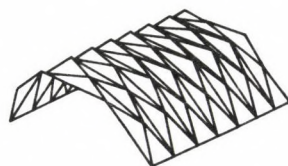
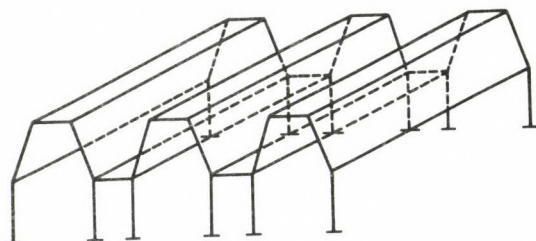


Fig. 5.

sequently, we have to set up the so-called three edge force equations in order to assure equal strains in the neighbouring plates along their common edges. In the following we will not deal with this kind of structure.

The plate elements of the second type are so short that a force acting along one edge does not cause any appreciable strain on the opposite edge. Hence there are no three edge force equations necessary. The individual (mostly triangular) plate elements transmit the loads onto their corner points, and the structure as a whole acts like a space frame, the "bars" of which are formed by the edges of the folded plate. Since these structures are mostly made of reinforced concrete, the connections of their "bars" can be considered rigid. Thus, folded plates with short elements are

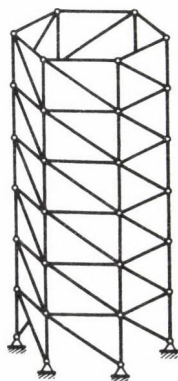


Fig. 6.

closely related to single-layer space frames with rigid joints and through them to bent shells.

We can find another group of structures, the members of which are related to membrane shells. Such is the single-layer space grid with hinged joints (Fig. 6), whose static behaviour essentially corresponds to that of membrane shells, with some differences, explained in /Kollár and Hegedűs, 1985/.

Membrane structures, made of coated fabric consisting of threads running in two perpendicular directions, also belong to this type, whether pneumatic or stressed (Figs 7 and 8). They deviate only in one respect from membrane shells: their shear rigidity is very low as compared with their tensile stiffness. Consequently, they exhibit a much larger shear deformation than ordinary membrane shells, which causes that, if the loads would give rise to high shearing stresses, these cannot develop, viz. the membrane deforms by shear to such an extent that it is no longer permissible to determine the internal forces on the basis of its original (undeformed) shape. The membrane thus behaves like the next structure: the cable net, which we intend now to investigate.

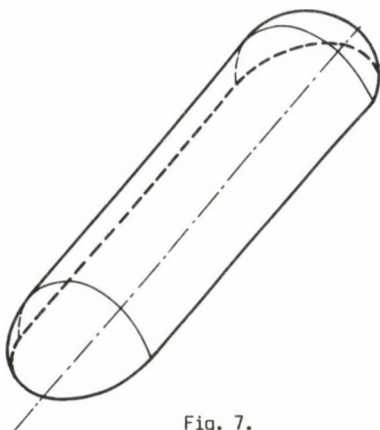


Fig. 7.

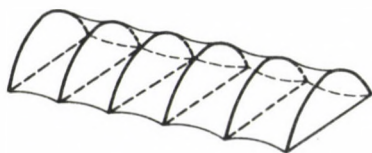


Fig. 8.

Cable nets differ from membrane shells in that respect that they have no in-plane shear rigidity at all. (Strictly speaking, we can give them a small but finite transverse rigidity by prestressing /Kollár, 1989/, but, in order to ensure a clearer treatment, we shall neglect this in the following.)

Consequently, in their original shape they cannot equilibrate loads which would cause shearing forces in them. The cable net must thus deform as long as it takes a new shape in which it can equilibrate the load without shearing forces. This new shape is called the funicular surface of the load. It also follows from this phenomenon that the cable net has to be analyzed by the large-deflection theory.

In Fig. 9 we sketched the relationships found so far between the various space structures.

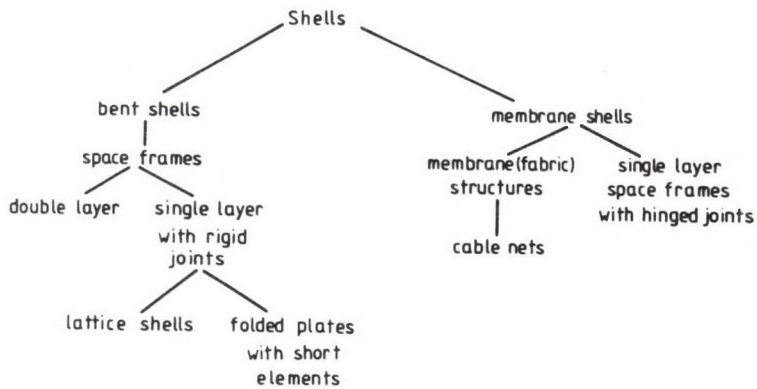


Fig. 9.

3. Structures with incomplete rigidity systems

Before we treat the problems of structural form, we have to investigate the consequences of missing rigidities.

Since space structures dealt with in this paper are formed according to a curved surface, it is possible to define on them tensile, bending, etc. rigidities referred to a cross section of unit width. We call the rigidity system of a space structure complete if it contains three membrane and three bending rigidities: tensile stiffnesses in both directions and shear stiffness; bending rigidities in both directions and torsional rigidity, and in addition, transverse shear rigidities in two directions. In

other words, all the elements in the main diagonal of the stiffness matrix have to be different from zero. (In order to be precise we also have to stipulate that the stiffness matrix be regular.)

The rigidity system of a bent shell is complete. On the other hand, the rigidity system of a membrane shell is incomplete because the three bending rigidities are missing.

The consequence of missing rigidities is that the structure needs special support arrangement to be kinematically determinate (stable). Hence membrane shells cannot be supported in an arbitrary way if we require that they remain kinematically determinate, i.e. that they should be able to carry any load by membrane forces. Necessary conditions for the fulfilment of this requirement have been given by Tarnai /1980-83/.

This problem does not arise with bent shells: they can be supported in an arbitrary way, provided equilibrium is ensured, they always remain kinematically determinate.

Single-layer space grids with hinged joints need support conditions similar to those of membrane shells.

There are structures which have not even all three membrane rigidities. Such are cable nets which have no in-plane shear rigidity. Moreover, the cables cannot take compression, so that they must be prestressed. From the latter fact it follows that cable nets can be built only according to surfaces with a negative Gaussian curvature, and even among them only those surfaces are suitable which correspond at every point to the equilibrium condition of the prestressed membrane (cable net).

The number of suitable surfaces is thus rather limited /Szabó and Kollár, 1984/.

The absence of shear rigidity causes that - even if the supports correspond to the static requirements of the prestressed form - the structure will not be kinematically determinate, but "movable"; it changes its form under various loads.

Membrane (fabric) structures show a similar behaviour, with the only difference that their material does have a shear rigidity, however small. Their behaviour thus represents a transition between those of membrane shells and cable nets. An interesting feature of fabric structures is that they can also be prestressed by air pressure, which adds a group of surfaces with zero or positive Gaussian curvature, suitable for building them, to those of negative Gaussian curvature of the cable nets.

4. Some remarks on structural forms

The basic meaning of structural form is "a form which is advantageous for a certain type of structure". This also means a certain degree of economy.

Such is, e.g. the form of the mushroom construction, as contrasted to flat slabs (without mushroom heads). However, related to structures with incomplete rigidities, structural form has a more restrictive sense: "a form which is necessary to build a certain type of structure".

In the case of membrane shells (and of single-layer space frames with hinged joints) the restriction extends only to the supports, but otherwise we are quite free to choose the form of the shell, provided the general rules of constructing membrane shells are observed (there should be no plane points or inflexions in the surface, no infinitely large forces arise in the shell, etc.).

We can formulate this restriction concerning the supports also the other way round: if the support conditions are given, the shape of the shell has to comply with the aforementioned static requirements in order to obtain a shell capable of carrying any load by membrane forces. As an example let us consider the temple shown in Fig. 10 /Kawaguchi, 1988/. Its side walls consist of cylindrical surfaces, which are supported along the bottom straight edge and along the two curved edges, but along the top straight edge it is acted upon by the load of the roof and is only supported in the horizontal plane. However, according to Tarnai's findings /Tarnai, 1980-83/, in order to obtain a shell capable of carrying any load by membrane forces alone, we would need a support in the tangential plane of the shell along the top edge. Consequently, this is not a structural form of the cylindrical membrane shells, thus for carrying the loads they have to develop bending moments. It was, in fact, necessary to provide beams with a considerable bending rigidity along their lines of fall. It follows from the foregoing that if we deviate from the structural forms of membrane shells, bending (and/or twisting) moments will develop, which has to be taken by appropriate structural elements.

With cable nets there are even more severe restrictions concerning the shape according to which such nets can be built.

Let us consider Fig. 11, which shows the Volley-ball Gymnasium in Beijing /Shen et al., 1989/.



Fig. 10.

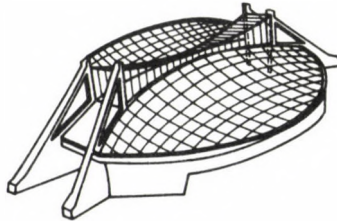


Fig. 11.

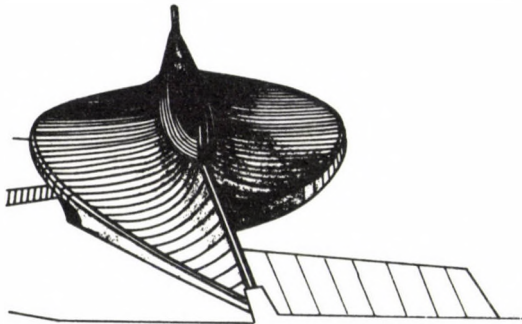


Fig. 12.

The shape of the two halves of the roof is the cable nets' structural form, so that this roof can be built as a cable net.

On the other hand, the Tokyo Olympic Swimming Hall (Fig. 12) considerably deviates from the structural form of cable nets /Tsuboi and Kawaguchi, 1966/. Consequently, this roof could be built only by using girders in one direction which can take bending.

Finally, fabric structures can be built only according to structural forms, because it is practically impossible to stiffen the fabric even in one direction against bending.

REFERENCES

1. Füzy, J.: Simulation of timber lattice shell without "in-plane" shear capacity by double-layer Cosserat surface. *Acta Techn. Acad. Sci. Hung.* 99 (1986), 287-296
2. Füzy, J. - Hegedűs, I.: Continuum analysis of doubly curved two-way trusses. *Proc. IASS Congress: 10 Years of Progress in Shell and Spatial Structures, 30 Anniversary of IASS. Madrid, 1989. Vol. 4.* (Laboratorio Central de Estructuras y Materiales; Ed.: del Pozo, F. and de las Casas, A.)
3. Kawaguchi, M.: A review of recent development of steel space structures in Japan. *Bulletin of the IASS, Vol. 29-1. (No. 96).* April 1988, 43-62
4. Kollár, L. - Hegedűs, I.: Analysis and design of space frames by the continuum method. *Akadémiai Kiadó, Budapest - Elsevier Science Publ., Amsterdam, 1985*
5. Kollár, L.: Stiffness problems of cable structures. *Proc. IASS Congress: 10 Years of Progress in Shell and Spatial Structures, 30 Anniversary of IASS. Madrid, 1989. Vol. 3. Membranes*
6. Shen, S.-Zh., Chen, X. - Zhao, Ch.: Design of two space structures for gymnasiums for Beijing 1990 Asian Games. *Proc. IASS Congress: 10 Years of Progress in Shell and Spatial Structures, 30 Anniversary of IASS. Madrid, 1989. Vol. 4.* (Laboratorio Central de Estructuras y Materiales; Ed.: del Pozo, F. and de las Casas, A.)
7. Szabó, J. - Kollár, L.: Structural design of cable-suspended roofs. *Akadémiai Kiadó, Budapest - Ellis Horwood, Chichester, 1984*
8. Tarnai, T.: The existence and uniqueness criteria of the membrane state of shells. *Acta Techn. Acad. Sci. Hung. T. Hyperbolic Shells: 91, 81-110; II. Parabolic Shells; 92, 67-88; III. Elliptic Shells. 96. 59-85. (1980-83)*
9. Tsuboi, Y. - Kawaguchi, M.: Probleme beim Entwurf einer Hängedachkonstruktion anhand des Beispiels der Schwimmhalle für die olympischen Spiele 1964 in Tokio. *Der Stahlbau* 35 (1966), 65-85

STABILITY OF SIMPLE STRUCTURES WITH NON-SMOOTH ENERGY FUNCTIONALS IN THE ONE-DIMENSIONAL CASE

KURUTZ, M.*

(Received: 27 December 1989)

This paper introduces the stability analysis of problems whose strain energy functional is not everywhere differentiable due to material irregularities or structural imperfections. Using the term of subdifferential and the convex analysis, the wide range of the stability problems of non-smooth functionals can be described mathematically in a perfect manner. All the problems having a so-called polygonal material law, like the plastic or locking behaviour, have a potential energy functional of not everywhere differentiable type. Since these phenomena can happen often in the practice, causing a considerably dangerous stability situation, or since this polygonal character can also be used for modelling some problems, it is necessary to clear them mathematically in a correct way.

In this paper the stability analysis of elastic-plastic, perfectly rigid-plastic, bi-, tri- or multilinearly elastic structures with lockings and imperfections will be presented by a very simple example. The general theory will be published elsewhere.

1. Introduction

In the general theory of the elastic stability it is well known that a stationary value of the total potential energy with respect to the generalized coordinates (the displacement parameters) is the necessary and sufficient condition for the equilibrium of the system. Furthermore, a complete relative minimum of the total potential energy with respect to the generalized coordinates is necessary and sufficient for the stability of an equilibrium state of the system /1/.

From the first condition we obtain one or more relations between the load and the displacement parameters. The diagrams of these functions are the equilibrium paths, and the intersections of them are the points of bifurcation separating the fundamental and the post-buckling or several further post-buckling equilibrium paths.

From the second condition we obtain the stability coefficients which are the elements of the Hessian matrix of the potential at the points of

*Kurutz, Márta, H-1118 Budapest, Serleg u. 8, Hungary

stationary. The stability coefficients help us to qualify not only the stability of the equilibrium states but also the stability of the equilibrium paths. Since the stability coefficients depend both on the load and the displacement parameters, they vary continuously along the equilibrium paths. Thus, the function of the stability coefficients in term of the displacement parameters as the function of the Hessian matrix can be spoken of.

All the basic axioms and terms mentioned above are related to the stability of elastic systems, on the basis of the general phenomenological law of the hyperelastic materials:

$$\sigma(\epsilon) = \frac{\partial W(\epsilon)}{\partial \epsilon} \quad \text{or} \quad \epsilon(\sigma) = \frac{\partial W^C(\sigma)}{\partial \sigma} . \quad (a)$$

Here $\sigma = \{\sigma_{ij}\}$ is the stress tensor and $\epsilon = \{\epsilon_{ij}\}$ is the strain tensor. Functionals $W(\epsilon)$ and $W^C(\sigma)$ are the strain and complementary strain energy densities, respectively, satisfying the variational inequalities

$$W(\epsilon_1) - W(\epsilon) \geq \sigma(\epsilon_1 - \epsilon)$$

and

$$W^C(\sigma_1) - W^C(\sigma) \geq \epsilon(\sigma_1 - \sigma)$$

as the conditions of the convexity of the functionals or, equivalently, the Drucker-stable character of the material.

If the functionals $W(\epsilon)$ or $W^C(\sigma)$ are continuously differentiable, the relations (a) correspond to a linear or non-linear hyperelastic material. If the material behaviour contains a polygonal-jump character in its stress-strain diagram (which can naturally be generalized to the non-uniaxial cases as well) then the relating energy density functionals, the so-called superpotentials, are non-smooth functions being not everywhere differentiable. Applying the term of subdifferential and the extremum terminology of the convex analysis, the classical derivation of the hyperelastic materials (a) can be extended to the non-elastic but stable (rigid, plastic, locking and their combinations type) materials in the form detailed in /3/ and /4/:

$$\sigma(\epsilon) \in \partial W(\epsilon) \quad \text{or} \quad \epsilon(\sigma) \in \partial W^C(\sigma) . \quad (b)$$

Here $\partial W(\epsilon)$ and $\partial W^C(\sigma)$ are the subdifferentials (the sets of the sub-

gradients) of the superpotentials $W(\varepsilon)$ and $W^C(\sigma)$ at the points ε and σ , respectively. So the actual $\sigma(\varepsilon)$ and $\varepsilon(\sigma)$ is among the elements of the set of subgradients. In this way, the non-elastic but stable materials can be handled in a quasi-hyperelastic manner, consequently, the stability problems of structures having materials like this can be analysed in a quasi-classical way.

In this paper the effect of several structural and material imperfections or irregularities leading to polygonal stress-strain diagrams and relating non-smooth energy functionals will be analysed. The analysis concerning all the mentioned cases will be introduced through the same one-dimensional example of the well-known hinged cantilever.

2. Stability of a rigid-plastic perfect structure

Figure 1.a shows a rigid cantilever with a support modelling the perfectly rigid-plastic behaviour of the structure by a friction like connection as the usual mechanical model of the rigid-plastic behaviour. (Note that the analysis relates to plastic and not to frictional problems.) Both the strain energy function and the relating constitutive law in Fig. 1.b and c are non-smooth functions being non-differentiable at its jump or break points. The plastic behaviour is characterized by the plastic moment limits M_{p1} and M_{p2} .

The total potential energy consists of the external and internal parts:

$$\pi(u, \vartheta) = \pi_{\text{ex}}(u) + \pi_{\text{in}}(\vartheta) . \quad (1)$$

Expressing the potential energy, kinematically admissible strain-displacement fields are needed. Using the correct displacement function

$$u = \ell(1 - \cos \vartheta) \quad (2)$$

as compatibility condition, the total potential energy of the perfect system, relating to the load increasing period of the loading process can be written as a non-smooth function, namely a superpotential /3/:

$$\pi(\vartheta) = -F\ell(1 - \cos \vartheta) + \begin{cases} M_{p1}\vartheta & \text{if } \vartheta \geq 0 \\ M_{p2}\vartheta & \text{if } \vartheta \leq 0 \end{cases} \quad (3)$$

where the first term is the potential of the external load and the second one is the internal energy of the plastic strains.

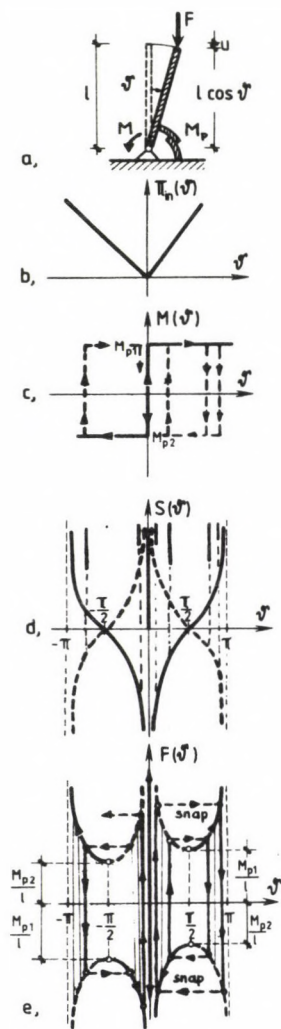


Fig. 1.

The condition of the equilibrium of the system relates to the first subdifferential of the total potential energy (3):

$$\partial\pi(\psi) = -F\ell \sin\psi + \begin{cases} M_{p1} & \text{if } \psi > 0 \\ [M_{p1}, M_{p2}] & \text{if } \psi = 0 \\ M_{p2} & \text{if } \psi < 0 \end{cases} \quad (4)$$

where the subdifferential at the point $\vartheta = 0$ consists of an interval $[M_{p1}, M_{p2}]$ as a set of subgradients. Furthermore, the stability of the equilibrium depends on the second subdifferential of the potential energy (3):

$$\partial^2 \pi(\vartheta) = -F\ell \cos \vartheta + \begin{cases} 0 & \text{if } \vartheta \neq 0 \\ +\infty & \text{if } \vartheta = 0 \end{cases} \quad (5)$$

In the case of non-smooth functions the condition of the equilibrium reads

$$0 \in \partial \pi(\vartheta) \quad , \quad (6a)$$

and the condition of the existence of critical forces is

$$0 \in \partial^2 \pi(\vartheta) \quad , \quad (6b)$$

namely, the zero has to be among the elements of the set of the first and the second subgradients. From the condition (6a) the functions of the equilibrium paths relating to the loading period can be obtained which also take the form of sets and intervals as elements

$$F(\vartheta) = \begin{cases} \frac{M_{p1}}{\ell \sin \vartheta} & \text{if } \vartheta > 0 \\ (+\infty, -\infty) & \text{if } \vartheta = 0 \\ \frac{M_{p2}}{\ell \sin \vartheta} & \text{if } \vartheta < 0 \end{cases} \quad (7)$$

From the condition (6b) the critical forces can be obtained:

$$F_{cr} = \begin{cases} \frac{M_{p1}}{\ell} & \text{if } \vartheta = \frac{\pi}{2} \\ +\infty & \text{if } \vartheta = 0 \\ -\frac{M_{p2}}{\ell} & \text{if } \vartheta = -\frac{\pi}{2} \end{cases} \quad (8)$$

The stability of the equilibrium paths can be qualified by the stability coefficients $S(\vartheta)$ obtained by substituting (7) for the second subdifferential (5)

$$S(\vartheta) = \begin{cases} -\frac{M_{p1}}{\operatorname{tg} \vartheta} & \text{if } \vartheta > 0 \\ [0, +\infty) & \text{if } \vartheta = 0 \\ -\frac{M_{p2}}{\operatorname{tg} \vartheta} & \text{if } \vartheta < 0 \end{cases} \quad (9)$$

signed in Fig. 1.d by full lines. This function contains the Hessian matrix relating to each of the stationary points of the loading phase. In this one-dimensional case, the Hessian matrix has only a single element for each value of ϑ . This element for regular points is a function value but for singular points it is an interval, like at $\vartheta = 0$. Thus, in this one-dimensional case, the analysis of the definiteness of the Hessian matrix is simplified to a sign control only. Consequently, the sign of the several parts of the function of the stability coefficients $S(\vartheta)$ in Fig. 1.d indicate directly* the stable, unstable or critical character of the several parts of the equilibrium paths in Fig. 1.e. The full lines indicate the stable and the broken lines show the unstable parts of the equilibrium paths. Thus, in the loading period, the equilibrium state is unstable if $-\frac{\pi}{2} < \vartheta < \frac{\pi}{2}$, while having $|\vartheta| > |\frac{\pi}{2}|$, the equilibrium state is stable, since the load $F > 0$ causes tension in the rod. Consequently, by any small disturbance, reaching the unstable equilibrium state at $-\frac{\pi}{2} < \vartheta < 0$ or at $0 < \vartheta < \frac{\pi}{2}$, the structure will snap dynamically as it can be seen in Fig. 1.e. Reaching the stable equilibrium state, the load can be increased again, or an unloading can be executed.

Till now the unloading of the structure has not been mentioned. This case is indicated in Fig. 1.c in the material behaviour in both directions, with the dissipated energy bounded by the loops. In Fig. 1.e also the equilibrium paths of some possible unloadings are illustrated.

Relating to an unloading period, starting the load decreasing at the value of plastic strain ϑ_p , the total potential energy has the form

$$\pi(\vartheta) = F\ell (1 - \cos \vartheta) + \begin{cases} M_{p1} \vartheta_p + M_{p2} (\vartheta_p - \vartheta) & \text{if } \vartheta_p \geq 0 \\ M_{p2} \vartheta_p + M_{p1} (\vartheta_p - \vartheta) & \text{if } \vartheta_p \leq 0 \end{cases} \quad (3a)$$

From the equilibrium condition

$$0 \in \partial \pi(\vartheta) = F\ell \sin \vartheta + \begin{cases} -M_{p2} & \text{if } \vartheta_p > 0 \\ [-M_{p1}, -M_{p2}] & \text{if } \vartheta_p = \vartheta \\ -M_{p1} & \text{if } \vartheta_p < 0 \end{cases} \quad (4a)$$

the equilibrium paths of the unloading process can be obtained

$$F(\vartheta) = \begin{cases} \frac{M_{p2}}{l \sin \vartheta} & \text{if } \vartheta_p > 0 \\ \left[\frac{M_{p2}}{l \sin \vartheta}, \frac{M_{p1}}{l \sin \vartheta} \right] & \text{if } \vartheta_p = \vartheta \\ \frac{M_{p1}}{l \sin \vartheta} & \text{if } \vartheta_p < 0 \end{cases} \quad (7a)$$

the second subdifferential of (3a)

$$\partial^2 \pi(\vartheta) = F l \cos \vartheta + \begin{cases} 0 & \text{if } \vartheta \neq \vartheta_p \\ +\infty & \text{if } \vartheta = \vartheta_p \end{cases} \quad (5a)$$

leads to the stability coefficients of the unloading phase

$$S(\vartheta) = \begin{cases} -\frac{M_{p2}}{\operatorname{tg} \vartheta} & \text{if } \vartheta_p > 0 \\ \left[+\infty - \frac{M_{p2}}{\operatorname{tg} \vartheta_p}, +\infty - \frac{M_{p1}}{\operatorname{tg} \vartheta_p} \right] & \text{if } \vartheta_p = \vartheta \\ -\frac{M_{p1}}{\operatorname{tg} \vartheta} & \text{if } \vartheta_p < 0 \end{cases} \quad (9a)$$

signed by broken lines in Fig. 1.d. In this way, the vertical equilibrium paths of unloading in Fig. 1.e are always stable, consequently, all the bifurcation points which are intersections of a vertical unloading path and an unstable path (the starting points of the snaps) are critical points. Then the possible critical forces can be given in the form of a function

$$F_{cr}(\vartheta) = \begin{cases} \frac{M_{p1}}{l \sin \vartheta} & \text{if } 0 < \vartheta \leq \frac{\pi}{2} \text{ and } -\pi < \vartheta \leq -\frac{\pi}{2} \\ \frac{M_{p2}}{l \sin \vartheta} & \text{if } -\frac{\pi}{2} \leq \vartheta < 0 \text{ and } \frac{\pi}{2} \leq \vartheta < \pi \end{cases} \quad (8a)$$

which function is, at the same time, the imperfection sensitivity function of the structure (broken line parts in Fig. 1.e).

In the case of some of the following problems, the case of the unloading will not be detailed. In spite of this fact, the possibility of the phenomenon will not be excluded. The problem will be fully analysed elsewhere.

3. Stability of a rigid-plastic imperfect structure

Figure 2.a shows a rigid-plastic cantilever structure with a small strain imperfection ϵ . In Fig. 2.b and c the non-smooth functions of the strain energy and the material law can be seen.

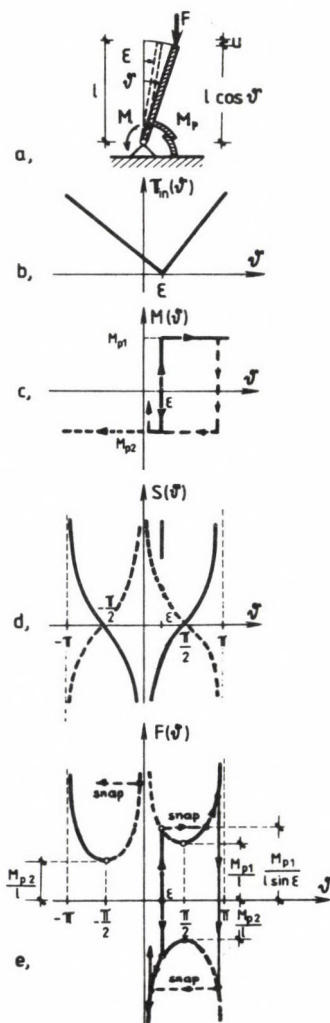


Fig. 2.

In this case the total potential energy of the loading period reads

$$\pi(\vartheta) = -Fl(1 - \cos \vartheta) + \begin{cases} M_{p1}(\vartheta - \varepsilon) & \text{if } \vartheta \geq \varepsilon \\ M_{p2}(\vartheta - \varepsilon) & \text{if } \vartheta \leq \varepsilon \end{cases} \quad (10)$$

According to the condition of the equilibrium of the structure in the case of non-smooth functions, the zero has to be among the elements of the set of the subgradients which build the subdifferential of the superpotential (10)

$$0 \in \partial \pi(\vartheta) = -Fl \sin \vartheta + \begin{cases} M_{p1} & \text{if } \vartheta > \varepsilon \\ [M_{p1}, M_{p2}] & \text{if } \vartheta = \varepsilon \\ M_{p2} & \text{if } \vartheta < \varepsilon \end{cases} \quad (11)$$

from which the equilibrium paths of the loading phase can be obtained:

$$F(\vartheta) = \begin{cases} \frac{M_{p1}}{l \sin \vartheta} & \text{if } \vartheta > \varepsilon \\ \left[\frac{M_{p1}}{l \sin \varepsilon}, \frac{M_{p2}}{l \sin \varepsilon} \right] & \text{if } \vartheta = \varepsilon \\ \frac{M_{p2}}{l \sin \vartheta} & \text{if } \vartheta < \varepsilon \end{cases} \quad (12)$$

Further we show that

$$\partial^2 \pi(\vartheta) = -Fl \cos \vartheta + \begin{cases} 0 & \text{if } \vartheta \neq \varepsilon \\ +\infty & \text{if } \vartheta = \varepsilon \end{cases} \quad (13)$$

thus, by substituting (12) for (13), the elements of the Hessian matrix namely the stability coefficients can be formed:

$$S(\vartheta) = \begin{cases} -\frac{M_{p1}}{\operatorname{tg} \vartheta} & \text{if } \vartheta > \varepsilon \\ \left[+\infty - \frac{M_{p1}}{\operatorname{tg} \varepsilon}, +\infty - \frac{M_{p2}}{\operatorname{tg} \varepsilon} \right] & \text{if } \vartheta = \varepsilon \\ -\frac{M_{p2}}{\operatorname{tg} \vartheta} & \text{if } \vartheta < \varepsilon \end{cases} \quad (14)$$

Note that the Hessian matrix has interval elements at the point $\vartheta = \varepsilon$. From the signs of the stability coefficients in Fig. 2.d, the stability circumstances of the equilibrium paths in Fig. 2.e can be determined.

Thus the critical forces are

$$F_{cr} = \begin{cases} \frac{M_{p1}}{l} & \text{if } \vartheta = \frac{\pi}{2} \\ \frac{M_{p1}}{l \sin \varepsilon} & \text{if } \vartheta = \varepsilon \\ -\frac{M_{p2}}{l} & \text{if } \vartheta = -\frac{\pi}{2} \end{cases} \quad (15)$$

Obviously, if $\varepsilon = 0$, then the perfect case of (8) is spoken of. Similarly to the perfect case, the function of the possible critical forces, depending on the snaps and the starting points of the unloadings, can be given as

$$F_{cr}(\vartheta) = \begin{cases} \frac{M_{p1}}{l \sin \vartheta} & \text{if } 0 < \vartheta \leq \varepsilon \text{ or } -\pi < \vartheta \leq -\frac{\pi}{2} \\ \frac{M_{p2}}{l \sin \vartheta} & \text{if } -\frac{\pi}{2} \leq \vartheta < 0 \text{ or } \pi - \varepsilon \leq \vartheta < \pi \end{cases} \quad (15a)$$

if ε is positive. Note that if the imperfection ε is negative, the detailed procedure is naturally valid but can be reflected with respect to the vertical axis.

4. Stability of a rigid-plastic locking structure

Fig. 3.a illustrates the rigid-plastic cantilever with a small locking type imperfection. It means that if $\epsilon_1 > \vartheta > \epsilon_2$ the cantilever can rotate without any restriction or resistance. This phenomenon yields a highly non-smooth behaviour in the relating functions. Fig. 3.b and c show the strain energy function and the constitutive law /4/.

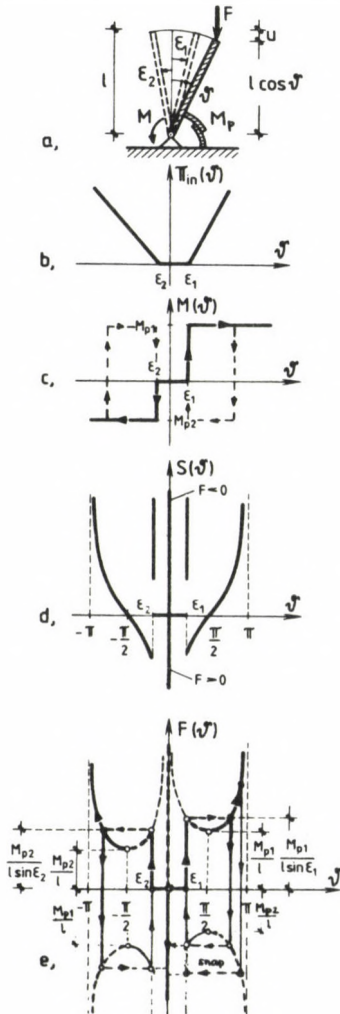


Fig. 3.

The total superpotential of the loading period has the form of

$$\pi(\vartheta) = -Fl (1 - \cos \vartheta) + \begin{cases} M_{p1}(\vartheta - \varepsilon_1) & \text{if } \vartheta \geq \varepsilon_1 \\ 0 & \text{if } \varepsilon_2 \leq \vartheta \leq \varepsilon_1 \\ M_{p2}(\vartheta - \varepsilon_2) & \text{if } \vartheta \leq \varepsilon_2 \end{cases} \quad (16)$$

so the condition of the equilibrium relates to its first subdifferential

$$0 \in \partial\pi(\vartheta) = -Fl \sin \vartheta + \begin{cases} M_{p1} & \text{if } \vartheta > \varepsilon_1 \\ [0, M_{p1}] & \text{if } \vartheta = \varepsilon_1 \\ 0 & \text{if } \varepsilon_2 < \vartheta < \varepsilon_1 \\ [M_{p2}, 0] & \text{if } \vartheta = \varepsilon_2 \\ M_{p2} & \text{if } \vartheta < \varepsilon_2 \end{cases} \quad (17)$$

The qualification of the equilibrium depends on the second subdifferential of (16)

$$\partial^2\pi(\vartheta) = -Fl \cos \vartheta + \begin{cases} 0 & \text{if } \vartheta \neq \varepsilon_1 \text{ and } \vartheta = \varepsilon_2 \\ +\infty & \text{if } \vartheta = \varepsilon_1 \text{ or } \vartheta = \varepsilon_2 \end{cases} \quad (18)$$

From (17) we obtain the equilibrium paths of the loading phase

$$F(\vartheta) = \begin{cases} \frac{M_{p1}}{l \sin \vartheta} & \text{if } \vartheta > \varepsilon_1 \\ \left[0, \frac{M_{p1}}{l \sin \varepsilon_1} \right] & \text{if } \vartheta = \varepsilon_1 \\ 0 & \text{if } \varepsilon_2 < \vartheta < \varepsilon_1 \\ (-\infty, +\infty) & \text{if } \vartheta = 0 \text{ and } \varepsilon_2 \leq 0 \leq \varepsilon_1 \\ \left[0, \frac{M_{p2}}{l \sin \varepsilon_2} \right] & \text{if } \vartheta = \varepsilon_2 \\ \frac{M_{p2}}{l \sin \vartheta} & \text{if } \vartheta < \varepsilon_2 \end{cases} \quad (19)$$

Substituting (19) for (18), the stability coefficients are obtained

$$S(\vartheta) = \begin{cases} -\frac{M_{p1}}{\operatorname{tg} \vartheta} & \text{if } \vartheta > \varepsilon_1 \\ (+\infty, +\infty - \frac{M_{p1}}{\operatorname{tg} \varepsilon_1}) & \text{if } \vartheta = \varepsilon_1 \\ 0 & \text{if } \varepsilon_2 < \vartheta < \varepsilon_1 \\ (+\infty, +\infty - \frac{M_{p2}}{\operatorname{tg} \varepsilon_2}) & \text{if } \vartheta = \varepsilon_2 \\ -\frac{M_{p2}}{\operatorname{tg} \vartheta} & \text{if } \vartheta < \varepsilon_2 \end{cases} \quad (20)$$

for the qualification of the equilibrium paths of the loading phase as we can see in Fig. 3.d and e.

Thus the set of the critical forces is

$$F_{cr} = \begin{cases} \frac{M_{p1}}{l} & \text{if } \vartheta = \frac{\pi}{2} \\ \frac{M_{p1}}{l \sin \varepsilon_1} & \text{if } \vartheta = \varepsilon_1 \text{ and } \varepsilon_1 < \frac{\pi}{2} \\ 0 & \text{if } \vartheta = 0 \\ \frac{M_{p2}}{l \sin \varepsilon_2} & \text{if } \vartheta = \varepsilon_2 \text{ and } \varepsilon_2 > -\frac{\pi}{2} \\ -\frac{M_{p2}}{l} & \text{if } \vartheta = -\frac{\pi}{2} \end{cases} \quad (21)$$

with a rather dangerous critical force among its elements: the zero force relating to the initial position!

Dealing with the unloading process, taking the potential energy

$$\pi(\vartheta) = F l (1 - \cos \vartheta) + \begin{cases} M_{p1}(\vartheta_p - \varepsilon_1) + M_{p2}(\vartheta_p - \vartheta) & \text{if } \vartheta_p \geq \varepsilon_1 \text{ and } \vartheta \geq \varepsilon_1 \\ 0 & \text{if } \varepsilon_2 \leq \vartheta \leq \varepsilon_1 \\ M_{p2}(\vartheta_p - \varepsilon_2) + M_{p1}(\vartheta_p - \vartheta) & \text{if } \vartheta_p \leq \varepsilon_2 \text{ and } \vartheta \leq \varepsilon_2 \end{cases} \quad (16a)$$

into account and considering the dynamical snaps, the function of the possible critical forces as the imperfection sensitivity function of the structure reads

$$F_{cr}(\vartheta) = \begin{cases} \frac{M_{p1}}{l \sin \vartheta} & \text{if } \vartheta = \varepsilon_1 \text{ or } -\pi < \vartheta \leq -\pi + \varepsilon_2 \\ 0 & \text{if } \vartheta = 0 \\ \frac{M_{p2}}{l \sin \vartheta} & \text{if } \vartheta = \varepsilon_2 \text{ or } \pi - \varepsilon_1 \leq \vartheta < \pi \end{cases} \quad (21a)$$

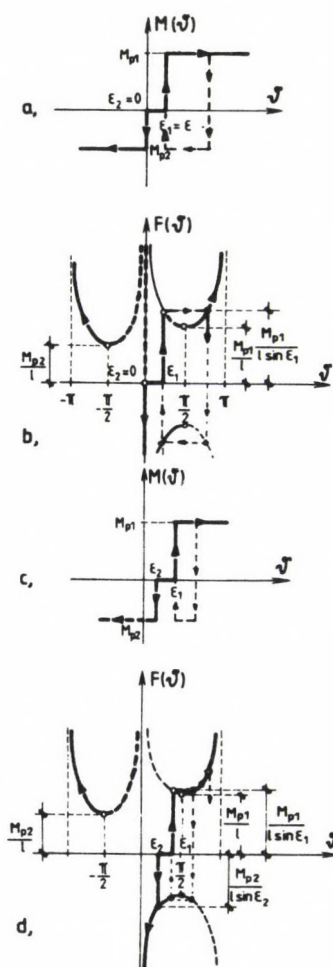


Fig. 4.

It is important to observe that between the values of ϵ_1 and ϵ_2 , except for $\vartheta=0$, the structure has no load bearing capacity. Here it can not be in equilibrium, consequently, subjected to any non-zero force the structure will move without any resistance. Moreover, in the initial position, if $\vartheta=0$, the equilibrium state is always unstable if the structure is subjected to any arbitrary positive force. It is very dangerous since the neighbouring states of the unstable initial state are the states of the free moving.

Figure 4 shows two variations of the locking effect. Fig. 4.a and b relate to the special case of the detailed problem if $\epsilon_2 = 0$. Fig. 4.c and d show the case of an internal locking if both ϵ_1 and ϵ_2 are positive.

5. Stability of an elastic-plastic perfect structure

Figure 5.a,b and c show the cantilever with an elasto-plastic support, the strain energy and the material behaviour characterized by the modulus of elasticity as the spring constant c and by the plastic moment limits M_{p1} and M_{p2} .

The total potential energy of the loading period reads

$$\pi(\vartheta) = -F\ell(1-\cos\vartheta) + \begin{cases} M_{p1}(\vartheta - \frac{\vartheta_{e1}}{2}) & \text{if } \vartheta \geq \vartheta_{e1} \\ \frac{1}{2}c\vartheta^2 & \text{if } \vartheta_{e2} \leq \vartheta \leq \vartheta_{e1} \\ M_{p2}(\vartheta - \frac{\vartheta_{e2}}{2}) & \text{if } \vartheta \leq \vartheta_{e2} \end{cases} \quad (22)$$

where $\vartheta_{e1} = \frac{M_{p1}}{c}$ and $\vartheta_{e2} = \frac{M_{p2}}{c}$ are the elastic strain limits. The condition of the equilibrium is

$$0 \in \partial\pi(\vartheta) = -F\ell \sin\vartheta + \begin{cases} M_{p1} & \text{if } \vartheta \geq \vartheta_{e1} \\ c\vartheta & \text{if } \vartheta_{e2} \leq \vartheta \leq \vartheta_{e1} \\ M_{p2} & \text{if } \vartheta \leq \vartheta_{e2} \end{cases} \quad (23)$$

from which the equilibrium paths of the loading phase seen in Fig. 5.e are

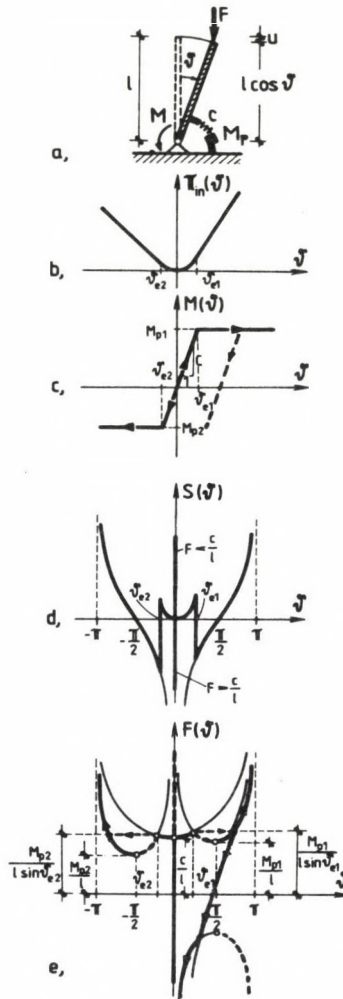


Fig. 5.

$$F(\psi) = \begin{cases} \frac{M_{p1}}{l \sin \psi} & \text{if } \psi \geq \psi_{e1} \\ \frac{c \psi}{l \sin \psi} & \text{if } \psi_{e2} \leq \psi \leq \psi_{e1} \\ (-\infty, +\infty) & \text{if } \psi = 0 \\ \frac{M_{p2}}{l \sin \psi} & \text{if } \psi \leq \psi_{e2} \end{cases} \quad (24)$$

with the relating critical forces

$$F_{cr} = \begin{cases} \frac{M_{p1}}{l} & \text{if } \vartheta = \frac{\pi}{2} \text{ and } \vartheta_{e1} < \frac{\pi}{2} \\ \frac{M_{p1}}{l \sin \vartheta_{e1}} & \text{if } \vartheta = \vartheta_{e1} \text{ and } \vartheta_{e1} \leq \frac{\pi}{2} \\ \frac{c}{l} & \text{if } \vartheta = 0 \\ \frac{M_{p2}}{l \sin \vartheta_{e2}} & \text{if } \vartheta = \vartheta_{e2} \text{ and } \vartheta_{e2} \geq -\frac{\pi}{2} \\ -\frac{M_{p2}}{l} & \text{if } \vartheta = -\frac{\pi}{2} \text{ and } \vartheta_{e2} \geq -\frac{\pi}{2} \end{cases} \quad (25)$$

knowing that the critical forces belonging to $|\vartheta| = \left| -\frac{\pi}{2} \right|$ will never be reached because of the snaps. In Fig. 5.e also an unloading path is illustrated.

It is worth to be mentioned here that the equilibrium paths (24) and the critical forces (25) in Fig. 5.e depend on the ratio existing among the material constants c , M_{p1} and M_{p2} . The relative position of the three curves and the intersection of them are determined by the ratio of

$$\vartheta_{e1} = \frac{M_{p1}}{c} \quad \text{and} \quad \vartheta_{e2} = \frac{M_{p2}}{c}.$$

If, for example, the elastic modulus c would be decreased by constant plastic limits, causing the increase of ϑ_{e1} and ϑ_{e2} , then the plastic paths could be covered by the elastic one, resulting no critical forces within the interval $-\frac{\pi}{2} < \vartheta < \frac{\pi}{2}$. Similar behaviour could be observed by increasing the plastic moment limits M_{p1} and M_{p2} compared with the elastic modulus c .

To qualify the equilibrium paths we need

$$\partial^2 \pi(\vartheta) = -Fl \cos \vartheta + \begin{cases} 0 & \text{if } \vartheta_{e2} > \vartheta > \vartheta_{e1} \\ [0, c] & \text{if } \vartheta = \vartheta_{e1} \text{ or } \vartheta = \vartheta_{e2} \\ c & \text{if } \vartheta_{e2} < \vartheta < \vartheta_{e1} \end{cases} \quad (26)$$

and substituting (24) for it, the stability coefficients seen in Fig. 5.d are obtained:

$$S(\psi) = \begin{cases} -\frac{M_{p1}}{\operatorname{tg} \psi} & \text{if } \psi > \psi_{e1} \\ \left[-\frac{M_{p1}}{\operatorname{tg} \psi_{e1}}, c(1 - \frac{\psi_{e1}}{\operatorname{tg} \psi_{e1}}) \right] & \text{if } \psi = \psi_{e1} \\ c(1 - \frac{\psi}{\operatorname{tg} \psi}) & \text{if } \psi_{e2} < \psi < \psi_{e1} \\ \left[-\frac{M_{p2}}{\operatorname{tg} \psi_{e2}}, c(1 - \frac{\psi_{e2}}{\operatorname{tg} \psi_{e2}}) \right] & \text{if } \psi = \psi_{e2} \\ -\frac{M_{p2}}{\operatorname{tg} \psi} & \text{if } \psi < \psi_{e2} \end{cases} \quad (27)$$

6. Stability of an elastic-plastic imperfect structure

Figure 6.a, b and c show the behaviour of the previously analysed structure with a small imperfection of strain type, which means an initial unsymmetry ε .

In this case the total potential energy in the loading phase is as follows

$$\pi(\psi) = -F L (1 - \cos \psi) + \begin{cases} M_{p1}(\psi - \frac{\psi_{e1}}{2} - \varepsilon) & \text{if } \psi \geq \varepsilon + \psi_{e1} \\ \frac{1}{2} c(\psi - \varepsilon)^2 & \text{if } \varepsilon - \psi_{e2} \leq \psi \leq \varepsilon + \psi_{e1} \\ M_{p2}(\psi - \frac{\psi_{e2}}{2} - \varepsilon) & \text{if } \psi \leq \varepsilon - \psi_{e2} \end{cases} \quad (28)$$

Thus, the condition of the equilibrium is

$$0 \equiv \partial \pi(\psi) = -F L \sin \psi + \begin{cases} M_{p1} & \text{if } \psi \geq \varepsilon + \psi_{e1} \\ c(\psi - \varepsilon) & \text{if } \varepsilon - \psi_{e2} \leq \psi \leq \varepsilon + \psi_{e1} \\ M_{p2} & \text{if } \psi \leq \varepsilon - \psi_{e2} \end{cases} \quad (29)$$

from which we obtain both the fundamental and the post-buckling equilibrium paths:

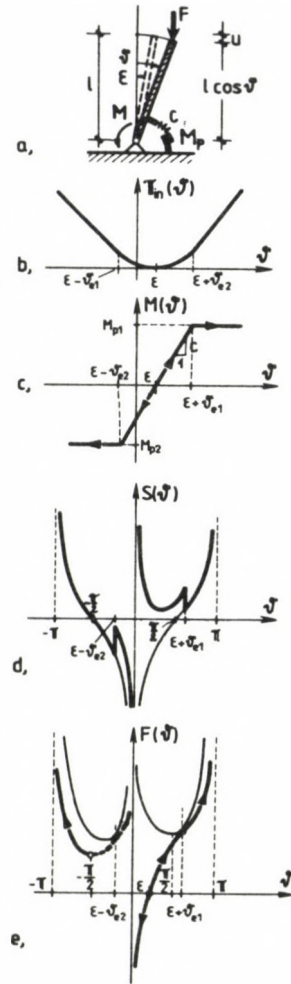


Fig. 6.

$$F(v) = \begin{cases} \frac{M_{p1}}{l \sin v} & \text{if } v \geq \epsilon + v_{e1} \\ \frac{c(v - \epsilon)}{l \sin v} & \text{if } \epsilon - v_{e2} \leq v \leq \epsilon + v_{e1} \\ \frac{M_{p2}}{l \sin v} & \text{if } v \leq \epsilon - v_{e2} \end{cases} \quad (30)$$

thus, the critical forces depending on the ratio of M_{p1} , M_{p2} , c and ϵ also in Fig. 6.e are

$$F_{cr} = \begin{cases} \frac{M_{p1}}{l} & \text{if } \vartheta = \frac{\pi}{2} \text{ and } \varepsilon + \vartheta_{e1} \leq \frac{\pi}{2} \\ \frac{M_{p1}}{l \sin(\varepsilon + \vartheta_{e1})} & \text{if } \vartheta = \varepsilon + \vartheta_{e1} \text{ and } \varepsilon + \vartheta_{e1} \leq \frac{\pi}{2} \\ \frac{M_{p2}}{l \sin(\varepsilon - \vartheta_{e2})} & \text{if } \vartheta = \varepsilon - \vartheta_{e2} \text{ and } \varepsilon - \vartheta_{e2} \geq -\frac{\pi}{2} \\ -\frac{M_{p2}}{l} & \text{if } \vartheta = -\frac{\pi}{2} \text{ and } \varepsilon - \vartheta_{e2} \geq -\frac{\pi}{2} \end{cases} \quad (31)$$

Since only the last condition is fulfilled, in Fig. 6.e only a single critical force can be spoken of. Furthermore

$$\partial^2 \pi(\vartheta) = -Fl \cos \vartheta + \begin{cases} 0 & \text{if } \varepsilon - \vartheta_{e2} > \vartheta > \varepsilon + \vartheta_{e1} \\ [0, c] & \text{if } \vartheta = \varepsilon + \vartheta_{e1} \text{ or } \vartheta = \varepsilon - \vartheta_{e2} \\ c & \text{if } \varepsilon - \vartheta_{e2} < \vartheta < \varepsilon + \vartheta_{e1} \end{cases} \quad (32)$$

so that the stability coefficients in Fig. 6.d are

$$S(\vartheta) = \begin{cases} -\frac{M_{p1}}{\operatorname{tg} \vartheta} & \text{if } \vartheta > \varepsilon + \vartheta_{e1} \\ \left[-\frac{M_{p1}}{\operatorname{tg}(\varepsilon + \vartheta_{e1})}, c(1 - \frac{\vartheta_{e1}}{\operatorname{tg}(\varepsilon + \vartheta_{e1})}) \right] & \text{if } \vartheta = \varepsilon + \vartheta_{e1} \\ c(1 - \frac{\vartheta - \varepsilon}{\operatorname{tg} \vartheta}) & \text{if } \varepsilon - \vartheta_{e2} < \vartheta < \varepsilon + \vartheta_{e1} \\ \left[-\frac{M_{p2}}{\operatorname{tg}(\varepsilon - \vartheta_{e2})}, c(1 + \frac{\vartheta_{e2}}{\operatorname{tg}(\varepsilon - \vartheta_{e2})}) \right] & \text{if } \vartheta = \varepsilon - \vartheta_{e2} \\ -\frac{M_{p2}}{\operatorname{tg} \vartheta} & \text{if } \vartheta < \varepsilon - \vartheta_{e2} \end{cases} \quad (33)$$

The unloading process is similar to that of the perfect version of the problem seen in Fig. 5.c and e.

7. Stability of an elastic-plastic locking structure

Concerning to the Fig. 7.a, b and c, the total superpotential of the loading period reads

$$\pi(\vartheta) = -Fl(1 - \cos \vartheta) + \begin{cases} M_{p1}(\vartheta - \frac{\vartheta_{e1}}{2} - \varepsilon_1) & \text{if } \vartheta \geq \varepsilon_1 + \vartheta_{e1} \\ \frac{1}{2}c(\vartheta - \varepsilon_1)^2 & \text{if } \varepsilon_1 \leq \vartheta \leq \varepsilon_1 + \vartheta_{e1} \\ 0 & \text{if } \varepsilon_2 \leq \vartheta \leq \varepsilon_1 \\ \frac{1}{2}c(\vartheta - \varepsilon_2)^2 & \text{if } \varepsilon_2 - \vartheta_{e2} \leq \vartheta \leq \varepsilon_2 \\ M_{p2}(\vartheta - \frac{\vartheta_{e2}}{2} - \varepsilon_2) & \text{if } \vartheta \leq \varepsilon_2 - \vartheta_{e2} \end{cases} \quad (34)$$

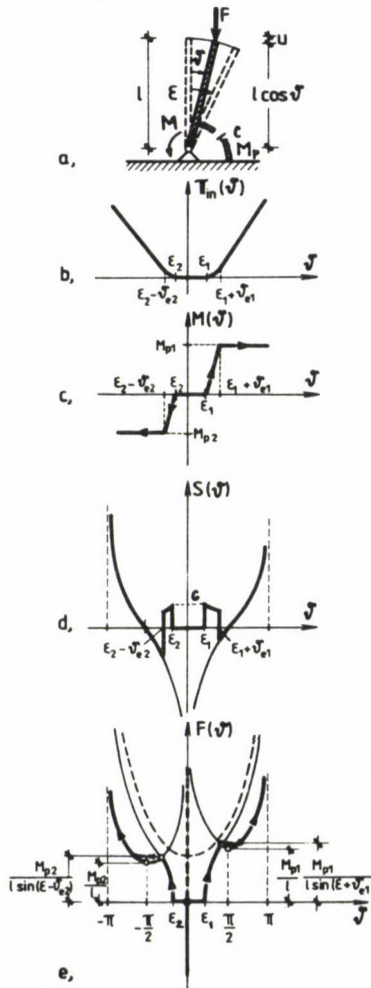


Fig. 7.

from the first subdifferential of which the equilibrium conditions

$$0 \leq \partial \pi(\vartheta) = -F l \sin \vartheta + \begin{cases} M_{p1} & \text{if } \vartheta \geq \varepsilon_1 + \vartheta_{e1} \\ c(\vartheta - \varepsilon_1) & \text{if } \varepsilon_1 \leq \vartheta \leq \varepsilon_1 + \vartheta_{e1} \\ 0 & \text{if } \varepsilon_2 \leq \vartheta \leq \varepsilon_1 \\ c(\vartheta - \varepsilon_2) & \text{if } \varepsilon_2 - \vartheta_{e2} \leq \vartheta \leq \varepsilon_2 \\ M_{p2} & \text{if } \vartheta \leq \varepsilon_2 - \vartheta_{e2} \end{cases} \quad (35)$$

and the equilibrium paths can be obtained

$$F(\vartheta) = \begin{cases} \frac{M_{p1}}{l \sin \vartheta} & \text{if } \vartheta \geq \varepsilon_1 + \vartheta_{e1} \\ \frac{c(\vartheta - \varepsilon_1)}{l \sin \vartheta} & \text{if } \varepsilon_1 \leq \vartheta \leq \varepsilon_1 + \vartheta_{e1} \\ 0 & \text{if } \varepsilon_2 \leq \vartheta \leq \varepsilon_1 \text{ except for } \vartheta = 0 \\ (-\infty, +\infty) & \text{if } \vartheta = 0 \text{ and } \varepsilon_2 \leq 0 \leq \varepsilon_1 \\ \frac{c(\vartheta - \varepsilon_2)}{l \sin \vartheta} & \text{if } \varepsilon_2 - \vartheta_{e2} \leq \vartheta \leq \varepsilon_2 \\ \frac{M_{p2}}{l \sin \vartheta} & \text{if } \vartheta \leq \varepsilon_2 - \vartheta_{e2} \end{cases} \quad (36)$$

with the referring critical forces:

$$F_{cr} = \begin{cases} \frac{M_{p1}}{l} & \text{if } \vartheta = \frac{\pi}{2} \text{ and } \varepsilon_1 + \vartheta_{e1} \leq \frac{\pi}{2} \\ \frac{M_{p1}}{l \sin(\varepsilon_1 + \vartheta_{e1})} & \text{if } \vartheta = \varepsilon_1 + \vartheta_{e1} \text{ and } \varepsilon_1 + \vartheta_{e1} \leq \frac{\pi}{2} \\ 0 & \text{if } \varepsilon_2 < \vartheta < \varepsilon_1 \\ \frac{M_{p2}}{l \sin(\varepsilon_2 - \vartheta_{e2})} & \text{if } \vartheta = \varepsilon_2 - \vartheta_{e2} \text{ and } \varepsilon_2 - \vartheta_{e2} \geq -\frac{\pi}{2} \\ -\frac{M_{p2}}{l} & \text{if } \vartheta = -\frac{\pi}{2} \text{ and } \varepsilon_2 - \vartheta_{e2} \geq -\frac{\pi}{2} \end{cases} \quad (37)$$

Figure 7.d and e represents the results of the analysis. Note, that also in this case, similarly to the case of Fig. 3, the most dangerous critical force relates to the initial state with the value of $F_{cr} = 0!$

8. Stability of a polygonally linear elastic-plastic structure

In Fig. 8 there is given a stress-strain diagram being in tension tri-linearly elastic and in compression simple elastic-plastic. All the

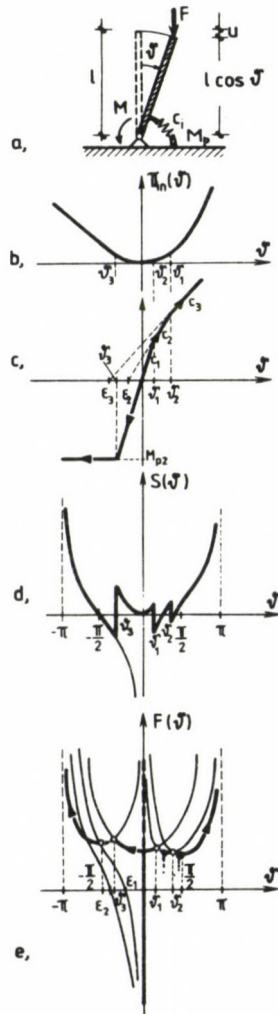


Fig. 8.

multi-linear cases can be taken as elastic material with strain imperfections into account. To the first modulus of elasticity c_1 no imperfection belongs, namely $\varepsilon_1 = 0$. The second linear part characterized by c_2 has an imperfection of ε_2 indicating by the section point of its line with the coordinate axis σ . Similarly, the third part also has an imperfection ε_3 . In this way we can analyse the problem similarly to the case of Fig. 6. The boundary line of all the curves forms an equilibrium path with section points referring to the changes of the type of the materials. The unloading process, along the multilinearly elastic parts, uses the same stress-strain diagram as the loading process has, since elastic materials have no energy dissipation. After plastification, the unloading takes place elastically, so it can be handled as an imperfection. The full analysis of the unloading will be detailed elsewhere.

Conclusion

On the basis of the presented method the stability analysis of structures with monotone increasing polygonal material law and relating non-smooth strain energy functionals can be investigated. The quasi-elastic exact analysis has been introduced through a simple one-dimensional example. Obviously, the method can be extended to more-dimensional problems. In this case the analysis of the definiteness of the Hessian matrix at the singular points needs the use of the interval arithmetics. Otherwise, since the exact analysis in multi-dimensional case, even for classical elastic problems, is mathematically rather complicated, for the non-smooth stability problems an approximate analysis is suggested.

REFERENCES

1. Thompson, J.M.T. - Hunt, G.W.: A general theory of elastic stability, Wiley, London. (1973)
2. Gáspár, Zs. (to be published): Application of the catastrophe theory in stability analysis of structures. In: Kollár, L. et al.: Special problems of structural stability, Akadémiai Kiadó, Budapest (in Hungarian)
3. Panagiotopoulos, P.D.: Inequality problems in mechanics and applications. Convex and non-convex energy functions. Birkhauser, Basel. (1985)
4. Kurutz, M.: Analysis of generalized conditional joints as subdifferential constitutive models, Mech. of Struct. and Mach. 15 (2), (1987), 123-151
5. Gáspár, Zs.: Imperfection-sensitivity at near-coincidence of two critical points, J. Struct. Mech. (1), (1985), 43-45.
6. Thompson, J.M.T. - Hunt, G.W.: Elastic instability phenomena. Wiley, Chichester, (1984)

A BANDWIDTH REDUCTION PROCESS FOR SUBSTRUCTURAL FINITE ELEMENT METHOD

PÁCZELT, I.* - SZABÓ, T.**

(Received: 27 November 1989)

Bandwidth reduction of the stiffness matrix of a substructure is obtained by solution of a steady-state heat transfer problem. The problem can be solved under the following conditions: zero temperature at the interface nodal points, rest of the surface of the body isolated from the environment, and uniform internal heat generation throughout the volume of the substructure.

Bandwidth reduction is obtained by renumbering of nodal points according to decreasing nodal temperatures. In this paper, the properties of the heat transfer problem are discussed and the efficiency of the proposed process is illustrated by a few examples.

1. Introduction

As is well known, banded matrices are produced in application of the finite element method /1/.

A possible advantage of bandwidth reduction is that the solution might require a smaller number of arithmetic operations and main or back storage locations.

In the program system FEM-3D /2/, the installed equation solver /3/ requires that the interface nodal point unknowns be placed at the end of total unknowns NEQ of the substructure.

The number of slave nodal point unknowns are denoted by LEQ. ND denotes the number of interface nodal point unknowns that is the size of interface stiffness matrix $ND = NEQ - LEQ$.

To the authors' best knowledge, no bandwidth reduction process under the above conditions has been published yet. The classic Cuthill, McKee /4/ and Cuthill /5/ algorithms are based on graph theory.

In this work, thermal transfer analogy is used for bandwidth reduction. Topologically, the same finite element mesh that has been generated for static and dynamic analysis of the structure is applied to the

*Páczelt, István, H-3529 Miskolc, Perczel Mór u. 30, Hungary

**Szabó, Tibor, H-3529 Miskolc, Aulich u. 26, Hungary

heat transfer problem. It is assumed that the temperature is zero at the interface nodal points, uniform internal heat is generated in all elements and the boundary of the structure is isolated.

The theoretical background of application of the finite element method to thermal transfer problems is presented e.g. in [7].

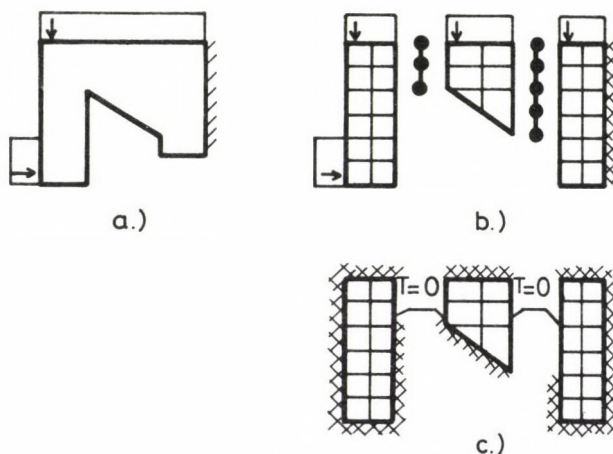


Fig. 1.1.

The two-dimensional structure in Fig. 1.a is divided in 3 substructures for static analysis. In Fig. 1.1.c, the boundary conditions of the thermal transfer problem are shown.

2. Heat transfer equation

The heat flow equilibrium in the interior of the body is described by Fourier's differential equation:

$$\nabla \cdot (\underline{K} \cdot \nabla T) + q^B = c \frac{\partial T}{\partial t} \quad (2.1)$$

where ∇ - Hamilton's differential operator
 T - temperature field
 \underline{K} - diagonal matrix of the thermal conductivities
 q^B - rate of heat, generated per unit volume
 t - time.

The following boundary conditions are stipulated:

- given temperature over surface S_1 ,
- heat-flow boundary condition $q = q^{FL}$ for surface S_2 ,
- heat-convection boundary condition

$$q = h(T_{\infty} - T)$$

for surface S_3 , where h is the convection coefficient, T_{∞} is the ambient temperature.

Thus conditions

$$T = T_{\infty} \quad x \in S_1 \quad (2.2)$$

$$k_n(\nabla T \cdot \underline{n}) = 0 \quad x \in S_2, (S_3) \quad (2.3)$$

must be satisfied, where \underline{n} denotes the direction of the normal to the surface, k_n is the thermal conductivity of the body ($k_n = \underline{n} \cdot \underline{K} \cdot \underline{e}$, $\underline{e}^T = [111]$).

If field T satisfies the boundary conditions along S_1 and the equations belonging to the stationary condition of the functional are

$$I = \frac{1}{2} \int_{(v)} \left[\nabla T \cdot \underline{K} \cdot \nabla T + 2 \left[q^B - c \frac{\partial T}{\partial t} \right] \right] dV \quad (2.4)$$

$$- \int_{(S_2)} q^{FL} T dS + \frac{1}{2} \int_{(S_3)} h(T - T_{\infty})^2 dS ,$$

then T will be the exact solution. For the steady-state condition, the underlined term is zero.

3. Bandwidth reduction finite elements

A simplified functional can be derived, taking into consideration the conditions mentioned earlier:

$$I = \frac{1}{2} \int_{(v)} \nabla T \cdot \underline{K} \cdot \nabla T dV - \int_{(v)} q^B T dV , \quad (3.1)$$

that is neither heat flow nor heat convection is present. At the interface

nodal points on surface S_1 , temperature $T = T_{\infty} = 0$ shall have priority. One, two and three dimensional finite elements are presented in the next sections.

3.1 One-dimensional line element

Assume that the temperature changes linearly along a line element

$$T = T_i + \frac{T_j - T_i}{L} x \quad (3.2)$$

where T_i, T_j are nodal point temperatures. The cross-section, length and thermal conductivity of the prismatic line element are denoted by A, L and k , respectively. (3.1) can be written as

$$I = \frac{1}{2} A \begin{bmatrix} T_i & T_j \end{bmatrix} \left(\frac{k}{L} \begin{bmatrix} 1 & -1 \\ -1 & 1 \end{bmatrix} \begin{bmatrix} T_i \\ T_j \end{bmatrix} - 2q^B \begin{bmatrix} \frac{L}{2} \\ -\frac{L}{2} \end{bmatrix} \right). \quad (3.3)$$

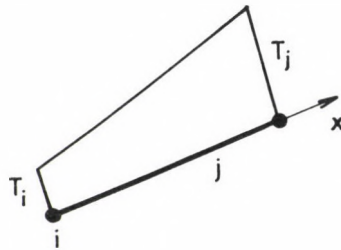


Fig. 3.1.

Important in respect of bandwidth reduction is only the topology of the finite element mesh. For this reason we take

$$A = k = L = 1 \quad \text{and} \quad q^B = 2 \quad (3.4)$$

Thus the heat conductivity matrix and internal heat generation vector \underline{f} can be written as

$$\underline{S} = \begin{bmatrix} 1 & -1 \\ -1 & 1 \end{bmatrix}, \quad \underline{f} = \begin{bmatrix} 1 \\ -1 \end{bmatrix}, \quad (3.5)$$

respectively.

3.2 Two-dimensional plane element

Taking into consideration the bandwidth reduction aspect, we derive the two-dimensional element according to /1/ but the actual x, z coordinates

shall be replaced by \tilde{x} , \tilde{z} varying in the range of

$$-1 \leq \tilde{x} \leq 1 ,$$

$$-1 \leq \tilde{z} \leq 1 ,$$

respectively.

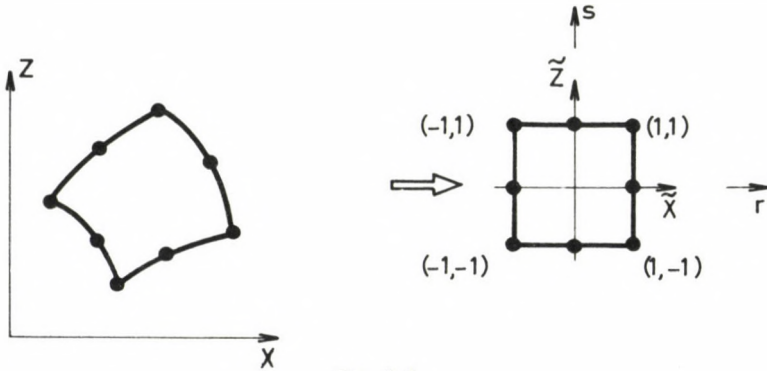


Fig. 3.2.

In this case, the Jacobian matrix is an identity matrix since the derivatives with respect to \tilde{x}, \tilde{z} are equal to the derivatives with respect to local coordinates r, s .

To derive matrix \underline{S} and vector \underline{f} , we use 2×2 Gauss integration orders. On the basis of (3.1) and taking

$$\underline{K} = \begin{bmatrix} k_x & 0 \\ 0 & k_z \end{bmatrix} = \begin{bmatrix} 1 & 0 \\ 0 & 1 \end{bmatrix} , \quad q^B = 1 ,$$

the following integrals can be written:

$$\underline{S} = \sum_{i=1}^2 \sum_{j=1}^2 \underline{B}^T(r_i, s_j) \underline{E} \underline{B}(r_i, s_j) W_i W_j \quad (3.6)$$

$$\underline{f} = \sum_{i=1}^2 \sum_{j=1}^2 \underline{N}^T(r_i, s_j) W_i W_j \quad (3.7)$$

where W_i, W_j are Gauss numerical integration weights at sampling points r_i, s_j , respectively,

$$\underline{N} = [N_1, \dots, N_i, \dots, N_8] ; \quad \underline{B} = [B_1, \dots, B_i, \dots, B_8] ;$$

$$N_i = N_i(r,s) \text{ shape function, } \underline{B}_i = \begin{bmatrix} \frac{\partial N_i}{\partial x} \\ \frac{\partial N_i}{\partial z} \end{bmatrix} = \begin{bmatrix} \frac{\partial N_i}{\partial r} \\ \frac{\partial N_i}{\partial s} \end{bmatrix}$$

\underline{E} - identity matrix of the second order.

3.3 Three-dimensional element

Similarly to the two-dimensional isoparametric element, actual coordinates x, y, z are replaced by natural coordinates. Using 3×3 Gauss integration order for (3.1), the conductivity matrix can be written as

$$\underline{S} = \sum_{i=1}^3 \sum_{j=1}^3 \sum_{k=1}^3 \underline{B}^T(r_i, s_j, t_k) \underline{E} \underline{B}(r_i, s_j, t_k) w_i w_j w_k \quad (3.8)$$

$$\underline{f} = \sum_{i=1}^3 \sum_{j=1}^3 \sum_{k=1}^3 \underline{N}^T(r_i, s_j, t_k) w_i w_j w_k \quad (3.9)$$

where $q^B = 1$, $\underline{K} = \underline{E}$ identity matrix of the third order.

$$\underline{N} = [N_1, \dots, N_i, \dots, N_{20}] ; \quad \underline{B} = [B_1, \dots, B_i, \dots, B_{20}] ;$$

$$\underline{B}_i^T = \left[\frac{\partial N_i}{\partial r} ; \frac{\partial N_i}{\partial s} ; \frac{\partial N_i}{\partial t} \right]$$

$N_i = N_i(r,s,t)$ shape function,

r_i, s_j, t_k sampling points of Gauss integration,

w_i, w_j, w_k integration weights.

4. Renumbering of nodes

By solution of the linear equation system produced on the basis of (3.1) for a substructure, the nodal point temperatures can be obtained. Bandwidth reduction can be obtained by renumbering of nodal points or nodal point unknowns only if they are ordered according to decreasing temperatures.

Note that this process can be used for profile (frontwidth) reduction. In this case, element renumbering takes place in accordance with decreasing medium temperatures of the elements.

5. Effect of the original boundary and fitting conditions on the thermal model

Some points are constrained. In case the support is a single beam or truss or spring with one end clamped, assembly of these elements is not necessary for the thermal solution. Otherwise, the temperature of the point connecting these single elements would be higher than desirable. That is why matrix $\underline{\underline{S}}$ and vector \underline{f} are zero for these elements.

In special modelling cases like excentric connections, periodicity and initial gaps, the slave nodal numbers are replaced by master ones for the thermal transfer solution.

6. Examples

To test the efficiency of the proposed reduction process, we take examples of /8/ to compare the results. Since no example has been found for substructure bandwidth reduction, we choose an arbitrary node as an interface in the example of beam structure used for comparison. In the examples of /8/, one node is selected to start renumbering based on the graph theory. The bandwidth depends on the first node selection.

6.1 First example

The beam structure according to /8/ is shown in Fig. 6.1.1.

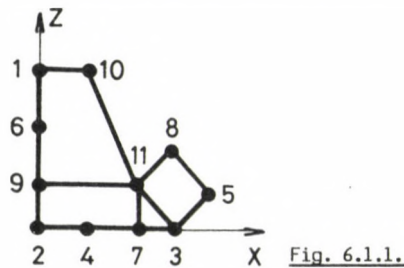


Fig. 6.1.1.

Starting renumbering with different nodal points, the compared results are tabulated in Table 6.1.

Table 6.1

| Starting point | Original | 1 | 2 | 3 | 4 | 5 | 6 | 7 | 8 | 9 | 10 | 11 | Bandwidth |
|----------------|----------|----|----|----|----|----|----|---|----|---|----|----|-----------|
| 5 | thermal | 2 | 3 | 9 | 6 | 11 | 1 | 7 | 10 | 4 | 5 | 8 | 4 |
| | /8/, /4/ | 9 | 11 | 3 | 8 | 1 | 10 | 5 | 2 | 7 | 6 | 4 | 4 |
| 1 | thermal | 11 | 6 | 2 | 5 | 1 | 10 | 3 | 4 | 8 | 9 | | 4 |
| | /8/, /4/ | 1 | 6 | 9 | 10 | 11 | 2 | 8 | 7 | 4 | 3 | | 4 |
| | /8/, /6/ | 1 | 5 | 8 | 6 | 10 | 2 | 7 | 11 | 4 | 3 | 9 | 6 |
| 8 | thermal | 2 | 3 | 10 | 4 | 9 | 1 | 7 | 11 | 5 | 6 | 8 | 4 |
| | /8/, /6/ | 9 | 6 | 3 | 5 | 2 | 8 | 4 | 1 | 7 | 10 | 11 | 10 |

The original numbering scheme can be found in the head of the Table 6.1. The renumbered schemes and bandwidths of methods /4/, /6/ and /8/ and the proposed 'thermal' procedure are shown for different starting points. The bandwidths are defined by the maximum of the difference between the nodal numbers. In the above examples the thermal method resulted in narrowest bandwidth.

6.2 Second example

A simple strain model, a C shaped machine tool frame is shown in Fig. 6.2.1. It is supported at two points, one of them fully constrained. The structure is loaded by two forces $F = 250$ kN in opposite directions.

Frame "C" consists of three substructures shown in Fig. 6.2.2. The linear static problem was solved by the application of eight nodal isoparametric elements of the program system FEM-3D. The FEM-3D consists of four modules (FEM1-4).

Parameters of the mesh and computation are listed in Table 6.2 where

NUMNP - number of nodal points

NUMEL - number of elements

NEQ - number of equations

LEQ - number of slave degrees of freedom

MBAND - bandwidth

NBLK - number of blocks of the stiffness matrix

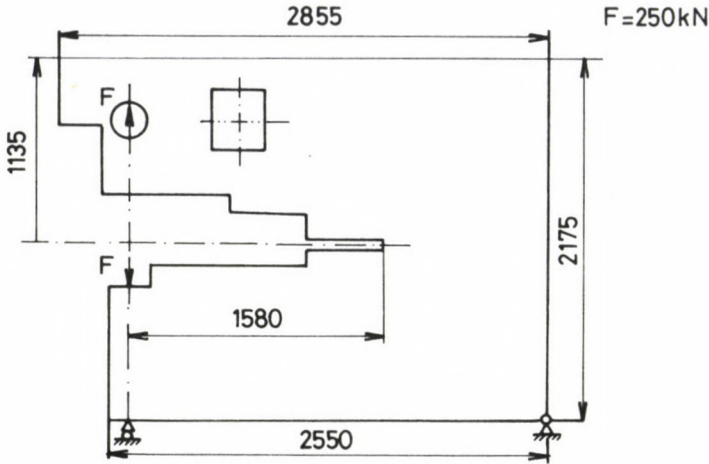


Fig. 6.2.1.

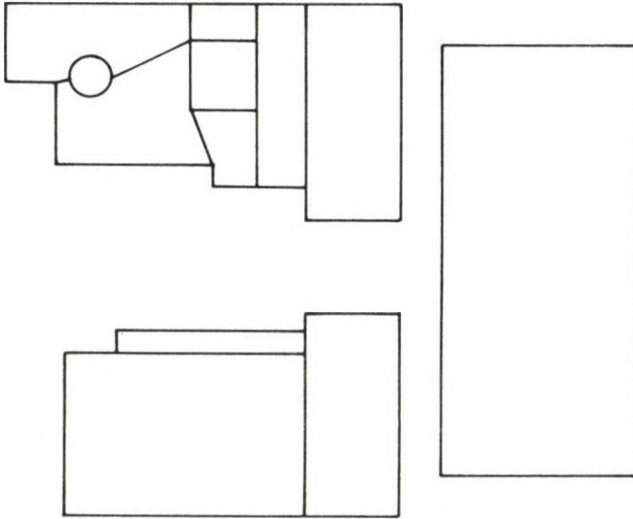


Fig. 6.2.2.

NBLL - number of blocks of the load vector

MAXT - maximum number of real constants of a block.

Data in brackets refer to the case of bandwidth reduction.

By applying the proposed bandwidth reduction process, the total computation time could be decreased by 33 minutes and the required back storage by 90 blocks.

Figure 6.2.3 shows the temperature distribution along the lines of the first substructure. It can be seen that the temperature is zero at the interface points but it is increasing in the direction towards the left.

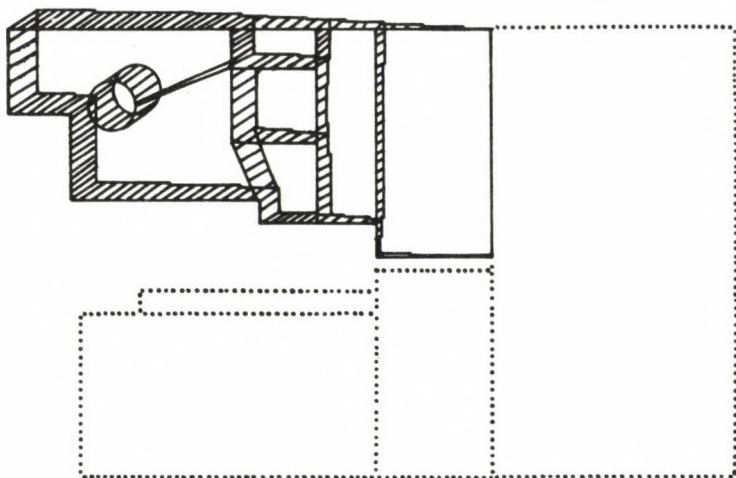


Fig. 6.2.3.

Table 6.2

| Parameters | Substructures | | | Main structure |
|--|--------------------------------|-------|-------|------------------------|
| | 1. | 2. | 3. | |
| NUMNP | 593 | 517 | 331 | 46 |
| NUMEL | 170 | 154 | 92 | 0 |
| NEQ | 1186 | 1033 | 660 | 92 |
| LEQ | 1136 | 991 | 568 | - |
| MBAND | 610 | 987 | 250 | 92 |
| | (114) | (106) | (192) | (92) |
| NBLK | 72 | 76 | 40 | 3 |
| | (33) | (27) | (38) | (3) |
| NBLL | 1 | 1 | 1 | 1 |
| Computation time | FEM1: 4 min (13 min 36 sec) | | | FEM3: 1 min (1 min) |
| IBM PC AT | FEM2: 70 min (27 min 4 sec) | | | FEM4: 6 min (6 min) |
| Total computation time: 81 min (48 min) | | | | |
| MAXT = 2000 | | | | |

REFERENCES

1. Zienkiewicz, O.C.: The finite element methods in engineering, McGraw Hill, London-New York, 1971
2. Égert, J. - Herpai, B. - Nándori, F. - Páczelt, I. - Sárközi, L. - Szabó, T.: Characteristics of a substructural finite element programming system for IBM AT compatible PC. Proceedings of ICED 88, Volume 3, 231-236, Edition GTE-Heurista 1988, ed. by V. Hubka - J. Barátossy - U. Pighini
3. Wilson, E.L. - Dohevey, H.H.: Solution for reduction of equilibrium equations for large complex structural systems. Advances in Engineering Software, Vol. 1. No1 (1978), 19-25.
4. Cuthill, E. - McKee, J.: Reducing the bandwidth of sparse symmetric matrices. Proceedings of the 24th National Conference of the ACM, Brandon Systems Press: NJ, 157-172
5. Cuthill, E.: Several strategies for reducing the bandwidth of matrices. In Rose and Willoughby (1972), 157-166
6. King, I.P.: An automatic reordering scheme for simultaneous equations derived from network systems. Int. J. Numer Meth. Eng. 2, 523-533
7. Klaus-Jürgen, Bathe: Finite element procedures in engineering analysis. Prentice-Hall, Inc., Englewood Cliff, New Jersey 07632, 1982
8. Sergio, Pissanetzky: Sparse Matrix Technology, Academic Press Inc. New York, Toronto, 1984

IDENTIFICATION OF DAMPING PARAMETERS IN LINEAR VIBRATING SYSTEMS WITH "FOLLOWER" LOAD

POPPER, GY.*

(Received: 12 July 1988)

A very effective non-derivative minimization method has been used for identification. The measured values of the stationary solution are simulated. The instabilizing effect of the "follower" force upon the process of identification of damping parameters on the basis of amplitudes has been shown.

1. Formulation of the problem

Consider the damped linear vibrating system with n degrees of freedom in Fig. 1 to be a chain of n rigid members in plane. Each bar is of length l and mass m_i , $i = 1, \dots, n$. In the cylindric hinges, there are springs supplying a return moment proportional to the relative rotation of the members. Spring constants of the hinges are c_i , $i = 1, \dots, n$. The hinges also contain a device (not illustrated) supplying a damping moment proportional to the relative angular velocity of the members, the moment damping coefficient in the hinge i being d_i , $i = 1, \dots, n$. Force P_n applied to the free chain end is constant during motion and it acts in the same direction as the last member. Hence, it is a so-called "follower" force.

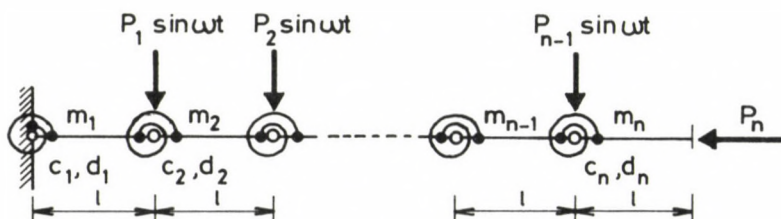


Fig. 1.

*Popper, György, H-1016 Budapest, Szirtes u. 28/A, Hungary

With the intermediate nodes of the chain disturbed by forces $P_{i-1} \sin \omega t$, $i = 2, \dots, n$, we want to find damping coefficients $d = (d_1, \dots, d_n)$ minimizing the integral (2) over given interval $\omega_0 \leq \omega \leq \omega_N$, where $v(\omega; d)$ is the stationary solution and $\tilde{v}(\omega)$ contains its values in points $\omega_0 < \omega_1 < \dots < \omega_N$ (determined e.g. by measurements).

Details are explained in the next section. The above assumption was made first by Bosznay /2/.

2. Some prerequisites of identification

The parametric identification of some dynamic problems can be mathematically formulated as follows. Assume a vector function $v(\omega; d)$ with ℓ real elements. ω is a real independent variable e.g. circular frequency (or time) and $d = (d_1, \dots, d_n)$ is a real vector of unknown parameters. Function $v(\omega; d)$ that is $v: [\omega_0, \omega_N] \times R^n \rightarrow R^\ell$, is generally given as a computer subroutine (a rather time-consuming calculation) and the derivatives of v are not available in practice or if indeed at all, not in the required form.

Function $v(\omega; d)$ represents a class of models (their responses) for identification of a real mechanical structure. Its actual response (known e.g. from measurements) is given by a real vector function $\omega \rightarrow \tilde{v}(\omega)$ with ℓ elements.

We are looking for the "best" model of the structure within the mentioned class of models. That is we want to find a vector $d^* = (d_1^*, \dots, d_n^*)$, minimizing over R^n the norm of error function

$$v(\omega; d) - \tilde{v}(\omega) \quad , \quad (1)$$

given over interval $\omega_0 \leq \omega \leq \omega_N$.

Since the error (1) is a vector with ℓ real elements, we may use the Euclidean norm

$$\|v(\omega; d) - \tilde{v}(\omega)\|_2 = ((v(\omega; d) - \tilde{v}(\omega))^T (v(\omega; d) - \tilde{v}(\omega)))^{1/2}$$

and, assuming that this real function is square-integrable over $[\omega_0, \omega_N]$, the integral norm

$$\| \|v(\omega; d) - \tilde{v}(\omega)\|_2\|^2 = \int_{\omega_0}^{\omega_N} \|v(\omega; d) - \tilde{v}(\omega)\|_2^2 d\omega$$

can be used.

Hence the mentioned identification problem is equivalent to the determination of a minimizer $d^* = (d_1^*, \dots, d_n^*)$ of the integral

$$J(d) = \int_{\omega_0}^{\omega_N} (v(\omega; d) - \tilde{v}(\omega))^T (v(\omega; d) - \tilde{v}(\omega)) d\omega \quad (2)$$

In practice, the analytical form of $v(\omega; d)$ is not available and response $\tilde{v}(\omega)$ of the actual structure is known only for fixed values of ω , say $\omega_0 < \omega_1 < \dots < \omega_N$. Therefore, integration can be carried out only by means of numerical methods. If e.g. the trapezoidal rule for non-equally spaced abscissa is used, we will have

$$J(d) \approx f^T(d) S f(d), \quad (3)$$

where

$$f(d) = \begin{bmatrix} v(\omega_0; d) - \tilde{v}(\omega_0) \\ v(\omega_1; d) - \tilde{v}(\omega_1) \\ \vdots \\ v(\omega_N; d) - \tilde{v}(\omega_N) \end{bmatrix} \quad (4)$$

is a vector with $m = l(N+1)$ function-elements and

$$S = E_l \times S_{N+1} \quad (5)$$

is the direct product of the identity matrix of order l and diagonal matrix

$$S_{N+1} = \frac{1}{2} \langle \omega_1 - \omega_0, \omega_2 - \omega_0, \omega_3 - \omega_1, \dots, \omega_N - \omega_{N-2}, \omega_N - \omega_{N-1} \rangle. \quad (6)$$

Since $\omega_0 < \omega_1 < \dots < \omega_N$, S is a symmetric positive definite matrix and thus the right-hand side of (3) means the square of the so-called elliptic norm of vector f .

Thus minimization of integral $J(d)$ and, consequently, identification of vector $d = (d_1, \dots, d_n)$ can be reduced to minimization of the elliptic norm of a function

$$f: R^n \rightarrow R^m, \quad m \geq n,$$

that is to minimization of functional

$$F(d) = \|f(d)\|^2 = f^T(d) S f(d) \quad (7)$$

where S is a real symmetric positive definite (weighting) matrix of order m .

3. Equations of motion

The equations of motion of the system assume a slight in-plane motion and use the transversal displacement of bar element end points $y_0 = 0, y_1; i = 1, \dots, n$ as co-ordinates (see Fig. 2).

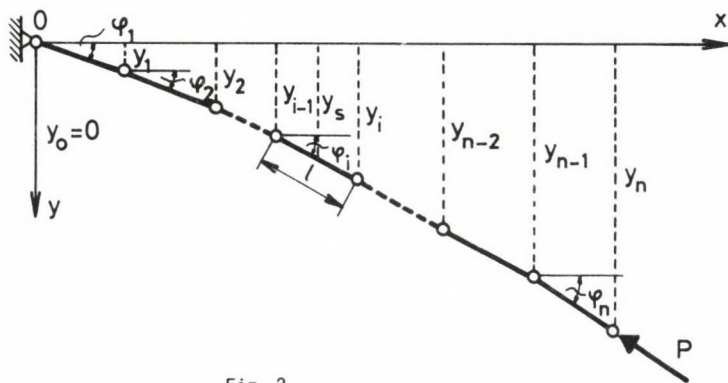


Fig. 2.

Motion energy of the bar chain is

$$T = \frac{1}{2} \dot{y}^T M \dot{y},$$

where the elements of vector \dot{y} are velocities \dot{y}_i , $i = 1, \dots, n$ and

$$M = \frac{1}{6} \begin{bmatrix} 2(m_1+m_2) & m_2 & & & \\ m_2 & 2(m_2+m_3) & m_3 & & \\ & m_3 & 2(m_3+m_4) & m_4 & \\ & & \ddots & \ddots & \ddots \\ & & & m_{n-1} & 2(m_{n-1}+m_n) \\ & & & & m_n & 2m_n \end{bmatrix} \quad (8)$$

is the so-called mass matrix, always positive definite.

Potential energy of return moments supplied by hinge springs, proportional to the relative rotation of bar elements, is given by relationship

$$V = \frac{1}{2} y^T \tilde{C} y, \quad$$

where the elements of vector y are coordinates y_i ; $i = 1, \dots, n$ and

$$\tilde{C} = \begin{bmatrix} \tilde{C}_{11} & \tilde{C}_{12} & \tilde{C}_{13} & & & \\ \tilde{C}_{21} & \tilde{C}_{22} & \tilde{C}_{23} & \tilde{C}_{24} & & \\ \tilde{C}_{31} & \tilde{C}_{32} & \tilde{C}_{33} & \tilde{C}_{34} & \tilde{C}_{35} & \\ & \cdot & \cdot & \cdot & \cdot & \\ & \tilde{C}_{n-2,n-4} & \tilde{C}_{n-2,n-3} & \tilde{C}_{n-2,n-2} & \tilde{C}_{n-2,n-1} & \tilde{C}_{n-2,n} \\ & & \tilde{C}_{n-1,n-3} & \tilde{C}_{n-1,n-2} & \tilde{C}_{n-1,n-1} & \tilde{C}_{n-1,n} \\ & & & \tilde{C}_{n,n-2} & \tilde{C}_{n,n-1} & \tilde{C}_{nn} \end{bmatrix} \quad (9)$$

is the so-called spring matrix, always positive definite, with elements

$$\left. \begin{aligned} \tilde{C}_{ii} &= \frac{1}{\ell^2} (c_i + 4c_{i+1} + c_{i+2}) \\ \tilde{C}_{i,i+1} &= \tilde{C}_{i+1,i} = -\frac{2}{\ell^2} (c_{i+1} + c_{i+2}) \\ \tilde{C}_{i,i+2} &= \tilde{C}_{i+2,i} = \frac{1}{\ell^2} c_{i+2} \end{aligned} \right\} \quad i = 1, \dots, n-2$$

$$\tilde{C}_{n-1,n-1} = \frac{1}{\ell^2} (c_{n-1} + 4c_n), \quad \tilde{C}_{n,n} = \frac{1}{\ell^2} c_n$$

$$\tilde{C}_{n-2,n} = \tilde{C}_{n,n-1} = -\frac{2}{\ell^2} c_n$$

and $\tilde{C}_{ij} = 0$ otherwise.

Effect of damping moments supplied by the device, proportional to the relative angular velocity of the bar elements, can be expressed by means of dissipation function

$$F = \frac{1}{2} \dot{y}^T D \dot{y},$$

where the so-called damping matrix D has the same five-diagonal form as the spring matrix (9) and it is positive definite because of the viscous damping force. Elements D_{ij} of matrix D are given by formulae

$$\left. \begin{aligned} D_{ii} &= \frac{1}{\ell^2} (d_i + 4d_{i+1} + d_{i+2}) \\ D_{i,i+1} &= D_{i+1,i} = -\frac{2}{\ell^2} (d_{i+1} + d_{i+2}) \\ D_{i,i+2} &= D_{i+2,i} = \frac{1}{\ell^2} d_{i+2} \end{aligned} \right\} \quad i = 1, \dots, n-2$$

$$D_{n-1,n-1} = \frac{1}{\ell^2} (d_{n-1} + 4d_n), \quad D_{nn} = \frac{1}{\ell^2} d_n$$

$$D_{n-1,n} = D_{n,n-1} = -\frac{2}{\ell^2} d_n$$

and $D_{ij} = 0$ otherwise, where d_i , $i = 1, \dots, n$, is the damping coefficient in hinge i .

The effect of disturbing forces $P_i \sin \omega t$ applied to nodes $i = 1, \dots, n-1$ of the chain and the effect of "follower" force P_n applied to the free chain end (see Fig. 1) are expressed by the vector of generalized forces,

$$Q = P \sin \omega t + R y$$

where

$$P = [P_1, \dots, P_{n-1}, 0]^T$$

and

$$R = \frac{P_n}{\ell} \begin{bmatrix} 2 & -1 & & & \\ -1 & 2 & -1 & & \\ & \ddots & \ddots & \ddots & \\ & & -1 & 2 & -1 \\ & & & 0 & 0 \end{bmatrix}$$

is a tri-diagonal non-symmetric matrix of order n .

Substituting into the Lagrange motion equation,

$$\frac{d}{dt} \left(\frac{dT}{d\dot{y}} \right) + \frac{dF}{d\dot{y}} + \frac{dV}{dy} = Q,$$

we obtain

$$M\ddot{y} + D\dot{y} + \tilde{C}y = P \sin \omega t + R_y$$

Rearranging:

$$M\ddot{y} + D\dot{y} + Cy = P \sin \omega t \quad (10)$$

where

$$C = \tilde{C} - R$$

with the elements

$$\left. \begin{aligned} C_{ii} &= \frac{1}{l^2} (c_i + 4c_{i+1} + c_{i+2}) - \frac{2}{l} P_n \\ C_{i,i+1} &= C_{i+1,i} = -\frac{2}{l^2} (c_{i+1} + c_{i+2}) + \frac{P_n}{l} \\ C_{i,i+2} &= C_{i+2,i} = \frac{1}{l^2} c_{i+2} \end{aligned} \right\} \quad i = 1, \dots, n-2$$

$$C_{n-1,n-1} = \frac{1}{l^2} (c_{n-1} + 4c_n) - \frac{2}{l} P_n, \quad C_{nn} = \frac{1}{l^2} c_n$$

$$C_{n-1,n} = -\frac{2}{l^2} c_n + \frac{P_n}{l}, \quad C_{n,n-1} = -\frac{2}{l^2} c_n$$

and $C_{ij} = 0$ otherwise.

Like matrices \tilde{C} and D , matrix C is also a five-diagonal band matrix of order n but it is non-symmetric because $C_{n-1,n} \neq C_{n,n-1}$.

If we are looking for the particular solution of the differential equation (10), expressing stationary vibration, in a form

$$y(t) = a \sin \omega t + b \cos \omega t \quad (11)$$

then, substituting it into the equation (10), we will obtain the system of linear algebraic equations of order $2n$

$$\begin{bmatrix} C - \omega^2 M & -\omega D \\ \omega D & C - \omega^2 M \end{bmatrix} \begin{bmatrix} a \\ b \end{bmatrix} = \begin{bmatrix} P \\ 0 \end{bmatrix}. \quad (12)$$

Solution of this system of equations is vector

$$v(\omega; d) = \begin{bmatrix} a(\omega; d) \\ b(\omega; d) \end{bmatrix} \quad (13)$$

occurring in the integral (2), that is $v: [\omega_0, \omega_N] \times \mathbb{R}^n \longrightarrow \mathbb{R}^{2n}$.

The j -th element of vector function (11),

$$y_j = a_j \sin \omega t + b_j \cos \omega t ,$$

describes the vibration of the j -th bar element end point with amplitude $\sqrt{a_j^2 + b_j^2}$. Hence the j -th and $(n+j)$ -th element of solution $v(\omega; d)$ of equation (12) mean components a_j and b_j of this amplitude.

The elements of vector

$$\tilde{v}(\omega) = \begin{bmatrix} \tilde{a}(\omega) \\ \tilde{b}(\omega) \end{bmatrix} \quad (14)$$

are values specified for the corresponding elements of vector $v(\omega; d)$.

The measured values of the stationary solution i.e. the elements of the vector (14) were simulated as follows: The stationary solution of system $v(\omega; d^0)$ i.e. the values of amplitude-components $a_i(\omega)$, $b_i(\omega)$, $i = 1, \dots, n$ in points $\omega_0, \omega_1, \dots, \omega_N$ were computed with given damping coefficients $d^0 = (d_1^0, \dots, d_n^0)$ and then subjected to small perturbations according to formula

$$\begin{aligned} \tilde{v}_i(\omega_j) &= (1 + 10^k \alpha_{ij}) v_i(\omega_j; d^0), \quad i = 1, \dots, 2n; \\ j &= 0, \dots, N, \end{aligned}$$

where $\alpha_{ij} \in [-1, 1]$ are pseudorandom numbers generated according to normal distribution and k is a negative integer expressing the "magnitude" of perturbation.

With these simulated amplitude-components used as input data, the corresponding damping coefficients, $d^k = (d_1^k, \dots, d_n^k)$, were calculated again using the minimization method, recommended.

Sensitivity of the identification process i.e. variation of the norm of error $d^k - d^0$ as a function of k is shown in Fig. 3.

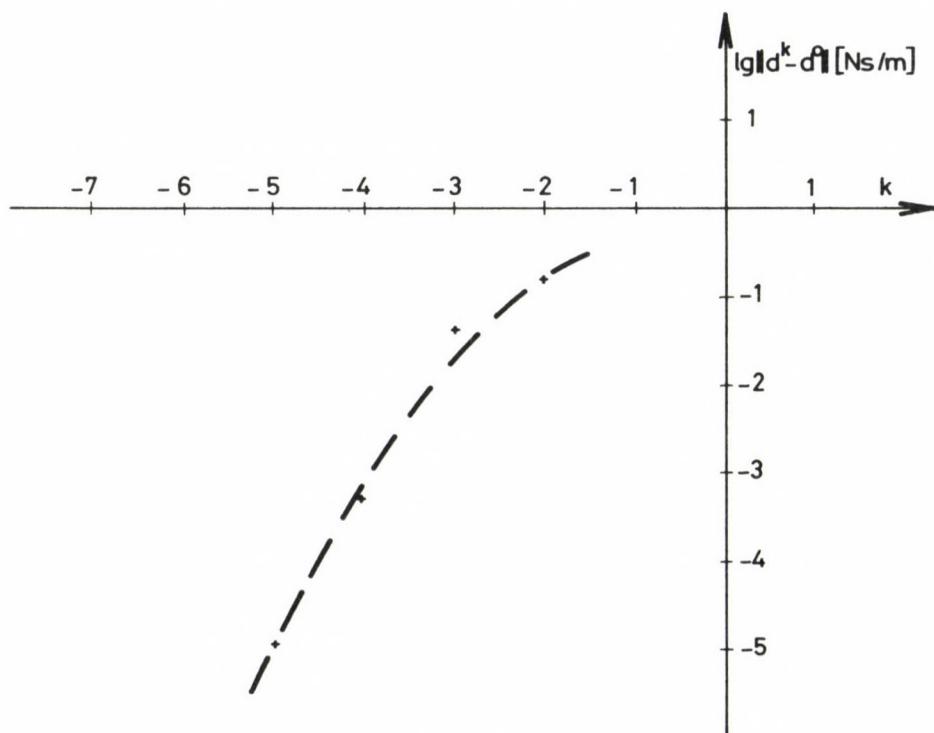


Fig. 3.

The disturbing forces and the follower force have been specified. Substituting (13) and (14) into (4), we obtain a function

$$f : R^n \longrightarrow R^m, \quad m = 2n(N + 1),$$

and identification of the damping coefficients has been reduced to minimization of the elliptic norm (7) of f .

4. Minimization method

To minimize the elliptic norm of function $f: R^n \rightarrow R^m$, $m \geq n$, a numerically very efficient non-derivative method suggested in [1] has been used. A variant of the Gauss-secant method has been combined with singular value decomposition of matrices.

A comparison of the secant method with a few non-derivative minimization methods shows that, as compared with any other method included in the comparison, the secant method needs much less functional values to be calculated for production of the minimizing vector to the same accuracy in case of the test functions used, the difference being an order of magnitude.

Each step of the Gauss-secant iteration includes the solution of a system of linear equations of number n . In the vicinity of minimizer d^* of functional (7), the linear independence of the columns of their matrices is gradually reducing, resulting in instability of the method.

This instability can be avoided by decomposition of the matrices into singular values as a method to solve the mentioned system of linear equations. In this way, the coefficient matrix of rank r and of spectral condition number σ_1/σ_n is deflated to a matrix of spectral condition number σ_1/σ_r , where σ_1 and σ_n are the largest and the smallest singular value, respectively, while σ_r is the smallest positive singular value.

This procedure is functionable until the coefficient matrix becomes equal to zero matrix. However, a zero matrix means that the solution has been obtained.

For details see [1].

5. Conclusions

The results of numerical computation shown in Fig. 4 and 5 can be summarized as follows: In case of conservative load, a small change in the amplitude-elements results in small changes in the damping coefficients (see Fig. 4). This result applies also to small values of the follower force but above a certain value, the conditions of the problem are gradually destroyed (see Fig. 5). This limit of the follower force depends on the actual frequency range.

In case of simulation of the measured values without perturbations, the damping coefficients assumed can be accurately identified. Mathemati-

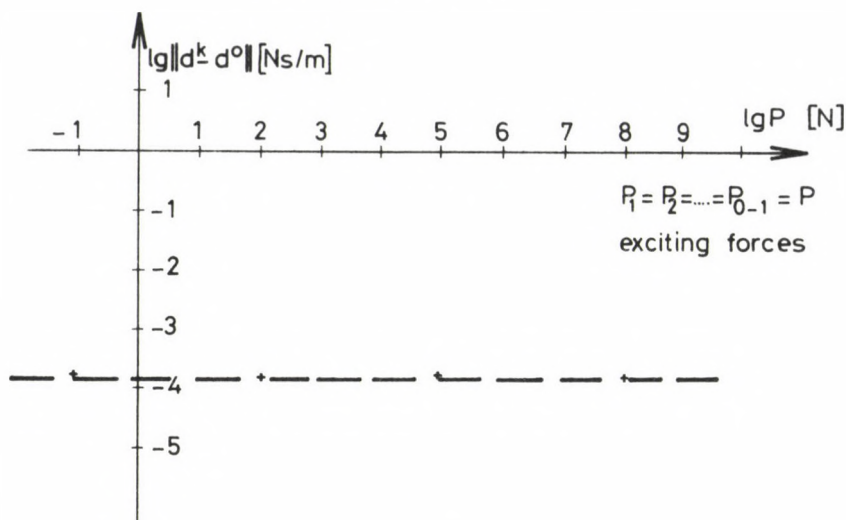


Fig. 4.

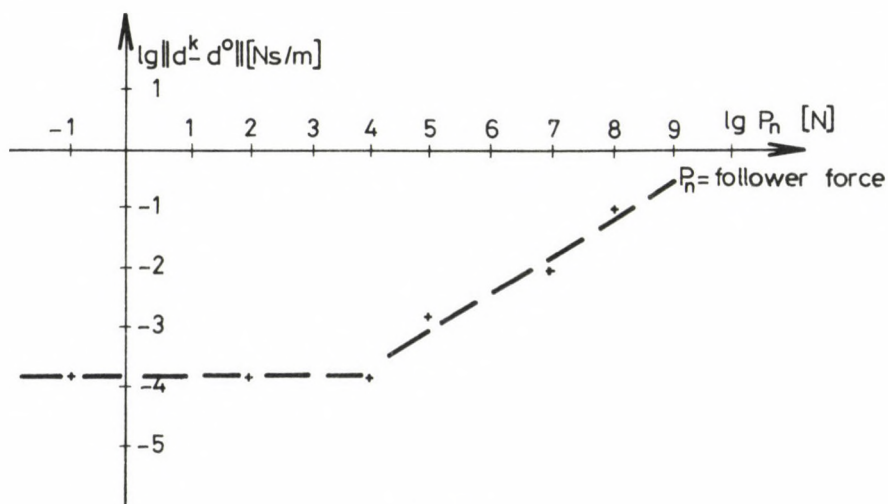


Fig. 5.

cally this corresponds to the special case when the minimum value of functional (7) is equal to zero.

REFERENCES

1. Popper, Gy. - Csizmás, F.: Minimization by the secant method, with an application to identification of frames. Acta Techn. Hung., 100, 3-4. 1988
2. Bosznay, Á.: Private communication

THE GENERAL STATE CHANGE EQUATION OF BAR STRUCTURES

ROLLER, B.*

(Received: 10 January 1990)

The role of time in the general analysis of the state change of bar structures is considered. The concept of influence arrays and some new variants of the superposition integral for linear elastoviscous materials are introduced. These new variants can be used to describe any sort of loading distribution. A sample problem is shown based on the 2nd principle of Colonetti. The state change integral transformation can be used in the matrix integral equation of trusses published formerly by the author.

1. Introduction

The state change equation of the 1st order theory of bar structures provides a concise synthesis of the classical theory of structures /19/ and contains the following assumptions: the structure is completely linear elastic; displacements in loading are infinitesimally small compared with the size of the structure; the equilibrium condition for the initial shape of the structure assumes no loading.

In the case of loads of unlimited measure that create small deformation, the state equation may be solved by conventional computation methods. The computational results confirm the required assumptions about the displacements and the constitutive equations. In fact, this method doesn't require a real state change analysis. By omitting the assumption of complete elasticity and, instead, introducing either elastoplastic /8/ or elastoviscous /2/ materials, a kind of state change analysis can be developed. In the treatment of elastoplastic materials, the concept of time has no role in the analysis, but the quality of the material (and consequently the state of the structure) changes.

Elastoviscous materials introduce a time element into the analysis and change the quality and state of the structure as well.

The introduction of plasticity makes the original linear problem nonlinear. The introduction of viscosity, on the other hand, results in either

*Roller, Béla, H-1027 Budapest, Mártírok útja 54, Hungary

a linear or non-linear problem depending the form of the constitutive law /1/. Amplification of the basic equations can be performed in both directions. The first direction results in a problem that requires mathematical programming for a computer solution /28/. The second direction, considered by the author, can be solved by a linear matrix integral equation /17/. Proper mathematical tools of the solution can be found in /3/.

Structures with conditional constraints /10/, /12/ also undergo a kind of state change. Linearity ceases in case of structures containing joints caulking or locking during the loading process /9/, /13/.

Each of the previously mentioned references deals only with linear geometry. This supposition is unacceptable in the analysis of cable nets. Hungarian researchers are active in the analysis of large displacements of suspended roofs over a long period of time /21/; thus, a 1st order analysis is unacceptable.

With fully linear elastic materials, the shape of the structure alters as a consequence of the loading process. Secondary shape effects in the equilibrium equations result in a kind of altering state even in case of small displacements. The analysis of this altering state is known as the 2nd order theory of the state equations. This theory treats the altering state as a hypermatrix equation and contains a matrix \underline{D} that registers the effects of the geometry in the equilibrium equations. Thus, displacements are involved in the equations.

An exact analysis of the altering state can be performed only by making use of a 3rd order theory that takes into account large displacements as well /22/, /25/. The 3rd order theory considers the equations of the 2nd order theory plus a hypervector of generalized forces. This hypervector contains the displacements and the generalized stresses as differentials. The concept is based upon an initial value problem belonging to an initial state that provides an equilibrium path. The resulting equations are published in /22/ and the numerical treatment of the equilibrium path is detailed in /4/. The 3rd order theory has been used in stability analysis /5/ and in the field of post-critical behavior /20/. The eigenvalue problem contained in /23/ has been generalized to the case of an eigenvalue problem with several parameters /18/. Mathematical solution tools are available in /15/.

An obvious extension of the state equation /19/ dealing with structural dynamics /7/ should be mentioned here. Processes of vibration can be analysed by a classic method which is numerically well treated. This treat-

ment can include viscous and hysteretical effects. Making use of a geometrical stiffness matrix to be found in /18/, a geometrical stiffness matrix dependent on frequency has been developed that includes the effects of shear stress and is suitable for the vibration analysis of bar structures /6/. Plates, folded shells, box girders, etc., can be constructed analytically by using the concept of bar structures having a pattern of stripes that make up the more complicated structures. Some analytical complications are introduced that are not present in simple bar structures but - on the other hand - the degrees of freedom are reduced. Problems due to inhomogeneous boundary conditions have been mastered and efficient methods of calculating continuous beams, boxes and curved bridges have been compiled. Thus, many detailed problems in bridgebuilding construction have been solved /26/, /27/. The reference publications take into account initial strains that are most important in the analysis of bridges and other structures.

In summary, the aforementioned papers provide a basis for development of a quite general altering state equation of bar structures that considers large displacements, branches of the equilibrium path, any kind of constitutive law, general materials of rheonomic behavior with the connection between structural joints and the loading distribution as a function of time for the real parameter of the state change being time itself. This problem remains to be treated by scientists.

2. Influence arrays

The loading effects of a bar can be included in the theory of structures most simply as a quantity depending on two independent variables. If the quantity changes continuously, we will deal with an influence or loading function. If changes occur in a discrete manner, an influence matrix may be used (influence lines and influence surfaces are not considered).

An influence function can be generalized as follows. Let C be a function of eight independent variables. Considering continua, we have

$$C = C(x, y, z, t; \xi, \eta, \zeta, \tau) \quad (1)$$

where x, y, z characterize a selected point of the continuum analyzed at the

moment t . ξ, η, ζ define (generally) another point of the continuum influenced by e.g. an impulsive force at the moment $\tau \leq t$.

C is denoted as the Generalized Influence Function. In case of bar structures, the influence may be analyzed for each bar

$$\begin{aligned} C &= C_{ij}(x, t, \xi, \tau) & i, j &\in (1, 2, \dots, r) \\ x &\in (0, L_i) & \xi &\in (0, L_j) & t &\in (0, T) & \tau \leq t &\in (0, T) \end{aligned} \quad (2)$$

$T \Rightarrow \infty$, but we can consider just a set of data containing finite number of elements.

(Instead of the usual concentrated forces, we make use of a unit impulse or stationary load.)

We may discretize the four continuous variables and denote the adequate values interpreted in a local frame as

$$\begin{aligned} x_i &= \frac{m}{n} L_i & t_k &= \frac{0}{p} T \\ m &= 0, 1, \dots, n & 0 &= 0, 1, \dots, p & \tau_\ell &\leq t_\ell \\ \xi_j &= \frac{m}{n} L_j & \tau_k &= \frac{0}{p} T \end{aligned}$$

$n + 1$ = number of intervals on L_i , $0/p$ = relative time interval.

Influence C may now be represented by an array of four dimensions:

$$C = C_{i,j,k,\ell} \quad (3)$$

This array is defined as an influence array.

Since each bar of a structure may be divided into several parts containing a different cross-section each and a different load may act upon each part, we can form more arrays of type (3) for the same structure. Other definitions differing from (3) may be presented as well - for instance, by enumerating nodes rather than bars.

As an example, consider the bar structure of Fig. 1. Part a) of the figure shows the arrangement and the load of the structure. Part b) shows a movable unit load chosen as an impulse. Next to the loading profile shown by graph $r(t)$, the time dependence function of the output resulting from an input Dirac-delta impulse load /11/ is presented. Part c) has a

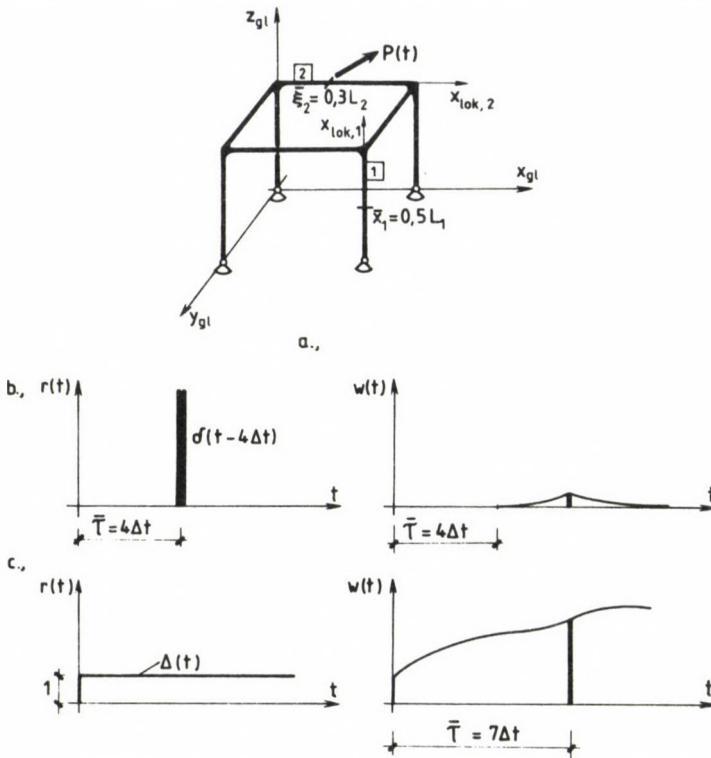


Fig. 1.

similar content showing the results from a stationary load. Note the ordinates of the function $M_{tw,1}$. Bars are divided in $K = 10$ parts. The figure illustrates the physical meaning of element C/5,7,3,4/ of the influence array; e.g., the influence from a twisting moment at cross-section $x_1 = 0.5L_1$ due to a force acting upon cross-section $\xi_2 = 0.3l_2$. Force $P(t)$ is variable in time. Any t time interval may be selected by the analyst. The impulse is described by Dirac distribution $\delta(t-\tau)$ defined by

$$\tau \neq t \quad \delta(t-\tau) = 0, \quad \int_{-\infty}^{\infty} \delta(t-\tau) d\tau = 1 \quad (4)$$

(see /11/).

The process function describing a permanent load is the Heaviside function:

$$0 > t \quad \Delta(t-\tau) = 0, \quad 0 \leq t \quad \Delta(t-\tau) = 1 \quad (5)$$

The computational method used in obtaining the elements contained in the influence array depends on certain circumstances of the loading that is on whether the space and time depending part of the altering state are separate or not; and on the choice of the constitutive law. Referring to a truss on three supports made of homogeneous material and selecting a quite simple example of a linear elastic time invariant material, we obtain a problem which is separable. Consider, also, a stationary load and make use of the "Second Particular Correspondency Principle" due to Colonetti /14/. Using Young's modulus as $E = 1 \text{ N cm}^{-2}$ and instants $t = \tau = 0$, the influence array can be determined so as to compile the influence matrix (e.g., that of the stress elements). The elements of this matrix shall be multiplied by the values of the creep-function calculated at appropriate periods /14/.*

3. Several variants of the creep and relaxation integral

The behavior of linear elastoviscous time invariant materials, which are consequently in a uniaxial state of stress, is described by the superposition integral of Boltzmann and Volterra /2/. We demonstrate the use of this formula in the case described in Fig. 2. The loading distribution $r(t)$, is at least piece-wise continuous. The response function, $H(t)$, resulting from the input Heaviside function $\Delta(t)$, is the beginning of the deduction. Making use of this, horizontal strips on $r(t)$ are performed. The results can be written as:

$$R(t) = r(t) H(0) + \int_0^t r(\tau) \dot{H}(t-\tau) d\tau \quad (6)$$

In the case of creep, we have

$$R_C(t) = r(t) J(0) + \int_0^t r(\tau) K_C(t-\tau) d\tau \quad (7)$$

In the case of relaxation, we have

$$R_R(t) = r(t) Y(0) = \int_0^t r(\tau) K_R(t-\tau) d\tau \quad (8)$$

* /14/ refers to the last two sentences of the introduction as well.

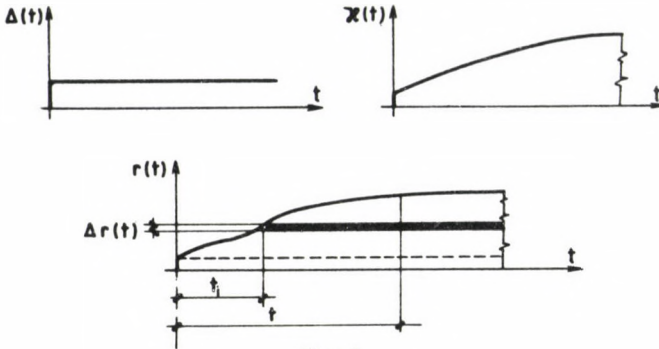


Fig. 2.

where $J(t)$ is the creep compliance function and $Y(t)$ is the stress relaxation function. Furthermore, $k_c = I_c(t)$ are the creep kernel and relaxation kernel respectively. The first part of (8) is an instantaneous response, the second part is the after-effect.

An alternate form of (6) may be derived by making use of integration by parts. Let

$$r(t) = \dot{s}(t), \quad \text{thus} \quad s(t) = \int_0^t r(\tau) d\tau$$

$$\text{then} \quad \int_0^t r(\tau) \dot{H}(t-\tau) d\tau = s(\tau) \dot{H}(t-\tau) \Big|_0^t - \int_0^t s(\tau) \frac{d\dot{H}(t-\tau)}{d\tau} d\tau$$

the first term is $s(t) \dot{H}(0) - s(0) \dot{H}(t)$, while the second is

$$\int_0^t s(\tau) \ddot{H}(t-\tau) d\tau$$

where $()'$ denotes a derivative with respect to $(t-\tau)$, furthermore

$$\int_0^t s(\tau) \dot{H}(t-\tau) d\tau = \int_0^t \ddot{H}(t) s(t-\tau) d\tau$$

The integral on the left side is a convolution. Also

$$s(0) = \int_0^0 r(\tau) d\tau = 0$$

holds, thus

$$R(t) = r(t) H(0) + s(t) \dot{H}(0) + \int_t^0 \ddot{H}(t) s(t-\tau) d\tau \quad (9)$$

Instantaneous effects are represented by two members of this formula. Repeating this algorithm, we get

$$R(t) = r(t) H(0) + s(t) \dot{H}(0) + u(t) \ddot{H}(0) + \int_0^t \ddot{H}(t) u(t-\tau) d\tau \quad (10)$$

where $s(t) = \dot{u}(t)$. Thus

$$u(t) = \int_0^t s(\tau) d\tau \quad \text{and} \quad u(0) = 0.$$

Besides

$$s(\tau) = \int_0^\tau r(\tau^1) d\tau^1$$

where τ^1 is an intrinsic variable. Thus

$$u(t) = \int_0^t s(\tau) d\tau = \int_0^t \int_0^\tau r(\tau^1) d\tau^1 d\tau$$

Making use of notations

$$a) \quad r^i(t) H^i(0) = \int_0^t \int_0^\tau \dots \int_0^{\tau^{i-1}} r(\tau^{i-1}) d\tau^i \dots d\tau^1 d\tau \cdot \frac{d^i H(0)}{d\tau^i},$$

b) τ_i denotes the i -th intrinsic variable

$$c) \quad v(t) = \int_0^t \int_0^\tau \dots \int_0^{\tau^{(n-1)}} r[\tau^{(n-2)}] d\tau^{(n-2)} \dots d\tau_1 d\tau, \quad (11)$$

we obtain finally

$$R(t) = \sum_{i=0}^n r^i(t) H^i(0) + \int_0^t H^{(n+1)}(\tau) v(t-\tau) d\tau \quad (11)$$

The instantaneous load effect is shown in (11) by a sum while the aftereffect is shown by a multiple integral. With (11) we can determine the response (8) choosing an arbitrary n , being selected from the point of view of the computing machinery used for the computations.

Formula (6) is applied in the general form by systems theory. Viscoelasticity also makes use of (6); but with respect to Fig. 2, we know either the creep function (which is the strain due to unit stationary stress) or the stress relaxation (the stress due to unit stationary strain).

Both main characteristics of the material were determined in such a way that the base of the constitutive law had been stated via spring and piston models (Maxwell, Kelvin-Voigt, Poynting-Thomson, Burgers, etc.) and afterwards the differential equation of the model was integrated. Results were compared by experiments. The selected system of springs and pistons were used for calculations and compared to experimental results for slow deformation.

In the field of Civil Engineering, material tests are most suitably (or easily) made by applying a stationary dead load or a stationary initial strain. In electrical engineering, we can readily produce impulse loads of circuits by use of a momentary short circuit and such loads are frequently used for testing. It can be shown that (6) is valid for test functions like impulse as well, by starting the analysis with an integral concept of Lebesgue rather than that of Riemann. Considering the development of laboratory techniques, it is quite probable that Civil Engineering will change over to impulse loading or impulsive initial strain in the future. Thus time consuming tests will be replaced by more efficient and thrifty methods.

Formula (6) is called Boltzmann-Volterra superposition principle (integral) in Civil Engineering and Duhamel integral in Electrical Engineering. These equations can be derived from a stationary load (input) in such a manner that the conventional integral concept of Riemann can be used. Consider Fig. 3 input b) is the superposition of inputs c) and d). Let the response of (t) be $H(t)$.

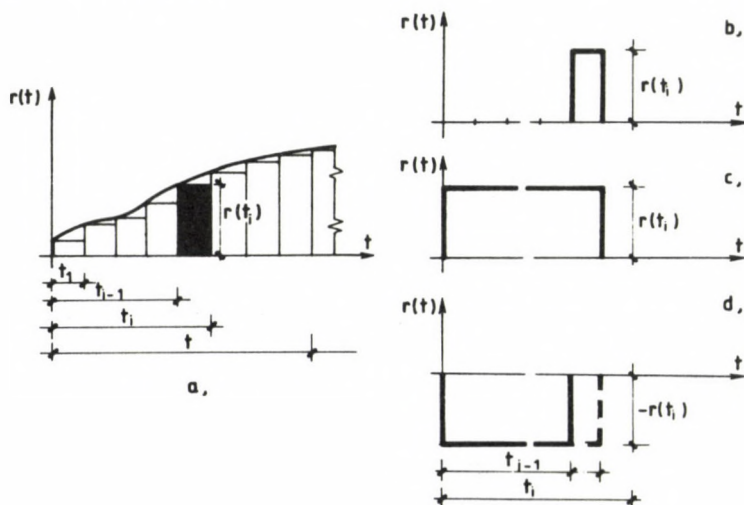


Fig. 3.

The response of input c) is

$$r(t_i)H(t-0) - r(t_i)H(t-t_i) ,$$

while that of input d) is

$$-r(t_i)H(t-0) + r(t_i)H(t-t_{i-1})$$

The response of input b) is

$$\Delta R_i = r(t_i) [H(t-t_{i-1}) - H(t-t_i)] \quad (12)$$

Summing up the effects of n inputs gives

$$\sum_{i=1}^n \Delta R_i = \sum_{i=1}^n r(t_i) [H(t-t_{i-1}) - H(t-t_i)] \quad (13)$$

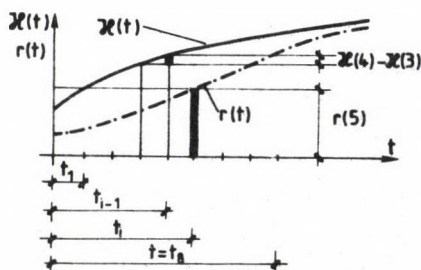


Fig. 4.

Interpretation of the expression after the summation symbol is shown by the example sketched in Fig. 4 where $i = 5$ and $n = 8$. After a limiting process and some transformations well known from /2/, we obtain equation (6) once again.

Formula (13) can be evaluated by numerical integration. The integration step is not necessarily unique and integrability does not presume continuity; i.e., the loading distribution may contain practically any kind of function or distribution. Thus, impulse loads can be approximated as well.

The superposition integral can also be approximated by using a step function as a test function. This function is defined by

$$t < t_{i-1}, \quad t > t_i \quad \nabla(t-t_i) = 0, \quad \text{else } \nabla(t-t_i) = 1$$

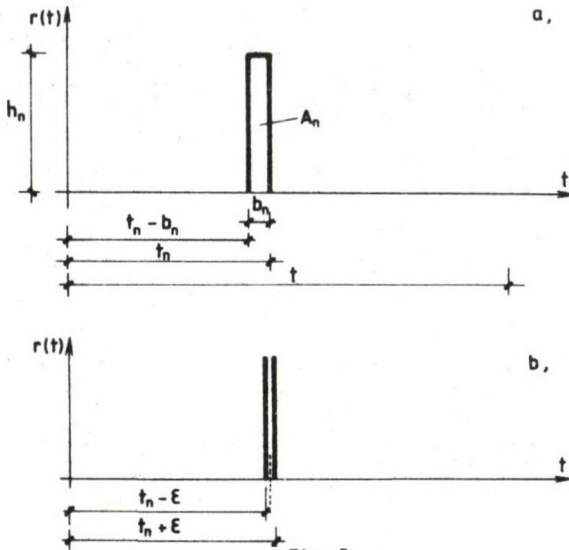


Fig. 5.

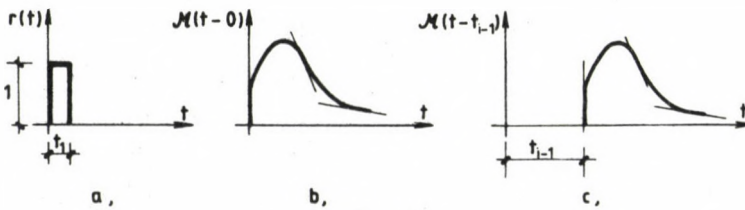


Fig. 6.

Suppose that a material in an axial state of stress has a response due to a step function as shown in Fig. 5. It is shown by experiment that this response is time invariant. So (Fig. 6)

$$M(t) \equiv M(t, 0) \equiv M(t-0) \quad \text{and} \quad M(t, t_{i-1}) = M(t-t_{i-1})$$

By definition input $r(t) \nabla(t)$ has a response $r(t)M(t)$ and input $r_i(t_i) \nabla(t-t_{i-1})$ is followed by $r(t_i)M(t-t_{i-1})$. Thus, any loading pattern can be approximated by a staircase of step loads as shown in Fig. 7a. A part of the input induces the response $K_i = r(t_i)M(t-t_i)$ and the sum of the inputs has an output

$$\sum_{i=1}^n \Delta K_i = \sum_{i=1}^n r(t_i) M(t-t_i) \quad (14)$$

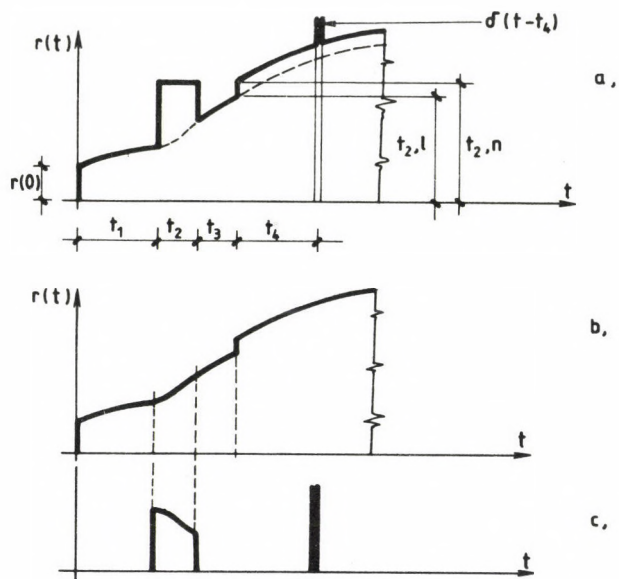


Fig. 7.

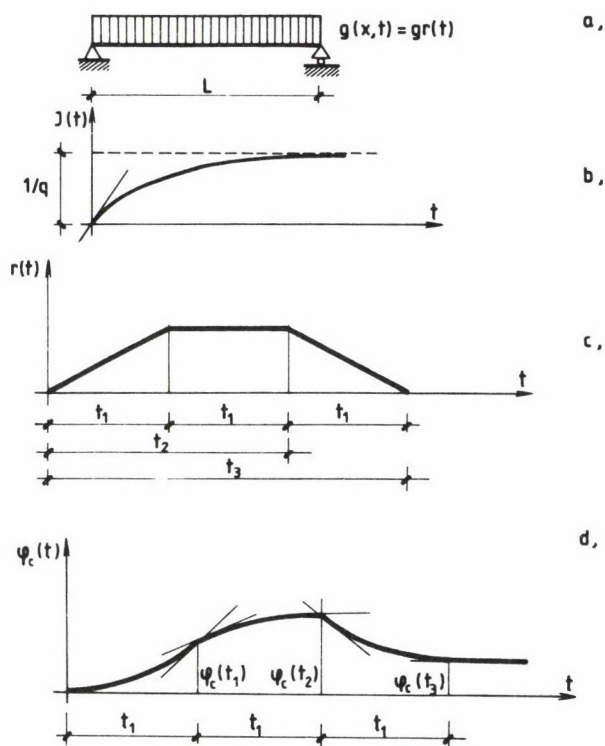


Fig. 8.

If the physical meaning of the relationships is concordant, (13) and (14) represent the same result. The latter is suitable for computations but more cumbersome to obtain laboratory results. Nevertheless it is possible to obtain procedures controlling each other.

In case of a quite general loading distribution, numerical integration can be performed (Fig. 7). The effect of loading distribution of Fig. 7 may be obtained by superposition of loads given by 7b and 7c.

Similar ideas may be used in foundation engineering where tests are made on sample soils and where the load may vary seriously; e.g., a containment foundation.

4. A sample problem

A test problem has been solved by analytical and numerical methods. A simpler variant of the problem is contained in /2/. The analytical method of solution resulted in definite integrals discussed in /11/. The load of a simply supported beam is $g(x,t) = g \cdot r(t)$ /see Fig. 8/. The constitutive law of the material is that of Kelvin-Voigt, the creep compliance function is given by

$$J(t) = \frac{1}{q_0} [1 - \exp(-\lambda t)] \quad \lambda = \frac{q_0}{q_1}$$

The loading distribution contains three linear parts:

$$\begin{array}{ll} 0 \leq t \leq t_1 & r(t) = t/t_1 \\ t_1 \leq t \leq t_2 & r(t) = 1 \\ t_2 \leq t \leq t_3 & r(t) = 3-t/t_1 \end{array}$$

else $r(t) = 0$

The deflection function is

$$v(x,t) = v(x) \varphi_c(t)$$

with

$$v(x) = \frac{gL^4}{24 I} \left[\left(\frac{x}{L} \right) - 2 \left(\frac{x}{L} \right)^3 + \left(\frac{x}{L} \right)^4 \right]$$

and

Diagram no. 1

Parameters: $q_0 = 130$ [kN/cm²], $\lambda = 1/6$ [1/h], $t_1 = 1$ [days]Function values at points $t = k \cdot t_1$ ($k = 0.5, 1, 1.5, 2, 2.5, 3, 3.5$)

- 1 . 1.958299E-03
- 2 . 5.804454E-03
- 3 . 1.245572E-02
- 4 . 1.335587E-02
- 5 . 9.507718E-03
- 6 . 7.551418E-03
- 7 . 7.551418E-03

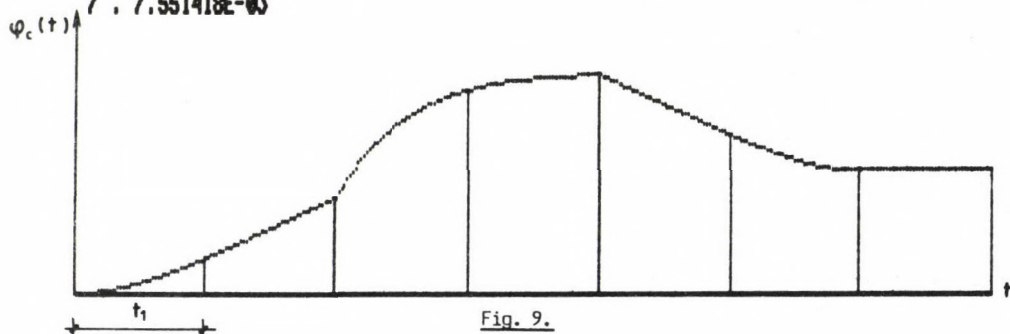
cm² kN⁻¹

Diagram no. 2

Parameters: $q_0 = 130$ [kN/cm²], $\lambda = 1/12$ [1/h], $t_1 = 2$ [days]Function values at points $t = k \cdot t_1$ ($k = 0.5, 1, 1.5, 2, 2.5, 3, 3.5$)

- 1 . 2.183337E-03
- 2 . 5.804453E-03
- 3 . 1.245572E-02
- 4 . 1.335587E-02
- 5 . 9.734755E-03
- 6 . 7.551419E-03
- 7 . 7.551419E-03

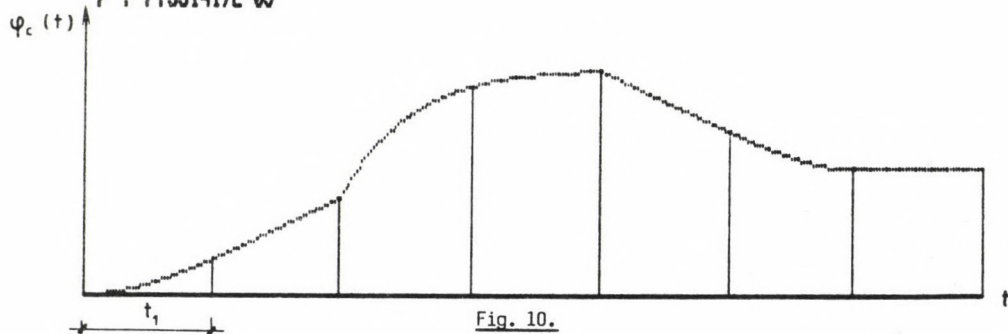
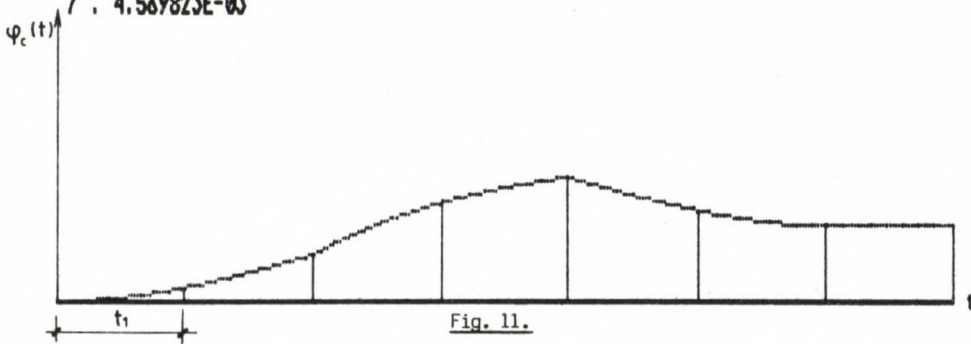
cm² kN⁻¹

Diagram no. 5

Parameters: $q_0 = 170$ [kN/cm²], $\lambda = 1/430$ [1/h], $t_1 = 30$ [days]Function values at points $t = k \cdot t_1$ ($k = 0.5, 1, 1.5, 2, 2.5, 3, 3.5$)

1. $8.720258E-04$ cm² kN⁻¹
2. $2.835805E-03$
3. $5.939531E-03$
4. $7.405628E-03$
5. $5.441849E-03$
6. $4.569823E-03$
7. $4.569823E-03$



$$0 \leq t \leq t_1 \quad \varphi_{c1}(t) = \frac{1}{q_0} \left\{ \frac{t}{t_1} - \frac{1}{\lambda t_1} [1 - \exp(-\lambda t)] \right\}$$

$$t_1 \leq t \leq t_2 \quad \varphi_{c2}(t) = \varphi_{c1}(t_1) + \frac{1}{q_0} \{1 - \exp[-\lambda(t-t_1)]\}$$

$t_2 \leq t \leq t_3$ $\varphi_{c1}(1)$ has to be transposed.

The deflection function, $\varphi_c(t)$, has been calculated for several numerical cases. Some results are presented in Fig. 9, 10 and 11, the calculations were checked with formula (13).

REFERENCES

1. Findley, W.N. - Lai, I.S. - Onaran, K.: Creep and relaxation of nonlinear viscoelastic materials. North Holland Publ. Comp., Amsterdam - New York, Oxford, 1976
2. Flügge, W.: Viscoelasticity 2. rev. ed., Springer, Berlin-Heidelberg-New York, 1975
3. Fodor, G.: Laplace Transforms in Engineering. Akadémiai Kiadó, Budapest, 1965
4. Gáspár, Zs.: Large Deflection Analysis of Bar Structures. Acta Techn. 87/1-2 (1978) 49-58
5. Gáspár, Zs.: Stabilitätsprüfung von Stabkonstruktionen. Acta Techn. 72/3-4 (1972) 315-322
6. Györgyi, J.: Frequency Dependent Geometrical Stiffness Matrix for the Vibration Analysis of Beam Systems. Per. Pol. Civ. Eng. Vol. 25. No. 3-4. (1981) 151-163

7. Györgyi, J.: Viscous and Hysteretic Damping in Vibration of Structures. Per. Pol. Civ. Eng. Vol. 29. No. 1-2 (1985) 23-31
8. Kaliszky, S.: Plasticity. Theory and Engineering Applications, Elsevier, Amsterdam-Oxford-New York-Tokyo 1989
9. Kaliszky, S.: The Analysis of Structures with Conditional Joints. Journal of Structural Mechanics. Vol. 6. No. 2. (1978) 195-210
10. Kaliszky, S. - Nédli, P.: Analysis of Elastoplastic Structures by Mathematical Programming, Acta Techn. 83 (1978) 205-212
11. Korn, G.A. - Korn, T.M.: Mathematical Handbook for Scientists and Engineers, McGraw Hill, New York 1968
12. Kurutz, M.: State Change Analysis of Structures with Generalized Conditional Joints. Per. Pol. Civ. Eng. Vol. 25. No. 3-4 (1981) 169-189
13. Kurutz, M.: Analysis of Plastic Load Capacity of Plane Frameworks by Kinematic Loading, Per. Pol. Civ. Eng. Vol. 18. No. 1-2 (1974) 71-82
14. Lipták, L.: Betonszerkezetek kúszása és a harántkontrakció. Kandidátusi értekezés tételei, Budapest, 1966. (Creep of RC structures and the transversal contraction, Ph.D. thesis).
15. Popper, Gy. - Gáspár, Zs.: Numerical methods for Solving Eigenvalue Problems of Lambda Matrices of Degree m . Acta Techn. 94/3-4 (1989) 103-109
16. Roller, B.: Viszkoelasztikus tartók állapotváltozási vizsgálata. Építés-építészettudomány IX. 3-4, Budapest, 1979, 221-239 (Altering state analysis of viscoelastic structures)
17. Roller, B.: Integral Equations for Linear Elasto-Viscous Skeletons. Per. Pol. Civ. Eng. Vol. 25. No. 3-4 (1981) 211-226
18. Roller, B. - Gáspár, Zs.: Generalization of the Stability Analysis of Elastic Systems, Per. Pol. Civ. Eng. Vol. 18. No. 1-2, (1974) 109-119
19. Szabó, J.: The Equation of State Change of Structures. Per. Pol. Mech. Eng. Vol. 17. No 1, (1971) 55-71
20. Szabó, J. - Gáspár, Zs.: Bolshie peremesheniya i poslekriticheskie sostoaniya stersnevnykh konstrukcii. Uspehy Mekhaniki 1/1-2 (1978) 171-181
21. Szabó, J. - Kollár, L.: Structural Design of Cable-Suspended Roofs. Akadémiai Kiadó, Budapest, 1984
22. Szabó, J. - Roller, B.: Rúdszerkezetek elmélete és számítása. Műszaki Könyvkiadó, Budapest 1971 (Theory and Computation of Bar Structures, in Hungarian)
23. Szabó, J. - Roller, B.: Anwendungen der Matrizenrechnung auf Stabwerke. Akadémiai Kiadó, Budapest 1978
24. Szabó, J. - Rózsa, P.: Die Matrizengleichung von Stabkonstruktionen. Acta Techn. Tom. 71. Fasc. 1-2 (1971) 131-146
25. Szabó, J. - Rózsa, P.: Grosse Verschiebungen von Stabkonstruktionen. Acta Techn. Tom. 73. Fasc. 1-2 (1972) 53-60
26. Szilágyi, Gy.: Quelques applications de la méthode des bandes finies. Mémoires AIPC, Vol. 34-II, Zürich 1974, 149-168
27. Szilágyi, Gy.: Inhomogeneous Boundary Conditions for Finite Strips. Per. Pol. Civ. Eng. Vol. 25. No. 3-4 (1981), 227-241
28. Vásárhelyi, A. - Grósz, M.: Elasto-Plastic Analysis of Continuum Structures by Nonlinear Programming. System Modelling and Optimization Proc. of 12. IFIP Springer Verlag 1984, 1008-1019

ATTRactions AND RISKS OF THE ANALOGIES

SCHARLE, P.*

(Received: 27 December 1989)

Analogous formulations taken from geodesy and mechanics may prove to be fruitful in developing, interpreting, even extending the well-known models. A detailed verification of the analogies, however, may lead to auxiliary conditions or limitations even in the conventional cases.

Introduction

Theories are not developing in the different fields of science simultaneously. Matching of the physical ideas, mathematical principles and analytical techniques or delay in the possible discoveries depend on the level of information, trends of mode, authority of the scientific schools, etc. Therefore, a comparative analysis of the scientific fields may result in very interesting lessons.

The mathematical ideas and tools, applied in physical sciences are common. We are using the same concepts and procedures to describe and formulate the most different problems. Even the geometry itself may be interpreted as a branch of physical sciences, and from the Noether-theorem it follows that the "conservation principles" are nothing but different interpretations of the same mathematical thesis. Therefore,

- one can establish analogies between different physical phenomena or processes, and may chose the same mathematical model to describe them - then the deeper understanding of the analogy inspires elaboration of less developed theories;

- identical mathematical models may be chosen by chance or deliberately, aware of their power to solve different physical problems not necessarily known to be analogous - in this case, the range of validity of the models shall be investigated and real analogies can be either discovered or rejected. Both aspects mentioned may be illustrated by analogies (either true or false) in relation to the concept of entropy. Starting from the

*Scharle, Péter, H-1112 Budapest, Mérédek u. 60, Hungary

phenomenological theory of heat, the entropy differential can be postulated as

$$dS = \frac{\delta Q}{T} \quad (1)$$

where δQ stands for the increment of heat and T denotes the temperature. Analogous concepts of geotechnical entropy (Moroto, 1976), economic entropy (Szabó, 1981, Bródy et al., 1986) etc. were defined then. Many interesting results have been obtained in this way. Nevertheless, the interpretation of dual intensive fields (corresponding to temperature) and that of the maximum entropy principle have remained ambiguous, even impossible in most cases and, as a rule, these analogies seem to be vulnerable. On the other side, starting with the entropy as it is defined in mathematical statistics,

$$S = - \sum_{(i)} p_i \ln p_i \quad , \quad (2)$$

different entropies can be defined (even within the framework of the same particular theory) without conflicting with duality problems (Brown, 1978, Lőrincz, 1986). However, in these cases the phenomena involved differ from the classic interaction problems, and no field theories have been posed (Scharle, 1989).

Closer and more fruitful analogies had been established in cases, where the ideas were connected with powerful, widely used mathematical concepts, theses and proofs relating to quadratic forms. The mathematical theory of quadratic surfaces, the Legendre-transformation, the classic interpretations and applications elaborated in the mechanical problems offer an appropriate basis for constructive analogies. Nevertheless, even in these cases, one has to be cautious in establishing correspondences. An interesting example presented in the next section shows that the most convincing analogies may have weak points and this shall be taken into account when we wish to exploit them.

Analogous extremum principles in geodesy and mechanics

The mechanical models - particularly the classic ones formulated many decades ago - serve as a good basis for establishing analogies. We could refer to the well known correspondence between the Kirchhoff-theory of electric networks and the theory of bar structures. However, passing by

this precisely elaborated example we shall draw the attention to a recent development, connecting some problems of geodesy and mechanics.

Starting with mechanical description, we assume that the reader is familiar with the theory of bar structures as it was formulated some two decades ago in the simple form of

$$\begin{bmatrix} 0 & G^T \\ G & F \end{bmatrix} \begin{bmatrix} u \\ s \end{bmatrix} + \begin{bmatrix} q \\ 0 \end{bmatrix} = \begin{bmatrix} 0 \\ 0 \end{bmatrix} \quad (3)$$

(Szabó, Roller, 1971), comprising both equilibrium and compatibility equations. The classic variational principles (formulated as the extrema of the potential and complementary energies) were derived as well (Roller, Szentiványi, 1974), and a more general stationarity condition of the Hellinger-Reissner functional, derived in the form of

$$-\frac{1}{2} s^T F s - q^T u - r^T (u-v) - s^T G u = \text{extr!} \quad (4)$$

proved to be equivalent to (3)* (Scharle, Szabó, 1974).

Turning to geodetic description and following a recent paper of Moritz (1988) we shall start with the most common procedure of "adjustment by parameters". Comprising the unknown scalar parameters (distances or angles, for example) in the vector x , design matrix A which informs about the arrangement and combination of the parameters shall be set up. Instead of direct determination, the transformed data of Ax can be observed. In general, number n of the measured quantities exceeds number m of the unknown parameters (therefore, the column vectors of A set out the m -dimensional subspace Ω_m of the n -dimensional vector space - Fig. 1). The observation equations are given then in the form of

$$l + v = Ax \quad (5)$$

*In the equations of (3) and (4) the following notations were used

- u - vector of the unknown nodal displacements
- v - vector of the prescribed nodal displacements
- s - vector of the unknown nodal forces
- q - vector of the given active nodal forces
- r - vector of the unknown reaction forces
- G - matrix of the geometric data
- F - matrix of the flexibility coefficients

where l denotes the measured data and v stands for the unknown corrections. Because the reliability of the measurements may differ from each other, it is natural to prescribe the condition

$$\frac{1}{2} v^T P v = \min! \quad (6)$$

for the vector v . Here P denotes the weight matrix, not necessarily identical with the unit matrix $I = [\delta_{ij}]$. This is the well-known least squares principle.

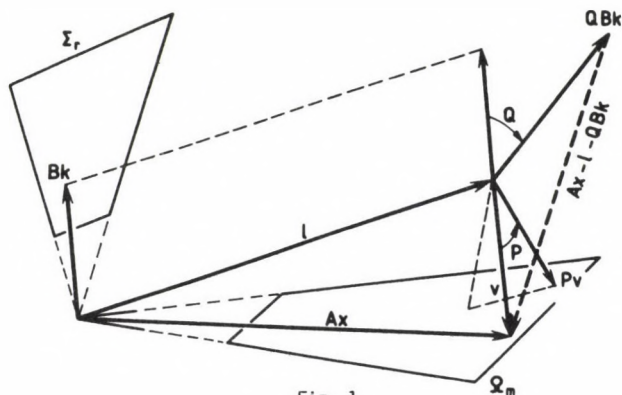


Fig. 1.

In the dual approach one can consider the linear equations relating the corrected observations

$$B^T(l + v) = 0 \quad (7)$$

(we assume that no additive constants occur in these equations). Because the number r of these equations is determined as $r = n - m$, the column vectors of B can be identified as the base vectors of r -dimensional space Σ_r , orthogonal to subspace Ω_m in the n -dimensional space, in the sense of $B^T A = 0$ (Fig. 1). The unknown vector of corrections can be expressed now as

$$v = QBk \quad (8)$$

where k stands for another set of r parameters (complementary to x) and $Q = P^{-1}$ denotes the covariance matrix. Using notation $w = B^T l$ for the "re-

siduals" we obtain the normal equation from (7) as

$$B^T Q B k + w = 0 \quad . \quad (9)$$

The adjoint extremum principle can be obtained (using k as a vector of the Lagrangian multipliers) from (6) and (7) in the form of

$$\frac{1}{2} k^T B^T Q B k + k^T w = \text{extr!} \quad (10)$$

Starting with these preliminaries Moritz shows that, by defining the distance between two points in the n -dimensional space (Fig. 2) by

$$d(p, q) = d^T P d \quad , \quad (11)$$

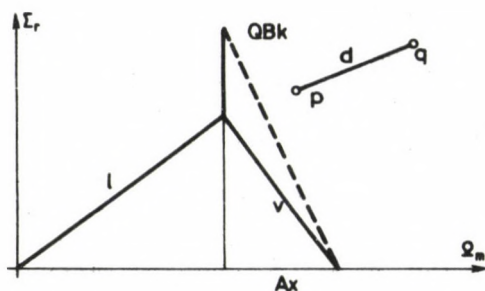


Fig. 2.

the adjoint formulations (6) and (10) can be obtained as

$$\frac{1}{2} (Ax - 1)^T P (Ax - 1) = \text{extr!} \quad (12a)$$

and

$$\frac{1}{2} (1 + QBk)^T P (1 + QBk) = \text{extr!}, \text{ respectively.} \quad (12b)$$

According to the well-known projection theorem, the orthogonality condition can be obtained as

$$A^T P (Ax - 1) = 0 \quad . \quad (13)$$

This means that the column vectors of A are normal to vector v in the sense of the inner product weighted by the metric matrix P .

Extensions and remarks

Note that the more general variational principles (referred to in continuum mechanics as the Hellinger-Reissner and the Hu-Washizu principles) can be easily interpreted in the Moritz-presentation. Consider vector $Ax - 1 - QBk$ as shown in Fig. 1. The bilinear form of

$$\frac{1}{2}(Ax - 1 - QBk)^T P(Ax - 1 - QBk) \quad (14)$$

can be resolved and simplified. In this way we obtain the generalized extremum principle

$$\frac{1}{2}(x^T A^T P A x + k^T B^T Q B k) - 1^T P^T A x - 1^T B k = \text{extr!} \quad (12c)$$

which corresponds to the Hu-Washizu principle and can be considered as a slight generalization of the Hellinger-Reissner principle. The stationarity conditions with respect to x and k are equations (13) and (9), respectively. Note that metric matrix P can be interpreted as an analogy to the constitutive matrices occurring in the mechanical models.

These coincidences could be considered as another argument for the perfect analogy between the mechanical and geodetical treatment. Nevertheless, this correspondence can be accepted with a delicate distinction only. In the mechanical models, namely, the extremum conditions can be formulated as error principles in an energy space defined with a single metric of a unique bilinear form (Scharle, 1976). In the geodetic models presented by Moritz, two different metrics are used simultaneously:

a) the orthogonality of the subspaces Ω_m and Σ_r is established with unit matrix I ,

$$B^T A = 0 \quad \text{and} \quad A^T B = 0 ;$$

b) the distances between the points of space $\Omega_m \cup \Sigma_r$ are measured with weighted metric matrix P .

We would not say that either of these metrics should be abandoned or could be eliminated. Even the difference disappears in the trivial case of $P = I$. Further analyses may clear up other interesting lessons, too. Nevertheless, this example shows that discovering and exploiting an analogy may have attractions and risky points, as well.

Acknowledgements

The author is deeply indebted to Dr. Gy. Alpár, who helped to elaborate this paper with valuable remarks and comments.

REFERENCES

1. Bródy, A. - Martinás, K. - Sajó, K.: Gazdasági és termodinamikai mérés, Közgazdasági Szemle, 1986, 1, 19-27
2. Brown, C.B.: The use of maximum entropy in the characterization of granular materials, in Continuum Mechanical and Statistical Approaches in the Mechanics of Granular Materials, (ed.: Cowin, S.C., Satake, M.), Gakujutsu Bunken Fukyu-kai, 1978, 98-108
3. Lőrincz, J.: A talajok szétosztályozásáról, MTA Műszaki Mechanikai Tanszéki Kutatócsoport IV. Tudományos ülészaka, Tanulmányok, 1986, 60-68
4. Moritz, H.: Reciprocity relations and analogies to elastostatics in least squares adjustment, Manuscripta Geodaetica (1988), 13, 156-163
5. Moroto, N.: A new parameter to measure degree of shear deformation of granular material in triaxial compression tests, Soils and Foundations, 1976, 4, 1-10
6. Roller, B. - Szentiványi, B.: Extrémum-tételek és alkalmazásaik a rúd- és felületszerkezetek másodrendű elméletében, MTA Műszaki Mechanikai Tanszéki Munkaközösség Tudományos ülészaka, 1974, Tanulmányok, 35-46
7. Scharle, P.: On the relationship between different approximating methods, Acta Technica, 82, 1976, 53-59
8. Scharle, P.: Thermodynamic aspects suggested for granular materials, Proceedings of the XII International Conference on Soil Mechanics and Foundation Engineering (Rio de Janeiro), 1989, 164-166
9. Szabó, J. - Roller, B.: Rúdszerkezetek elmélete és számítása, Műszaki Kiadó, 1971
10. Szabó, J.: Az építőipari technológiai váltás optimalásának makroökonomiai feltételei (manuscript), 1981. november
11. Szabó, J. - Scharle, P.: Über die Beziehungen zwischen der Theorie der Stabkonstruktionen und der Kontinuumaufgabe, Acta Technica, 79, 1974, 51-62

HIGHER-ORDER INFINITESIMAL MECHANISMS

TARNAI, T.*

(Received: 28 December 1989)

In this paper importance of the term "higher-order infinitesimal mechanism" is explained and different definitions of it are surveyed. Difficulties in the determination of the order of infinitesimal mechanisms are pointed out and it is shown how to overcome them. To help the understanding examples are also presented.

1. Introduction

In a paper on structural rigidity, among others the following two questions have been listed by Tarnai (1980) for future research:

(A) What criterion determines whether self-stress stiffens an assembly which is both statically and kinematically indeterminate?

(B) How can matrix methods be used to decide whether kinematical indeterminacy takes the form of an infinitesimal or a finite mechanism?

Koiter (1984) in his note on a preliminary version of the paper by Pellegrino and Calladine (1986) dealing with these two questions pointed out that a distinction only between infinitesimal and finite mechanisms is inadequate to deal with all possible cases of both statically and kinematically indeterminate structures; and since the second question cannot be answered directly, he suggested replacing it by the following question:

(B*) How can matrix methods be used to decide whether kinematical indeterminacy takes the form of an infinitesimal mechanism of the first order or of a higher order?

In both questions (A) and (B*) and also in their answers the term "higher-order infinitesimal mechanism" plays a crucial role.

The aim of this paper is to show the different approaches in defining infinitesimal mechanisms of higher order and to call attention to the special importance of higher-order infinitesimal mechanisms in the answer to question (A) given by Pellegrino and Calladine (1986) and generalized by Kuznetsov (1988).

*Tarnai, Tibor, H-1037 Budapest, Kolostor u. 17, Hungary

2. The notion of higher-order infinitesimal mechanism

2.1 Koiter's definition

Koiter (1984) has introduced a classification of infinitesimal mechanisms, which makes possible a more correct treatment of both statically and kinematically indeterminate structures. This classification consists of infinitesimal mechanisms of the first order (identical to infinitesimal mechanisms in the linear theory of structures) and infinitesimal mechanisms of the second and higher orders. Finite mechanisms are called of infinite order, and they are considered as exceptions.

Koiter (1984) has defined "an infinitesimal mechanism of the first order by its property that any infinitesimal displacement of the mechanism is accompanied by second order elongations of at least some of the bars. An infinitesimal mechanism is called of second (or higher) order, if there exists an infinitesimal motion such that no bar undergoes an elongation of lower than the third (or higher) order".

Tarnai (1984a) has tried to formulate Koiter's definition mathematically in the following way. Consider a bar-and-joint assembly which contains b bars and consider a system of infinitesimal displacements of the joints. Let us denote an infinitesimal displacement component of a characteristic joint by δ and the elongation of the bar k due to δ by e_k . Produce the power-series expansion of e_k in δ :

$$e_k = a_{1k}\delta + a_{2k}\delta^2 + a_{3k}\delta^3 + \dots \quad (k = 1, 2, \dots, b) \quad (1)$$

The structure is called infinitesimal mechanism if there exists a system of infinitesimal displacements of joints such that in (1) $a_{1k} = 0$ for $k = 1, 2, \dots, b$.

Definition 1 (Tarnai, 1984a): An infinitesimal mechanism is of order n ($n \geq 1$) if there exists a system of infinitesimal displacements of joints such that in (1) $a_{1k} = a_{2k} = \dots = a_{nk} = 0$ for $k = 1, 2, \dots, b$, but there exists no system of infinitesimal displacements of joints such that in (1) $a_{n+1,k} = 0$ for $k = 1, 2, \dots, b$, that is, there exists at least one bar m , $m \in \{1, 2, \dots, b\}$, such that $a_{n+1,m} \neq 0$.

A structure is an infinitesimal mechanism of infinite order if there exists a system of infinitesimal displacements of joints such that in (1) $a_{ik} = 0$ for $i = 1, 2, \dots$ and $k = 1, 2, \dots, b$.

Finite mechanism may be defined as a structure in which there exists a finite motion such that the elongation of every bar is zero.

Since every finite mechanism locally is an infinitesimal mechanism, it follows from the above definitions that every finite mechanism necessarily is an infinitesimal mechanism of infinite order. Its reverse, however, in general, is not valid.

Consider an infinitesimal mechanism with elongation in the bars:

$$e_k = C_k e^{-\frac{1}{\delta^2}} \quad (k = 1, 2, \dots, b) \quad (2)$$

where e on the right-hand side is the base of the natural logarithms and C_k ($k = 1, 2, \dots, b$) are constants. Forming its power-series expansion in δ (at point $\delta = 0$) we obtain $a_{ik} = 0$ for $i = 1, 2, \dots$ and $k = 1, 2, \dots, b$. The structure with bar elongation (2) is an infinitesimal mechanism of infinite order, but is not a finite mechanism since if $\delta \neq 0$ then $e_k \neq 0$.

Thus, we suggest making a distinction between infinitesimal mechanisms of infinite order and finite mechanisms.

So we have two classes of mechanisms: (a) infinitesimal and (b) finite mechanisms. And class (a) contains subclasses of infinitesimal mechanisms of the first, second, third, ..., infinite order.

Example 1 (Tarnai, 1984b). We show a simple example of both statically and kinematically indeterminate structures in which the kinematic indeterminacy can take the form of an infinitesimal mechanism of arbitrary order and also a finite mechanism. The structure in Fig. 1 consists only of one bar whose lower end is fixed against translations but free to rotate and upper end can slide in a rigid-walled plane slot. Let us apply a polar coordinate system r, φ (Fig. 2).

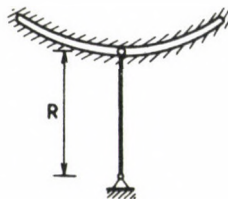


Fig. 1.

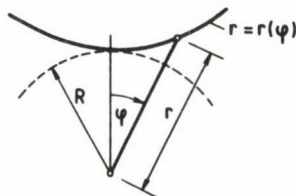


Fig. 2.

Let the equation of the slot curve be

$$r = R + C_1 \psi^{n+1} + C_2 e^{-\frac{1}{\psi^2}} \quad (3)$$

where C_1 and C_2 are constants and n is an integer. If $C_1 \neq 0$ and $n = 0$ then the structure is not an infinitesimal mechanism at $\psi = 0$. If $C_1 \neq 0$ and $n \geq 1$ then the structure is an infinitesimal mechanism of the n -th order at $\psi = 0$. If $C_1 = 0$ and $C_2 \neq 0$ then the structure is an infinitesimal mechanism of infinite order at $\psi = 0$. If $C_1 = C_2 = 0$ then the structure is a finite mechanism.

2.2 Connelly's definition

In mathematics the term n -th-order infinitesimal mechanism is not known but n -th-order flex is known instead, and it means practically the same.

Connelly (1980) has defined n -th-order flex in the following way. Let p_1, p_2, \dots, p_j be j points in the 3-space. Let E be a collection of b unordered pairs of these points. We call E the bars and $p = (p_1, \dots, p_j)$ the joints of a framework F . A bar is denoted by the indices of the two joints connected by the bar: $\{\ell, m\}$. We say a flex of a framework F is a continuous path for $0 \leq t \leq 1$, $p(t) = (p_1(t), \dots, p_j(t))$ such that the length of any bar $|p_\ell(t) - p_m(t)|$, $\{\ell, m\} \in E$, is constant in t , and $p(0) = p$. Consider a vector R of b elements: $R(p, q) = (\dots, (p_\ell - p_m) \cdot (q_\ell - q_m), \dots)$, where $p = (p_1, \dots, p_j)$, $q = (q_1, \dots, q_j)$ and the dot denotes the scalar product.

Definition 2 (Connelly, 1980): An n -th-order flex of a vector p of a framework is a sequence of n vectors, $p', p'', \dots, p^{(n)}$ such that

$$\sum_{i=0}^h \binom{h}{i} R(p^{(i)}, p^{(h-i)}) = 0 \quad (h = 1, 2, \dots, n) \quad (4)$$

These are derivatives of $R(p,p) = \text{constant}$ n times, where $p = p(t)$ is regarded as a function of the parameter t and $p^{(i)}$ is the i th derivative of $p(t)$.

Let us suppose that joints l and m are joined by bar k . So, $|p_l(t) - p_m(t)| = l_k + e_k$ where l_k is the length of bar k in rest position and e_k is its elongation. In (4), in fact, derivatives of $(p_l - p_m)^2 = (l_k + e_k)^2$ are formed. It is easy to show that

$$\left. \frac{d^i}{dt^i} (l_k + e_k)^2 \right|_{t=0} = 0 \quad (i = 1, 2, \dots, n)$$

if and only if

$$\left. \frac{d^i}{dt^i} e_k \right|_{t=0} = 0 \quad (i = 1, 2, \dots, n) .$$

If $t = \delta$ then the derivatives $e_k^{(i)}(0)$ multiplied by $(i!)^{-1}$ are the coefficients a_{ik} in Maclaurin's series of e_k , so we have arrived at Tarnai's (1984a) formulation of Koiter's definition. Thus, it seems that Definitions 1 and 2 are equivalent, but these definitions seem to characterize the motion rather than the assembly.

2.3 Gáspár's definition

Gáspár (1989) pointed out that neither Definition 1 nor 2 stresses that the maximum of the first non-vanishing coefficients in (1) should be considered for all the possible systems of displacements of joints such that at least one displacement component is a linear function of δ , but this is an immanent feature of Koiter's definition.

Gáspár suggested an improvement of Definition 1 (and 2) and suggested defining the order of an infinitesimal mechanism in the following way. Consider a system of infinitesimal displacements of joints of the mechanism and consider the elongations of bars as functions of a displacement component of one of the joints. Consider the lowest order elongation in each bar, and take the minimum of these lowest orders decreased by one. Then produce systems of infinitesimal displacements of joints in all the possible ways and take the maximum of these minima as the order of the infinitesimal mechanism.

Tarnai (1989) has formulated Gáspár's definition mathematically in the following way.

Consider a bar-and-joint assembly, constituting and infinitesimal mechanism, in which b bars elongate and j joints translate when the infinitesimal mechanism is excited. Let one of the components of the displacement vector of the joint characterizing the infinitesimal mechanism be denoted by δ . Consider δ as a scalar parameter of the system of motions, so displacement vector of every joint is a function of δ , that is, the displacement vector $\underline{\delta}_l$ of the l th joint is

$$\underline{\delta}_l = \underline{\delta}_l(\delta) \quad l \in \{1, 2, \dots, j\}.$$

but we can define such a function arbitrarily in several ways:

$$\underline{\delta}_{lr} = \underline{\delta}_{lr}(\delta) \quad r \in \Gamma \quad (5)$$

where Γ is a set of subscripts of all the possible functions. Let joints l and m be connected by bar k , then the elongation e_{kr} of bar k is a function of displacement vectors $\underline{\delta}_{mr}$ and $\underline{\delta}_{lr}$ of the joints m and l :

$$e_{kr} = e_{kr}(\underline{\delta}_{mr}, \underline{\delta}_{lr}).$$

However, because of (5), e_{kr} is a function of δ , and we can produce its MacLaurin's series expansion at point zero:

$$e_{kr} = \sum_{i=1}^{\infty} a_{kr} \delta^i. \quad (6)$$

Definition 3 (Tarnai, 1989): An assembly is an n th-order infinitesimal mechanism if for the coefficients a_{kr} in (6)

$$n = \max_r \min_k \left\{ h \mid a_{kr} = a_{kr} = \dots = a_{kr} = 0, a_{kr(h+1)} \neq 0 \right\} \quad (7)$$

$$k \in \{1, 2, \dots, b\}, r \in \Gamma.$$

If there is a bar k which does not elongate, that is, $e_{kr} = 0$ and so $a_{kr} = 0$ for $i = 1, 2, \dots$ then, for that k , h should be considered infinite.

To illustrate this definition we present the following Example 2. Let the length of all the bars in Fig. 3 be equal to the unity. Here x is the horizontal displacement of joint A, $2y$ is the vertical displacement of joint B. Because of symmetry we consider the elongations of bars 1 and 2 to

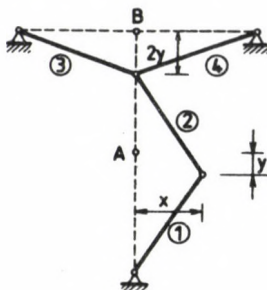


Fig. 3.

be equal (they are denoted by e_1), and the elongations of bars 3 and 4 to be equal (they are denoted by e_3):

$$e_1 = \sqrt{(1-y)^2 + x^2} - 1 = \frac{1}{2}(-2y + y^2 + x^2) - \frac{1}{8}(-2y + y^2 + x^2)^2 + \dots$$

$$e_3 = \sqrt{1 + (2y)^2} - 1 = 2y^2 - 2y^4 + \dots$$

(It should be noted that if generalizing the deformation we would break the symmetry, e.g. $e_1 \neq e_2$, then the first non-vanishing coefficient in (6) could increase for one of the bars but would decrease for the other, finally the minimum of them would decrease. But the aim is to increase the minimum as much as possible.)

$$\left. \begin{array}{l} \text{If } y = 0 \text{ then } e_1 = \frac{x^2}{2} - \dots \\ e_3 = 0 \end{array} \right\} \min h = 1$$

$$\left. \begin{array}{l} \text{If } y = Cx \text{ then } e_1 = \frac{1}{2} \left[-2Cx + (C^2 + 1)x^2 \right] - \dots \\ e_3 = 2C^2x^2 - \dots \end{array} \right\} \min h = 0$$

$$\left. \begin{array}{l} \text{If } y = Cx^2 \text{ then } e_1 = \frac{1}{2} \left[(-2C + 1)x^2 + C^2x^4 \right] - \dots \\ e_3 = 2C^2x^4 - \dots \end{array} \right\} \min h = 1$$

$$\left. \begin{array}{l} \text{in particular, } C = \frac{1}{2} : e_1 = \frac{x^4}{8} - \dots \\ e_3 = \frac{x^4}{2} - \dots \end{array} \right\} \min h = 3$$

$$\text{If } y = Cx^N, N \geq 2 \text{ then } \left. \begin{aligned} e_1 &= \frac{1}{2}(-2Cx^N + C^2x^{2N} + x^2) - \dots \\ e_3 &= 2C^2x^{2N} - \dots \end{aligned} \right\} \min h = 1 ,$$

$$\text{If } y = \frac{x^2}{2} + \frac{x^4}{8} \text{ then } \left. \begin{aligned} e_1 &= \frac{1}{2}\left(\frac{x^6}{8} + \frac{x^8}{64}\right) - \dots \\ e_3 &= \frac{x^4}{2} + \frac{x^6}{4} + \frac{x^8}{32} - \dots \end{aligned} \right\} \min h = 3 ,$$

$$\text{If } y = \frac{x^2}{2} + \frac{x^4}{8} + \frac{x^6}{16} \text{ then } \left. \begin{aligned} e_1 &= \frac{1}{2}\left(\frac{5}{64}x^8 + \frac{x^{10}}{64} + \frac{x^{12}}{256}\right) - \dots \\ e_3 &= 2\left(\frac{x^4}{4} + \frac{x^6}{8} + \frac{5}{64}x^8 + \frac{x^{10}}{64} + \frac{x^{12}}{256}\right) - \dots \end{aligned} \right\} \min h = 3 ,$$

In general, if we want to eliminate the second-order term in e_1 it is necessary that y contains the term $x^2/2$. In this case, however, e_3 will always contain a fourth-order term. Thus, the minimum exponent will never exceed 4. Consequently

$$n = \max(\min h) = 3 ,$$

that is, the assembly in Fig. 3 is a third-order infinitesimal mechanism. It is interesting to mention that practically the same assembly was published by Connelly (1980) and Kuznetsov (1988), and those authors said the assembly to be a second-order infinitesimal mechanism. However, we believe that our result here obtained by Definition 3 is correct.

The method applied here seems to be awfully laborious. However, this is only for the sake of illustrating the concept of the definition, that is, producing a set of minima and taking its maximum. In fact, the procedure can be made systematic and simple.

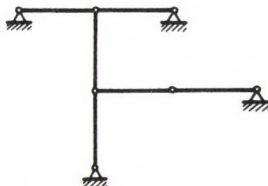
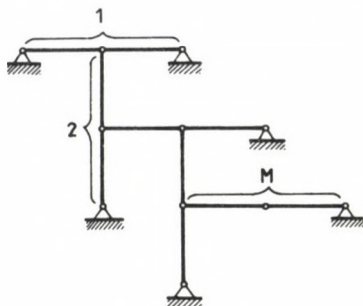


Fig. 4.



Example 3. In a similar way, it can be shown that the assembly in Fig. 4 is a 7th-order infinitesimal mechanism. In the general case, where the assembly is composed of M three-hinged arches (Fig. 5), it is a 2^M -1st-order infinitesimal mechanism. If $M \rightarrow \infty$ we obtain an infinitesimal mechanism of infinite order.

Some other examples of higher-order infinitesimal mechanisms can be seen in (Pellegrino, 1986).

3. Difficulties in the determination of the order of an infinitesimal mechanism

Connelly (1989) has called attention to problems which the different definitions, especially Definition 3, can have.

(a) Parametrization of a system of displacements of joints is important but difficult, as without a precisely defined proper parametrization the order of any mechanism seems to be infinite. Namely, if $\underline{\delta}_\ell(\delta)$ is the displacement vector for any joint ℓ , we can define a new displacement vector $\underline{\delta}_\ell(\delta) = \underline{\delta}_\ell(\delta^2)$. When we compute the first minimum in Definition 3, it is twice as large for the second function and so can be made arbitrarily large. This is the reason why Connolly (1980) did not mention the parametrization explicitly /c.f. (Connolly and Whitely, 1988)/. However, we think that this problem is eliminated by the fact that in the parametrization we supposed one displacement component to be a linear function of the parameter (the displacement component itself is considered as the parameter). So, a reparametrization mentioned by Connolly is not possible.

(b) In Example 2, due to Definition 3, it is assumed that the displacement x is linear in δ . Connolly thinks that it is not always possible directly to choose a displacement component in the first-order for some joint. He has mentioned that this would happen, for instance, for the case $x^3 = y^2$, near the point (0,0). Connolly has concluded that he is not at all sure that there is a good definition of higher-order infinitesimal mechanism. We think that we can always parametrize the system of displacements, such that a displacement component of one joint is a linear function of the parameter (in such a way that after parametrization the term of the lowest power should be linear). With this, however, some difficulties can occur, for instance: multi-valuedness of functions, loss of analyticity, lack of differentiability. These problems are discussed in the subsequent subsections.

(c) In Definition 3 (and also in Definition 1) it is supposed that there exists Maclaurin's series (6), that is, the elongation functions are analytic at $\delta = 0$. The lack of analyticity causes problem in Example 1 if the slot curve is defined as

$$r = \begin{cases} R + \varphi^3 & \text{if } \varphi \geq 0 \\ R + \varphi^2 & \text{if } \varphi \leq 0 \end{cases}.$$

It is an infinitesimal mechanism at $\varphi = 0$ because $\left. \frac{dr}{d\varphi} \right|_{\varphi=0} = 0$, but we cannot define the order of the mechanism due to Definitions 1, 2, 3. However, we can produce the one-sided Maclaurin's series. With this modification Definition 3 constitutes the infinitesimal mechanism to be of order 2.

(d) In certain cases it can occur that even one-sided Maclaurin's series does not exist. A good example for that is Example 1 if the slot curve is defined as $r = R + \Psi$ such that $\Psi^2 = \varphi^3$ mentioned by Connolly. At the point (R,0) the function $r(\varphi)$ has one-sided derivatives of arbitrary order: $r'_+(0) = 0$ but $r^{(i)}_+(0) = +\infty$ ($-\infty$) for $i = 2, 3, \dots$. Definition 3 with one-sided derivatives does not work, but Definition 2 with one-sided derivatives does and results in a first-order infinitesimal mechanism, because it does not need the first non-vanishing derivative to be bounded. So Definition 3 can be modified for more general cases with one-sided derivatives in the following way:

Definition 4: An assembly is an n-th-order infinitesimal mechanism if

$$n = \max_{\gamma} \min_k \left\{ h \mid e_{k\gamma+}^{(i)}(0) = 0 \quad \text{for } i = 1, \dots, h; e_{k\gamma+}^{(h+1)}(0) \neq 0 \right\},$$

$k \in \{1, 2, \dots, b\}, \gamma \in \Gamma$, where $e_{k\gamma+}^{(i)}(0)$ denotes the i-th one-sided derivative of $e_{k\gamma}(\delta)$ at point $\delta = 0$. In this definition, if there exists a k for which $e_{k\gamma}(\delta) \equiv 0$ and so $e_{k\gamma+}^{(i)}(0) = 0$ for $i = 1, 2, \dots$ then, for that k , h should be considered infinite.

However, elongations in bars of engineering bar-and-joint structures are, in general, analytic functions so definitions in Section 2 can be used. The minimax property in Definition 3 is an important feature, but the definition itself does not seem to be very convenient for practical application. Although the notion "higher-order infinitesimal mechanism" is a purely geometrical term, to simplify the analysis Koiter (1989) suggested the introduction of elasticity in the bars, that is, the use of the elastic energy function of the assembly and interpretation of the infinitesimal mechanism as the buckling mode of the truss under zero loading. Koiter noted: "The stability of equilibrium in this critical case of neutral equilibrium may be investigated by the nonlinear theory of elastic stability (Koiter, 1945). The outcome of the analysis is stability of an even order $2(n+1)$ indicating an infinitesimal mechanism of order n ." Here not the actual elastic properties of the bars are required but only fictive ones which can be different for the different bars.

Koiter's idea overcomes the difficulties mentioned by Connelly, since the form of the excited mechanism is considered as the buckling mode and so it gives the way how to parametrize the motion. It reduces the calculation work necessary due to Definition 3 and using the elastic energy it automatically satisfies the extremum properties (7).

Turning back to Example 2 Koiter pointed out that if one introduces a Lagrange type strain:

$$\epsilon_1 = -y + \frac{1}{2}(x^2 + y^2), \quad \epsilon_3 = 2y^2,$$

then obtains the elastic energy for equal bars as

$$C \left\{ \left[-y + \frac{1}{2}(x^2 + y^2) \right]^2 + 4y^4 \right\}.$$

He remarked: "The 'buckling mode' is $y = 0$, $x = a$ (arbitrary), the stability investigation requires minimization of energy with respect to y for fixed a (infinitesimal). Result is for energy proportional to $a^8 + \text{h.o.}$, confirming infinitesimal mechanism of 3rd order."

Proposition of Koiter can be easily understood if we take the first derivative of the energy with respect to y equal to zero. Then we obtain

$$y - \frac{1}{2}x^2 + \frac{1}{2}y^2 + \frac{1}{2}x^2y + \frac{17}{2}y^3 = 0 \quad .$$

By keeping the lowest-order terms in y and x and neglecting the higher-order terms we have $y = x^2/2$. Substituting $x = a$ and $y = a^2/2$ in the energy expression we arrive at Koiter's conclusion. The great advantage of Koiter's idea is that it directly gives the required $y = y(x)$ function.

4. Stiffening effect of prestress

Let us turn back to question (A) and consider the structure in Fig. 1 with slot curve equation $r = r(\varphi)$. This structure is both statically and kinematically indeterminate at $\varphi = 0$ if

$$\left. \frac{dr}{d\varphi} \right|_{\varphi=0} = 0 \quad . \quad (8)$$

Suppose that the basic position of the bar is at $\varphi = 0$ and (8) is satisfied. Let us now investigate whether prestress in the bar can stiffen this structure (self-stress may impart a first-order stiffness to the structure).

Let the upper end of the bar be subjected to a horizontal force P . Describe the equilibrium of the structure in a displaced position. The load P and reactions S and N acting in the joint in the slot have to be in equilibrium. Here S is the force in the bar and N is a force whose line of action is perpendicular to the slot curve. The relationship between P and S in accordance with Fig. 6 is

$$P = S(\sin \varphi + \tan \alpha \cos \varphi) \quad .$$

Since due to Fig. 6

$$\begin{aligned} x &= r \sin \varphi \quad , \\ y &= r \cos \varphi \end{aligned}$$

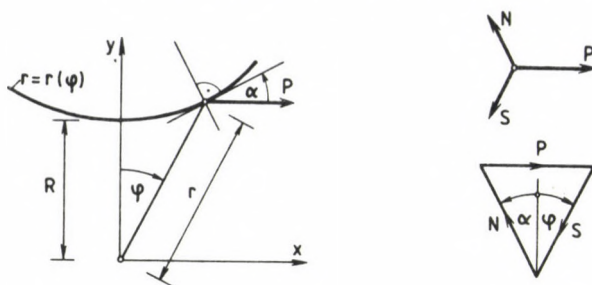


Fig. 6.

and

$$\frac{dx}{d\varphi} = \frac{dr}{d\varphi} \sin \varphi + r \cos \varphi ,$$

$$\frac{dy}{d\varphi} = \frac{dr}{d\varphi} \cos \varphi - r \sin \varphi ,$$

we have

$$\tan \alpha = \frac{dy}{dx} = \frac{\frac{dr}{d\varphi} \cos \varphi - r \sin \varphi}{\frac{dr}{d\varphi} \sin \varphi + r \cos \varphi}$$

and so

$$P = S \frac{\frac{dr}{d\varphi}}{\frac{dr}{d\varphi} \sin \varphi + r \cos \varphi} . \quad (9)$$

Forming its first derivative we obtain

$$\begin{aligned} \frac{dP}{d\varphi} = & \frac{dS}{d\varphi} \frac{\frac{dr}{d\varphi}}{\frac{dr}{d\varphi} \sin \varphi + r \cos \varphi} + \\ & + S \frac{\frac{d^2r}{d\varphi^2} r \cos \varphi - 2 \left(\frac{dr}{d\varphi} \right)^2 \cos \varphi + \frac{dr}{d\varphi} r \sin \varphi}{\left(\frac{dr}{d\varphi} \sin \varphi + r \cos \varphi \right)^2} . \end{aligned} \quad (10)$$

In the forthcoming we suppose that

$$-\infty < S \Big|_{\varphi=0} < +\infty \quad (11)$$

and

$$\left(\frac{dS}{d\varphi} \frac{dr}{d\varphi} \right) \bigg|_{\varphi=0} = 0 \quad (12)$$

which mean that the force S in bar is finite at $\varphi = 0$, and the derivative $dS/d\varphi$ at $\varphi = 0$ is finite or if it is infinite then - as φ approaches zero - $dr/d\varphi$ tends to zero in order higher than $dS/d\varphi$ tends to infinity.

Let us analyse the $P - \varphi$ diagram at $\varphi = 0$. It is easy to see due to (8) and (9) that $P \big|_{\varphi=0} = 0$ for arbitrary finite value of S .

Consider now the case in which the structure has no prestress, that is, $S \big|_{\varphi=0} = 0$. By introducing $\varphi = 0$ into (10) and considering (8) and (12) we obtain

$$\frac{dP}{d\varphi} \bigg|_{\varphi=0} = 0,$$

that is, the structure has no first-order stiffness at $\varphi = 0$.

Consider now the case in which the structure has prestress, that is, $S \big|_{\varphi=0} \neq 0$. By introducing $\varphi = 0$ into (10) and considering (8) and (12) we obtain

$$\frac{dP}{d\varphi} \bigg|_{\varphi=0} = \frac{1}{R} \cdot S \bigg|_{\varphi=0} \cdot \frac{d^2r}{d\varphi^2} \bigg|_{\varphi=0}. \quad (13)$$

(13) vanishes if $(d^2r/d\varphi^2) \big|_{\varphi=0} = 0$, that is, in the cases of the infinitesimal mechanisms of second or higher order and finite mechanisms.

Thus, this example well illustrates Pellegrino's and Calladine's (1986) statement modified by Koiter (1984): Self-stress may impart first-order stiffness to a both statically and kinematically indeterminate structure if the kinematical indeterminacy takes the form of an infinitesimal mechanism of the first order. Second- and higher-order infinitesimal mechanisms and finite mechanisms cannot be linearly stiffened by self-stress. This statement has a great importance in structural engineering practice (Kollár, 1988).

5. Conclusions

(1) Koiter's (1989) definition of an infinitesimal mechanism of n th order is: "An infinitesimal mechanism is of the n th-order ($n = 1, 2, \dots$) if it involves no elongation of any bar up to and including the n th order but exhibits an elongation of order $(n+1)$ in at least one bar." We presented and compared different mathematical formulations of this definition and we discussed the problems arising when we want to formulate mathematically this definition. If a displacement component of one joint is a linear function of the parameter of motion and one-sided derivatives are used then Definition 4 seems to be the most general formulation of the discussed ones.

(2) Using Koiter's (1989) idea one can avoid the mathematical problems and can determine the order of an infinitesimal mechanism if considers the form of the excited mechanism as a buckling mode and applies nonlinear theory of elastic stability.

(3) To illustrate Pellegrino and Calladine's (1986) statement modified by Koiter (1984) we presented an example of a both statically and kinematically indeterminate structure and showed that prestress cannot impart first order stiffness to it if it is a second- or higher-order infinitesimal mechanism.

(4) This paper gave a brief account of what happened in the research on higher-order infinitesimal mechanisms during the last few years. Several problems remained to solve, so further research is needed in this field. An interesting question is, for instance: Does the order of an infinitesimal mechanism change under a projective transformation?

Acknowledgements

I thank Professors W.T. Koiter and R. Connelly and Dr. Zs. Gáspár for helpful discussions. Research reported here was supported by OTKA Grant No. 744 awarded by the Hungarian Scientific Research Foundation.

REFERENCES

1. Connelly, R.: The rigidity of certain cabled frameworks and the second-order rigidity of arbitrarily triangulated convex surfaces. *Advances in Mathematics* 37 (1980), 272-299

2. Connelly, R.: Private communication to the author (1989)
3. Connelly, R. - Whiteley, W.: Second-order rigidity and pre-stress stability. (Preprint) Université de Montreal, Centre de recherches mathématiques (1988)
4. Gáspár, Zs.: Private communication to the author (1989)
5. Koiter, W.T.: On the stability of elastic equilibrium (In Dutch). Thesis, H.J. Paris, Amsterdam (1945), English translation: (a) NASATT F-10, 833, (1967), (b) AFFDL TR 70-25 (1970)
6. Koiter, W.T.: On Tarnai's conjecture with reference to both statically and kinematically indeterminate structures. Lab. Report No.788 (1984), Delft Univ. Tech.
7. Koiter, W.T.: Private communication to the author (1989)
8. Kollár, L.: Rigidity problems of cable structures (In Hungarian). Közlekedésépítés- és Mélyépítéstudományi Szemle 38 (1988), 241-248
9. Kuznetsov, E.N.: Underconstrained structural systems. Int. J. Solids Structures 24 (1988), 153-163
10. Pellegrino, S.: Mechanics of kinematically indeterminate structures. Ph.D. Dissertation, University of Cambridge (1986)
11. Pellegrino, S. - Calladine, C.R.: Matrix analysis of statically and kinematically indeterminate frameworks. Int. J. Solids Structures 22 (1986), 409-428
12. Tarnai, T.: Problems concerning spherical polyhedra and structural rigidity. Struct. Topology 4 (1980), 61-66
13. Tarnai, T.: Comments on Koiter's classification of infinitesimal mechanisms. (Manuscript). Hung. Inst. Build. Sci. Budapest, October 1984a
14. Tarnai, T.: Infinitesimal mechanisms and stiffening effect of prestress. (Manuscript). Hung. Inst. Build. Sci. Budapest, November 1984b
15. Tarnai, T.: Infinitesimal mechanisms. (Manuscript). Hung. Inst. Build. Sci. Budapest, February 1989

ANALYSIS OF THE STRUCTURES FOR DYNAMIC EFFECTS WITH MATHEMATICAL PROGRAMMING

VÁSÁRHELYI, A.* - LÓGÓ, J.*

(Received: 27 December 1989)

In case of dynamical analysis, the state variables depend on time. In the primal case, the equilibrium equations and the limits of the complementary elastic and kinetic energies are constraints and the sum of complementary energies is found in the objective function. The Stieltjes derivatives are used to form the dual problem. It is bounded by the compatibility equations and energy-limits and the sum of elastic and kinetic energies can be found in the objective.

1. Introduction

Dynamic problems usually are solved as an eigenvalue problem of discretized structures /11, 13/. The mathematical background is some types of direct time integration methods where the number of unknowns and equations is identical. Most of them are related to the so-called "tangent stiffness" method /5, 7, 8/ in which the stiffness matrix of the system is adjusted at every loading step.

In the Seventies a new direction developed on the basis of mathematical programming procedures. However, the problem is solved as a linear complementarity problem /6/.

The aim of this paper is to present an other type of solution of dynamic problems by mathematical programming.

2. Basic idea

The differential equations concerning structures are transformed into an unconstrained minimization problem by the help of variational methods and they are decomposed into a pair of constrained minimization problem.

*Vásárhelyi, Anna, H-1126 Budapest, Kiss J. alt. u. 34, Hungary

**Lógó, János, H-1118 Budapest, Regős u. 7, Hungary

Decomposition has not a unique solution, it is executed in such a way that the primal-dual problems have a physical meaning. The primal and dual variables are intensive and extensive from a mechanical point of view, respectively. The objective functions contain the different types of energies.

The state variables (e.g. stresses, strains, etc.) are given in the vector space by vector-scalar functions in case of equilibrium state. The structures are discretized that is the vector space is supposed to be an n dimensional space in the global coordinate system. A state vector is ordered to each vector which point at the direction of a discretized point with maximum 6 independent components given in the local coordinate system.

The time dependent state variables are given in both local and global coordinate systems, but they are vector-vector-function quantities. In the following, the small displacement theory is supposed to be valid that is the position vectors are time independent.

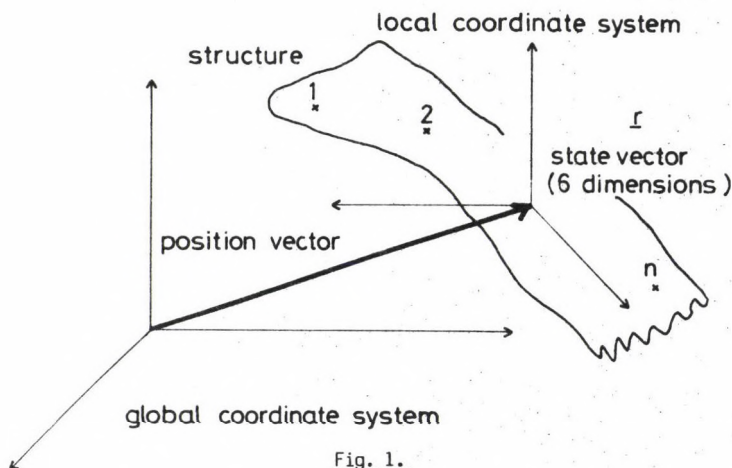


Fig. 1.

3. Mathematical Background

The time dependent state variables are approximated by an orthogonal polynomial system [10]:

$$r(t) = \sum_{i=1}^{\infty} \alpha_i P_i(t) \quad P_i(t) \in L^2 \quad (1)$$

In the local coordinate system, we have to determine:

$$\underline{r}(t) = \sum_{j=1}^6 \sum_{i=1}^{\infty} \alpha_i^j P_i(t) \underline{e}_j \quad (2)$$

where \underline{e}_j is the unit vector in the local system.

The th unknown in the global system can be written as:

$$\underline{x}^L(t) = (a_1^L, a_2^L, a_3^L, r_1^L(t), r_2^L(t), \dots, r_6^L(t)) \quad (3)$$

The dual problem is formed on the basis of Kuhn-Tucker conditions /1, 2/ by the help of a Stieltjes derivate which is the inverse operation of the Stieltjes integral /3, 14/.

The Stieltjes derivate:

$$\frac{df(x(t))}{dx(t)} = \frac{d \int \hat{f}(x(t)) dx(t)}{dx(t)} = \frac{\dot{f}(x(t))}{\dot{x}(t)} \quad (4)$$

$$\dot{x}(t) \neq 0$$

$$\begin{aligned} \text{because } f(x) &= \int \dot{f}(x(t)) dt + c = \int \dot{f}(x(t)) \frac{\dot{x}(t)}{\dot{x}(t)} dt + c = \\ &= \int \frac{\dot{f}(x(t))}{\dot{x}(t)} dx(t) + c \quad \dot{x}(t) \neq 0 \end{aligned}$$

Statement: The following primal and the deduced dual problems have the same Euler-Lagrange equation and it expresses Newton's second law.

$$\text{Primal: } \min \left\{ 0.5 \int \underline{\sigma} dt \underline{m}^{-1} \int \underline{\sigma} dt \mid \underline{\phi}^* \int \underline{\sigma} dt + \int \underline{f} dt = 0 \right\} \quad (5)$$

The dual is formed according to the Wolfe procedure which is based on the Kuhn-Tucker theorem. The Stieltjes derivatives:

$$\nabla_{\underline{\sigma}} \left(\int \underline{\sigma} dt \underline{m}^{-1} \int \underline{\sigma} dt \right) = \frac{\underline{\sigma}}{\underline{\sigma}^j} \underline{m}^{-1} \int \underline{\sigma} dt \quad \nabla_{\underline{\sigma}} (\underline{\phi}^* \underline{\sigma}) = \underline{\phi} \frac{\underline{\sigma}}{\underline{\sigma}^j} \quad (j=1, \dots, 6n)$$

The dual problem:

$$\max \left\{ \int \underline{\sigma} dt \underline{m}^{-1} \int \underline{\sigma} dt + (\underline{\phi}^* \int \underline{\sigma} dt + \int \underline{f} dt) \underline{x} \mid \underline{\phi} \frac{\underline{\sigma}}{\underline{\sigma}^j} \underline{x} + \frac{\underline{\sigma}}{\underline{\sigma}^j} \underline{m}^{-1} \int \underline{\sigma} dt = 0 \right\}$$

$$\underline{\sigma}^j \neq 0$$

$$\min \left\{ 0.5 \int \underline{\sigma} dt \underline{m}^{-1} \int \underline{\sigma} dt - \underline{x} \int \underline{f} dt \mid \underline{x} \underline{\Phi} + \underline{m}^{-1} \int \underline{\sigma} dt = 0 \right\} \quad (6)$$

The variational problem of the primal case:

$$\int (0.5 \int \underline{\sigma} dt \underline{m}^{-1} \int \underline{\sigma} dt + \underline{y} (\underline{\Phi}^* \int \underline{\sigma} dt + \int \underline{f} dt)) dt \quad (7)$$

The variation of the basic function according to $\underline{\sigma}$:

$$\delta_{\underline{\sigma}} : \int \left(\int (\underline{\sigma} + \underline{\varepsilon} \underline{\eta}) dt \underline{m}^{-1} \int (\underline{\sigma} + \underline{\varepsilon} \underline{\eta}) dt + \underline{y} \underline{\Phi} (\underline{\sigma} + \underline{\varepsilon} \underline{\eta}) + \underline{y} \int \underline{f} dt \right) dt \quad (8)$$

The extremal value according to $\underline{\varepsilon}$:

$$\frac{\partial}{\partial \underline{\varepsilon}} : \int \left(\int \underline{\eta} dt \underline{m}^{-1} \int (\underline{\sigma} + \underline{\varepsilon} \underline{\eta}) dt + \underline{y} \underline{\Phi} \int \underline{\eta} dt \right) dt \quad (9)$$

$$\frac{\partial}{\partial \underline{\varepsilon}} \Big|_{\underline{\varepsilon}=0} : \int \left(\underline{m}^{-1} \int \underline{\sigma} dt + \underline{y} \underline{\Phi} \right) \int \underline{\eta} dt dt = 0 \quad \int \underline{\eta} dt \neq 0$$

It follows:

$$\underline{m}^{-1} \int \underline{\sigma} dt + \underline{y} \underline{\Phi} = 0 \quad (10)$$

Let be the Lagrangian multiplier $\underline{y} = \underline{\dot{u}}$

The variation of the function (7) according to \underline{y} :

$$\delta_{\underline{y}} : \int (0.5 \int \underline{\sigma} dt \underline{m}^{-1} \int \underline{\sigma} dt + (\underline{y} + \underline{\varepsilon} \underline{\eta}) (\underline{\Phi}^* \int \underline{\sigma} dt + \int \underline{f} dt)) dt$$

the extremal value according to $\underline{\varepsilon}$ for $\underline{\varepsilon} = 0$:

$$\int (\underline{\Phi}^* \int \underline{\sigma} dt + \int \underline{f} dt) \underline{\eta} dt = 0 \quad (11)$$

That is:

$$\underline{\Phi} \int \underline{\sigma} dt + \int \underline{f} dt = 0 \quad (12)$$

Taking into consideration the meaning of Lagrangian multipliers and combining (10) and (12) in one system:

$$\underline{M} \underline{\ddot{u}} + \underline{f} = 0 \quad (13)$$

where:

$$\underline{\underline{M}} = -\underline{\underline{\Phi}} \underline{\underline{m}}^{-1} \underline{\underline{\Phi}}$$

this is the Euler-Lagrange equation originated from the primal problem.

The variational problem concerning dual case:

$$\int \left\{ 0.5 \int \underline{\underline{\sigma}} dt \underline{\underline{m}}^{-1} \int \underline{\underline{\sigma}} dt - \underline{\underline{u}} \int \underline{\underline{f}} dt + \underline{\underline{x}}^* (\underline{\underline{\Phi}} + \underline{\underline{m}}^{-1} \int \underline{\underline{\sigma}} dt) \right\} dt \Rightarrow \min \quad (14)$$

$$\begin{aligned} \partial_{\sigma}: \int \left\{ 0.5 \int (\underline{\underline{\sigma}} + \underline{\underline{\epsilon}} \underline{\underline{\eta}})^* dt \underline{\underline{m}}^{-1} \int (\underline{\underline{\sigma}} + \underline{\underline{\epsilon}} \underline{\underline{\eta}}) dt - \underline{\underline{u}}^* \int \underline{\underline{f}} dt + \underline{\underline{x}}^* (\underline{\underline{u}} \underline{\underline{\Phi}} + \right. \\ \left. + \underline{\underline{m}}^{-1} \int (\underline{\underline{\sigma}} + \underline{\underline{\epsilon}} \underline{\underline{\eta}}) dt) \right\} dt \end{aligned} \quad (15)$$

the extremal value according to $\underline{\underline{\epsilon}}$ for $\underline{\underline{\epsilon}} = 0$:

$$\int (\int \underline{\underline{\eta}}^* dt \underline{\underline{m}}^{-1} \int \underline{\underline{\sigma}} dt + \underline{\underline{x}}^* \underline{\underline{m}}^{-1} \int \underline{\underline{\eta}} dt) dt = 0 \quad (16)$$

taking out $\int \underline{\underline{\eta}} dt$ we get the following equation, for $\underline{\underline{\eta}} \neq 0$:

$$\int \underline{\underline{\sigma}} dt = -\underline{\underline{x}}$$

The Lagrangian multiplier is substituted into (14):

$$\begin{aligned} \partial_{\sigma}: \int \left\{ 0.5 \int (\underline{\underline{\sigma}} + \underline{\underline{\epsilon}} \underline{\underline{\eta}})^* dt \underline{\underline{m}}^{-1} \int (\underline{\underline{\sigma}} + \underline{\underline{\epsilon}} \underline{\underline{\eta}}) dt - \underline{\underline{u}}^* \int \underline{\underline{f}} dt - \right. \\ \left. - \int \underline{\underline{\sigma}}^* dt (\underline{\underline{u}} \underline{\underline{\Phi}} + \underline{\underline{m}}^{-1} \int (\underline{\underline{\sigma}} + \underline{\underline{\epsilon}} \underline{\underline{\eta}}) dt) \right\} dt \end{aligned} \quad (17)$$

$$\frac{\partial}{\partial \underline{\underline{\epsilon}}} \Big|_{\underline{\underline{\epsilon}}=0} : \int (-\int \underline{\underline{\eta}}^* dt \underline{\underline{m}}^{-1} \int \underline{\underline{\sigma}} dt - \int \underline{\underline{\eta}} dt \underline{\underline{u}}^* \underline{\underline{\Phi}}) dt = 0 \quad (18)$$

If $\int \underline{\underline{\eta}} dt \neq 0$:

$$\underline{\underline{m}}^{-1} \int \underline{\underline{\sigma}} dt + \underline{\underline{u}}^* \underline{\underline{\Phi}} = 0 \quad (19)$$

The variation of (14) according to $\underline{\underline{u}}$:

$$\begin{aligned} \delta_{\underline{\underline{u}}} : \int (-\int (\underline{\underline{u}} + \underline{\underline{\epsilon}} \underline{\underline{\eta}}) \int \underline{\underline{f}} dt - \int \underline{\underline{\sigma}} dt (\underline{\underline{u}} + \underline{\underline{\epsilon}} \underline{\underline{\eta}}) \underline{\underline{\Phi}} - 0.5 \int \underline{\underline{\sigma}} dt \underline{\underline{m}}^{-1} \int \underline{\underline{\sigma}} dt) dt \\ \delta_{\underline{\underline{\epsilon}}} \Big|_{\underline{\underline{\epsilon}}=0} : \int (-\int \underline{\underline{\eta}} \int \underline{\underline{f}} dt - \int \underline{\underline{\sigma}} dt \underline{\underline{\eta}} \underline{\underline{\Phi}}) dt = 0 \quad \text{if } |\underline{\underline{\eta}}| \neq 0 : \end{aligned}$$

$$\int \underline{f} dt + \int \underline{\sigma}^* dt \underline{\Phi} = 0 \quad (20)$$

The Euler-Lagrange equation concerning the dual problem consists of (19) and (20):

$$\underline{M} \underline{\ddot{u}} + \underline{f} = 0$$

The statement is right.

4. Model of the dynamic problems without dumping

Suppose that:

- the material of the structures is linear elastic,
- the mass and flexibility of the structures are time independent,
- the small displacement theory is valid,
- the external loads are given by time functions.

The external loads are decomposed into two parts: the first causes elastic deformations, while the second moves the structures /4/. The inner forces are divided in a similar way.

The primal problem of the dynamic analysis can be written by the help of the primal problem of Newton's law (5) merging with the primal associated with the elastic problems /12/.

The material of the structure has an attitude which shows how much energy can be taken on elastic and dynamic way during a time interval respectively. From this fact the inequalities derive in the mathematical programming model. According to the second assumption these inequalities became limits for the stresses.

The integrals of the energy functions concerning the domain of the structure are approximated by the Gaussian numerical method.

$$-\int_{t_1}^{t_2} \underline{f}_e(t) dt - \int_{t_1}^{t_2} \underline{f}_d(t) dt + \int_{t_1}^{t_2} \underline{f}(t) dt = 0 \quad (a)$$

(21)

$$\underline{B}^* \int_{t_1}^{t_2} \underline{\sigma}_e dt + \int_{t_1}^{t_2} \underline{f}_e(t) dt = 0 \quad (b)$$

$$\underline{\Phi}^* \int_{t_1}^{t_2} \underline{\sigma} dt + \int_{t_1}^{t_2} \underline{f}(t) dt = 0 \quad (c.)$$

$$\sigma_e \leq \sigma_{EL} \quad (21) \quad (d)$$

$$\sigma_d \leq \sigma_{DL} \quad (e)$$

$$\sum_{i=1}^G \varrho_i \int_{t_1}^{t_2} \underline{\sigma}_e d\sigma_e + \sum_{i=1}^G \frac{\varrho_i}{m} \int_{t_1}^{t_2} \underline{\sigma}_d \int_{t_1}^{t_2} \underline{\sigma}_d dt dt \rightarrow \min \quad (f)$$

where: B is the transfer matrix for elastic part /9/,

$\underline{\Phi}$ is transfer matrix for dynamic part,

$\underline{f}_e, \underline{f}_d$ are the decomposed external load, respectively,

$\underline{\sigma}_{EL}, \underline{\sigma}_{DL}$ are the elastic and the dynamic limit stresses, respectively

$\underline{\sigma}_e, \underline{\sigma}_d$ are elastic and dynamic stresses, respectively,

ϱ_i are the Gaussian weights,

G is the number of the Gaussian points.

unknowns: $\sigma_e, \sigma_d, f_e, f_d$

The Stieltjes derivatives of 21.a - 21.f:

| number of eq. | ∇f_e | ∇f_d | $\nabla \sigma_e$ | $\nabla \sigma_d$ |
|---------------|----------------------|---------------------|---|--|
| 21.a | $-\frac{f_e}{f_e^j}$ | $\frac{f_d}{f_d^j}$ | 0 | 0 |
| 21.b | $\frac{f_e}{f_e^j}$ | 0 | $B \frac{\sigma_e}{\sigma_e^j}$ | 0 |
| 21.c | 0 | $\frac{f_d}{f_d^j}$ | 0 | $\underline{\Phi} \frac{\sigma_d}{\sigma_d^j}$ |
| 21.d | 0 | 0 | 1 | 0 |
| 21.e | 0 | 0 | 0 | 1 |
| 21.f | 0 | 0 | $\sum_{i=1}^G \varrho_i \underline{\sigma}_e$ | $\sum_{i=1}^G \varrho_i^{-1} \frac{\sigma_d^* \int \sigma_d dt}{\sigma_d^j}$ |
| | | | | (j=1,...,6n) |

Assigning the dual variables (X , Y , Z) in the order of the equations and taking into consideration inequalities (d) and (e) as constraints:

$$-X \frac{f_e}{f_e^j} + Y \sum_{i=1}^G \frac{f_e}{f_e^j} \vartheta_i = 0 \quad (j = 1, \dots, 6n) \Rightarrow \underline{X} = \underline{Y} \quad (22)$$

$$-X \frac{f_d}{f_d^j} + Z \sum_{i=1}^G \frac{f_d}{f_d^j} \vartheta_i = 0 \quad (j = 1, \dots, 6n) \Rightarrow \underline{X} = \underline{Z} = \underline{Y} \quad (23)$$

Using these conditions:

$$\underline{X} \underline{B} \frac{\sigma_e}{\sigma_e^j} + \sum_{i=1}^G \vartheta_i \underline{F} \underline{\sigma}_e = 0 \quad (j = 1, \dots, 6n) \quad (a)$$

$$\underline{X} \underline{\Phi} \frac{\sigma_d}{\sigma_d^j} + \sum_{i=1}^G \vartheta_i \frac{\sigma_d^* \int \sigma_d dt}{\sigma_d^j} = 0 \quad (j = 1, \dots, 6n) \quad (b)$$

$$\sigma_e \leq \sigma_{EL} \quad (c)(24)$$

$$\sigma_d \leq \sigma_{DL} \quad (d)$$

$$\begin{aligned} & \sum_{i=1}^G \vartheta_i \int_{\underline{F}} \sigma_e d\sigma_e + \sum_{i=1}^G \vartheta_i \int_{t_1}^{t_2} \sigma_d \int_{t_1}^{t_2} \sigma_d dt dt + \underline{X}^* \left[- \int_{t_1}^{t_2} \underline{f}_e(t) dt - \int_{t_1}^{t_2} \underline{f}_d(t) dt \right. \\ & \left. + \int_{t_1}^{t_2} \underline{f}(t) dt \right] + \underline{X}^* \left[\underline{B} \int_{t_1}^{t_2} \sigma_e dt + \int_{t_1}^{t_2} \underline{f}_e(t) dt \right] + \underline{X} \left[\underline{\Phi} \int_{t_1}^{t_2} \sigma_d dt \right. \\ & \left. + \int_{t_1}^{t_2} \underline{f}_d(t) dt \right] \rightarrow \max \quad (e) \end{aligned}$$

It follows that from equations (a) and (b):

$$\underline{X}^* \underline{B} + \sum_{i=1}^G \underline{F} \underline{\sigma}_e \vartheta_i = 0$$

$$\underline{X}^* \underline{\Phi} + \sum_{i=1}^G \vartheta_i \int \sigma_d dt = 0$$

Substituting the equalities into the objective function, it can be re-written in the following form:

$$\sum_{i=1}^G q_i \int_{\sigma_e} \underline{f}_e d\sigma_e - \sum_{i=1}^G q_i \int_{\sigma_e} \underline{f}_e dt + \sum_{i=1}^G m^{-1} q_i \int_{t_1}^{t_2} \sigma_d \int_{t_1}^{t_2} \sigma_d dt dt - \\ - \sum_{i=1}^G m^{-1} q_i \int_{t_1}^{t_2} \sigma_d dt \int_{t_1}^{t_2} \sigma_d dt + \underline{x}^* \int_{t_1}^{t_2} \underline{f} dt \longrightarrow \max$$

It follows from (23/a) and (23/b) that $X = u$, which satisfies (e). That means that the dual variable of the time integral of the inner force is the displacement velocity.

In case no feasible solution is obtained over the domain bounded by limit stresses on the surface determined by the equilibrium equations, the structure has a resonance.

Control:

Both the primal and the dual conditions have to be satisfied at the extremal point.

$$\begin{aligned} - \int_{t_1}^{t_2} \underline{f}_e(t) dt - \int_{t_1}^{t_2} \underline{f}_d(t) dt + \int_{t_1}^{t_2} \underline{f}(t) dt &= 0 \\ \underline{B}^* \int_{t_1}^{t_2} \sigma_e dt + \int_{t_1}^{t_2} \underline{f}_e(t) dt &= 0 \\ \underline{\Phi}^* \int_{t_1}^{t_2} \sigma_d dt + \int_{t_1}^{t_2} \underline{f}_d(t) dt &= 0 \\ \underline{u}^* \underline{B} + \sum_{i=1}^G q_i \int_{t_1}^{t_2} \sigma_e dt &= 0 \quad - \int_{t_1}^{t_2} \underline{u} dt \sum_{i=1}^G q_i \int_{t_1}^{t_2} \sigma_e dt = \int_{t_1}^{t_2} \sigma_e dt \\ \underline{u}^* \underline{\Phi} + \sum_{i=1}^G m^{-1} q_i \int_{t_1}^{t_2} \sigma_d dt &= 0 \longrightarrow -\underline{u}^* \sum_{i=1}^G m^{-1} q_i \int_{t_1}^{t_2} \sigma_d dt = \int_{t_1}^{t_2} \sigma_d dt \end{aligned} \quad (25)$$

Using the last equations we get:

$$\begin{aligned}
 - \int_{t_1}^{t_2} \underline{u} \, dt \, \overbrace{\underline{B}^* \underline{F}^{-1} \underline{B}}^{\underline{K}} \underline{e} + \int_{t_1}^{t_2} \underline{f}_e(t) dt = 0 \\
 \overbrace{\underline{u} \, \underline{\Phi}^* \underline{m} \, \underline{\Phi}}^{\underline{M}} \underline{e} + \int_{t_1}^{t_2} \underline{f}_d(t) dt = 0
 \end{aligned} \quad (26)$$

Introducing \underline{K} and \underline{M} the following equation is obtained:

$$- \int_{t_1}^{t_2} \underline{u} \, dt \, \underline{K} - \underline{\dot{u}} \, \underline{M} + \int_{t_1}^{t_2} \underline{f}(t) dt = 0 \quad (27)$$

After derivation of this expression with respect to time we obtained the wellknown differential equation of the dynamic analysis.

$$\underline{M} \, \ddot{u}(t) + \underline{K} \, u(t) + \underline{f}(t) = 0 \quad (28)$$

5. Numerical example

Consider a simple bar structure of homogenous, isotropic material. The dimensions can be seen on Fig. 2. The mass of the structure is 214 kg, the cross-sectional dimensions $(EA) = 0.25 \text{ kN}$, the flexibility $(EI) = 0.12 \text{E-3 kNm}^2$.

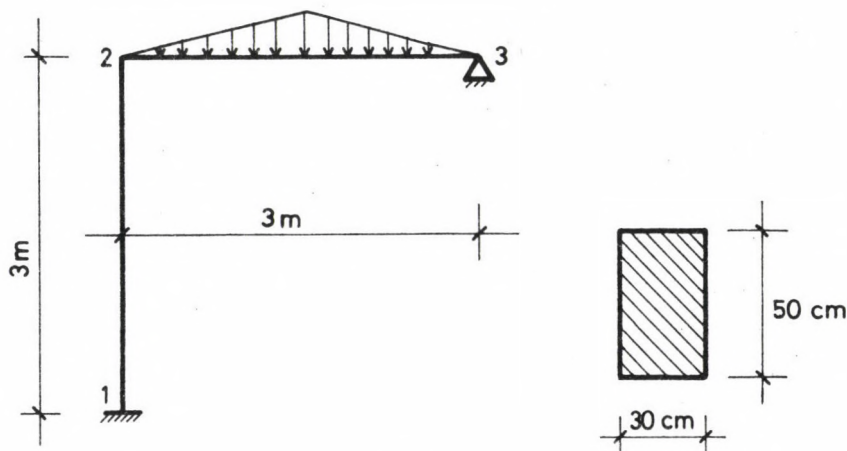


Fig. 2.

The external load acts in three time periods and increases linearly with time. For the calculation the external force was reduced to nodes 2 and 3.

The unknowns are bending moment (M_1 , M_2) and shear force (T_2), taken into consideration as lagged variables in three steps in the time. The problem was solved as a dynamic programming problem by the help of the program package CONOPT.

The result can be seen in Table 1.

The diagrams of bending moments:

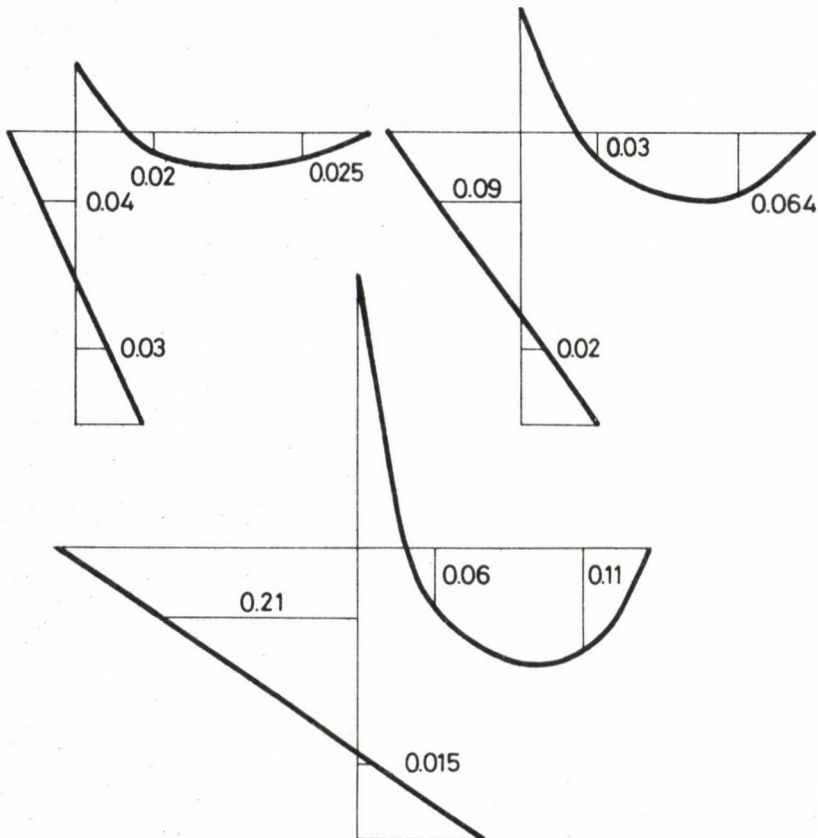


Fig. 3.

Table 1

| | Time period | | |
|-------|-------------|---------|---------|
| | 1 | 2 | 3 |
| T_2 | 79.29 | 119.25 | 268.30 |
| M_1 | 150.00 | 225.00 | 506.50 |
| M_2 | -145.71 | -218.50 | -492.80 |

REFERENCES

1. Bazaraa, M.S. - Shetty, C.M.: Nonlinear Programming Theory and Algorithms. John Wiley & Sons, New York, 1979
2. Bhakta, P.C. - Roychandhuri, S.: Optimization in Banach Spaces. Jour. of Math. Analysis and Applications, No. 134, 1988, 460-470
3. Daniell, P.J.: Differentiation with Respect to a Function of Limited... Trans. Amer. Math. Soc. No. 19. 1918, 353-362
4. Duda, A.: Zum Kontaktproblem Schale- Deformierbarer Baugrund. Conf. "Theoretische und Experimentelle Baumechanik-Forschung und Anwendung", Dresden Sept. 12-14, 1989
5. Owen, D.R.J.: Implicit Finite Element Methods for Dynamic Transient Analysis of Solids with Particular Reference to Nonlinear Solutions. In. J. Donéa (ed.), Advanced Structural Dynamics, London, Appl. Science Pubs. 1980, 123-152
6. Polizzotto, C.: A Quadratic Programming Approach to Dynamic Elastoplasticity. Trans. Int. Conf. on Structural Mechanics in Reactor Technology, SMIRT-8, Brussels, August 19-23, paper B4/5, Vol. B, 1985, 185-190
7. Sayegh, A.H. - Rubinstein, A.F.: Elastic-plastic Analysis by Quadratic Programming. J. Eng. Mech., Div. ASCE, EM6, 1972, 1547-1572
8. Stricklin, J.A. - Haisler, W.E.: Formulation of Solution Procedures for Nonlinear Structural Analysis. Computer & Structures 7, 1977, 125-136
9. Szabó, J. - Roller, B.: Anwendung Matrizenrechnung auf Stabwerke. Akadémiai Kiadó Budapest, 1978
10. Szökefalvi-Nagy, B.: Valós függvények és függvénysorok (in Hungarian). Tankönyvkiadó, Budapest, 1961
11. Tornósy, Á.: Analysis of Bar Structures For Seismic Effect in Engineering Practice. University Doctoral Thesis, Budapest, 1987
12. Vásárhelyi, A. - Lógó, J.: Analysis of Elastic Structures by Mathematical Programming. Periodica Polytechnica (in print)
13. Vértés, Gy.: Structural Dynamics. Elsevier, Amsterdam - Oxford - New York - Tokyo, 1985
14. Young, W.H.: On Integrals and Derivates with Respect to a Function. Proc. London Math. Soc. No. 15. 1914-15, 35-63

INVESTIGATION OF NONLINEAR BEHAVIOUR OF BUILDING STRUCTURES UNDER DYNAMIC LOAD

VÉRTES, GY.*

(Received: 11 January 1990)

A method has been presented for the analysis of composite building structures under earthquake and other dynamic load, assuming an elasto-plastic material model. In final account, the problem can in any case be reduced to the solution of a secondorder differential equation with nonlinear coefficients to be expressed by continuous functions.

1. Introduction

In investigation of the effect of external dynamic loads (earthquake, blast of wind, explosion etc.) upon the structure of buildings, it is often necessary that stresses beyond the limit of elasticity or in other words, plastic deformations be permitted considering that loads of this type are an extraordinary case. In case of a simple structure, the diagram of the so-called elasto-plastic material model can be used to describe the process of load transfer. However, if the structure consists of structural elements for which the yield load is different because of their different size or location, this simple diagram will not apply to the structure as a whole because the different elements become plastic in case of different deformations. The situation is still more complicated in case of dynamic loads because of the significant contribution of the time factor: the different structural elements may arrive at the elastic limit at a different time each. In case of a structure where the centre of rotation and the centre of mass are not coincident, the 'coupled motion' (that is displacement and rotation taking place simultaneously) results in additional complications in predicting the place and time of elastic and plastic deformations.

It follows from what has been said that investigation of the dynamic effects is a rather complicated problem especially if also a potential

*Vértés, György, H-1075 Budapest, Madách tér 6, Hungary

plastic deformation is taken into consideration and the problem is considerably simplified also in the international literature /3/, /4/. This work is intended to provide a practicable method for investigation of the effect of dynamic loads which, based on acceptable approximations, supplies results of sufficient accuracy for practice. In the method, the response of the structural elements of the building to forces acting upon them is taken into consideration as realistically as possible.

The method described below assumes a linearly elastic - perfectly plastic behaviour of the different structural elements of the building in response to horizontal forces acting upon them and only horizontal displacement of the slabs of the building as a result of horizontal dynamic loads (such as earthquake, impact load etc.). According to the method, first the multilinear force-displacement diagrams are determined in accordance with the elastoplastic material model and then these curves are replaced with curves that can be characterized by polynomials. In this way, the problem has been reduced to the solution of a system of differential equations of the second order and of variable coefficient.

2. The model taken as a basis for calculations

For buildings with framework or wall system, a model has been selected for calculations, where the structure to be investigated is a system consisting of masses of a number equal to the number of floors of the building and the masses interconnected elastically are represented by rigid disks in the plane of the different roofs (in the horizontal plane). Since the force is acting in horizontal direction, the different masses are assumed to move only in their own plane. There is a constrained elastic connection between the lowest mass and the soil as well as between the other masses and those above or below them. In accordance with the general system of planar displacements, the constraints are capable of bringing about forces and moments. In addition to these constraints, also a damping constraint directly proportional to the rate of velocity of displacement and rotation has been taken into consideration as schematically illustrated for two adjacent masses (mass k and mass $k+1$) in Fig. 1.

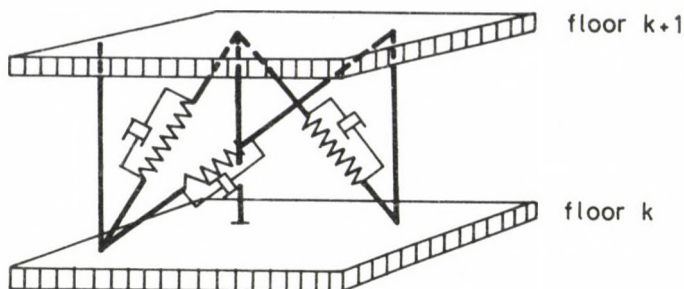


Fig. 1.

3. System of equations used for dynamic calculations

On the basis of the detail drawing of the model given in Fig. 1, the equation of motion for the i -th floor of a multistoreyed building can be written in a co-ordinate system where the origin is arbitrary but vertically coincident for each floor (0) and the direction of the x - y axes is identical for each floor (global co-ordinate system), taking into consideration an exciting force of horizontal direction, in the following form (for derivation see /1/ while calculation of the coefficients is described later in this work):

$$\begin{aligned}
 m_i(\ddot{x}_i - y_i^S \ddot{\phi}_i) + k_{il,xx} x_1 + \dots + k_{in,xx} x_n + \\
 + k_{il,xy} y_1 + \dots + k_{in,xy} y_n + \\
 + k_{il,x\phi} \phi_1 + \dots + k_{in,x\phi} \phi_n + \\
 + c_{il,xx} \dot{x}_1 + \dots + c_{in,xx} \dot{x}_n + \\
 + c_{il,xy} \dot{y}_1 + \dots + c_{in,xy} \dot{y}_n + \\
 + c_{il,x\phi} \dot{\phi}_1 + \dots + c_{in,x\phi} \dot{\phi}_n = P_{ix}(t)
 \end{aligned}$$

$$\begin{aligned}
 m_i(\ddot{y}_i + x_i^S \ddot{\phi}_i) + k_{il,yy} y_1 + \dots + k_{in,yy} y_n + \\
 + k_{il,yx} x_1 + \dots + k_{in,yx} x_n + \\
 + k_{il,y\phi} \phi_1 + \dots + k_{in,y\phi} \phi_n + \\
 + c_{il,yy} \dot{y}_1 + \dots + c_{in,yy} \dot{y}_n + \\
 + c_{il,yx} \dot{x}_1 + \dots + c_{in,yx} \dot{x}_n +
 \end{aligned}$$

$$\begin{aligned}
& + c_{il,y\phi} \dot{\phi}_1 + \dots + c_{in,y\phi} \dot{\phi}_n = p_{iy}(t) \\
& - y_i^s m_i \ddot{x}_i + x_i^s m_i \ddot{y}_i + J_{O1} \ddot{\phi}_i + \\
& + k_{il,\phi\phi} \phi_1 + \dots + k_{in,\phi\phi} \phi_n + \\
& + k_{il,\phi x} x_i + \dots + k_{in,\phi x} x_n + \\
& + k_{il,\phi y} y_i + \dots + k_{in,\phi y} y_n + \\
& + c_{il,\phi\phi} \dot{\phi}_1 + \dots + c_{in,\phi\phi} \dot{\phi}_n + \\
& + c_{il,\phi x} \dot{x}_1 + \dots + c_{in,\phi x} \dot{x}_n + \\
& + c_{il,\phi y} \dot{y}_1 + \dots + c_{in,\phi y} \dot{y}_n = M_{oi}(t) \quad (i = 1, 2, \dots, n)
\end{aligned}$$

Accordingly, the matrix form of the system of equations for the entire building can be written, as follows (the co-ordinates in the equations as well as the typical points associated with the roof being illustrated in Fig. 2):

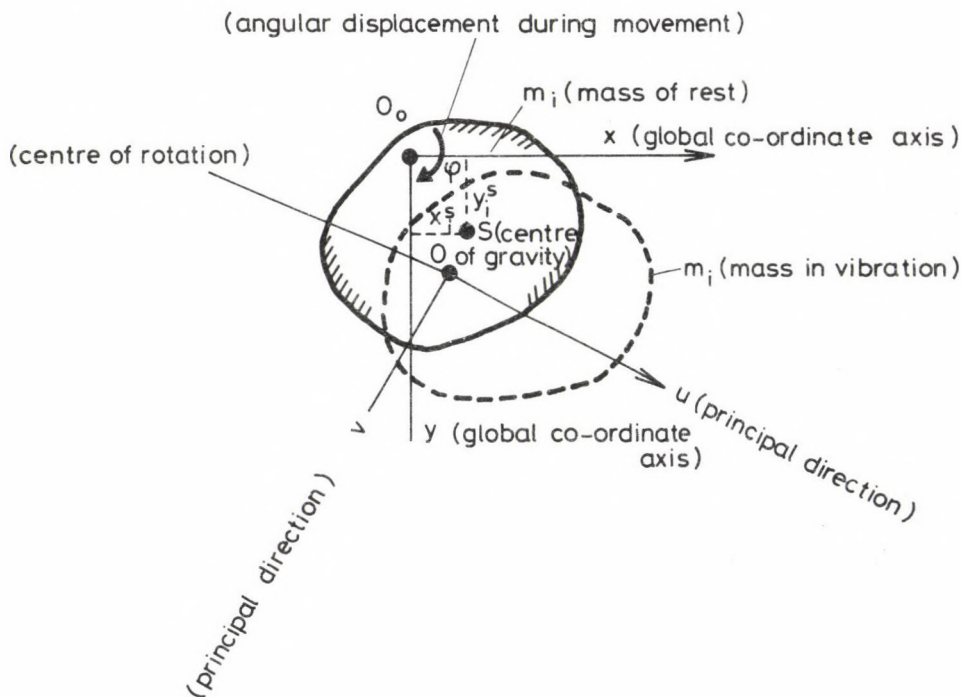


Fig. 2.

$$\underline{\underline{A}} \underline{\underline{d}} + \underline{\underline{C}} \underline{\underline{d}} + \underline{\underline{K}} \underline{\underline{d}} = \underline{\underline{p}}(t) \quad (5.27)$$

where:

$$\underline{\underline{A}} = \begin{bmatrix} \underline{\underline{M}} & 0 & -\underline{\underline{Y}}_S \underline{\underline{M}} \\ 0 & \underline{\underline{M}} & \underline{\underline{X}}_S \underline{\underline{M}} \\ -\underline{\underline{Y}}_S \underline{\underline{M}} & \underline{\underline{X}}_S \underline{\underline{M}} & \underline{\underline{J}}_0 \end{bmatrix} \quad (\text{hypermatrix})$$

$$\underline{\underline{M}} = \langle m_1, m_2, \dots, m_n \rangle \quad (\text{mass diagonal matrix})$$

$$\underline{\underline{J}} = \langle J_{01}, J_{02}, \dots, J_{0n} \rangle \quad (\text{mass inertia diagonal matrix})$$

J_0 being the moment of inertia of the mass concentrated on the roof with respect to origin of the co-ordinate system,

$$\underline{\underline{X}}_S = \langle x_1^S, x_2^S, \dots, x_n^S \rangle \quad (\text{diagonal matrix of x-co-ordinates in the centre of mass})$$

$$\underline{\underline{Y}} = \langle y_1^S, y_2^S, \dots, y_n^S \rangle \quad (\text{diagonal matrix of y-co-ordinates in the centre of mass})$$

$$\underline{\underline{K}} = \begin{bmatrix} K_{xx} & K_{xy} & K_{x\phi} \\ K_{yx} & K_{yy} & K_{y\phi} \\ K_{\phi x} & K_{\phi y} & K_{\phi\phi} \end{bmatrix} \quad (\text{stiffness hypermatrix})$$

$$\underline{\underline{C}} = \begin{bmatrix} C_{xx} & C_{xy} & C_{x\phi} \\ C_{yx} & C_{yy} & C_{y\phi} \\ C_{\phi x} & C_{\phi y} & C_{\phi\phi} \end{bmatrix} \quad (\text{damping hypermatrix})$$

$$\underline{\underline{d}} = \begin{bmatrix} x \\ y \\ \phi \end{bmatrix} \quad (\text{hypervector containing displacement co-ordinates})$$

$$\underline{\underline{p}}(t) = \begin{bmatrix} p_x \\ p_t \\ M_0 \end{bmatrix} \quad (\text{load hypervector})$$

4. Stiffness matrix of the system of equations

In addition to the solution of the system of equations in general, difficulties arise in determination of the elements of the stiffness matrices. Determination of these elements will therefore be discussed in detail below. First the centre of rotation of the building cross sections (0), their principal directions of stiffness (u, v, θ), forces acting in these directions, resulting in unit displacement (p_u, p_v) and the force couple resulting in unit rotation in the centre of rotation (M_i) shall be determined from the relationships given below [1] (for definitions see Fig. 3).

$$\operatorname{tg} 2\alpha = \frac{2C}{A-B} \quad (5.28)$$

$$p_{u,v} = \frac{A+B}{2} \pm \sqrt{\left(\frac{A-B}{2}\right)^2 + C^2} \quad (5.29)$$

$$M_i = \sum_{i=1}^m y_i p_{ixx} - 2 \sum_{i=1}^m x_i y_i p_{ixy} + \sum_{i=1}^m x_i^2 p_{iyy} \quad (5.30)$$

Co-ordinates of the centre of rotation (0):

$$y'_0 = \frac{B}{N} \left[\sum_{i=1}^m y'_i p_{ixx} - \sum_{i=1}^m x'_i p_{ixy} \right] + \frac{C}{N} \left[\sum_{i=1}^m x'_i p_{ixx} - \sum_{i=1}^m y'_i p_{ixy} \right] \quad (5.31)$$

$$x'_0 = \frac{A}{N} \left[\sum_{i=1}^m x'_i p_{iyy} - \sum_{i=1}^m y'_i p_{ixy} \right] + \frac{C}{N} \left[\sum_{i=1}^m y'_i p_{ixx} - \sum_{i=1}^m x'_i p_{ixy} \right] \quad (5.32)$$

In the relationships

$$A = \sum_{i=1}^m p_{ixx}, \quad B = \sum_{i=1}^m p_{iyy}, \quad C = \sum_{i=1}^m p_{ixy}, \quad N = AB - C^2.$$

(Note that, because of nonlinearity, the above relationships vary as a function of time.)

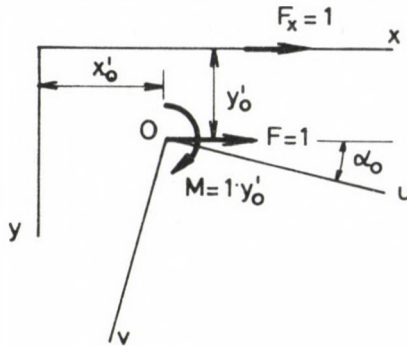


Fig. 3.

First, as usually, the flexibility matrix shall be determined instead of the stiffness matrix, the elements of which contain the displacements (rotations) resulting from unit forces (force couples). Illustrated in Fig. 3 are the centre of rotation and principal directions of stiffness in the co-ordinate system for the i -th floor, determined in the way described above.

Let force $F = 1$ be plotted in the direction of axis x . The displacements resulting from this force can be determined in the following way:

In the general case, the floor is displaced in directions x and y due to combined motion and, in addition to this displacement, the floor may experience also angular displacement (rotation). Let these displacements be denoted by a_{xx} , a_{xy} , $a_{x\phi}$. With the force reduced to the origin of the co-ordinate system, a force $F = 1$ and a moment $M = 1y'_0$ are obtained. Furthermore, with force F decomposed into components of direction u and direction v , $F_u = 1 \cdot \cos \alpha_0$ and $F_v = 1 \cdot \sin \alpha_0$, respectively. Displacements p_u , p_v associated with unit forces have been written above. From these, the numerical value of force resulting in unit displacement (spring constant): $k_u = \frac{1}{p_u}$, $k_v = \frac{1}{p_v}$, respectively. The numerical value of force couple resulting in unit rotation can similarly be obtained: $K_\phi = \frac{1}{M_1}$. Accordingly, displacements of the centre resulting from force F_x are

$$u = \cos \alpha_0 k_u$$

$$v = \sin \alpha_0 k_v$$

$$\phi = y'_0 k_\phi$$

and, from these, the effect of force $F_x = 1$ that is displacement in the direction of axis x and y (e_{xx} , e_{xy} , respectively) and rotation of the centre of the co-ordinate system (ϕ_x) can be obtained:

$$e_{xx} = \cos^2 \alpha k_u + \sin^2 \alpha k_v + y_0' k_\phi$$

$$e_{xy} = \sin \alpha \cos \alpha (k_u - k_v) - x_0' k_\phi$$

$$\phi_y = x_0' k_\phi .$$

Quite similarly, the following displacements are obtained for force $F_y = 1$ acting upon the y axis:

$$e_{yy} = \sin^2 \alpha k_u + \cos^2 \alpha k_v + x_0' k_\phi$$

$$e_{yx} = \sin \alpha \cos \alpha (k_u - k_v) - y_0' k_\phi$$

$$\phi_y = x_0' k_\phi .$$

On the basis of what has been written above, the flexibility matrix (\underline{N}) of the system can be calculated. With this inverted, the stiffness matrix ($\underline{K} = \underline{N}^{-1}$) can be obtained as well.

5. Stiffness in case of a complex structure, taken into consideration on the basis of the elasto-plastic material model

In Fig. 4, a simple system consisting of one single mass is illustrated, indicating the elastic-plastic force-displacement relations.

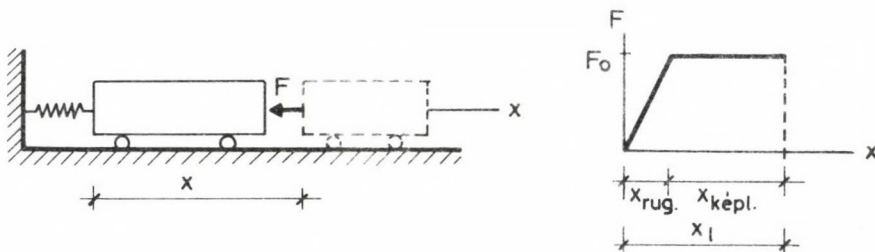


Fig. 4.

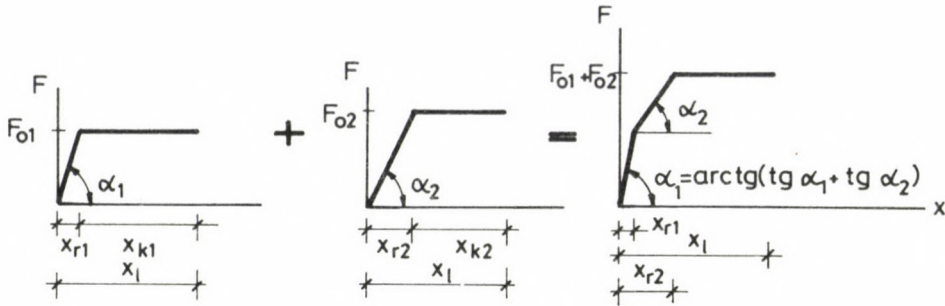


Fig. 5.

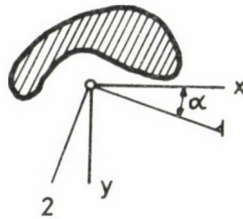


Fig. 6.

In case of more springs connected in parallel, with a different force resulting in yield for each, a polygonal diagram is obtained for force-displacement as shown for two springs of different characteristic in Fig. 5. The polygonal diagram can be replaced with a general polynomial (of the n -th degree) properly osculating the polygon (the accuracy being increased by increasing the degree of the curve) to produce a continuous function in this way, representing the relation between the resultant of forces acting upon the mass and displacement.

The same principle can be applied to the case of bent beams. Fig. 6 shows the cross section of a bent beam, indicating the principal directions of inertia. According to the Figure, forces F_1 and F_2 shall be acting upon the shear centre of another cross section denoted by k , parallel to the appropriate displacements, in order to displace cross section i of a Hookean homogeneous prismatic rod parallel to principal directions 1 and 2 to an extent of Δ_1 and Δ_2 , respectively. The magnitude of the forces is given by relationships

$$F_1 = HJ_2 \cdot \Delta_{1 \text{ ik}}$$

$$F_2 = HJ_1 \cdot \Delta_{2 \text{ ik}}$$

based on the theory of the strength of materials.

(In the relationships, H is a factor depending on the material, conditions of support and location of cross sections of the rod.)

Let then, again in cross section i, an arbitrary co-ordinate system xy be plotted to determine what an external force resulting in unit displacement of the shear centre of the cross section in the direction of axis x shall be acting upon cross section k. If axis x is not coincident with the principal direction, the force resulting in displacement will not be parallel to axis x but it can be characterized by components p_{xx} and p_{xy} of direction x and y, respectively. The magnitude of the component in direction 1 or 2 of the mentioned unit displacement in the direction of axis x, including an angle α with principal direction 1, is $1 \cos \alpha$ or $-1 \sin \alpha$ as suggested by Fig. 5, 9. To bring about these displacements, forces

$$Q_1 = HJ_2 \cos \alpha$$

$$Q_2 = -HJ_1 \sin \alpha \quad ,$$

acting in the direction of axis 1 or 2, are required. Force components p_{xx} and p_{xy} to be found are given by the sum of projections of these forces in direction x and y, respectively, that is

$$p_{xx} = Q_1 \cos \alpha - Q_2 \sin \alpha = H(J_1 \sin^2 \alpha + J_2 \cos^2 \alpha)$$

$$p_{xy} = Q_1 \sin \alpha - Q_2 \cos \alpha = -\cos \alpha \sin \alpha H(J_1 - J_2) \quad .$$

Forces p_{yy} and p_{yx} shall act in direction y and x, respectively to result in unit displacement of the investigated cross section in direction y. These forces can be determined in a way similar to the above determination to obtain

$$p_{yy} = H(J_1 \cos^2 \alpha + J_2 \sin^2 \alpha)$$

$$p_{yx} = -\cos \alpha \sin \alpha (J_1 - J_2) H = p_{xy} \quad .$$

Values p_{xx} , p_{yy} and $p_{xy} = p_{yx}$ so determined are also called stiffness factors.

In case of more interconnected beams, the stiffness factor can be produced as the sum of the different stiffness factors. Consider a case where the force-displacement diagram complies with the elasto-plastic material model. Now, in accordance with diagram $F_1 - \Delta_1$ or $F_2 - \Delta_2$, relationships p_{xx} , p_{yy} and p_{xy} are equal to the sum of angular coefficients of the diagrams. A staggered diagram is obtained as an illustration as seen for p_{xx} in Fig. 7. In case of a complex cross section (more independent elements), the sum of displacements associated with unit force is used in the relationships serving to determine the centre of rotation, principal directions of stiffness etc., the illustration resulting in a multistep diagram (Fig. 7). Now we have to write relationships $\sum p_{ixx}$, $\sum p_{iyy}$ and $\sum p_{ixy}$ in the form of approximate continuous functions. Thus, considering the values associated with the different steps to be tangents of the sides of a polygonal diagram, the integral of the staggered diagram that is a polygonal diagram can be obtained (Fig. 8), which can be replaced with a suitably selected polynomial of the n -th degree. With this polynomial determined, the continuous functions of the stiffness factors can be obtained as derivatives of this polynomial.

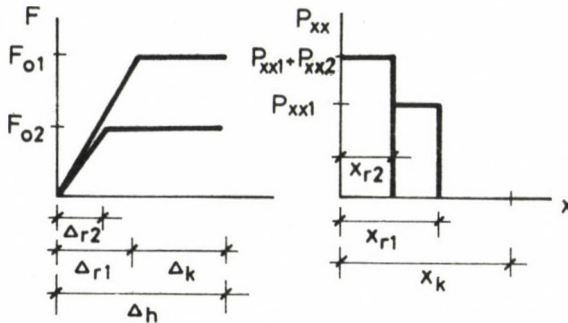


Fig. 7.

The result of this effort is that the relationships that have been used to determine the coefficients of the kinetic equation can be expressed as a continuous instead of a constant function of x , y , ϕ . In the system of equations, this means that the elements of stiffness matrix \underline{K} are not constant and in case of earthquake, the load vector will not be constant

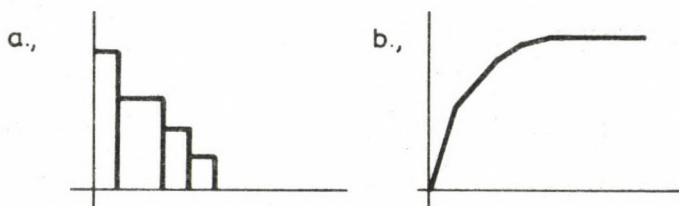


Fig. 8.

either because the components of the force and moment depend on the centre of rotation of the first storey.

Introduction of notation

$$\sum p_{ixx} = Af_1(x_i); \quad \sum p_{iyy} = Bf_2(y_i); \quad \sum p_{ixy} = Cf_3(x_i, y_i)$$

results in modification of the above relationships as follows:

Forces acting in the principal directions, resulting in unit displacement:

$$P_U = \frac{Af_1(x) + Bf_2(y)}{2} + \left[\left(\frac{Af_1(x) - Bf_2(y)}{2} \right)^2 + C^2 f_2(xy)^2 \right]^{1/2}$$

$$P_V = \frac{Af_1(x) + Bf_2(y)}{2} - \left[\left(\frac{Af_1(x) - Bf_2(y)}{2} \right)^2 + C^2 f_2(xy)^2 \right]^{1/2}$$

Inclination angle of principal directions:

$$\alpha_0 = \text{arctg} \frac{Cf_3(xy)}{Af_1(x) - Bf_2(y)}$$

With notation

$$N = Af_1(x) Bf_2(y) + Cf_3(x, y)^2$$

introduced, co-ordinates of the centre of rotation:

$$y'_0 = \frac{Bf_2(y)}{N} [Df_1(x) + Ef_3(xy)] + \frac{Cf_3(xy)}{N} [Ff_2(y) - Ef_3(xy)]$$

$$x'_0 = \frac{Af_1(x)}{N} [Ff_2(y) + Ef_3(xy)] + \frac{Cf_3(xy)}{N} [Df_1(x) - Ef_3(xy)]$$

6. Plotting of the resistive force - displacement diagram

Determination of the $F - \Delta$ diagram in different cases occurring in practice has been discussed in detail in par 5, taking into consideration that in case of complex structures, part of the structure is elastic while the other part plastic. The initial section of the $F - \Delta$ diagram can be determined in this way and the relationship can be applied to determination of maximum displacement (load) resulting from a single shock wave (blast of wind, explosion). However, in case of dynamic loads or variable direction (e.g. earthquake), a hysteretic curve is obtained for $F - \Delta$ as shown in Fig. 9.

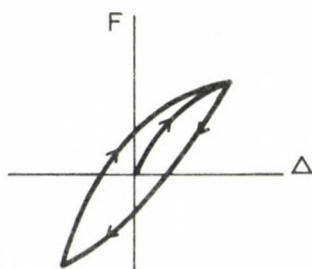


Fig. 9.

This considerably more general diagram had been determined analytically by Jennings /2/ and practical calculations and experiments proved that it could be successfully used to simulate the response of actual building structures to forces acting upon them. Let the function describing relation $F - \Delta$, determinable on the basis of par 5, be denoted by $F = F_1^{(\Delta)}$ in the first phase of loading. Then, according to Jennings, the following relationship will exist in case of load of opposite direction of if the load discontinues:

$$\frac{F - F_0}{2} = F_1 \frac{\Delta - \Delta_0}{2},$$

where F_0 and Δ_0 are the displacement and force, respectively taking place before the loading process reversed (Structures and materials that meet these requirements are called Masing-type structures and materials because Masing was the first to define the curve). Applicability of the curve to cases where damping effect is prevailing was proved also by Herrera (1965),

Lazan (1968) and Marsal (1967) /2/. Thus the hysteretic diagram or a degraded type of it can be used also to investigate the effects of earthquake and it yields acceptable values for the functions included in the theoretical relationships. At the same time, the practical applicability of the method as a whole seems to be proved.

REFERENCES

1. Vértés, G.: Structural Dynamics, Elsevier Sc. Publishers, Amsterdam, 1985
2. Newmark, N.M. - Rosenblueth, E.: Fundamentals of Earthquake Engineering, Prentice Hall, N.H. 1971
3. Sbo, H.: Nonlinear Vibrations of Gradually Changing Beams, Journal of Sound and Vibration, 72.3, October 1980
4. Bielac, D.: Behaviour of Building with Nonlinear Structures, Earthquake Engineering and Structural Dynamics, 6.1, January-February 1987

BOOK REVIEW

Sándor Kaliszky: Plasticity. Akadémiai Kiadó, Budapest, 1989 (pp. 505)

The recent book of Sándor Kaliszky on plasticity in English language is a modernized and amplified version of the 1975 edition written in Hungarian language, including now the recent results of research. The book has been intended first of all for engineers and research people but it can be used as a text-book by anybody familiar with the fundamentals of the theory of strength.

The first three chapters introduce the reader in the fundamentals of elasticity and plasticity, giving, in particular, definitions, field equations and extremum principles where the author restricts himself to small deformations and linearly elastic and ideally plastic bodies. Presented in the fourth chapter are the basic problems of plasticity (ultimate plasticity of a rod under tension, onset of this state, twisted rod, thick-walled spherical bodies and tubes under internal pressure) while in the fifth chapter, the reader becomes familiar with the equation system for two-dimensional problems (two-dimensional plastic flow, state of plane stress), the theory of field of slip lines and the method of solution based on this theory where the solution of problems presented contributes considerably to better understanding of the theory.

Discussed in the sixth chapter are the plastic behaviour of bent rods and rod type structures under complex load and the ultimate load capacity while the seventh chapter deals with the same problem for shells and plates. The author deals with determination of the lower (statically permissible) and upper (kinematically permissible) limits of load in detail, discussing also the fundamental principles of design on the basis of these limits that is design of the structure for minimum load. Written in this chapter are the basic equations of mathematical programming for load capacity and stability of rod type structures and optimum weight.

The eight chapter gives a brief description of the models of other than ideally plastic, non-elastic bodies for plastic (isotropic, kinematic and generalized) hardening, granular materials and viscous materials.

The ninth chapter which is the last chapter in the book deals with the dynamic problems of plastic structures. It gives a summary of the fundamental principles adopted for the description of non-elastic behaviour of structures under impact pressure essentially on the basis of the model of rigid-plastic bodies but it also shows how other effects (rate of deformation, large displacements, elastic deformation) can be taken into consideration. Two approaches, together with the process of solution, are presented for treatment of the problems and examples are given to illustrate the application of the process.

The style of the book is simple and comprehensible, easy to understand even for beginners in the field of mechanics and ample examples and illustrations contribute to better understanding. The work of research people is facilitated by references of a number of more than 400. The book is outstanding in that it represents an engineers' philosophy, offering thus a valuable help for the solution of practical engineering problems.

Mrs. P. Elter

PRINTED IN HUNGARY

Akadémiai Kiadó és Nyomda Vállalat, Budapest

NOTICE TO CONTRIBUTORS

Papers in English* are accepted condition that they have not been previously published or accepted for publication.

Manuscripts in two copies (the original type-written copy plus a clear duplicate one) complete with figures, tables, and references should be sent to

Acta Technica
Nádor u. 7. I. 118
Budapest, Hungary
H-1051

Although every effort will be made to guard against loss, it is advised that authors retain copies of all material which they submit. The editorial board reserves the right to make editorial changes.

Manuscripts should be typed double-spaced on one side of good quality paper with proper margins and bear the title of the paper and the name(s) of the author(s). The full postal address(es) of the author(s) should be given in a footnote on the first page. An abstract of 50 to 100 words should precede the text of the paper. The approximate locations of the tables and figures should be indicated on the margin. An additional copy of the abstract is needed. Russian words and names should be transliterated into English.

References. Only papers closely related to the author's work should be referred to. The citations should include the name of the author and/or the reference number in brackets. A list of numbered references should follow the end of the manuscript.

References to periodicals should mention: (1) name(s) and initials of the author(s); (2) title of the paper; (3) name of the periodical; (4) volume; (5) year of publication in parentheses; (6) numbers of the first and last pages. Thus: 5. Winokur, A., Gluck, J.: Ultimate strength analysis of coupled shear walls. American Concrete Institute Journal 65 (1968) 1029-1035

References to books should include: (1) author(s)' name; (2) title; (3) publisher; (4) place and year of publication. Thus: Timoshenko, S., Gere, J.: Theory of Elastic Stability. McGraw-Hill Company, New York, London 1961.

Illustrations should be selected carefully and only up to the necessary quantity. Black-and-white photographs should be in the form of glossy prints. The author's name and the title of the paper together with the serial number of the figure should be written on the back of each print. Legends should be brief and attached on a separate sheet. Tables, each bearing a title, should be self-explanatory and numbered consecutively.

Authors will receive proofs which must be sent back by return mail.

Authors will receive 50 reprints free of charge.

*Hungarian authors can submit their papers also in Hungarian.

Periodicals of the Hungarian Academy of Sciences are obtainable
at the following addresses:

AUSTRALIA

C.B.D. LIBRARY AND SUBSCRIPTION SERVICE
Box 4886, G.P.O., Sydney N.S.W. 2001
COSMOS BOOKSHOP, 145 Ackland Street
St. Kilda (Melbourne), Victoria 3182

AUSTRIA

GLOBUS, Höchstädtplatz 3, 1206 Wien XX

BELGIUM

OFFICE INTERNATIONAL DES PERIODIQUES
Avenue Louise, 485, 1050 Bruxelles
E. STORY-SCIENTIA P.V.B.A.
P. van Duyseplein 8, 9000 Gent

BULGARIA

HEMUS, Bulvar Ruszki 6, Sofia

CANADA

PANNONIA BOOKS, P.O. Box 1017
Postal Station "B", Toronto, Ont. M5T 2T8

CHINA

CNPICOR, Periodical Department, P.O. Box 50
Peking

CZECHOSLOVAKIA

MAD'ARSKA KULTURA, Národní třída 22
115 66 Praha
PNS DOVOZ TISKU, Vinohradská 46, Praha 2
PNS DOVOZ TLAČE, Bratislava 2

DENMARK

EJNAR MUNKSGAARD, 35, Nørre Søgade
1370 Copenhagen K

FEDERAL REPUBLIC OF GERMANY

KUNST UND WISSEN ERICH BIBER
Postfach 46, 7000 Stuttgart 1

FINLAND

AKATEEMINEN KIRJAKAUPPA, P.O. Box 128
00101 Helsinki 10

FRANCE

DAWSON-FRANCE S.A., B.P. 40, 91121 Palaiseau
OFFICE INTERNATIONAL DE DOCUMENTATION ET
LIBRAIRIE, 48 rue Gay-Lussac
75240 Paris, Cedex 05

GERMAN DEMOCRATIC REPUBLIC

HAUS DER UNGARISCHEN KULTUR
Karl Liebknecht-Straße 9, DDR-102 Berlin

GREAT BRITAIN

BLACKWELL'S PERIODICALS DIVISION
Hythe Bridge Street, Oxford OX1 2ET
BUMPUS, HALDANE AND MAXWELL LTD.
Cowper Works, Olney, Bucks MK46 4BN
COLLET'S HOLDINGS LTD., Denington Estate,
Wellingborough, Northants NN8 2QT
WM DAWSON AND SONS LTD., Cannon House
Folkstone, Kent CT19 5EE
H. K. LEWIS AND CO., 136 Gower Street
London WC1E 6BS

GREECE

KOSTARAKIS BROTHERS INTERNATIONAL
BOOKSELLERS, 2 Hippokratous Street, Athens-143

HOLLAND

FAXON EUROPE, P.O. Box 167
1000 AD Amsterdam
MARTINUS NIJHOFF B. V.

Lange Voorhout 9-11, Den Haag
SWETS SUBSCRIPTION SERVICE
P.O. Box 830, 2160 Sz Lisse

INDIA

ALLIED PUBLISHING PVT. LTD.
750 Mount Road, Madras 600002
CENTRAL NEWS AGENCY PVT. LTD.
Connaught Circus, New Delhi 110001
INTERNATIONAL BOOK HOUSE PVT. LTD.
Madame Cama Road, Bombay 400039

ITALY

D. E. A., Via Lima 28, 00198 Roma
INTERSCIENTIA, Via Mazzè 28, 10149 Torino
LIBRERIA COMMISSIONARIA SANSONI
Via Lamarmora 45, 50121 Firenze
SANTO VANASIA, Via M. Macchi 58
20124 Milano

JAPAN

KINOKUNIYA COMPANY LTD.
Journal Department, P.O. Box 55
Chitose, Tokyo 156
MARUZEN COMPANY LTD., Book Department
P.O. Box 5050 Tokyo International, Tokyo 100-31
NAUKA LTD., Import Department
2-30-19 Minami Ikebukuro, Toshima-ku, Tokyo 171

KOREA

CHULPANMUL, Phenjan

NORWAY

TANUM-TIDSKRIFT-SENTRALEN A.S.
Karl Johansgata 43, 1000 Oslo

POLAND

WĘGIERSKI INSTYTUT KULTURY
Marszałkowska 80, 00-517 Warszawa
CKP I W, ul. Towarowa 28, 00-958 Warszawa

ROUMANIA

D. E. P., Bucuresti
ILEXIM, Calea Grivitei 64-66, Bucuresti

SOVIET UNION

SOYUZPECHAT — IMPORT, Moscow
and the post offices in each town
MEZHDUNARODNAYA KNIGA, Moscow G-200

SPAIN

DIAZ DE SANTOS Lagasca 95, Madrid 6

SWEDEN

ESSELTE TIDSKRIFTSCENTRALEN
Box 62, 101 20 Stockholm

SWITZERLAND

KARGER LIBRI AG, Petersgraben 31, 4011 Basel

USA

EBSCO SUBSCRIPTION SERVICES
P.O. Box 1943, Birmingham, Alabama 35201
F. W. FAXON COMPANY, INC.
15 Southwest Park, Westwood Mass. 02090
MAJOR SCIENTIFIC SUBSCRIPTIONS
1851 Diplomat, P.O. Box 819074,
Dallas, Tx. 75381-9074
READ-MORE PUBLICATIONS, INC.
140 Cedar Street, New York, N. Y. 10006

YUGOSLAVIA

JUGOSLOVENSKA KNJIGA, Terazije 27, Beograd
FORUM, Vojvode Mišića 1, 21000 Novi Sad